VERTICAL MIXING OF OZONE IN THE VERY STABLE NOCTURNAL BOUNDARY LAYER

by

JENNIFER ANN SALMOND

BA., University of Oxford, 1995

M.Sc., University of Birmingham, 1996

A THESIS SUBMITTED IN PARTIAL FULFILMENT OF
THE REQUIREMENTS FOR THE DEGREE OF

DOCTOR OF PHILOSOPHY

in

THE FACULTY OF GRADUATE STUDIES

(Department of Geography)

We accept this thesis as conforming
to the required standard

THE UNIVERSITY OF BRITISH COLUMBIA

July 2001

In presenting this thesis in partial fulfilment of the requirements for an advanced degree at the University of British Columbia, I agree that the Library shall make it freely available for reference and study. I further agree that permission for extensive copying of this thesis for scholarly purposes may be granted by the head of my department or by his or her representatives. It is understood that copying or publication of this thesis for financial gain shall not be allowed without my written permission.

Department of GEOGRAPHY

The University of British Columbia
Vancouver, Canada

Date 10-SEPT-2001

Abstract

Significant increases in nocturnal ozone concentration have been observed near the surface in regions of complex terrain. These temporally isolated features are characterised by a sudden increase ('spike') in ozone concentrations superimposed upon spatially uniform background concentrations of near zero. They typically occur during the summer months when synoptic conditions support the development of the very stable nocturnal boundary layer (NBL). Although localised, these 'spikes' in ozone concentration may have environmental and health consequences and play a significant role in determining diurnal pollutant budgets.

During the summer of 1998 a field experiment was conducted in the Lower Fraser Valley, British Columbia, to investigate the relationship between near surface ozone concentrations and the structure of the NBL. This thesis examines the hypothesis that nocturnal spikes in surface ozone concentration result from vertical mixing processes which temporarily couple the residual layer to the surface layer, facilitating the transport of ozone stored aloft to the surface. The study uses a comparatively new quantitative analytical tool – wavelet analysis – to objectively isolate periods of intermittent turbulence observed in the near surface layers through the field campaign. A new technique is developed to isolate the flux associated with only the turbulent ('burst') component of each time series, and to provide revised estimates of scalar fluxes.

Despite the dominance of ozone sinks in the surface layer, localised spikes in ozone concentration were observed throughout the Lower Fraser Valley during the field campaign. At the field site these were well correlated with periods of increased turbulence associated with the presence or rapid break-down of the nocturnal low-level jet and the development of down-valley winds. However, spikes in surface concentration were also shown to be sensitive to surface nitrogen monoxide concentrations and ozone concentration aloft. Ozone concentrations were highly variable throughout the residual layer, and the largest spikes in surface concentration coincided with periods when ozone concentrations in excess of 80 ppb were observed aloft. Whilst the results demonstrate that vertical mixing processes can play a significant role in determining local surface concentrations, in regions of complex coastal terrain the role of advection in the NBL cannot be ignored.

Table of Contents

Table of Tables

Table of Figures

List of symbols and abbreviations

a_x	constant
b	position
b_x	constant
f(t)	function at time t
c	scalar quantity
C_δ	scale independent constant for wavelet
C_ψ	constant depending on the wavelet chosen
CFS	Canadian Forces Station
d	zero-plane displacement length
db4	'Daubechies 4' wavelet
g	acceleration due to gravity
GVRD	Greater Vancouver Regional District
hv	ultra-violet radiation
j	scale number
k	frequency index
L	Monin Obukhov length scale
LLJ	low-level jet
LFV	Lower Fraser Valley
M	catalyst
n	specific point in the series
N	total number of data points in the series
NBL	nocturnal boundary layer
N_{bv}	Brunt-Vaisala frequency
NO	nitrogen monoxide
NO_2	nitrogen dioxide
NO_x	oxides of nitrogen
O·	oxygen free radical
O_2	oxygen
O_3	ozone
P_k	red noise spectrum
ppb	parts per billion

PDT	Pacific Daylight Time
Ri	gradient Richardson number
Ri_c	critical Richardson number
RL	residual layer
s	scale
S_c	sources and sinks of scalar c
SBL	stable boundary layer
t	time
T^*	temperature scale
u	east - west wind vector
u^*	friction velocity
U_j	u, v, w directions for j = 1,2,3
v	north - south wind vector
w	angular frequency
$\overline{W}^2(b)$	wavelet variance at each scale b
W_n	generic wavelet coefficient
$W_\psi f$	wavelet coefficient for each scale (a) and position (b)
W^{fg}	product of wavelet coefficients for time series f and g
W^{*fg}	product of the complex conjugate of time series f and g
X_j	x, y, z directions for j = 1,2,3
z	height above the earth surface
α	lag –1 auto-correlation of the signal
δj	number of sub-intervals per octave
σ^2	variance
σ_w	standard deviation of vertical velocity
σ_T	standard deviation of temperature
ψ_m	dimensionless wind shear
ψ_T	dimensionless temperature gradient
θ_v	virtual potential temperature
$\psi[(t-b)/a]$	mother wavelet
υ_c	molecular viscosity

Acknowledgements

Financial support for this thesis was provided by a Commonwealth Scholarship, University Graduate Fellowship and NSERC grants to Dr. Ian McKendry. I gratefully acknowledge the hard work and support of my supervisor Dr. Ian McKendry, who gently encouraged me to develop my own ideas and research agenda whilst continually providing opportunities for debate and discussion. Thanks also go to Dr. Tim Oke whose timely wisdom often helped put things into perspective, Dr. Roland Stull who patiently taught me the value of taking risks whilst striving for the seemingly impossible, and Dr. Douw Steyn who challenged me to think in new ways. Special thanks goes to Vincent Kujala for the many hours spent helping me to write computer programs, to Chris Jeffery who regularly helped out with the maths and to Ian McKendry, Andrew Murphy and Laura Rempel for helping to check the final drafts.

The fieldwork for this thesis would not have been possible without the enthusiastic support of Markus Kellarhals, Clair Hanson and Kathy Ostermann who worked in the field all night and often all day for several days at a time without complaining. Thanks also goes to Diane Pellerin, Vincent Kujala, Joel Torcolini, Ian Owens and Juliet Rowson who kept us awake during the small hours of the morning. I also gratefully acknowledge the support of Chief Madill and staff at CFS Aldergrove and the Air Traffic Controllers at Abbotsford who handled our many requests for tethersonde flights.

I will always treasure the years I have spent in Canada completing this thesis. The friendship and support I have received from friends and colleagues in the Department of Geography has at times been overwhelming. While there are too many people to thank in person a few deserve a special mention for their help, especially during the hard months when I struggled with Lyme's disease. These include Diane Pellerin, Wendy Hales, Beth Gilchrist, Bob Wilson, and Kate Williams whose support went beyond the call of duty. Thanks also go to Laura Beattie, Juliet Rowson and Phil Kelly for their continued support through the years, and to my office mate Laura Rempel for the many and varied discussions which livened up the days.

I am also indebted to my family for their unconditional emotional and financial support through the tough times and for joining with me in celebrating the good times. This thesis would have been a lot harder without the weekly telephone calls of encouragement. I would also like to give special thanks to Clair Hanson who has been my confidante and best friend throughout the

last 6 years. Thank you for everything you have done to support me, both practically and emotionally, through the PhD process. Finally, I am enormously grateful to Andrew without whose immeasurable love and generosity this thesis would still be under construction. Thank you for all your help and understanding both at home and at work.

Chapter 1: Introduction and aims

Increasing recognition of the deleterious impact of photochemical pollutants on human health (Lippmann 1989) and the natural environment (Reich & Amundson 1985) has sparked an 'explosion' in air quality monitoring world wide (Derwent et al. 1995). Although data from each location have a unique signature (Altshuller 1986), distinct diurnal cycles in near-surface pollutant concentrations can be identified (Baldsley et al. 1994; Garland & Derwent 1979; Harrison et al. 1978; Kleinman et al. 1994; Steinberger & Ganor 1980; Zaveri et al. 1995). The characteristics of these temporal patterns are pollutant specific (Harrison et al. 1978), determined by the complex interaction between pollutant emissions, chemistry, meteorological controls on dispersion and depositional processes operating within the boundary layer (Reitebuch et al. 2000).

High concentrations of photochemical pollutants are predominantly associated with strong temperature inversions, stagnant quasi-stationary high pressure systems which limit the vertical and horizontal dispersion of pollutants (Kleinman et al. 1994; McKendry et al. 1990; McKendry 1994; Pryor et al. 1995). When this scenario occurs in regions where high emissions of anthropogenic pollutants (particularly from vehicular exhausts) are common, periods of poor air quality known as 'summer smog episodes' may persist for several days. During smog episodes near-surface concentrations of photochemical pollutants exhibit a marked diurnal periodicity, with high concentrations observed during the day and low concentrations (often near zero) recorded at night (Beyrich et al. 1996; Kelly et al. 1984). In regions of complex terrain this periodicity has been linked to pollutant dispersion patterns resulting from advection by thermo-topographical wind systems and vertical mixing mechanisms which couple pollutant reservoirs aloft with the surface (Millan et al. 1996).

Under these conditions, processes operating in the very stable nocturnal boundary layer (NBL), which determine the three dimensional distribution of pollutants, surface based pollutant sinks and pollutant storage aloft, may have a significant impact on near-surface concentrations during a pollution episode (Neu 1995). The breakdown of the stable layer and resulting entrainment of the residual layer shortly after dawn, has been shown to be particularly significant in understanding the diurnal cycles of surface photochemical pollutants (Berkowitz et al. 2000; Beyrich et al. 1996; Hastie et al. 1993; Zaveri et al. 1995; Zhang & Rao 2000).

Attempts have been made to quantify the relationship between pollution stored in the residual layer and near-surface concentrations the following day using simple semi-empirical models (Neu 1995; Neu et al. 1994). These have shown mixed success (Teichmann et al. 1997) and may be hindered in part by a failure to consider the three dimensional characteristics of pollutant advection and vertical mixing processes in the nocturnal boundary layer. However, research suggests that more than half the daily surface concentrations of one photochemical pollutant, ozone, can be accounted for by entrainment from pollutant reservoirs aloft (Kelly et al. 1984; Kleinman et al. 1994; Lehning et al. 1998; Millan et al. 2000).

Our current understanding of the turbulent and meteorological processes controlling pollutant dispersion in the NBL has been limited by a focus on surface based monitoring networks (Hastie et al. 1993). From this information alone, only inferences may be made about the nature and characteristics of processes operating aloft (Berkowitz et al. 2000). Thus despite a recognition of the importance of pollutant levels in the residual layer on near-surface air quality (Banta et al. 1997; Banta et al. 1998; Berkowitz & Shaw 1997; Bigler-Engler & Brown 2000; Gusten et al. 1997; Martin et al. 1991; Millan et al. 2000; Zaveri et al. 1995; Zhang & Rao 2000), concentrations in the residual layer are typically treated as invariant in time and space (Neu et al. 1994).

This assumption is particularly inappropriate in regions of complex terrain where localised thermo-topographical wind systems play an important role in determining both pollutant dispersion pathways within the residual layer and the characteristics of the nocturnal boundary layer (Banta et al. 1997; Beyrich et al. 1996; Kleinman et al. 1994; Martin et al. 1991; Zhang et al. 1998). Unfortunately, little is known about the three dimensional distribution of pollutants within the nocturnal thermo-topographic wind systems and to date these influences have been largely neglected in the literature (Pisano et al. 1997).

Although difficult to characterise and poorly understood, turbulent fluxes in the very stable NBL may also have important practical implications for air quality. Significant increases in ozone concentration (occasionally more than half the previous day's maximum) have been observed near the surface during the night (Corsmeier et al. 1997; Loffler-Mang et al. 1997; Reitebuch, et al. 2000; Samson 1978; Seibert et al. 2000; Zurita & Castro 1983). They usually occur during the summer months when synoptic conditions support the development of the very stable nocturnal boundary layer. These temporally isolated features are distinguished by a sudden increase (hereafter termed a 'spike') in ozone concentrations (Corsemeier et al. 1997).

Ozone production is limited at night and removal mechanisms (such as deposition and chemical titration) dominate in the surface layers (Zaveri et al. 1995). This results in a positive gradient in ozone concentration between the surface and the residual layer (Broder & Gygax 1985; Colbeck & Harrison 1985; Garland & Derwent 1979). Given the prevailing patterns of low ozone concentrations in the near-surface layers, and the likely persistence of higher concentrations aloft, these pollution 'spikes' may therefore be a result of the vertical mixing generated by turbulence.

Turbulence in the very stable NBL is typically weak and intermittent, often governed by local shear and thermal instabilities unrelated to surface characteristics (Stull 1988). Localised bursts of turbulence, generated by mechanisms such as the low level jet, may temporarily couple the residual layer with the stable boundary layer and could generate sufficient vertical mixing to transport pollutants from the residual layer to the surface (Teichmann et al. 1997). If the turbulence coincides with the advection of high pollutant concentrations in the residual layer this may lead to localised periods of poor air quality at the surface (Corsmeier et al. 1997).

However, the characteristics of turbulence (and hence the turbulent fluxes) are difficult to determine in the very stable NBL. Turbulence is typically non-stationary, dominated by a variety of different frequency regimes, and shows a poorly defined spectral gap (Mahrt 1999). Measurements are often made at or near to instrumental limits and are highly sensitive to surface conditions. Flux estimates are sensitive to choice of averaging length and it may be hard to identify intermittent scalar fluxes from within averaged data sets (Mahrt et al. 1996). Standard spectral analysis techniques and theory are ill-suited to the characteristics of weak intermittent turbulence without significant data reduction (through quality control) or correction procedures.

The occurrence and potential significance of these 'spikes' in nocturnal pollutant concentrations has been frequently over-looked in the literature. This is in part due to the intermittency of nocturnal turbulence and the nature of the averaging techniques used. However, these increases in ozone concentration may have environmental and health consequences for local populations. Recent studies have demonstrated that increased levels of ozone concentration at night may be critical to determining the negative response of vegetation to ozone (Musselman & Massman 1999) and increase levels of accumulated 24 hour exposure. Further it is theoretically possible that nocturnal ozone concentrations may temporarily exceed hourly air quality standards (Loffler-Mang et al. 1997). The identification of vertical mixing processes operating in the very stable NBL also has significant implications for pollutant concentrations in

the residual layer and may affect the daily temporal autocorrelation of ozone concentrations during a pollution episode (Banta et al. 1997; Beyrich et al. 1996; Gusten et al. 1997; Lehning et al. 1998; Neu 1995; Zhang & Rao 2000).

Clearly, advection and vertical mixing processes operating in the very stable nocturnal boundary layer (which to date remain poorly understood), may affect ozone concentrations in the residual layer. In 1995 Neu opined that the reduction of ozone concentrations in the residual layer (due to advection and vertical mixing processes) is 'too large to be neglected'. Since then, other authors, notably Teichmann et al. (1997) and Gusten et al. (1997), have tried to quantify the changes in ozone concentration which occur in the stable layer and residual layer of the nocturnal boundary layer. Although these studies hint at the significance of the processes operating in the nocturnal boundary layer in determining diurnal pollutant budgets, few satisfactory quantitative conclusions have been reached. Thus the relative importance of in-situ emissions and chemical production of pollution versus advection and vertical mixing of pollutants stored within the boundary layer in determining surface concentrations remain unknown (Berkowitz et al. 2000; Neu et al. 1994).

1.1 Study rationale

The purpose of this thesis is to design and carry out a field experiment to study the vertical distribution of ozone within the context of the turbulent and meteorological characteristics of the very stable NBL. Although significant increases in nocturnal near-surface ozone concentration have been observed in regions of complex terrain, little is known about their causes or the consequences for diurnal pollutant cycles throughout the airshed. Thus a more thorough understanding of the vertical mixing processes operating in the very stable NBL is sought. Within this context, this thesis examines the hypothesis that increased ozone concentrations at the surface are the result of vertical mixing processes which couple the residual layer to the surface layers and facilitate the transport of ozone stored aloft to the surface.

The study uses a comparatively new quantitative analytical tool – wavelet analysis – to objectively isolate, and quantitatively analyse, the characteristics of intermittent turbulence observed near the surface during the field campaign. Unlike traditional analytical methods such as eddy correlation or Fourier analysis, wavelet analysis is well suited to highly non-stationary signals and can be used to elucidate multi-scale features, transient phenomena and singularities within the data set. Thus the potential of wavelet analysis as an effective tool for identifying the

frequency and duration of pollution events, isolating turbulent processes from other processes operating in the nocturnal boundary layer (such as gravity waves) and the calculation of energy and co-spectra is investigated.

In order to address the research gaps outlined in Chapters 2 and 3, the study focuses on the processes operating in the Lower Fraser Valley (LFV), an urbanised region of complex terrain located on the south-west coast of British Columbia.

The objectives of this thesis are to:

1. Quantitatively describe the frequency and magnitude of nocturnal spikes in ozone concentration as observed at the site
2. Identify spatial and temporal patterns in nocturnal spikes in ozone concentration throughout the Lower Fraser valley
3. Describe the temporal variations in the vertical distribution ozone concentrations in the very stable nocturnal boundary layer
4. Determine the meteorological structure and evolution of the characteristics of the very stable nocturnal boundary layer
5. Describe the characteristics of mesoscale thermo-topographical wind systems and ascertain their importance in determining the horizontal advection of ozone over the site
6. Identify the characteristics of the nocturnal boundary layer during periods of increased ozone concentration at the surface
7. Demonstrate the potential of a comparatively new analytical tool - wavelet analysis - to provide an insight into the characteristics of turbulence in the very stable nocturnal boundary layer
8. Develop techniques to objectively isolate and quantitatively analyse the characteristics of turbulence in the surface layers of the very stable NBL using wavelet analysis
9. Examine the role different processes (such as the nocturnal low-level jet, development of down-valley wind regimes and presence of gravity waves) in generating near surface turbulence
10. Calculate turbulent fluxes using wavelet-based methodologies

11. Develop a new wavelet based, conditional sampling technique to extract intermittent turbulent 'fluxes' from 30 minute time series

12. Compare the relative importance of vertical mixing and advection mechanisms in the determination of near surface pollution concentrations at the chosen site.

This information will aid the overall assessment of the characteristics and significance of these intermittent turbulent bursts to local surface air quality at the field site. It is hoped that the results of this study will provide a basis for understanding the importance of nocturnal vertical mixing processes in these types of environments. Such an enhanced understanding of the processes operating in three dimensions throughout the diurnal evolution of the boundary layer is necessary for the development of rational mesoscale and regional air quality models and coherent pollutant abatement strategies (Wotawa & Kromp-Kolb 2000). This has implications for air quality management in regions of complex coastal terrain world-wide.

Chapter 2: The very stable nocturnal boundary layer

2.1 Introduction

Several mechanisms have been proposed to explain observed diurnal variations in surface pollutant concentrations. In most environments, hourly changes in concentration are too great to be explained simply by variations in local emissions or chemical reactions (Kleinman et al. 1994; Hastie et al. 1993; Wotawa et al. 2000; Lehning et al. 1996). Pollutant transport and dispersion is determined both by changes in the turbulent structure of the boundary layer and trends in pollutant advection. The temporal and spatial characteristics of the processes determining three dimensional pollutant dispersion in regions of complex coastal terrain have yet to be fully understood. Thus the specific characteristics of the diurnal pollutant cycles in these regions cannot be easily translated into our current (largely horizontal, 2-dimensional) understanding of pollutant sources and sinks. A representative sample of the relevant literature is reviewed to demonstrate the characteristics and diurnal evolution of the boundary layer and mesoscale airflow patterns and their relevance to developing an understanding of pollutant cycles (Douglas & Kessler 1991; Moore et al. 1991b; Moore et al. 1991a; Nester 1995).

Emphasis here is placed on conditions which promote the incidence of high concentrations of a single photochemical pollutant, ozone. The primary reasons for the choice of ozone are:

a) the extensive existing knowledge base concerning both its fundamental chemistry and emission of precursors
b) the recognition of its deleterious effect on human health and the environment
c) the abundance of this pollutant within the study area
d) the availability of monitoring equipment to study its distribution in 3-dimensions

2.2 Pollutant distribution in the boundary layer

The concentration of a pollutant (c) at a given location in time or space can be expressed mathematically using a conservation of mass equation (Equation 2.1). This treats the section of the boundary layer of interest as a permeable box. The concentration of any pollutant can then be determined by analysis of the horizontal and vertical flows at the boundaries of the delimited area. Clearly no such concrete boundaries exist in the atmosphere and the usefulness of this

approach is affected by the limits chosen. However the equation does present a useful starting point for discussion and can be used to investigate the relative importance of in-situ emissions, advection and vertical fluxes in determining the concentration of pollutants (Freytag 1987; Lehning et al. 1998).

For any atmospheric constituent, assuming horizontal homogeneity for the mean and turbulent flux terms and negligible mean vertical velocity, the budget can be represented by:

$$\frac{\partial \overline{c}}{\partial t} + \overline{u}_j \frac{\partial \overline{c}}{\partial x_j} = \upsilon_c \frac{\partial^2 \overline{c}}{\partial x_j^2} + S_c + \frac{\partial \left(\overline{u_j' c'}\right)}{\partial x_j} \qquad (2.1)$$

Term I	Term II	Term III	Term IV	Term V
Storage	Advection	Molecular diffusion	Sources / sinks	Flux divergence

where:

υ_c	molecular viscosity
c	scalar quantity
S_c	sources and sinks of scalar c
U_j	u, v, w directions for j = 1,2,3
X_j	x, y, z directions for j = 1,2,3
t	time

Term IV describes the importance of sources and sinks of ozone. The chemical behaviour of ozone in the boundary layer has been well documented (Hastie et al. 1996). Ozone is a secondary pollutant formed downwind of urban areas as a result of the photo-dissociation of nitrogen dioxide in the atmosphere (Equation 2.2). A number of conditions must be met for the formation of ozone, including the availability of solar radiation (*hv*) and the presence of organic catalysts (M) (Equation 2.3) (Pisano et al. 1997). Thus ozone production is negligible at night.

$$NO_2 + hv \longrightarrow NO + O\cdot \qquad (2.2)$$

$$O\cdot + O_2 + M \longrightarrow O_3 + M\cdot \qquad (2.3)$$

Ozone is a highly volatile substance which reacts rapidly with nitrogen monoxide (hereafter NO, Equation 2.4), thus it is typically destroyed at the surface in urban areas where

exhaust fumes provide an abundant supply of NO. This reaction forms nitrogen dioxide (hereafter NO_2), setting up a complex chain of reactions between the three substances.

$$NO + O_3 \longrightarrow NO_2 + O_2 \qquad (2.4)$$

The balance between the concentrations of ozone, NO and NO_2 is determined both by anthropogenic emissions of photochemical precursors and environmental conditions. In urban areas ozone concentrations are likely to be comparatively low as a result of this reaction. Thus although ozone typically has a life time in the atmosphere of the order of a few days, it may be difficult to trace its dispersion pathways particularly in an urban context. Measurements of NO and NO_2 are therefore essential to establish the photochemical status of the air at the surface (Hayden et al. 1997).

Ozone is primarily removed from the atmosphere as a result of surface deposition (Pisano et al. 1997). Deposition velocities are however highly dependent on the type of surface (Millan et al. 2000; Van Dop et al. 1977). Since ozone is virtually insoluble in water deposition is a particularly important removal mechanism in rural areas (where NO emissions are low) away from water bodies (Galmarini et al. 1997). Unfortunately little is known about deposition rates at night due to difficulties of measurement (Seinfeld & Pandis 1997). Night-time fluxes have also been traditionally ignored, especially in reference to plant responses due to both lower ozone concentrations and plant conductance rates during the night (Musselman & Massman 1999).

In Equation 2.1 Term I represents the storage or residual concentration of the pollutant in the atmosphere during the previous time period. In the context of the diurnal ozone cycle the magnitude of this term will vary with time. Term II presents advection to the site of interest. In urbanised regions of complex coastal terrain horizontal homogeneity cannot be assumed. Given the proximity of urban areas within the airshed the chemical reactions between ozone, NO and NO_2 are unlikely to have formed an equilibrium. Thus concentrations of ozone are likely to vary in space and advection will be important in determining the balance of the equation. Due to the temporal and spatial scales chosen, Term III (molecular diffusion) is likely to be negligible within the context of this study.

Term V, the flux divergence term, describes how the flux changes in space. Although both advection and flux divergence can occur in horizontal and vertical planes, advection typically dominates in the horizontal plane and flux divergence in the vertical. The balance

between each of these terms in the pollutant budget varies in time and space due to diurnal meteorological and anthropogenic controls on emissions, chemical reactions and dispersion.

2.3 Diurnal structure of the boundary layer

Most photochemical pollutants are emitted or formed within the boundary layer. Thus the mean and turbulent characteristics of the boundary layer determine the transportation, dispersion and storage of pollutants (Roussel et al. 1996; Kurzeja et al. 1991). The boundary layer is that part of the atmosphere that responds directly to the flows of mass, energy and momentum from the earth's surface, characteristically at timescales of an hour or less (Stull 1988).

The diurnal evolution of the boundary layer plays an important role in determining pollutant dispersion pathways and chemical properties of atmospheric pollutants (Zaveri et al. 1995). The diurnal structure of the boundary layer can be represented using a conceptual model. Three dominant components of the boundary layer can be identified; the convective mixed layer, the residual layer and the stable boundary layer. These are illustrated in Figure 2.1. A surface layer, which consists of the lowest 10% of the boundary layer may also be identified in both the mixed layer and the stable boundary layer (Stull, 1988).

This conceptual model represents a simplification of the boundary layer that is best developed over homogeneous land surfaces and under anticyclonic conditions (i.e. when there is low synoptic scale forcing). In regions of complex coastal terrain the evolution of the boundary layer is determined by the interaction between synoptic scale meteorology, mesoscale thermo-topographical circulatory systems and local surface characteristics. The relative importance of these factors varies in time and space. High concentrations of photochemical pollutants are predominantly associated with anti-cyclonic conditions, thus synoptic scale influences are not discussed here.

2.4 Convective mixed layer

The convective mixed layer develops soon after dawn as a result of thermal convection. Driven by solar heating of the earth's surface, convective turbulence entrains the less turbulent air from above and ensures vertical mixing within the boundary layer. During the early hours of the morning convective mixing processes entrain pollutants stored aloft from previous day(s)

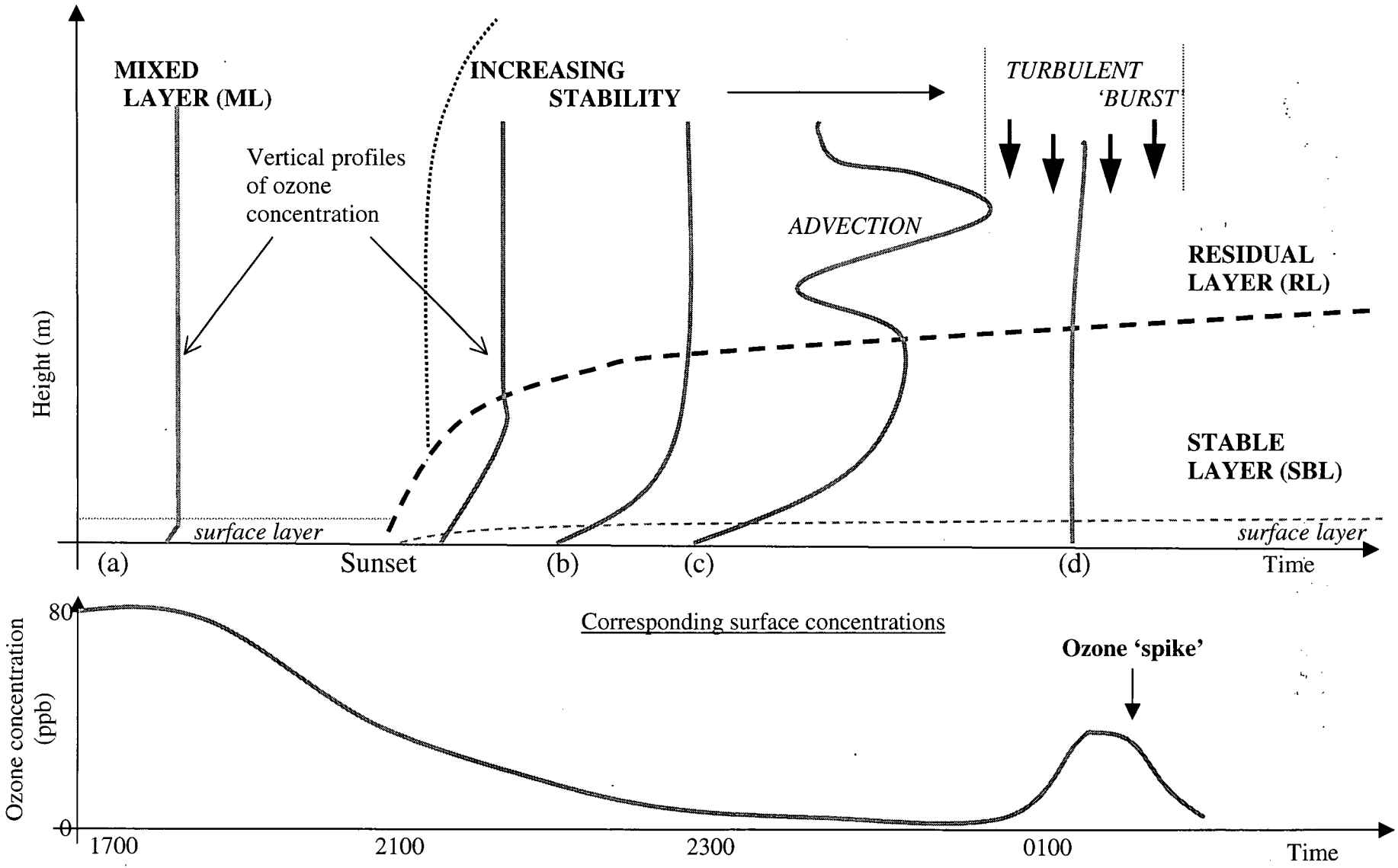

Figure 2.1 A conceptual model to describe the evolution of the nocturnal boundary layer (NBL), surface concentrations of ozone and vertical distribution of ozone

emissions (Beyrich et al., 1996). This fumigation of pollutants has a profound effect on air quality and may account for more than 50% of the daily maximum ozone concentration (Neu et al., 1994). As the levels of solar radiation increase, photochemical production of ozone may occur in both the residual and surface layers. Pollutant concentrations may be further enhanced by emissions directly into the mixed layer and advection throughout the boundary layer associated with the development of mesoscale flows. The complexity of these processes makes it difficult to determine how much of the increase in concentrations at any given point in time is directly attributable to vertical mixing processes alone. However, given well-mixed conditions surface measurements are likely to be representative of pollutant concentrations throughout the boundary layer.

Although concentrations of pollutants in the mixed layer show relative homogeneity in the vertical plane (profile a, Figure 2.1), concentrations in the horizontal plane may show considerable heterogeneity, particularly in regions of complex terrain. Thermo-topographical circulations are essentially driven by a thermal overturning of the atmosphere in the vertical (Atkinson 1981) generated by different thermal properties of the earth's surface which results in a diurnal reversal in wind direction. The resulting mesoscale circulatory systems such as sea breezes and mountain flows determine trajectories of air parcels and play a significant role in controlling pollutant transportation within an airshed (Lu & Turco 1995; Martin et al. 1991).

Observational, tracer and modelling experiments in a variety of environments have documented the importance of the transport of urban pollutants embedded in these flows in determining local air quality (Kelly et al. 1984; Altshuller 1986; Svensson 1996; Xu et al. 1996; Broder & Gygax 1985). These studies demonstrate that concentrations of ozone typically peak downwind of urban areas due to the daytime advection of both ozone and its precursors (Steyn et al. 1997). Photochemical production of ozone usually peaks with solar radiation in the early afternoon (Millan et al. 2000). In the Lower Fraser Valley Bottenheim et al. (1997) demonstrate that the rate of ozone formation (due to chemical reactions between precursors) in the urban plume may be as high as 8 ppb h^{-1}. Ozone concentrations in the plume can also decrease as they are advected downwind of urban areas if, for example, local sources of NO are mixed into the plume (Berkowitz et al. 2000). The timing of the observed surface maximum in ozone concentration depends on the balance between local concentrations of ozone, volatile organic compounds, NO_2 and NO, the rate of ozone formation, advection and depositional processes. In coastal locations, the timing of the penetration of the sea or lake breeze front can also be crucial

to determining the timing of maximum concentrations (Hastie et al. 1999; Buckley & Kurzeija 1997).

Thermo-topographical wind systems can interact with the diurnal characteristics of the boundary layer to generate complex three dimensional patterns in pollutant concentration (Martin et al., 1991). The existence of discrete elevated layers of pollutants has been well documented in regions of complex coastal terrain (Berkowitz et al. 2000; McKendry et al. 1997; Nester 1995; Lalas et al. 1987; McElroy & Smith 1986; Clark & Ching 1983; Wakamatsu et al. 1983). Formation of these layers is thought to be related to the interaction of slope flows, sea breezes and convective activity within the atmosphere (McKendry et al., 1997). As a result of vertical mixing processes these layers have the potential to affect surface pollution concentrations when the mixed layer depth grows to the height at which they are found (Millan et al. 2000; Hayden et al. 1997; Moore et al. 1991b). Thus in regions of complex terrain, vertical mixing processes are important in determining air quality even in the mixed layer (McKendry et al. 1997; McElroy & Smith 1993; McElroy & Smith 1986).

A gradual reduction in pollutant concentrations in the boundary layer during the afternoon is sometimes reported in the literature (Banta et al. 1997). This decrease is observed for a range of pollutants including ozone, suggesting it can be partially accounted for by the increased depth of the boundary layer (hence greater mixing volume). However, ozone concentrations in the mixed layer are also likely to decrease later in the day due to decreased rates of chemical formation as solar radiation levels drop.

2.5 Nocturnal boundary layer

2.5.1 Climatology and classification of nocturnal boundary layers

In order to facilitate data analysis, modelling and the comparison of experimental results between different sites, the NBL is typically classified into two types or regimes - the weakly stable nocturnal boundary layer and the very stable nocturnal boundary layer (Mahrt et al. 1998) (Table 2.1). Although many authors have suggested refinements and sub-categories to this classification system (Beyrich 1994; Kurzeja et al. 1991; Mahrt 1985), these have yet to be widely accepted within the literature and the dual scheme remains a useful basis for analysis.

The two categories are based on the turbulent characteristics of the stable boundary layer (SBL). The very stable regime develops primarily under anti-cyclonic conditions, associated

with light and variable winds and only intermittent turbulence in the stable surface layers. By comparison the weakly stable NBL develops under a more disturbed regime resulting in a continuously (if weakly) turbulent stable layer at the surface. Although the definitions of 'very stable' and 'weakly stable' lack consistency between studies, Mahrt et al. (1998) identify prototype definitions of the stability regimes which aid classification of any given set of observed conditions.

Table 2.1 Characteristics of different stability regimes in the nocturnal boundary layer (Mahrt et. al. 1998)

Characteristics	**Weakly stable / continuously turbulent**	**Very stable / intermittently turbulent regime**
Wind	Light to moderate, strong shear	Light and variable
Cloud cover	Clouds frequently present	Clear skies
Radiative cooling	Weak	Strong, particularly close to the surface
Turbulence	Continuous in time and with height throughout the stable layer. Consistently stronger and well established	Weak, spatial and temporal intermittent and can be isolated in layers above the surface. May be strongest at the top of the inversion layer
Structure of NBL	Text book NBL. Well marked transition between stable layer and residual layer	Poorly defined structure. Difficult to identify top of the stable boundary layer
Similarity theory	Applied with confidence	Inappropriate for the very stable case. Routinely fails.

High concentrations of photochemicals are primarily associated with anti-cyclonic conditions. In regions of complex terrain these conditions typically promote the development of the very stable boundary layer (Gusten et al. 1998). Thus the very stable boundary layer will form the basis of the following discussion.

2.5.2 Structure and formation

Stable stratification of the boundary layer develops shortly before sunset when the surface becomes cooler than the atmosphere immediately above it. The structure of the NBL is primarily determined by complex interactions between processes governing the static stability of the atmosphere and mechanical generation of turbulence (Stull 1988). In regions of complex terrain these processes include radiation, turbulence, advection, subsidence, terrain-induced flows, and wind shear throughout the NBL.

These processes can operate at a multitude of different heights and scales within the atmosphere, and it may be very difficult to identify a dominant control or process. The continued interaction between these processes further ensures that the NBL is continually evolving in time and space, hence equilibrium or steady-state conditions are rare. This makes it very difficult to observe and predict the transport pathways and diffusion of pollutants in the nocturnal boundary layer, particularly in regions of complex terrain (Bowen et al. 2000; Beyrich 1994).

Observations and model simulations point towards a layered structure of the nocturnal surface inversion (Beyrich & Weill 1993). Thermal stratification results from the radiative cooling of the surface that stabilises the layers of air that come into contact with it. The region of greatest static stability is found closest to the earth's surface and typically decreases with height. Once the rate of cooling is strong enough a temperature inversion may form near the surface. This region is the stable boundary layer (SBL) component of the NBL. During very stable conditions, the absence of a dominant forcing mechanism to generate turbulence results in a very shallow SBL (Coulter 1990).

The development of a very stable layer close to the surface allows the upper portions of the boundary layer to become de-coupled from surface layer forcings and a residual layer (RL) remains aloft (Pisano et al. 1997). This layer has similar characteristics to the mixed layer of the day before. This layer has reduced thermal stratification, and cooling predominantly results from clear air radiative flux divergence. This may be important to the structure of the boundary layer towards the end of the night as it may determine whether or not a stable layer exists above the wind shear zone at the top of the SBL (Beyrich & Weill 1993). Under anti-cyclonic conditions divergence near the surface and subsidence aloft can result in warm air being transported towards the surface from aloft affecting the structure of the NBL.

The SBL is essentially decoupled from the RL, thus pollutants such as NO which are emitted at or near the surface remain trapped within the SBL, resulting in elevated pollutant concentrations over time (Mahrt 1985). Alternatively, concentrations of other pollutants that are not emitted or formed directly within the SBL may remain constant or decrease over time. Due to the rapid reaction of ozone with surface based pollutants and effective deposition of ozone at the surface, concentrations decrease rapidly through the stable layer as shown in profiles b and c (Figure 2.1). By comparison, in the absence of advection or the release of NO directly into the residual layer, concentrations of ozone in the residual layer remain more constant and closely resemble those of the mixed layer of the previous day (profile c, Figure 2.1).

2.5.3 Depth of the stable boundary layer

Many questions remain regarding the basic structure of the very stable NBL. This is due in part to the temporal and spatial variability of the NBL and the significance of advection and limited measurements of fluxes throughout the NBL (Mahrt et al. 1979). Clearly, the depth of the SBL plays a significant role in determining the vertical distribution of atmospheric pollutants in the NBL. However, the top of the SBL is much more difficult to determine than for the convective boundary layer (or even the weakly stable NBL), and to date no single definition has been accepted (Beyrich 1994; Beyrich & Weill 1993; Mahrt et al. 1979). Several different thermal, dynamical and turbulent height scales have been proposed to identify the top of the SBL within the NBL. These include (Beyrich & Weill 1993; Stull 1988):

Momentum scales:

1) The height where wind speed reaches geostrophic speed
2) The height where winds become parallel to geostrophic flows
3) The height of the low-level wind speed maxima (or jet)

Thermal height scales:

1) The height of the surface inversion
2) The first discontinuity in the temperature profile
3) The height to which nocturnal cooling extends

Turbulent height scales:

1) The height where some turbulence parameter (stress, heat flux, TKE) has been reduced to a percentage (e.g. 10%,5%,2%,1%) of the surface layer value

2) The height where the Ri number reaches its critical value

These height scales, especially those between categories, are not well correlated with each other and may show different behaviour through the night (Beyrich & Weill 1993; Kurzeja et al. 1991). This is true even for observational studies, where depths are typically inferred from profiles of averaged quantities (Mahrt et al. 1979). This may be a result of processes such as clear air radiative cooling or advection operating in the residual layer, generating stable stratification aloft. Thus the depth of the SBL calculated from the surface inversion may occur 25% above the maximum wind speed zone due to radiational cooling (Mahrt et al. 1979). There is also little consistency between studies regarding fundamental issues such as whether the top, middle or bottom of the low-level jet constitutes the top of the SBL. Variations among artificial smoothing routines used to generated averaging profiles may also explain some of the differences in SBL height observed between categories (Mahrt et al. 1979).

Given the often distinct differences in pollutant profiles observed between the residual and surface layers, Beyrich et al. (1996b) suggest that these may be used to aid the identification of the top of the SBL. Unfortunately, whilst this has potential utility for the weakly stable NBL case, the strong static stability and layering of the NBL supports the existence of discrete layers of reactive pollutants which may be transported considerable distances within the NBL. This adversely affects the potential of a single pollutant to act as an atmospheric tracer. Given the difficulties associated with the thermal and dynamical diagnostic methods, Mahrt (1985) and Kurzeja et al. (1991) promote the use of turbulence measurements. However, definitions of the SBL depth which require the fluxes to reach zero are difficult to apply: fluxes may approach zero without actually reaching it, leaving room for subjective interpretation of the data. Further, the instruments used to determine vertical turbulence profiles, especially at night, are subject to the similar resolution limits (Chapter 3).

Studies trying to identify consistent trends in SBL evolution with time are fraught with difficulties. The temporal, spatial and vertical resolution of measurements are limited and assumptions of stationarity used to gain complete description of the NBL cannot be accurately

applied. Depths vary in time and space (particularly in regions of complex terrain) due to the continual evolution of boundary layer processes (such as the low-level jet), mesoscale flows and interaction from gravity waves (Kalthoff et al. 2000). Thus the design of an experiment and choice of parameters frequently depends on the site and scope of the study and instrument data available.

2.5.4 Advection and mesoscale flows

The wind structure of the NBL can be very complex and may continually evolve through the night (Stull 1988). Winds are typically light and variable (Mahrt et al. 1998). In the lower two - ten metres of the boundary layer winds are primarily determined by local topography, buoyancy, friction, and entrainment processes. In the upper layers synoptic and mesoscale forcings such as advection or subsidence are important. A wind speed maximum is usually present at the top of the SBL, which may develop into a nocturnal low-level jet (LLJ). Above the SBL wind speed and direction become gradually geostrophic. Discrete layers are common within the NBL, and they may display considerable 'azimuthal meandering' or horizontal motion (Kurzeja et al. 1991). Localised circulations may develop which are only reconnected with the onset of turbulence in the morning (Bader et al. 1987).

The contribution of advection processes in the very stable NBL is typically under-estimated. Surface measurements provide the false impression that transport in light winds is negligible (Banta et al. 1998). However, even in regions of homogeneous terrain, advection can play an important role in determining the characteristics of the very stable boundary layer and make a significant contribution to the heat and pollutant budgets (Howell & Sun 1999). During 'smog episodes' the nocturnal transport of pollutants by advection above the SBL may be considerably greater than previously expected and perhaps more important to determining pollutant dispersion within an airshed than the equivalent daytime flows (Banta et al. 1998).

Advection of pollutants into areas downwind of emissions sources by land breezes at night (often strengthened by katabatic drainage) and the existence of elevated pollutant layers is undisputed (Banta et al. 1998). This has been well documented in a number of coastal locations including Athens, Greece (Lalas et al. 1987; Nester 1995), Tokyo, Japan (Wakamatsu, 1983) and Los Angeles, USA (McElroy & Smith, 1993; Moore et al., 1991). The meandering and layered characteristics of mesoscale flows within the NBL result in a variety of different trajectories. Thus advection may result in the transport of either higher or lower pollutant concentrations than

the local daytime maximum depending on the origin and pathway of dispersion (Prevot et al. 2000), as portrayed in profile d, Figure 2.1.

Katabatic and downslope winds also have the potential to influence air quality near the surface within valley systems. Although the meteorological structure of these flows has been well studied, few experiments have considered the three-dimensional pollutant composition of these wind systems. During the daytime, pollutants entrained within upslope flows can be transported deep into tributary valleys and vented into the atmosphere at mountain tops (McKendry et al. 1990a; McKendry et al. 1990b; McKendry et al. 1997). Reversal of these diurnal wind patterns then results in the transport of this ozone rich air back towards the source area during the night (Loffler-Mang et al. 1997). However, the pathway of the flows is important in determining the concentration of ozone re-entering the main valley system. Depositional processes may act to cleanse air parcels as the air comes into contact with vegetation on valley side walls (Broder & Gygax 1985). This was observed in the Lower Fraser Valley by Banta et al. (1997). Their study demonstrated that the lowest 500 metres of the NBL were low in ozone whilst pulses of air containing high concentrations of pollutants existed aloft.

Transport of pollutants trapped within thermo-topographical circulatory systems and back into source areas (due to return wind flow patterns) may result in an escalation of pollutant concentrations over a period of several days (Kalthoff et al. 2000). The success of observational studies which aim to investigate this hypothesis has been hampered by the limited spatial and temporal resolution of data collection, and a tendency to focus on individual parts of the problem. Thus little is known about the three dimensional distribution of pollutants within these return wind flow patterns (McElroy & Smith 1986; Helmis et al. 1997).

In regions of complex coastal terrain, local/mesoscale wind systems are not only expected to affect the horizontal but also the vertical distribution of pollutants in the NBL. For example, shear stresses resulting from localised and often layered thermo-topographical flows generate increased turbulence and hence vertical mixing through the boundary layer (Haeger-Eugensson 1999). Turbulence can also result from differences in the thermal properties of advected layers. For example, cold air drainage is a common phenomenon in regions of complex terrain which may result in ponding and surging of cold air over warmer air from the valley. This may result in localised turbulence. Transport processes in the very stable NBL clearly play a key role in determining surface concentrations both during the night and following fumigation the next day.

2.5.5 Characteristics of turbulence in the very stable nocturnal boundary layer

Examining the turbulence characteristics of the NBL is complicated by a 'multiplicity of physical influences including clear air radiative flux divergence, elevated shear associated with low level jets, meandering motions, gravity waves, slope flows and increased sensitivity to surface heterogeneity' (Mahrt et al. 1998). Not surprisingly, previous studies have largely been restricted to homogeneous sites under ideal conditions (McMillen 1988; Kurzeja et al. 1991). Thus 'observational studies of the nocturnal boundary layer are rather incomplete' (Mahrt et al. 1979, 247).

Laboratory, numerical and field experiments have demonstrated that turbulence and vertical mixing can persist even in the very stable boundary layer (Howell & Sun 1999). Its characteristics and structure are determined by the relationship between the dynamic dampening by the thermal structure of the boundary layer and the mechanism generating turbulence (Bange & Roth 1999). However the complexity of the processes operating within the nocturnal boundary layer and the decoupling of mechanisms from surface based forcings makes it very difficult to both describe and model the NBL (Stull 1988). Although well studied, the characteristics of turbulence in the very stable NBL are poorly understood (Mahrt 1985; Koracin & Berkowicz 1988).

Turbulent parameters, though of perhaps the most direct relevance to air quality studies, are difficult to evaluate for the NBL (Koracin & Berkowicz 1988). Turbulence is typically weak, sporadic in time and patchy in space (Nappo & Johansson 1999), often existing in isolated layers or pockets (Bange & Roth 1999). Thus it is very difficult to obtain representative measurements at the surface and measurements are often made at or near instrumental limits.

Mechanical processes primarily generate turbulence in the NBL. These are typically associated with wind shear resulting from the nocturnal LLJ, the development of the geostrophic wind profile with height, skin friction and obstacles near the ground, and atmospheric motions (such as down-slope flows) generated by complex coastal terrain (Mahrt 1985). Wind shear usually results in turbulent mixing primarily in the horizontal plane. However, if the turbulent stresses are sufficient to overcome static stability, vertical mixing throughout a layer or layers may occur. Turbulence within the NBL at any height is governed primarily by localised shear instabilities and is only indirectly related to the surface fluxes (Stull 1988; Mahrt 1985; Finnigan 1999).

Although thermal turbulence is suppressed by stability, the presence of fog and stratocumulus can generate radiatively driven turbulence processes (Stull 1988). Wave activity is a common source of turbulence during stable conditions, particularly in regions of complex terrain (Coulter 1990). Breaking gravity waves may generate turbulence, whilst buoyant oscillations may act to enhance or suppress existing turbulence and can result in the transport of turbulent layers to different heights within the NBL (Stull 1988).

2.5.6 Role of the nocturnal low-level jet

Conditions in the stable nocturnal boundary layer frequently give rise to the development of a nocturnal LLJ (Thorpe & Guymer 1977; Frisch et al. 1992). The occurrence and characteristics of the LLJ can have a profound impact on the structure of the nocturnal boundary layer and the dispersion of pollutants in the very stable NBL. The nocturnal LLJ is a thin layer of fast moving air, usually located 100 - 300 m above the earth surface (Stull 1988). This results in a 'jet-like' shape in the wind profile, with marked shear in the layers above and below the often super-geostrophic wind maximum (Beyrich 1994). The maximum wind speed usually occurs four to seven hours after sunset in the northern hemisphere mid-latitudes, and a steady clockwise turning of the wind vector can be observed (Beyrich 1994). These jets usually have wind speeds of 10 to 20 m s^{-1} and may be several hundreds of kilometres wide and thousands of kilometres in length (Stull 1988). Thus pollutants embedded in the LLJ may be transported considerable distances from their source area (Hanna & Chang 1992).

As with many other characteristics of the NBL, different authors have used different criteria to identify the LLJ in the BL (Beyrich 1994). Stull (1988) suggests that some authors require wind speeds to be greater than 12/16/20 m s^{-1} or super-geostrophic, and occur either below 1000, 1500 or 2500 m in height. His pragmatic definition defines a LLJ when there is a relative wind speed maximum of at least 2 m s^{-1} greater than the wind speeds above it, which occurs in the lowest 1500 m of the BL. This definition will be used for the purpose of this thesis. Although the direction of the low-level jet is not included in any definitions it can be important in both identifying the key characteristics and origins of the LLJ (Whiteman et al. 1997).

The nocturnal LLJ results primarily from inertial processes and baroclinic pressure gradients (Frisch et al. 1992). De-coupling of the surface layers enables the acceleration of winds at higher levels. Due to the influence of the Coriolis force, inertial oscillations can result in the wind speeds becoming super-geostrophic (Beyrich 1994). Baroclinic pressure gradients

result from horizontal temperature gradients. These can be generated by differences in surface characteristics such as sloping terrain and result in changes in the geostrophic wind with height (Holton 1992).

The presence of the LLJ 'strongly influences the turbulent characteristics of the boundary layer' (Smedman et al. 1995). Unlike other atmospheric jets, which may form a localised turbulent maximum, the LLJ is associated with a decreased zone of turbulence (Mahrt et al. 1979). However, the shear associated with the LLJ can, over time, generate localised break-downs in stability (Haeger-Eugensson 1999). This may become sufficient to result in the break up of the jet, creating a burst of turbulence that temporarily couples the RL to the SBL. However, continued cooling of surface layers provides a hostile environment to the maintenance of turbulence. Since the source of turbulence has been removed (with the break up of the jet) stability in the NBL may be restored. This enables de-coupling of the layers and the former wind profile to re-establish which in turn promotes the re-development of the LLJ in a cyclical manner (Finnigan 1999; Derbyshire 1999). Turbulence associated with the LLJ is therefore intermittent, as the jet develops in dynamic equilibrium with forcing processes.

The role of the nocturnal jet in the generation of turbulence in the very stable NBL is contested. Whilst some authors observe an increase in turbulence associated with the LLJ (Corsmeier et al. 1997), others suggest that the presence of the LLJ acts to suppress turbulence generation in the SBL (Smedman et al. 1995). This has been attributed to the 'blocking' affect of the very stable layers (which support the development of the jet) that inhibit the passage of instabilities generated in the residual layer to the surface. Both Smedman et al. (1995) and Neu (1995) argue that the presence of the stable layers block the passage of gravity waves and hence turbulence associated with their breakdown. Since a number of processes in the very stable layer (and indeed the nocturnal LLJ itself) can generate gravity waves, the role of the jet in acting to enhance or suppress turbulence at the surface may be site specific.

Conditions in the very stable NBL do not always support the development of a LLJ. For example Beyrich (1994) notes that a low pressure gradient, local advection, and partial/temporal cloud cover may inhibit the development of the jet. Further mesoscale terrain induced flows may act to counteract or enhance the development of the jet. Continuous observation of the nocturnal jet is difficult to achieve without the use of a continuous remote sensor such as a sodar (Whiteman et al. 1997). However, even with this equipment, interpretation and analysis of the images is not without controversy, and the vertical resolution may render it difficult to ascertain

the precise characteristics of the jet. Thus determining spatial and temporal patterns in nocturnal LLJ characteristics (such as strength, height and pollutant concentration) remains a challenge to researchers.

2.5.7 Gravity wave - turbulence interactions

Weakly turbulent, statically stable environments are ideal for the formation and propagation of buoyancy waves (Stull 1988; Coulter 1990). Gravity waves can be generated by a number of different forcings including uneven terrain, thermo-topographical circulations, thunderstorms and frontal systems (Garratt 1982). To propagate, the waves must have frequencies of less than the Brunt-Vaisala frequency at any given height:

$$N_{bv}^2 = \frac{g\partial\theta_v}{\theta_v \partial z}$$ (Weber & Kurzeja 1991)

where:

N_{bv} Brunt-Vaisala frequency

θ_v Potential temperature

Scalar quantities may be transported vertically by the buoyant oscillations generated by gravity waves which may also affect the observed structure of the NBL (Rogers et al. 1995a; Rogers et al. 1995b). However, turbulence only results from breaking or trapped gravity waves. In regions of complex terrain waves are commonly formed as a result of topographic forcing. In this environment, wave activity associated with turbulence may be stronger than that generated by katabatic flows (Finnigan 1999).

Gravity waves and turbulence coexist in the very stable NBL (Mahrt 1985; Smedman et al. 1995). Wave-turbulence interaction can result in coupling of the planetary boundary layer with flows above it destroying the temperature structure and wind shear including the LLJ (Coulter 1990; Finnigan 1999). This interaction, although fundamental to our understanding of the very stable nocturnal boundary layer, is poorly developed (Chimonas 1999; Lee et al. 1997). Turbulence generated by breaking gravity waves may only be a factor of two smaller than turbulent scales, and breaking gravity waves result in sharp boundaries within data generating "red noise" at a variety of frequency responses within the signal. This makes it difficult to identify a spectral gap and thus it is very hard to isolate their characteristics using traditional analytical tools such as Fourier analysis.

2.6 Pollutant spikes in the nocturnal boundary layer

Penetration of active shear instabilities (resulting from mesoscale thermo-topographical wind systems, the nocturnal LLJ or breaking internal gravity waves for example) into the stable boundary layer can result in intermittent vertical mixing of scalar quantities (Beyrich 1994; Howell & Sun 1999). Despite the weak, sporadic and patchy characteristics of turbulent activity, vertical mixing can occur throughout the stable NBL. This intermittency enables the very stable NBL to act as 'a single entity, rather than a group of completely decoupled layers' (Stull 1988). Thus transport may occur between the stable and residual layers and pollutants that may otherwise be stored aloft are transported to the surface (profile d, Figure 2.1)

Temporal increases in concentration have been observed in the SBL for a range of pollutants, including ozone (Seibert et al. 2000; Reitebuch et al. 2000), volatile organic compounds (Prevot et al. 2000), isoprene (Starn et al. 1998), hydrogen peroxide (Das & Aneja 1994), carbon monoxide (CO) (Moxley & Cape 1997), nitrogen monoxide and particulate matter smaller than ten microns in diameter (PM_{10}) (McKendry 2000). Detailed study of the timing of these pollutant spikes reveals that pollutants such as CO, NO and PM_{10} are out of phase with pollutants such as ozone. This suggests different process-based explanations (McKendry 2000). Pollutants emitted primarily into the surface layer (CO, NO and PM_{10}) build up in the SBL until a burst of turbulence enables mixing through a deeper layer (Reitebuch et al. 2000). When this occurs the surface pollutants are diluted, whilst other pollutants from the residual layer such as ozone or isoprene are mixed to the surface (Starn et al. 1998).

Significant increases in ozone concentrations have been observed at night near the surface in a range of different environments (Coulter 1990; Corsmeier et al. 1997; Kalthoff et al. 2000; Neu 1995; Beyrich et al. 1996a). Increases tend to be well defined, followed by a substantial decrease in concentration and appear as a 'spike' in the data set. The phenomenon appears to be temporally and spatially highly variable (Loffler-Mang et al. 1997) and may easily be missed within data sets as a result of weekly or monthly averaging of hourly data. Despite increased study of this phenomenon a set of criteria to identify these downward bursts of pollutants has not been identified, nor has a descriptive label been attached.

Early studies by Kroening & Ney (1962) suggested that these spikes result from the mixing of ozone to the surface from the stratosphere (Steinberger & Ganor 1980). Whilst this mechanism may explain increases in ozone concentration during the passage of fronts (Beyrich

et al. 1996a), this is unlikely to explain increased ozone concentrations in the very stable boundary layer. Increases in ozone concentrations in mountain regions have also been reported where the site is located at an elevation close to the height of the RL layer (Gusten et al. 1997; Millan et al. 2000; Beyrich et al. 1996a). However, this cannot account for increases observed within valleys.

One of the first studies to attribute increased ozone concentrations in the stable layer to turbulence associated with the nocturnal LLJ was conducted by Samson (1978). More recent studies by Corsmeier et al. (1997), Beyrich et al. (1996) and Reitebuch et al. (2000) confirm the importance of the LLJ in generating sufficient turbulence to mix ozone from the residual layer to the surface. Interestingly, no comment is made in their work about the role or importance of gravity waves. By comparison Coulter (1990) shows that increases in ozone concentration, which correspond well to periods of turbulent activity lasting approximately 30 min, are preceded by wave activity.

Turbulence alone cannot account for increased surface concentrations of pollutants. Berkowitz et al. (2000) note that relatively large increases in surface ozone levels are preceded by the horizontal transport of aged plumes rich in ozone aloft. Understanding the interaction between advection and pollutant storage in the residual layer with turbulent mixing processes is therefore critical to identifying the importance of these processes on diurnal pollutant cycles.

2.7 Summary

The diurnal structure and evolution of the boundary layer plays an important role in determining the distribution of pollutants in time and space. Results of this survey demonstrate the importance of processes operating in the NBL to a comprehensive understanding of diurnal pollutant budgets, particularly in regions of complex terrain. Pollutants stored in the residual layer are rapidly entrained into the growing mixed layer the following day. The temporal auto-correlation of pollutants during a smog episode is therefore strongly influenced by horizontal advection and vertical mixing processes that determine pollutant dispersion in the very stable NBL. In view of the diverse and complex set of processes operating in the NBL it is perhaps not surprising that relatively little is known about the mean and turbulent properties of the nocturnal boundary layer or their variations in time and space (Weber & Kurzeja 1991).

Our current understanding of the characteristics and relative importance of vertical mixing and advection mechanisms is therefore hampered by a poor understanding of the

underlying processes operating in the very stable NBL (Nappo & Johansson 1999). Observational studies in the very stable NBL have been sporadic and limited by a focus on surface data. When vertical observations have been included in field experiments, the measurement regimes typically have a limited spatial and temporal resolution, and studies tend to focus primarily on meteorological rather than pollutant characteristics (Corsmeier et al., 1997).

Thus there is a continued need for further research into the three-dimensional distribution of pollutants within nocturnal thermo-topographical wind systems, and their implications for pollutant distribution in the very stable NBL. Further, due to the weak and intermittent characteristics, little is known about the spatial and temporal characteristics of the turbulence in the very stable NBL. This makes it difficult to accurately measure and calculate turbulent fluxes (Chapter 3). Thus the importance of vertical mixing mechanisms in determining pollutant concentrations in both the residual and stable layers remains to be established.

Chapter 3: Observation and analysis of turbulence in the very stable nocturnal boundary layer

3.1 Introduction

Turbulence measurement techniques and traditional data processing methods (such as the Fourier Transform) have severe limitations when applied to the very stable boundary layer (Mahrt 1985). Turbulence in the very stable NBL is highly localised in time and space. It is characterised by abrupt changes in variance (often by as much as an order of magnitude) within a short period of time (Coulter 1990; Howell & Sun 1999). Turbulence is typically intermittent, comprised of isolated clusters of eddies and rarely in equilibrium with surface conditions. As a result, individual experiments may be considered 'unrepresentative', or site specific, and are often limited by instrumental errors and uncertainties or tradeoffs in experimental design. Theories of turbulence and wave structure in the NBL are poorly developed. Thus, similarity theory and other stationary models currently used to interpret and predict the behaviour of the boundary layer cannot be easily applied to the very stable case (Rogers et al. 1995; Finnigan et al. 1984). Field experiments need to be carefully designed and measurement details thoroughly reported in order for results to make a meaningful contribution to the literature.

Our current understanding of processes operating in the very stable NBL stems from a small number of field experiments typically located in regions of homogeneous terrain. Given the complexity of the NBL and the difficulties associated with measuring turbulence in the very stable NBL this is perhaps not surprising. However, from an air quality perspective there is a 'need to develop and demonstrate techniques to make both measurements and prediction in far less ideal circumstances' (Hicks & McMillen 1988, 81; McMillen 1988). Whilst data measured under these conditions at non-ideal sites may not be suitable for determining universal laws (Derbyshire 1994), they can help develop an important part of our understanding of processes determining scalar transport and exchange near the land-surface interface (Lee & Black 1994).

The aim of this chapter is to review some of the difficulties associated with the accurate measurement and calculation of turbulent fluxes in the very stable nocturnal boundary layer. The characteristics of a comparatively new analytical tool - wavelet analysis - are also presented. The technique is discussed within the context of existing literature on atmospheric turbulence. The

potential contribution of the wavelet transform to the quantitative analysis of intermittent turbulence in the very stable nocturnal boundary layer is highlighted.

3.2 Measuring turbulence

3.2.1 Micrometeorological techniques

Turbulence is typically measured using micrometeorological instruments mounted on a tower above a particular surface. Micrometeorological instruments are labour intensive, demand large data storage capabilities and can be costly to maintain. Turbulence in the very stable NBL is weak, typically with standard deviations of vertical velocity of less than 0.20 m s^{-1}(Weber & Kurzeja 1991; Mahrt 1985). This is near the limits of instrument sensitivity. To date there are no accepted, objective and systematic methods for distinguishing between instrumental noise and plausible physical behaviour (Vickers & Mahrt 1997). Critical values must therefore be chosen to exclude contaminated data. Inappropriate sub-selection of data may lead to sampling errors or result in the systematic exclusion of low wind speed conditions creating a bias towards strong wind cases (and the weakly stable nocturnal boundary layer).

Information from these instruments can be used to calculate surface fluxes from an averaged area upwind of the tower – the flux 'footprint' (Horst & Weil 1994; Kharabata & Schuepp 1999). The 'field of view' of tower eddy-correlation measurements may be quite small (Schmid 1994). Due to the size of the eddies and the rate of transport, turbulent measurements in the NBL are particularly sensitive to small-scale heterogeneity of the surface. If the surface cover of the footprint area is heterogeneous, horizontal advection and vertical flux divergence may occur. This renders flux measurements inaccurate as representations of the surface area of interest.

Towers also cannot detect stationary eddies (Lee & Black 1994). Under cloudless nocturnal conditions, significant fluxes and vertical advection can preferentially develop at isolated patches in space corresponding to stationary updrafts (Sun et al. 1997). This is accentuated in regions of complex terrain where stationary features can be generated with convergence of drainage flows or by surfaces with different thermal properties (Mahrt 1998).

Few studies examine the spatial characteristics of intermittent turbulence (Mahrt 1985). Although turbulence sensors do exist for use in conjunction with tethersonde systems these are not widely available. Aircraft have been fitted with turbulence sensors and employed to capture

spatial trends (Bange & Roth 1999; Berkowitz et al. 2000; Berkowitz & Shaw 1997). This requires careful data analysis to remove contamination in the data sets resulting from the aircraft shape and flying speed. Assumptions also have to be made about spatial and temporal stationarity. These are rarely appropriate in the very stable NBL (Mahrt 1998). However, this approach does enable vertical and horizontal variations in turbulence to be studied through a greater depth of the SBL. Results from the small number of aircraft studies suggest that sharp boundaries exist between turbulent patches in the very stable NBL. These patches then have to be identified by arbitrary categories and fluxes calculated using conditional sampling techniques (Weber & Kurzeja 1991; Mahrt 1985).

3.2.2 Richardson numbers

Given the difficulties associated with the direct measurement of turbulent fluxes, the expense of aircraft and acoustic sensors and the limitations of surface based measurements, alternative methods for determining the turbulent state of the NBL have been sought. The most widely used variable to determine the turbulent state of the boundary layer is the Richardson number. This can be calculated from observations of the mean (or turbulent) structure of the boundary layer using instrumentation that is widely available.

Theory suggests that the behaviour of turbulence in the SBL is largely determined by the relationship between the buoyant and mechanical production terms in the turbulent kinetic energy budget (Derbyshire 1990). This forms the basis of the Richardson number. Although the Richardson number does not describe the intensity of the turbulence, the presence or absence of turbulence at a given point in time and space can be determined.

The gradient form of Richardson number (Equation 3.1) has been widely used in studies of the very stable NBL.

$$Ri = \frac{g}{\overline{\theta}_{\upsilon}} \frac{\partial \overline{\theta}_{\upsilon}}{\partial z} \left[\left(\frac{\partial \overline{u}}{\partial z} \right)^2 + \left(\frac{\partial \overline{v}}{\partial z} \right)^2 \right]^{-1}$$

(3.1)

Using this equation it is assumed that turbulent activity cannot be supported in the boundary layer where the Richardson number exceeds a critical value of Ri = 0.25. This parameter was developed and tested using surface data and assumes a very small difference in

height between measurements. However, it has been applied to data collected at a variety of height intervals (typically from towers, tethersonde systems or sodars) throughout the NBL.

In these cases the height difference between contiguous points is of the order of metres rather than centimetres. This raises the issue of the depth of the layer to be used in the calculation. Theoretically it may be more appropriate to use the bulk form of the Richardson number (Equation 3.2) when using widely spaced input measurements. Unfortunately, there is not a critical number associated with the bulk Richardson number, so authors typically apply the gradient form of the equation and use the critical value of $Ri_c = 0.25$.

$$Rb = \frac{g\Delta\overline{\theta}_v \Delta z}{\overline{\theta}_v\left[(\Delta\overline{u})^2 + (\Delta\overline{v})^2\right]} \qquad (3.2)$$

The Richardson number is highly scale dependent (Neu et al. 1994). Calculated values based on measurements of a thick layer of the atmosphere are typically considerably higher than values calculated within the layer (Garratt 1982). Further, local gradients within the SBL and weak wind shear may result in contamination of the data set as localised Richardson numbers approach infinity (Mahrt et al. 1998).

Due to the scale dependence of the Richardson number and its sensitivity to small gradients, a balance has to be achieved between the use of mean values in the profile and the risk of losing too much information. Thus a variety of different averaging techniques have been suggested. A number of authors exclude or round large values to Ri = 10 in order to avoid contamination of the data set by a few very large values (Mahrt et al. 1998).

The large variability in conditions in the NBL combined with the use of different mean heights and smoothing techniques (which often cannot be avoided (Derbyshire 1990)) in the calculation has resulted in a large range of Richardson numbers published in the literature. Even after significant averaging both within and between profiles, values of the order of five to ten are not uncommon and very few report negative values (Kunkel & Walters 1982; Lenschow et al. 1988; Nai-Ping et al. 1983; Weber & Kurzeja 1991; Garratt 1982; Mahrt 1985)

Considerable scatter is shown in the relationship between Richardson number and turbulent fluxes (Neu et al. 1994). This is partially a product of sampling errors and partially due to a phase lag between intermittent turbulence and mean shear (Mahrt 1985). The critical value of $Ri_c = 0.25$ has been contested within the context of vertical profiles through the stable

boundary layer. Kunkel & Walters (1982) report observing turbulence at Richardson numbers up to $Ri_c = 10.0$. Derbyshire (1994) suggest that the $Ri_c = 0.25$ may be locally specific, and that a range of values from $Ri_c = 0.21$ to as high as $Ri_c = 0.45$ may be appropriate.

Clearly, the concept of a single critical Richardson number for these types of conditions is a simplification (Finnigan 1999). This is especially true for unsteady, non-stationary and non-equilibrium conditions typical of the very stable nocturnal boundary layer. However, here I take the view (in agreement with Finnigan (1999) and Mahrt et al. (1979)) that in the absence of detailed micrometeorological measurements, the technique does provide a starting point for comparing the stability between layers and provide an indication of where turbulence might be expected to exist.

3.3 Calculation of turbulent fluxes

Temporal variability in turbulence (expressed both in terms of intermittency and non-stationarity) represents perhaps the most significant challenge to the interpretation of atmospheric data and the calculation of turbulent fluxes in stable conditions (Foken & Wichura 1996; Smedman et al. 1995; Howell & Sun 1999). Fluxes describe the transport of a scalar quantity per unit area with time. In order to calculate an accurate scalar flux, data recorded at a minimum of twice the frequency of the shortest wavelength (the Nyquist frequency) are averaged over a specified time period. The turbulent component is then generated as the difference between the mean state of the variable throughout the time period and each individual data point. The flux is equal to the mean product of the turbulent component of (for example) a scalar quantity with the turbulent component of either the horizontal or vertical transport term. This is the basis of the eddy-correlation method of calculating scalar fluxes.

3.3.1 Non-stationarity

Non-stationarity in the data set (defined as changes in the mean state over the chosen time period) results from a variety of atmospheric forcings including mesoscale circulatory systems (Mahrt et al. 1996), diurnal trends in the boundary layer (Mahrt 1998) and variations in cloud cover (McMillen 1988). Non-stationarity can affect the computed flux at scales larger than turbulence. Although when averaged over many records the effects may be negligible, at an individual scale contamination can be pronounced (Mahrt 1998).

Non-stationary records are ideally omitted from the data record as the calculation of the turbulent and mean component of the flux is flawed. This renders the flux calculations particularly sensitive to averaging length, detrending and filtering procedures (Mahrt 1985). However, without these forms of data conditioning, flux calculations are meaningless. The relative importance of the various sources of errors in the data set cannot be isolated (Mahrt 1998).

Given the inherent non-stationarity in conditions in the very stable NBL some authors have opted for short flux averaging lengths, of the order of 15 minutes (Weber & Kurzeja 1991; Kurzeja et al. 1991). The averaging length used to calculate turbulent fluxes must be long enough to ensure the appropriate statistical sampling of eddies in order to accurately represent conditions at the site. However, due to light wind speeds, and weak and intermittent turbulence, the use of 15 minute averaging periods may result in the sampling of only a small number of eddies in the NBL. This is a particularly serious source of error when fluxes are condensed using local averaging time periods of 5 minutes for data storage purposes (Mahrt et al. 1996). Other authors have therefore chosen to increase the averaging time from the standard daytime value of 30 minutes to one hour (Mahrt 1998) but these flux records are almost certainly contaminated by non-stationarities in the data set. The trade off between these two sources of error is an 'intrinsic feature of the very stable boundary layer' (Mahrt et al. 1998, 257) and the resulting variation in flux averaging lengths hinders comparison between studies.

The elimination of non-stationary time series may result in a significant loss of data at non-ideal sites when the very stable nocturnal boundary layer persists (McMillen 1988). Attempts to reduce the impact of non-stationarities in turbulent time series have traditionally involved linear detrending of the data set. However, there is no physical reason why the processes should be linear (Mahrt 1998). This technique is only really successful when there is a clear spectral gap in the data set, which is often hard to identify in nocturnal turbulence data due to the interaction between gravity waves and turbulence (Mahrt 1985; Smedman et al. 1995).

More advanced filters such as quadratic detrending and higher order filters have also been used to address the problem of stationarity including the use of a running mean rather than an arithmetic mean to calculate the turbulent component (McMillen 1988). However, such techniques risk contamination of the signal and may remove the inherent characteristics of the data sets such as jumps or irregularities. A further difficulty associated with detrending

procedures is that the Reynolds averaging terms ($\overline{w'\bar{\phi}}$ and $\overline{\bar{w}\phi'}$) no longer vanish. These terms may systematically account for 1/3 of the main term and thus the fluxes calculated can only be considered as 'order of magnitude estimates' (Mahrt 1985).

At best, detrending improves the quality of the data set and at worst it is not only ineffective but contaminates the data with an introduced bias. Given the inherent difficulties of applying the detrending procedures some authors opt to avoid detrending altogether and remove offending data sets from analysis. Almost by definition this also results in a biased sampling of the data set.

3.3.2 Intermittency

Quantitative flux estimates are also contaminated with sampling problems generated by the intermittency of the turbulence (Mahrt 1985). Observational studies by Weber & Kurzeja (1991) identify periods of isolated turbulence lasting 5 - 30 minutes near the surface in the NBL. Thus within any given 30 minute sampling period only a small portion of signal may be turbulent. This limits the number of eddies sampled and hence the statistical validity of the flux calculation. This also makes the physical interpretation of the spectra and cospectra difficult because the characteristics of the turbulence spectra are obscured by non-turbulent portions of the time period (Mahrt 1985).

One approach which avoids this problem involves the conditional sampling of time series. Turbulent periods may be isolated, cobbled together and studied as a unit to enable statistical analysis. This technique requires the choice of cut-off values to isolate the turbulent periods. Individual segments must also be scaled, using for example the standard deviation of the turbulence for each patch (Mahrt 1985). Unfortunately, isolating short periods of the time series generates considerable difficulties when analysing the spectral and co-spectral characteristics of the turbulent patches using traditional approaches such as the Fast Fourier Transform.

Quantifying intermittency within the record also presents a challenge. Mahrt (1989) distinguishes between local and global intermittency in the record. Local intermittency refers to the behaviour of the turbulence within the turbulent portion of the trace whilst global intermittency refers to the time between turbulent patches, which is of interest here.

The criteria for identifying the boundary between turbulent and non-turbulent portions of the signal are contested and frequently determined by eye (Bange & Roth 1999). Once the criteria have been established, global intermittency can be defined by comparing the turbulent and non-turbulent portions of the signal. However, there is no consistency as to how this may be effectively achieved. Mahrt et al. (1998) define an intermittency index for each eight minute section of the record, comparing the local standard deviation of the flux with the standard deviation of the 30 minute record length. Other indexes include ratios of the time period of the turbulent and non-turbulent sections of the record (Hagelberg & Gamage 1994) .

3.4 Analytical tools

3.4.1 Fourier analysis

Since the 1970's Fourier analysis has been the dominant technique used to analyse quantitatively large data sets generated by micrometeorological instruments (Collineau & Brunet 1993). This technique decomposes the signal into a series of sine and cosine functions. These are multiplied by a coefficient, which changes the amplitude of the wave. Fourier analysis therefore acts like a mathematical prism, breaking up the series into its set of composite frequencies. The resulting spectra and co-spectra can be used to calculate velocity and length scales, and provides useful insights into the processes operating in the boundary layer. Fourier analysis has been shown to be very effective in some scenarios, thus there is a strong temptation to apply the technique with little discretion. This has resulted in the use of the Fourier transform for applications to which it is not suited producing results with limited value (Hubbard 1998).

The results from Fourier filtering techniques are limited to the frequency domain. In frequency space, information about time is hidden in terms of phases. In theory, information about time can be extracted from the phases of the sine and cosine functions. However, in practice, the precision required to extract information about one instant of the signal from information dispersed through all the frequencies, renders this objective impossible. Thus all temporal information about the frequencies that compose the signal is lost to the investigator, obscuring important information about the processes operating (Jordan et al. 1997).

Fourier analysis, therefore, is not well suited to the analysis of intermittent turbulent data from the very stable nocturnal boundary layer. Further, in order to gain statistically significant results about the turbulent characteristics of the NBL, averages have to be made for periods of

time longer than the intermittent structures of interest. Thus the local event of interest in the time domain becomes an obscured global characteristic of the data in the frequency domain. It is then impossible to identify frequencies associated with turbulent and non-turbulent activity.

The sharp transitions between frequencies associated with intermittent turbulence are highly localised in time. Akin to the Heisenberg uncertainty principle, these events cannot also be band limited in frequency space. An abrupt event in a signal is therefore translated into a range of frequencies, resulting in a global change in the characteristics of the Fourier series. This makes it very hard to establish from the frequency data that a discontinuity has occurred and impossible to determine when it occurred. The absence of time references in frequency space renders the FFT more vulnerable to error magnification. For example if in a 1-hour signal an instrument error occurs during the last 5 minutes, the mistake will corrupt the entire Fourier transform.

3.4.2 Wavelet analysis

Given the preceding litany of difficulties, there is a clear need for a new quantitative mathematical technique to analyse intermittent turbulence in the very stable NBL in order to quantitatively assess the characteristics and importance of the associated scalar fluxes. Ideally, such a technique could be used to objectively isolate and analyse the turbulent 'bursts'. This would provide insight into the turbulent processes operating in the nocturnal boundary layer, whilst avoiding contamination from other processes, such as gravity waves or background noise in the signal.

Wavelet analysis is a comparatively new analytical tool that provides a potential alternative to Fourier analysis. The technique emerged independently in a number of different fields in the 1980's (Farge 1992). Wavelet analysis has increasingly been applied to the analysis of turbulence and is 'yielding important insights into boundary-layer processes' (Trevino & Andreas 1996, 271).

3.4.3 What is wavelet analysis?

Wavelet analysis is a mathematically rigorous tool used primarily in signal processing (Hagelberg & Gamage 1994; Collineau & Brunet 1993). The goal of wavelet analysis is (like Fourier analysis) to transform efficiently the information in a signal into coefficients which can be used to store, transmit, analyse, manipulate or reconstruct the original signal (Hubbard 1998).

It is considered to be both a departure from, and extension of, Fourier analysis. Perhaps the most significant difference between the two techniques is that wavelet analysis provides a 2-dimensional representation of the signal in time and frequency space. Thus it retains a time localisation associated with the frequencies identified. This enables information about how the dominant frequency modes vary through time to be determined from the data (Torrence & Compo 1998). In this way, it can be used to 'point to important features of a process and reveal structure not apparent from direct observation which are a key component of process understanding' (Kumar & FoufoulaGeorgiou 1997, 408).

A *wavelet* is a short piece of a wave or function, which consists of a few short oscillations within a specified time window, and is equal to zero at the asymptotic limits of the function. The wavelets must be 'wave-like' but not form a sustaining wave (Kumar & FoufoulaGeorgiou 1997). These form the 'elementary building blocks' in the decomposition, similar to the sine and cosine terms in a Fourier transform (Kumar & FoufoulaGeorgiou 1997).

Unlike Fourier analysis, however, wavelet analysis takes place at a variety of different scales using a family of wavelets. The wavelet family consists of the *mother wavelet* that defines the overall shape of the wave. The *daughter wavelets* are clones of the mother wavelet, which have been compressed or stretched and translated (or shifted along the signal) as shown in Figure 3.1.

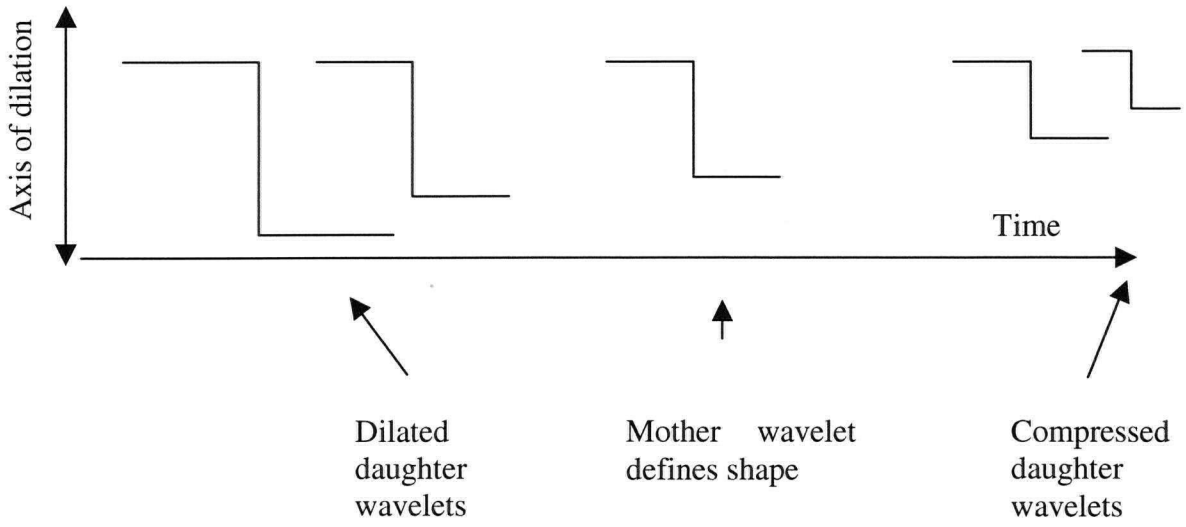

Figure 3.1 The relationship between Mother and Daughter wavelets based on the Haar wavelet

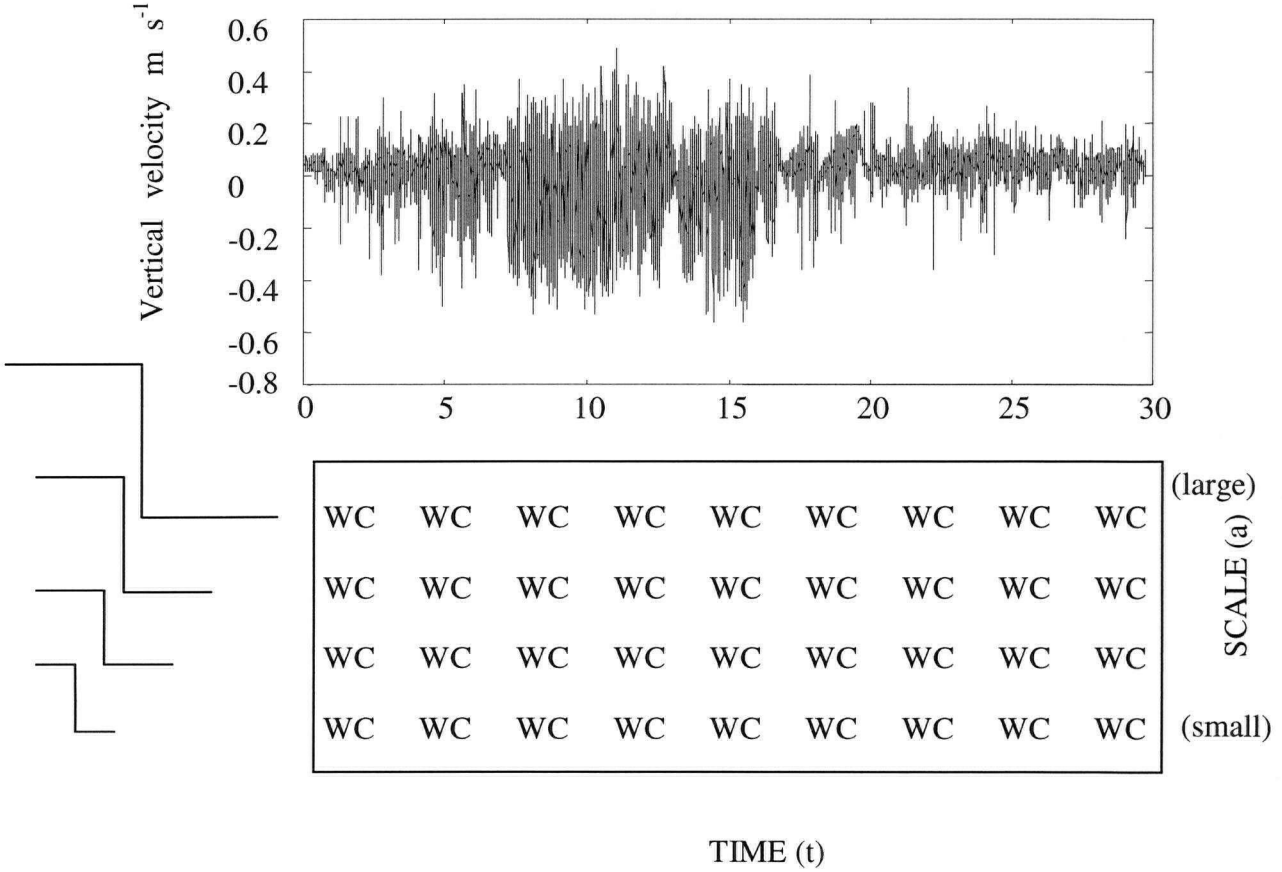

Figure 3.2 Example of a time series and resulting scalogram (b) following wavelet analysis at four scales

The signal is compared to the family of wavelets by taking the inner product of wavelet and the signal at different scales (a) and positions (b) along the signal, using Equation 3.3 (Gao & Li 1993), as shown in Figure 3.2.

$$W_\psi f(a,b) = \frac{1}{|a|^{1/2}} \int f(t)\psi\left(\frac{t-b}{a}\right)dt$$

(3.3)

where:

a	scale
b	position
t	time
$\psi[(t-b)/a]$	mother wavelet
$\|a\|^{1/2}$	scaling function to normalise energy content at each scale
f(t)	function at time t
$W_\psi f$	wavelet coefficient for each scale (a) and position (b)

The wavelet can be said to 'zoom in', allowing the features of the signal to be studied locally, with a level of detail matched to their scale. The large-scale features are then studied with broader wavelets at a lower resolution, and fine scale features with smaller wavelets at a higher resolution. The technique has been described as a 'mathematical microscope' (Hubbard 1998), with location and magnification corresponding to translation and dilation of the daughter wavelets, respectively. The information yielded about the signal is dependent on the analysing wavelet (or lens) selected (Trevino & Andreas 1996). This property is unique to wavelets (Lau & Weng 1995). The wavelet transform can be considered as 'a type of multi-channel tuned filter' (Hagelberg & Gamage 1994, 219). Wavelets at low frequencies filter out all information except low frequency trends, and high frequency wavelets only allow through high frequency energy (Hubbard 1998). It makes the technique 'especially useful for signals that are non-stationary, have short lived transient components, have features at different scales, or have singularities' (Kumar & FoufoulaGeorgiou 1997, 386). Therefore wavelets may be particularly appropriate for use in the time-frequency analysis of intermittent turbulence in the very stable NBL.

Table 3.1 Comparison between Fourier analysis and Wavelet Analysis

Characteristics	**Wavelet Analysis**	**Fourier Analysis**
Signal represented by:	The integral of the product between the signal and a family of wavelets	A series of sine and cosine functions
Domain of results	Time-frequency (2-dimensional)	Frequency only (1-Dimensional)
Response to errors in signal	Small changes in the signal correspond to small changes in wavelet coefficients thus errors are not magnified	Absence of time references in frequency space makes the FFT more vulnerable to error magnification
Sensitive to:	Missing data (less sensitive to noise in the data and the presence of non-stationary trends)	Missing data. Linear and non-linear trends. Irregular data.
Type of data best suited for analysis	Highly non stationary signals with sudden changes or discontinuities	Regular periodic signals & linear problems
Support by basis function	Strongly influenced by local events	Strongly influenced by global structures
Computational efficiency	For a data set size N, N calculations required	For a data set size N, N log N computations required
Scale of analysis	Signal studied at detail matched to scale	One scale used
Efficiency	Relatively few wavelet coefficients are required to capture a significant portion of the energy	Large number of sine and cosine functions required to capture the energy of an temporally localised signal
Disadvantages	Few examples currently available, frequency information less precise, some variation in results depending on wavelet choice	No information about temporal location of frequencies identified. Long averaging periods required for statistically significant results. Vulnerable to error magnification. A brief localised event in time will correspond to a wide range of Fourier coefficients.

The product of the wavelet transform is a series of *wavelet coefficients,* one for each point in the signal at each scale of analysis. The wavelet coefficient effectively measures the correlation between the shape of the wavelet and the corresponding segment of the signal. These coefficients provide a representation of the signal as an infinite series expansion consisting of dilated, or expanded and translated, versions of the mother wavelet. The wavelet coefficients for each scale and position can be displayed in a two-dimensional plot known as a scalogram, with the original time scale along the x-axis and scale along the y axis (see Figure 3.2). The wavelet coefficients are usually contoured to display the results efficiently. Wavelet analysis is compared to Fourier analysis in Table 3.1. In summary, wavelet analysis is a local, linear transform, which can preserve energy characteristics and provide a reversible time-frequency representation of a given signal.

3.4.4 Types of wavelet

There is an infinite number of different wavelets and wavelet-Fourier hybrids. A wavelet can consist of any piece of a wave or function, providing it meets the following criteria (Farge 1992). The wavelet must have an integral of zero such that the area under the curve and above the axis is equal to the area above the curve below the axis. The wavelet must have a mean equal to zero. The wavelet, though wave-like, must not form a sustaining wave but must asymptotically go to zero at plus and minus infinity. The wavelet must be also localised in time and, ideally, the frequency domain (Torrence & Compo 1998). Finally, it must be possible to define the inverse transform of the wavelet.

So far 'there is no consensus as to how hard one should work to choose the best wavelet for a given application and no firm guidelines about how to make such a choice' (Hubbard 1998, 88). However, 'the choice of a wavelet is neither unique nor arbitrary' (Kumar & FoufoulaGeorgiou 1997, 389). It requires a thorough understanding of the properties of the form of the wavelet transform chosen and the properties of the different wavelets.

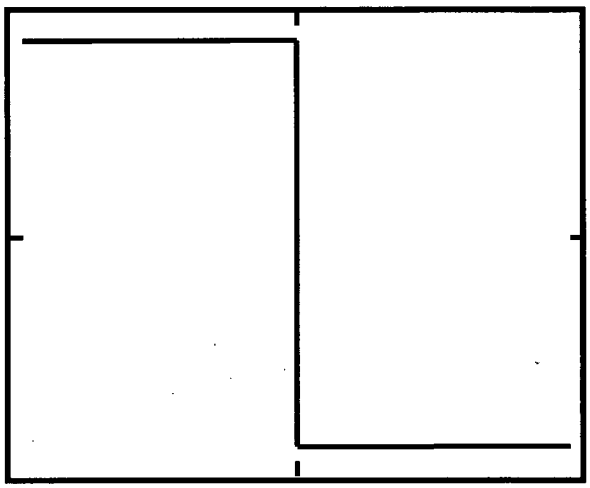

Haar Wavelet

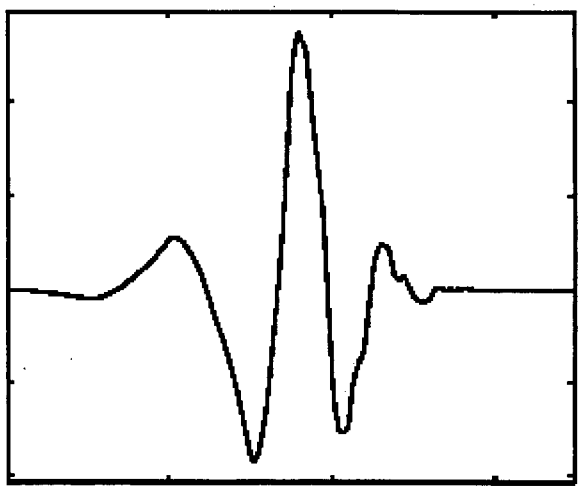

Daubechies '4' wavelet

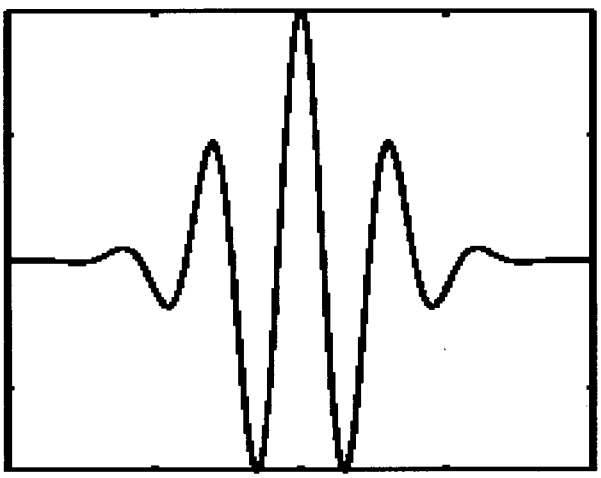

Morlet wavelet

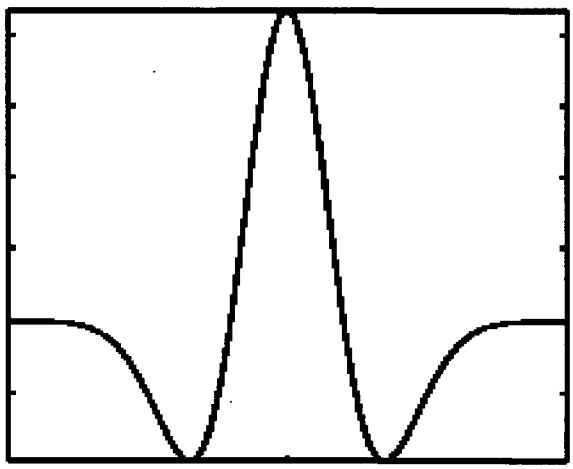

Mexican Hat wavelet

Figure 3.3 The shape of four common 'Mother' wavelets

The choice of the mother wavelet determines what type of information can be extracted from the transform. Like any analysis technique, the chosen representation places emphasis on some information within the signal at the expense of other information which may become 'hidden' in the transform (Kumar & FoufoulaGeorgiou 1997). Wavelets can be constructed to give small or zero coefficients when compared to a specified function. This generates 'vanishing moments' or parts of the function which the wavelet does not see. In an experiment, Trevino & Andreas (1996) illustrate that wavelet coefficients of an artificial data set (signal 'a') and the coefficients for signal 'a' plus a linear trend are very similar. From this information they argue that 'patterns in wavelet coefficients are insufficient evidence of turbulent structure and, therefore, caution must be exercised when interpreting geometrical structures present in the display of wavelet coefficients' (Trevino & Andreas 1996). However, their analysis was based on the Haar wavelet. The Haar wavelet is not ideally suited to the detection of linear trends, but rather the jumps or sudden events in the data set. Had a different wavelet transform been used which is more suited to the detection of linear trends, the results would have been different and the trend highlighted.

Whilst Trevino & Andreas (1996) rightly emphasise the limitation of the Haar wavelet, the same is not necessarily true for other types of wavelet analysis. Each individual wavelet has its own limitations. Wavelets based on second order difference functions offer no information about linear trends in the data set (Trevino & Andreas 1996). This property can be utilised to the advantage of the experimenter. For example, in turbulence analysis it is desirable to avoid contamination by non-stationary components of the signal such as linear trends. Thus, using long wavelet filters such as the Daubechies-4 wavelet to calculate variances, undesirable linear trends in the original data will not contaminate the results (Whitcher 2000 pers. comm.).

All mother wavelets have limitations in terms of the type of information they reveal about the time series and choices must be made in terms of representation, computational requirements and precision in time or frequency space. In the absence of other criteria, Lau & Weng (1995, 2394) argue that the choice of a wavelet which bears the most 'reasonable resemblance in form to the signal' will provide the most useful information from a wavelet transform. However, Collineau & Brunet (1993) suggest that particularly when using the discrete form of the wavelet transform and calculating the wavelet coefficients as a convolution in Fourier space, the frequency characteristics of the wavelet are of more importance than the temporal ones.

Some wavelets – such as the Morlet and Paul wavelets - have imaginary components analogous to the Fourier imaginary component. Results from such a complex wavelet transform can be divided into a real part and an imaginary part. This can be useful in providing information about phases within the data set (for use in distinguishing between gravity waves and turbulence, for example). Real wavelets capture both the positive and negative oscillations in time series as separate peaks in wavelet power. Complex wavelets tend to combine positive and negative peaks into a single broader peak. Thus, real wavelets are better suited to isolating peaks and discontinuities in the data sets (Torrence & Compo 1998). However, a plot of only the real or imaginary part will yield results similar to the 'real' wavelet (Torrence & Compo 1998). Torrence & Compo (1998) conclude that the same features can be identified at approximately the same locations using both the Mexican Hat (a 'real' transform) and the complex Morlet wavelet.

Authors disagree over the critical choices between wavelets. Hagelberg & Gamage (1994) argue that the critical choice between wavelet types is between symmetric and anti-symmetric wavelets. For example, in the analysis of turbulent signals the anti-symmetric wavelet will be highly coherent when it is positioned at the centre of the transition, whilst the symmetric wavelet will be coherent at the edges, effectively defining the region of the transition zone. However, Hagelberg & Gamage (1994, 238) argue further that the 'specific type of wavelet, and its regularity are less critical in applications to real data'.

There is some controversy surrounding the effect that wavelet choice has on the universality of results. Given that wavelet coefficients are the product of the wavelet and the signal, it is inevitable that the characteristics of the wavelet will be stamped on the results to some degree. Lau & Weng (1995) and Torrence & Compo (1998) discuss the qualitative effect of different wavelets on the scalogram. They show that whilst there are differences, primarily associated with the resolution of the coefficients in time and frequency space, comparing results from the two techniques (based on a knowledge of the characteristics of the wavelet chosen) can result in enhanced understanding of the processes. In contrast, Kumar & FoufoulaGeorgiou (1997) and Collineau & Brunet (1993) demonstrate that when the information from the wavelet transform is summarised (for example in the form of variances) there is little difference in the results due to choice of wavelets.

3.4.5 Continuous and discrete forms of wavelet analysis

Wavelet analysis can be undertaken at two different scales. The continuous form of the wavelet transform is computed by using smoothly varying values of translations and dilations of the daughter wavelets. In theory this analysis is infinitely continuous and studies the signal at all possible scales. The discrete form of the wavelet transform is computed using only a discrete and pre-selected number of scales. There are advantages and disadvantages associated with both types of transform.

A continuous transform is 'shift invariant', so the precise location of the start of analysis within the signal does not change the coefficients produced. The output from a continuous wavelet transform is used to plot a 2D scalogram. In this way the detailed changes in frequency with time can be visualised. The continuous form of the wavelet transform ensures that information about the signal is represented at every scale, and the peaks in the wavelet coefficients at all scales are represented.

However, this form of the technique provides an over-complete analysis of the signal and the individual wavelet coefficients are not independent of each other. Whilst the redundancy can be exploited to gain maximum information about a particular feature, it can also 'bring about undesired formal relations between the wavelet coefficients themselves' (Katul & Parlange 1995). Further, when looking at the results in frequency space, the redundant information contaminates the transform, appearing throughout the frequency data as noise similar to that expected from leakage in the FFT. Unlike leakage (caused by cut-offs at the end of a finite time series), this results from an intrinsic property of the wavelet analysis and can act to accentuate information obtained from the transform. This is useful for detecting jumps or breaks in the data set (Collineau & Brunet 1993). However, due to the redundancy within the coefficients this form of the wavelet transform is not energy preserving. Thus the estimates of variance are not reliable. Nevertheless, Howell & Mahrt (1994a) demonstrate that in practice there is very little difference in the variance and covariance calculated using continuous versus orthogonal transforms.

Whilst the continuous form of the wavelet transform may be preferable if the energetic characteristics of signal are not of interest, it is computationally intensive. For this reason, when real data sets are analysed the continuous wavelet transform is often discretised and performed at a selection of different scales. There remains redundant information in the transform but the

transform can no longer be used to recreate the original signal perfectly and some information is lost to the user.

The discrete wavelet transform (DWT) involves analysis at a subset of the translations and dilations available. The orthogonal form of the wavelet transform is a special type of DWT. Orthogonal scales are chosen and the signal analysed at scales differing by a factor of two, such that information is only encoded once. The number of wavelets used is the minimum required by sampling theory to allow for a perfect reconstruction of the signal. The transform contains the same number of points as the signal itself.

Each orthogonal wavelet family has a 'Father' or scaling function in addition to a mother wavelet, which determines 'the starting point for the analysis and makes it possible to compute the wavelet coefficients fast' (Hubbard 1998). The size of the scaling function also determines the finest resolution for analysis. Hence computational efficiency can be achieved without sampling, thereby minimising the risk of generating non-representative values. The signal is divided into segments, whereby a combination of the signal 'smoothed' by the father and details from the mother are calculated at each scale. Since this type of wavelet transform is energy preserving and satisfies the requirements of Parseval's theorem (Katul & Parlange 1995), the sum of the square of the wavelet transform is equal to the variance of the time series at each scale. 'This allows a clear and conventional physical interpretation of the expansion coefficients from the energetic point of view when applied to turbulence measurements' (Katul & Parlange 1995).

However, orthogonal wavelets are sensitive to the starting point of the analysis. A small shift in the start point can result in a large change in the coefficients at each scale and the position of the maximum variance. Torrence & Compo (1998) caution that in orthogonal analyses the number of convolutions at each scale is proportional to the width of the wavelet basis at that scale. This produces an aperiodic shift in the analysis that may generate a very different wavelet spectrum. Orthogonal wavelet analysis may therefore 'miss' information at scales between each octave. This can result in errors in the physical interpretation of the wavelet analysis (Lau & Weng 1995).

The non-decimated or maximal overlap form of the discrete wavelet transform (MODWT) forms a compromise between some of the desirable characteristics of the continuous and discrete forms of the wavelet transform. Essentially, the MODWT involves the computation

of wavelet coefficients at all scales like the continuous wavelet transform. It also calculates the coefficients for all points in the time series (unlike the DWT which restricts sample sizes to integers of the power 2). The coefficients are then sub-sampled and re-normalised at dyadic scales to generate the final coefficient matrix (Whitcher & Byers 2000). The MODWT is therefore shift invariant and the resulting variances calculated are insensitive to the starting point of analysis (Percival & Walden 2000). This type of wavelet analysis can be used to form the basis of a multiresolution analysis and is comparable to the FFT in terms of computational efficiency. Although not strictly orthogonal, this form of wavelet analysis is energy preserving (due to statistical sampling and averaging of the wavelet coefficients) and satisfies the requirements of Parseval's theorem (Percival & Walden 2000). It has been shown to be effective in time series analysis and is arguably more suited to calculation of variance and covariance within a data series.

Hubbard (1998) cautions that whilst it is dangerous to forget that different wavelets provide different information about the signal, there is also a very real trade off between time spent in search for the perfect wavelet and time spent evaluating the results. The old motto regarding 'horses for courses' seems appropriate here. The choice of the most appropriate wavelet is influenced by the need for the wavelet to be localised in the time or frequency domain, the shape of the events in the actual signal, and on the question asked.

3.4.6 Wavelet variance, spectra, co-spectra and cross-spectra

Like Fourier analysis, wavelet analysis can be used to calculate variance and spectra. Variance of the time series is defined from the wavelet transform as shown in Equation 3.4 (Torrence & Compo 1998).

$$\sigma^2 = \overline{W}^2(b) = \frac{1}{N}\sum_{n=0}^{N-1}\left|W_n(b)\right|^2 \qquad (3.4)$$

where:

$\overline{W}^2(b)$ Wavelet variance at each scale b

N Total number of data points in the series

n Specific point in the series

The spectral density function can be calculated using wavelet analysis by defining a wavenumber to correspond to each scale in wavelet analysis. To gain a true representation of the energy at each scale, discrete orthogonal forms of the wavelet transform (which satisfy the requirements of Parseval's theorem) and have compact support in the frequency domain must be used. Wavelet spectra have significant advantages over Fourier spectra. For example, judicious choice of wavelets avoids contamination by linear trends or the need for complex detrending of the data prior to analysis. Wavelet analysis also provides greater resolution at larger scales. Errors and subjectivity introduced due to the averaging of data points (and choice of bin sizes) are also avoided.

Choice of wavelet has been shown to bias the calculated spectra for artificial data sets which demonstrate a steep drop off in frequencies. This type of signal is not expected in atmospheric turbulence data. However, to ensure minimal effect of the wavelet on the results, the Haar wavelet is used to calculate spectra in Chapter 6. The wave numbers associated with the Haar wavelet can be calculated easily and the spectra have been compared previously to the spectra from FFT and reliably demonstrate good correlation for daytime data sets (Katul & Parlange 1995).

Using a complex wavelet such as the Morlet wavelet it is possible to define a type of cross-scalogram analogous to the co-spectra calculated using Fourier analysis (Equation 3.5). Thus it is also possible to define the phase between two variables, as shown in Equation 3.6. Information about the phase between vertical velocity and temperature can be used to identify whether gravity waves are present in the data set. Turbulence can be expected to generate a phase difference of 180^0 whilst in gravity waves the two variables are offset by 90^0.

$$W_f(a,b)^* \overline{W_g(a,b)} \qquad (3.5)$$

where:

W wavelet coefficient for time series f and g respectively

a scale

b dilation

$$\text{phase} = \tan^{-1} \frac{W_n^{fg}(b)}{W_n^{*fg}(b)} \tag{3.6}$$

where:

W^{fg} product of wavelet coefficients for time series f and g

b position

n point in series

W^{*fg} product of the complex conjugate of time series f and g

Like Fourier analysis, the wavelet coefficients can be converted back into the original time series using the simple inverse equation given in Equation 3.7a (Lau & Weng 1995).

$$f(t) = \frac{1}{C_\varphi} \int \frac{da}{a} \int db \frac{1}{(a)^{1/2}} \psi \frac{(t-b)}{a} W_{b,a} \tag{3.7a}$$

where:

C_ψ constant depending on the wavelet chosen (see 3.7a)

t time

b position

a scale

$W_{b,a}$ wavelet coefficient

$$C_\psi = \int_0^\infty \frac{|\psi(w)|^2}{w} dw \qquad < \infty \tag{3.7b}$$

where:

w angular frequency

Wavelet analysis can be effectively used to isolate the characteristics of the signal at one scale and use that information to reconstruct the signal at that scale without incurring any significant cut-off errors. This is akin to filtering the signal and is calculated using the inverse form of the wavelet transform.

3.4.7 Advantages and uses of wavelet analysis in the atmospheric sciences

Although wavelet analysis is a relatively new technique, it is proving to be a powerful tool for the analysis of signals containing non-stationary processes (Druilhet et al. 1994). Wavelet analysis has the potential to make a significant contribution to data analysis of climate and turbulent signals. It is a local transform, thus is well suited for the analysis of multi-scale features, transient phenomena and detection of singularities within data sets (Kumar & FoufoulaGeorgiou 1997; Lau & Weng 1995). Climate and turbulence signals are often non-stationary with a variety of frequency regimes operating either at localised points in time or spanning the entire series. They are therefore well suited to interrogation by the wavelet transform (Jordan et al. 1997). Thus, 'judiciously used this higher level of sophistication in our methods analysis will bring new insights and understanding of many complex phenomenon around us' (Kumar & FoufoulaGeorgiou 1997).

One of the first authors to utilise the wavelet transform in atmospheric science was Farge (1992). Since, there has been a 'virtual explosion in the number of wavelet papers appearing in professional journals' (Trevino & Andreas 1996, 271). Wavelet analysis can be used to efficiently store, manipulate and reconstruct data and has been used to identify and quantitatively analyse trends in a wide variety of different applications. For example, it has been used effectively to isolate and objectively determine the characteristics of climatic cycles such as those associated with El Nino (Torrence & Compo 1998; Howell & Mahrt 1994b).

Localisation in the time domain enables the frequency characteristics of individual phenomena to be isolated (Collineau & Brunet 1993; Kulkarni et al. 1999). Fourier filtering techniques cannot accomplish similar partitioning of signals because sharp transitions in the time domain are not band limited in the frequency domain. This is not such a problem for wavelet analysis because the frequency content under consideration is limited to a specific point in time (Hagelberg & Gamage 1994). This type of analysis of changing scale through time and its

quantification, 'almost without exception, provides an effective way for representing and interpreting experimental data of all types' (Trevino & Andreas 1996).

Wavelet analysis has also been successfully used as a filter to remove unwanted trends (such as non-stationarities) (Andreas & Trevino 1997) and noise from both climate and turbulence signals (Howell & Mahrt 1994b). For example, Howell & Mahrt (1994a) develop an 'adaptive multiresolution filter' based on the Haar wavelet to remove noise and small scale variance from the data sets from a turbulent data set and ENSO data set. Their filter acts as a running mean contained within a moving window. It is effective at identifying coherent regions within the signal that are embedded in noise and are otherwise obscured. White noise (random background noise), which has been traditionally difficult to remove from signals, can also be removed efficiently from signals by the elimination of very small coefficients in the transform. Unlike Fourier analysis, the wavelet transform can be used to remove trends without incurring cut-off errors.

To date, the main use of wavelet analysis in turbulence literature has been in the detection and analysis of coherent structures (Collineau & Brunet 1993; Katul et al. 1996). Coherent structures in velocity fields determine the spectral characteristics of the velocity signals and play an important role in flux transport. The presence of these in the data set generates a form of local intermittency that is hard to quantify using the Fourier transform. Wavelet analysis, a technique which 'encompasses many desirable features of traditional conditional sampling techniques' (Hagelberg & Gamage 1994, 240), provides an objective means for defining and quantifying intermittent events in a signal and enables partitions to be created which maintain the sharp edges of the events. Hagelberg & Gamage (1994) effectively separate the signals into structure and non-structure components using wavelet analysis to first identify the scale of the dominant structures and then to separate out information at that scale using the wavelet transform as a filter. Separating the signal in this way they evaluate the spectral characteristics of the separate components determining that, whilst the coherent structure component of the signal exhibits the traditional –5/3 gradient in the inertial range, the non-structure component has a –1 slope (Hagelberg & Gamage 1994).

Hudgins et al. (1993) and later Mayer et al. (1994) demonstrated that the wavelet transform can be used to calculate variance and spectra that are directly comparable to those calculated using the Fourier transform. The wavelet version, however, has the advantage of higher resolution at longer scales (Hudgins et al. 1993) and avoids the difficulties associated

with averaging and the arbitrary assignment of bin sizes to the data set. Wavelet analysis also enables the local definition of spectra in time or space (Perrier et al. 1995). Wavelet transform locally decomposes variance such that the peak in the spectra is determined by the width of the dominant local scale event. By comparison, variances calculated from Fourier spectra are affected by the periodicity of the event and include information about the spacing between events in calculated variances (Howell & Mahrt 1997).

Howell & Mahrt (1997) demonstrate that wavelet analysis can be effectively used to calculate turbulent fluxes. They use a fast algorithm based on the orthogonal Haar wavelet to construct cospectra at different resolutions from a spatial turbulence series collected from an aircraft. This is a form of multiresolution analysis. The resulting technique is akin to using an unweighted (non-over lapping) moving average window of different widths to calculate the fluxes. This enables the characteristics of the two signals to be compared at the same resolution, calculating a local covariance. This technique satisfies Reynolds averaging rules and the sum of the cospectra is equal to the flux. One of the advantages of this method of flux calculation is that the influence of non-stationarities in the data set is minimised. Using wavelet analysis to calculate fluxes also enables a 'measure of statistical confidence in the flux' to be retained (Howell & Sun 1999). Interestingly, although Galmarini & Attie (2000) successfully exploit the characteristics of the cross-scalogram to determine the spatial location of enhanced turbulent exchanges at the thermal internal boundary-layer, they use traditional analytical tools to calculate the turbulent fluxes from their aircraft data used in the early part of their paper.

Local scale averaging makes wavelet analysis ideal for calculating fluxes in non-ideal conditions when the time series is expected to be non-stationary. Not surprisingly therefore, Howell & Sun (1999) use the multi-resolution analysis (developed in Howell & Mahrt (1997)) to analyse the characteristics of turbulence in the nocturnal boundary layer. However, their work primarily explores the cut-off effects on the flux averaging time and an error term that they develop. Interestingly, although they do explore the issue of intermittency this is based on the division of the record into 10 minute sub-records rather than using the potential of wavelet analysis in a manner akin to the study of turbulence in the forest canopy by Collineau & Brunet (1993). They also do not discuss the potential of this technique for filtering the time series to remove noise and other processes, or the possibilities of distinguishing between gravity wave and turbulent transport. This has been successfully done in the middle troposphere by Sato & Yamada (1994).

3.4.8 A cautionary note

'It's a new tool, and one cannot apply it blindly to problems as shapeless as turbulence if it isn't calibrated first on academic signals that we know very well' Marie Farge quoted in p87 of Hubbard (1998).

'The often stated contention that wavelets are more suited than Fourier or other classical methods to the analysis and decomposition of non-stationary or random signals has aroused the curiosity' of the scientific community (Trevino & Andreas 1996, 271). As with all techniques, wavelet analysis has limitations. However, these have yet to be widely discussed in the literature (Trevino & Andreas 1996). This can result in the misinterpretation of results and inappropriate applications of wavelet analysis (Andreas & Trevino 1997). There is also a lack of proper normalisation and rigorous statistical significance tests leaving the technique open to criticism (Torrence & Compo 1998). However, these issues are currently being addressed in the literature (Howell & Mahrt 1997).

Although wavelet analysis provides information about the signal in time and frequency space, high resolution cannot be simultaneously achieved in both domains. Wavelet analysis adapts to the components of the signal (low frequencies corresponding to broader wavelets, and higher frequencies corresponding to thinner wavelets) and enables a broad range of information about the signal in time and frequency space to be gathered. However, low frequencies corresponding to broader wavelets are vague about time with a high precision in frequency space. Conversely, small wavelets are poorly localised in frequency space but accurately represented in time space. Further, given that stretching or compression changes the shape of the wavelet, the resolution, scale and frequency all change at once. Information about the frequency is thus less precise than for the Fourier transform, which must be considered when interpreting results.

The use of different size wavelets also means that care has to be taken when analysing a finite signal. Like Fourier analysis, the length of the signal can contaminate information in the wavelet transform, particularly at longer wavelengths. The area of the scalogram affected by this is known as the cone of influence and must be discarded from analysis. Care must also be taken with information contained in wavelet variances at longer wavelengths. Padding techniques have been used to minimise these effects.

'Wavelet coefficients combine information about both the signal and the wavelet' (Trevino & Andreas 1996, 286). This is not unlike the problems associated with the effects of instrumentation on measurement of turbulence. 'What we observe is not nature itself, but nature exposed to our method of questioning' (Heisenberg 1958). However, it does mean that the choice of wavelet can affect the patterns which are seen. In its most extreme form this can have the effect that the dominant patterns reveal as much about the choice of wavelet as the underlying processes.

The wide range of choices available in wavelet analysis has left the technique vulnerable to criticism as subjective and non-rigorous, with unrepeatable methodologies. Some of this criticism may stem from a comparison with Fourier analysis where the choices (which also affect results, introducing a degree of subjectivity) are masked behind a rhetoric of 'accepted procedure' in the quest for objective and consistent results. Farge (1992) argues that 'a common pitfall when using any kind of transform is to forget the presence of the analysing function in the transformed field, which may lead to severe misinterpretations, the structure of the analysing function being interpreted as characteristic of the phenomenon under study'.

3.5 Summary

The weak, intermittent and spatially variable characteristics of turbulence in the very stable nocturnal boundary layer hinder the accurate measurement and calculation of turbulent fluxes. Given the importance of vertical mixing mechanisms in determining near surface air quality outlined in Chapter 2, further research is clearly required to develop a quantitative understanding of its characteristics in time and space. Within this context, wavelet analysis has the potential to make a significant contribution to the analysis of turbulent fluxes in the very stable nocturnal boundary layer.

Chapter 4: Methods

This chapter provides a detailed overview of the 1998 field experiment designed and implemented to meet the objectives outlined in Chapter 1. The chapter begins with a detailed description of, and rationale for, the field site. This is followed by an outline of the instruments used, the type of data collected and the measurement regimes undertaken. Special consideration is given to the specific requirements of the micrometeorological instruments used to measure turbulent fluxes. Lastly, the quality of the turbulence data is assessed using a range of data quality control techniques.

4.1 Field site: The Lower Fraser Valley

The Lower Fraser Valley (LFV) is a triangular shaped valley located on the coast of the Strait of Georgia straddling the US/Canada border (Figure 4.1). It is a flat-bottomed valley, located only a few metres above sea-level, and orientated approximately WNW - ESE. The valley is bounded to the west and south-west by the Strait of Georgia and extends more than 200km from Vancouver to Hope. The Coastal Mountain ranges are located to the north extending to ~2000 m above sea level, whilst the Cascade Mountains to the South rise to ~1000 m above sea level.

The highest population density is found at the north west end of the valley where the Coast Mountain ranges meet the Strait of Georgia. Here, the city and suburbs of Vancouver support a population of approximately two million people in the Greater Vancouver Regional District (GVRD). Land use in the remainder of the valley is primarily arable farming with isolated pockets of deciduous and coniferous forestry. Scattered settlements, some sizeable, are mainly clustered along the Trans-Canada Highway (Highway #1). Tributary valleys to the North of the LFV are comprised of near pristine forest environments and recreational areas, sections of which form provincial parks.

Although much has been written regarding the air pollution meteorology of the LFV (McKendry et al. 1997; Banta et al. 1997; Pisano et al. 1997), little is known about the nocturnal vertical distribution of pollutants, turbulence, deposition velocities, or the structure of the very stable nocturnal boundary layer. Although this region is not 'ideal' in micrometeorological terms due to the proximity of complex terrain, its choice is justified by the need for nocturnal turbulent

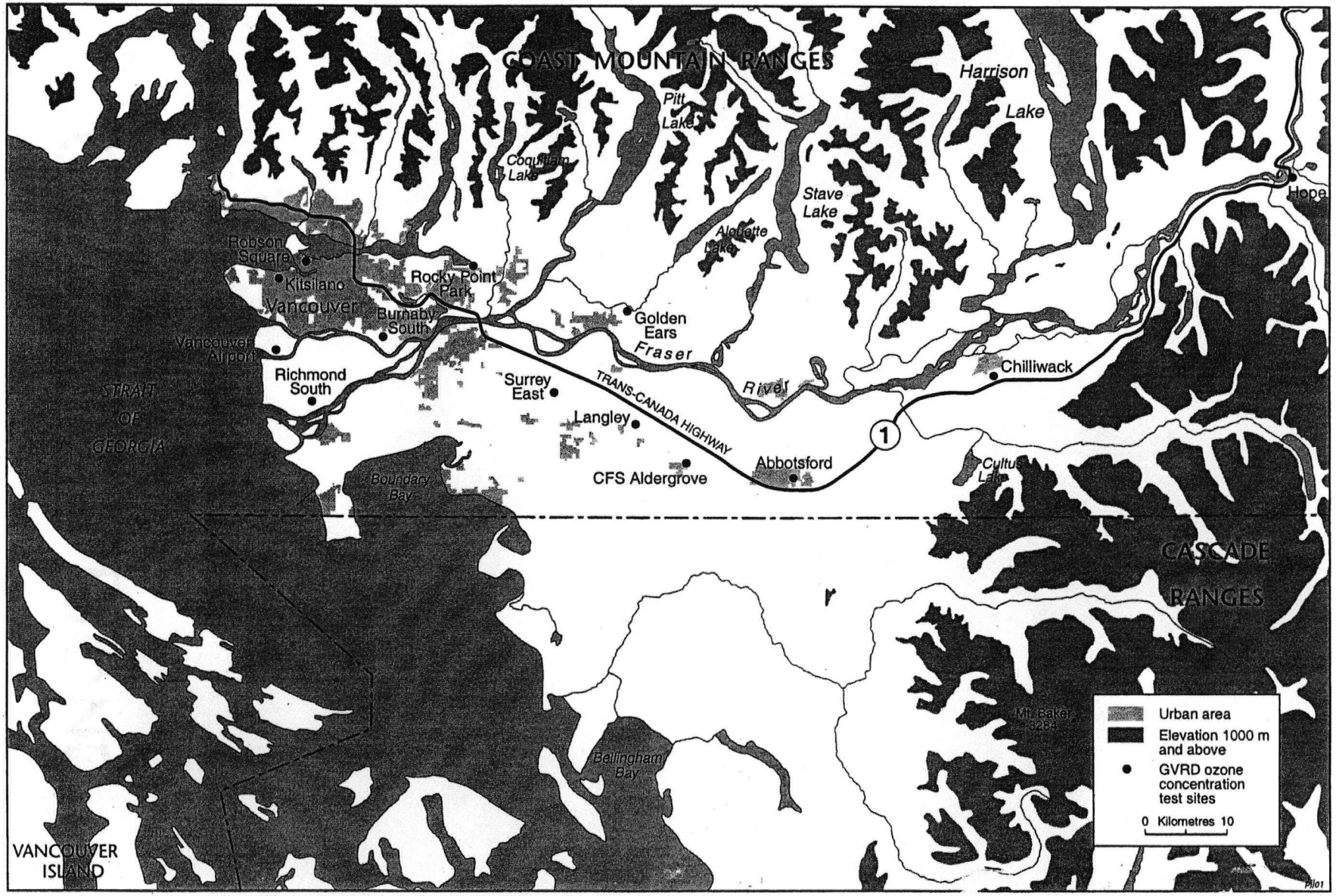

Figure 4.1 Map of the Lower Fraser Valley, British Columbia, Canada, illustrating the field site in Aldergrove, the proximity of the Trans-Canada highway and the location of the GVRD air quality monitoring stations included in this study

flux measurements in regions of complex coastal terrain (Hicks & McMillen 1988; McMillen 1988).

The GVRD and Environment Canada have a well-established surface air quality monitoring network in the region. During summer months, ozone concentrations in the LFV periodically exceed the Canadian Air Quality Objectives (Li et al. 1997). Episodes of poor air quality typically occur during anti-cyclonic conditions when subsidence generates an elevated inversion which traps surface pollutants within the airshed (McKendry 1994). The highest pollution concentrations are recorded at the eastern end of the valley (Steyn et al. 1997) and in the tributary valleys to the north (McKendry et al. 1990).

Nocturnal spikes in ozone concentration have been previously observed throughout the Lower Fraser Valley, particularly during periods of poor air quality, indicating that vertical transport mechanisms may play an important role in determining surface air quality in the region (McKendry 2000). In this environment, processes that affect diurnal pollutant cycles and trajectories have the potential to affect the health of local populations and vegetation (including areas of agriculture and pristine environments) located downwind of Vancouver.

4.1.1 Aldergrove

Within this context, the site chosen for the field experiment was the Canadian Forces Station (CFS) Aldergrove. This site provided a secure, grassland location with comparatively good fetch in the direction of the prevailing mesoscale winds as shown in Figure 4.2 and Figure 4.3. CFS Aldergrove is located 100 km east of Vancouver at 49^0 4.5' N, 122^0 28' E, 18 km WNW of Abbotsford. Other nearby townships include Langley, 16 km NW of the site, and Aldergrove located 2 km to the south. Highway #1 is located 2 km north of the site and runs NW-SE. CFS Aldergrove is situated in the middle of the valley away from the immediate influence of tributary valleys and in a region of comparatively simple terrain. The site was approved by the Aviation Authority for tethersonde flights up to 700 m throughout the night.

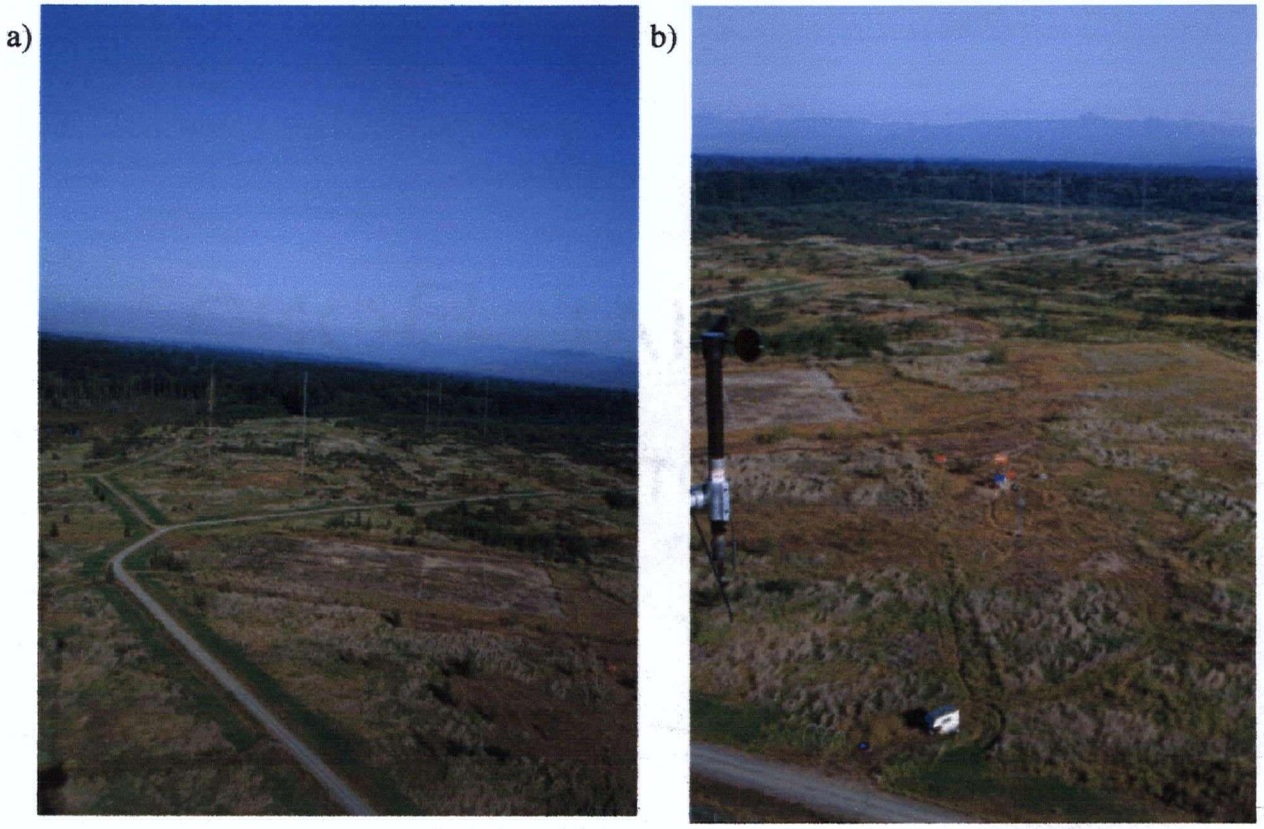

Figure 4.2 Photographs taken from the 80 m tower to show the typical fetch characteristics a) looking WNW and b) looking NNE from the tower

Figure 4.3 Aerial photograph (cropped from Vancouver and the Fraser Valley orthophotos on CD-ROM) to illustrate land-use within an approximately 500 m radius of the 8 m tower (marked with an X)

4.2 Field programme: continuous background monitoring

The field programme commenced on July 1st 1998 and extended until September 5th 1998. Due to the high maintenance and labour requirements of some of the field techniques employed during the field campaign, it was divided into two parts. The first part consisted of continuous, low maintenance, background monitoring over a period of months. The second part component involved several intensive observation periods (IOPs), each lasting 2 - 3 days. During the continuous monitoring phase background meteorological and pollution monitors were set up and data were collected continuously at a low temporal resolution. Turbulence data from a sonic anemometer were recorded throughout this period. Information regarding available and missing data is provided in Appendix 1.

4.2.1 Ozone measurements

In order to establish the local characteristics of the diurnal ozone cycle, a surface monitor was situated at the Aldergrove site throughout phase 1. Mean ozone concentrations were recorded at a height of 4 m at 5 minute intervals using a Monitor Labs 9811 ML analyser located at site 3 in Figure 4.4. The monitor was tested and calibrated to regulatory standards by the GVRD prior to, and following the field season, with minimal drift recorded. The instrument is considered accurate to within 1 ppb in the 0 - 600 ppb range. Data were collected between 1540 PDT July 7– 1035 PDT September 16 1998.

Data from the GVRD monitoring network throughout the LFV were used to supplement the spatial resolution of this data set and facilitate the quantitative analysis of surface advection processes. The monitoring locations of sites used in this study are shown in Figure 4.1.

4.2.2 Radiation and meteorological measurements

Basic meteorological and radiation measurements were made in order to provide background information regarding the local meteorology of the site. The measurement regime is outlined in Table 4.1. Meteorological instruments were mounted on an 8 m tower as shown in Figure 4.5 and Figure 4.7. The tower was located at site 1 in Figure 4.4. Radiation instruments were located on a separate 1 m high structure nearby (site 2 in Figure 4.4). Data were collected at 15 min intervals between 0115 PDT July 3rd and 1400 PDT September 4th 1998.

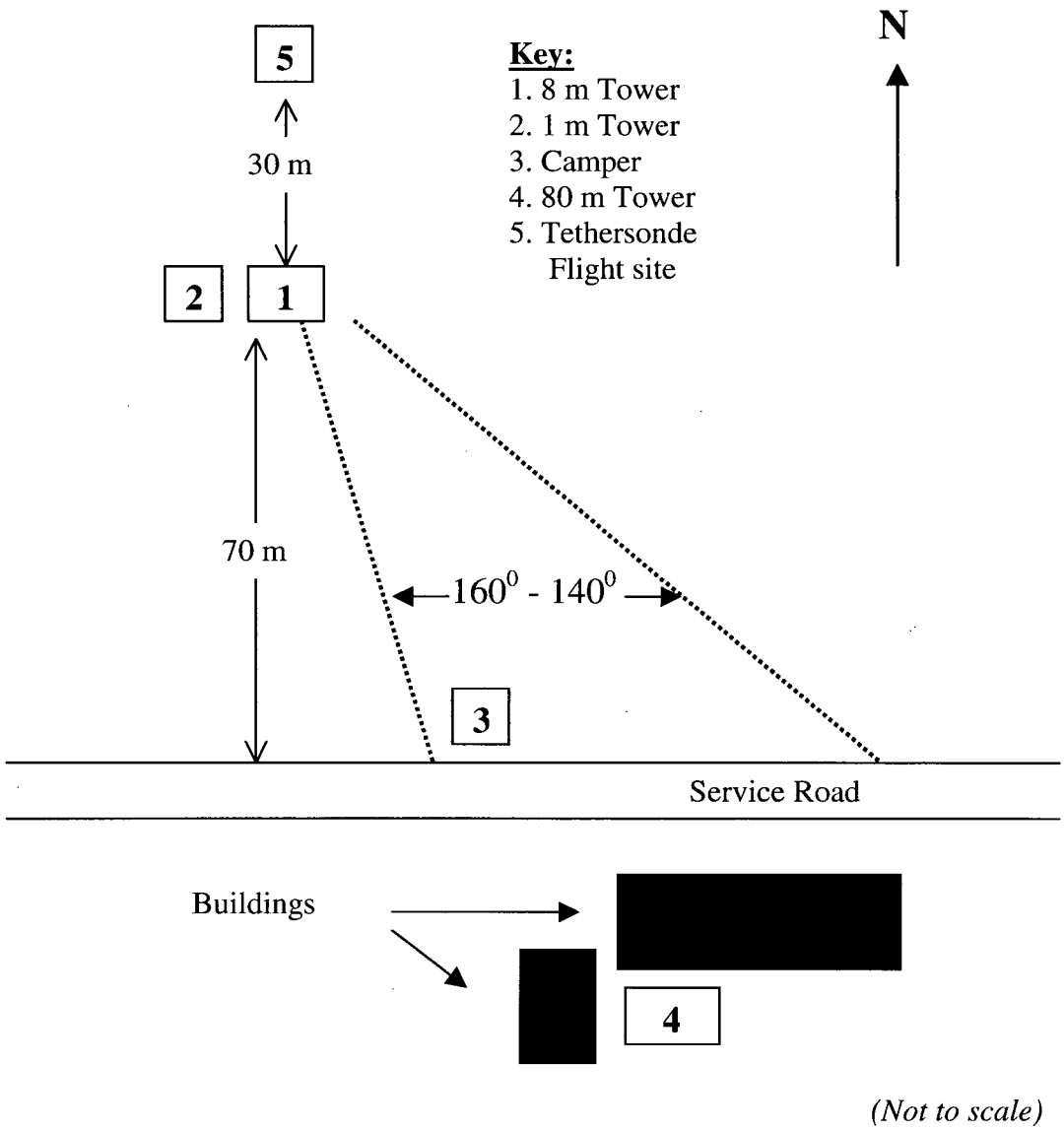

Figure 4.4 Schematic representation of the field site and location of instruments at CFS Aldergrove

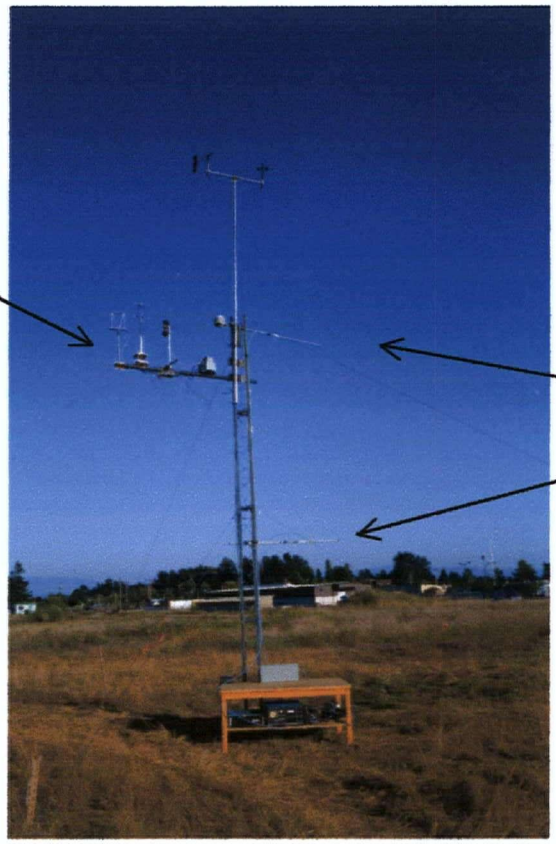

Figure 4.5 Photograph showing the 8 meter tower and instrument set-up

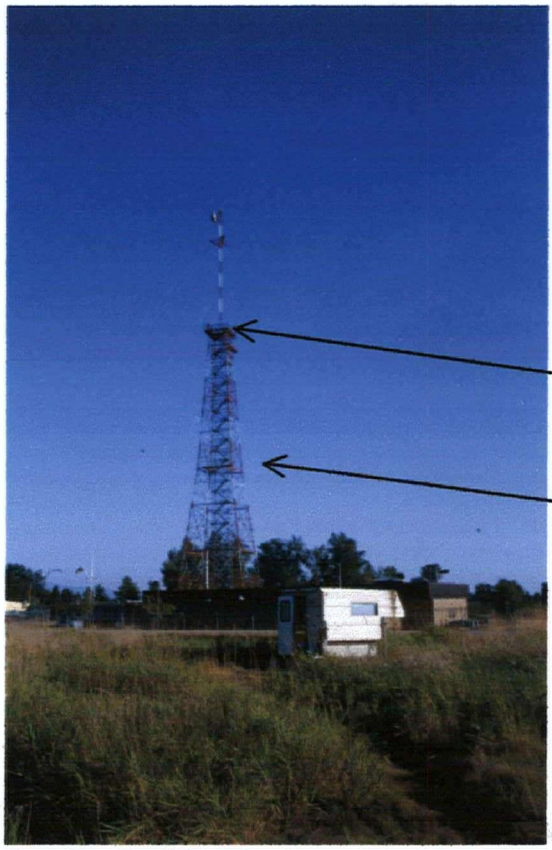

Figure 4.6 Photograph showing the 80 meter tower

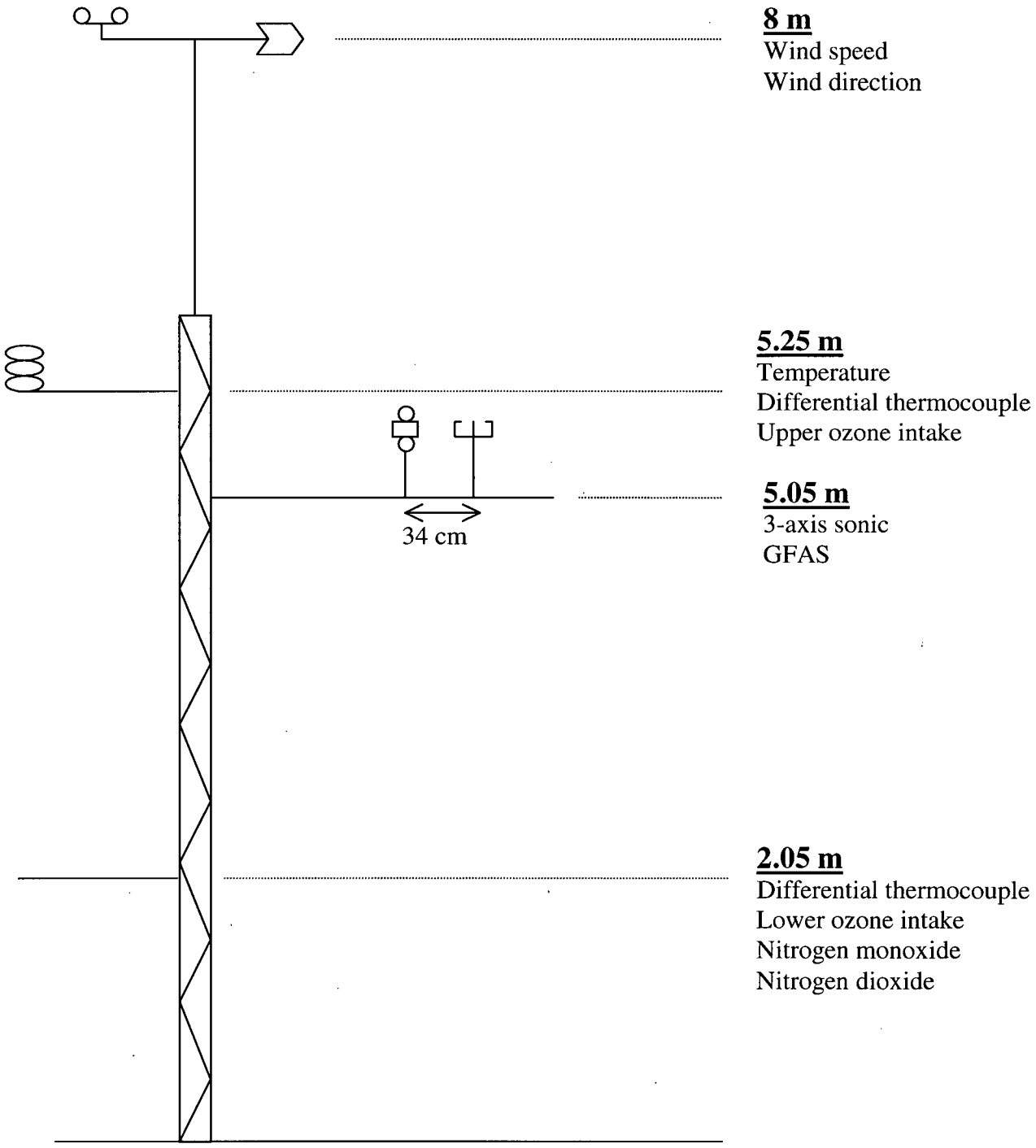

Figure 4.7 Position of meteorological and turbulence instruments on the 8 m tower

Table 4.1 Continuous background measurement regime

Instrument (Units)	**Height**	**Response time**	**Recording interval**
Site 1: 8 m Tower			
Temperature (^{0}C)	8.6 m	10 seconds	15 min
Wind speed (m s^{-1})	8.6 m	10 seconds	15 min
Wind direction (degrees)	8.6 m	10 seconds	15 min
Site 1b: 8 m Tower Micrometeorology			
Sonic anemometer	5.05 m	1/168 second	recorded at 21 Hertz, stored in 30 minute blocks
Site 2: 1 m Tower			
K up (W m^{-2})	1.0 m	10 seconds	15 min
K down (W m^{-2})	1.0 m	10 seconds	15 min
L down (W m^{-2})	1.0 m	10 seconds	15 min
Q* (W m^{-2})	1.0 m	10 seconds	15 min
Site 3: Camper			
Ozone (ppb)	4.0 m	less than 60 seconds	5 min
Site 4: 80 m Tower			
Wind speed (m s^{-1})	30 m/60 m	1 second	5 min
Thermocouple – differential mode (^{0}C)	30 m/60 m	1 second	5 min
Thermocouple – absolute mode (^{0}C)	30 m	1 second	5 min
Gill 3D anemometer (m s^{-1})	60 m	1 second	5 min

4.2.3 Richardson's number

A pre-existing 80 m tall steel-framed triangular tower (the main microwave communications tower), located near the middle of the naval base building, was used in the measurement program (site 4 in Figure 4.4, see also Figure 4.6). Anemometers were mounted at two heights (30 m and 60 m) along with both absolute and differential thermocouples to provide information for the calculation of Richardson numbers within the lowest layers of the stable boundary layer. The mean and standard deviation of the measurements were recorded at 5 minute intervals throughout the main observation period. Data were collected between 0855 PDT July 17th – 1455 PDT September 4th 1998.

4.2.4 Micrometeorology

CFS Aldergrove consists of a high density collection of buildings in the SE corner of the base, surrounded to the north and west by grassland, antennae fields and patchy woodland. A grassland site was chosen for the 8 m tower that supported micrometeorological sensors used to measure surface fluxes. This 0.25 m wide steel-framed triangular lattice tower was positioned 100 m to the NW of the main building area near the centre of a comparatively flat grassland area. Due to the close proximity of the buildings, data collected when the prevailing wind direction was between 140^0 - 160^0 were not used in analysis. The remainder of the fetch to the tower consisted of tall grasses (1.4 m) with occasional small trees and shrubs. The area of tall grasses extended between 500 - 1000 m from the tower, broken in the sector between 30^0 - 140^0 by the presence of a quiet road (22nd Street) at 300 m.

This field site is not 'ideal' from a micrometeorological perspective. The terrain is not perfectly flat nor is the vegetation homogeneous. The close proximity to the buildings, also undesirable from a micrometeorological perspective, was required for power supply purposes. However, the site is representative of land surface conditions in the Lower Fraser Valley and its use is justified by the need for flux measurements at non-ideal locations where there are real air quality problems to be addressed. The data collected are, however, unsuitable for determining universal laws.

A Gill three-axis ultrasonic anemometer (sonic) was utilised to measure the turbulent fluctuations in the wind field (u, v, and w) and temperature. The sonic was mounted on the tower 5.05 m above the ground using a 2 m steel boom (as shown in Figure 4.7) at site 2 in Figure 4.4.

Steel, rather than aluminium, was chosen to limit the effect of vibrations generated by wind. To minimise flow distortion, sensors were mounted on a boom orientated NW-SE along the valley. This orientation aided the collection of data from the wind directions of interest. The power supply and interface unit were located beneath the boom on the tower.

The height of the boom was carefully chosen to reflect the characteristics of the site, fetch and instrument response times (Gusten & Heinrich 1996; Businger 1986). Using the Source Area Model developed by Schmid (1997, 1994), the source area of the instrumented tower was estimated for an instrument height of 5.05 m (Zd ~ 4.05 m). The Roughness parameter was estimated as 0.3 based on tables from Davenport et al. (2000) and Wieringa (1993). The value chosen was at the high end of the range of values given for tall grassland regions interspersed with obstacles to take into consideration the heterogeneous characteristics of the local morphology and the impact of isolated trees on wind flow patterns (Fujita & Wakimoto 1982). Using this model, it was possible to determine that the fetch to the instruments is approximately 350 m when turbulence is fully developed. By comparison, under weakly stable conditions 90% of the flux is derived from an area up to 600 m downwind of the site. Under very stable conditions this distance increases to more than 1500 m and eventually to infinity. Excluding data from wind directions between 140^0 - 160^0, the minimum homogeneous fetch to the tower was 500 m, suggesting a height of 5 m was appropriate. Fujita & Wakimoto (1982) suggest that to avoid interference from localised obstacles up to 2 m in height, anemometers should be mounted at a height of 15 - 20 m. Increasing the boom height above 5 m may have been desirable to reduce the resolution demands on the instruments and limit the influence of the uneven ground surface immediately around the site. However, the boom was kept at 5.05 m in order to avoid difficulties induced by the presence of a woodland area and sewage ponds at distances of more than 500 m from the tower. Under very stable conditions the fetch is not likely to be perfectly representative of grassland conditions, however, given that the site is characteristic of patchy land use patterns in the LFV the resulting fluxes are of value here.

Data from the sonic anemometer were collected at 21 Hertz, transmitted to the camper van located at site one in Figure 4.4, and stored in 30 minute blocks using a Pentium 1 series desktop computer. As this instrument and data logging system were relatively robust, the sonic anemometer was run as a phase 1 instrument throughout the field season from 1230 PDT July 17 - 2400 PDT Sept 3 1998. The instrument responsible for turbulent scale measurements of scalar fluxes required more maintenance and thus was operated only during the IOPs.

4.3 Field programme: intensive observation periods (IOPs)

Several 2 - 3 day intensive observation periods (IOPs) were undertaken. A tethersonde system, high frequency ozone sensors and additional surface pollution monitors were maintained during these periods. IOPs were chosen to coincide with periods when synoptic conditions supported the development of high levels of ozone concentration. Observations were only commenced following several days of anticyclonic conditions, when forecasts predicted the continuance of the synoptic regime. Thus, detailed measurements were made only during periods with high daytime temperatures and clear skies. These conditions promoted the development of mesoscale circulatory systems and strong radiation heat losses at night, thereby enabling the development of a very stable nocturnal boundary layer. Five IOPs were chosen between July and September. In each case, measurements commenced during the afternoon on the first day and ceased around noon on the last day.

Intensive measuring periods were as follows:

July 21 - July 23 1998

July 26 - July 29 1998

August 08 - August 10 1998

August 12 - August 14 1998

August 30 - September 1 1998

4.3.1 Ozone and the oxides of nitrogen

Additional measurements of surface ozone were made at the site during intensive field studies using a switching system designed to record ozone concentrations at two different heights (5.25 m and 2.05 m). This was designed to calculate ozone fluxes using the flux gradient method to provide a back-up for the fast response ozone sensor. The switching system was built using the design of Kellerhals (1996). The two intakes were connected using equal lengths of Teflon tubing and air was pumped towards the ozone monitor to ensure minimal time delay. Mean concentrations were recorded at the two heights during alternate 10 minute intervals. The slightly longer averaging period (compared to the 9811 ML ozone monitor) was chosen to enable the instrument to equilibrate at different concentrations (Kellerhals, 1996). Differential and absolute thermocouples were also mounted at the two heights and data from these were

stored at 10 minute intervals. The two instruments were calibrated at the end of the data collection period.

Although it would have been ideal to collect data for the oxides of nitrogen at the same resolution throughout the measurement period, the sensitive nature of the instrument and its high power demands meant that measurements of nitrogen monoxide and nitrogen dioxide were limited to the last 2 of the intensive monitoring periods. During these periods, measurements were made at the eight metre tower and stored on a second data logger.

Table 4.2 Measurement regime during the IOPs

Instrument (SI Units)	**Height**	**Response time**	**Recording interval**
Site 1b: 8 metre tower micrometeorology			
Ozone (ppb)	5.85 m/2.65 m	10 seconds	10 min
Nitrogen monoxide (ppb)	5.85 m	10 seconds	10 min
Nitrogen dioxide (ppb)	5.85 m	10 seconds	10 min
Thermocouples (^{0}C)	5.85 m/2.65 m	10 seconds	10 min
GFAS ozone sensor (ppb)	5.05 m	~21 Hertz	recorded at 21 Hertz, stored in 30 minute blocks
Site 5: Tethersonde flight site			
Tethersonde Flights	0 - 800 m	less than 10 seconds	~ 2 seconds

4.3.2 Vertical profiles - Tethersonde system

An Atmospheric Instrumentation Research Inc. model tethersonde balloon system, equipped with a radiosonde meteorological sensor and an KZ-ECC ozonesonde (EN-SCI Corporation) was used to document the vertical characteristics of the boundary layer. The

ozonesonde measures ozone concentrations using a potassium iodide electrochemical cell. The changing current within the cell (proportional to the concentration of ozone in the intake sample) is relayed to the main meteorological package and transmitted to a receiver on the ground. The unit requires calibration and testing prior to usage and this was completed on site.

The system (meteorological and ozone sensors) was attached to the 5 m^3 balloon and a 1 km line winch system. Flights were made approximately hourly between 1700 PDT and 1100 PDT throughout the intensive measurement periods. Additional flights were made during the morning and evening transition phases and occasionally during the day to characterise the daytime boundary layer (see table Appendix 2). Flights typically lasted 45 - 60 minutes and ascended to an altitude of between 500 – 800 metres depending on the conditions and flight restrictions imposed by Air Traffic Control. Overall, an ascent rate of between 0.25 - 0.5 m s^{-1} was achieved which, with an instrument response time of 10 seconds, enabled a minimum vertical resolution of 5 metres. Time - height contours of tethersonde data for nights used to calculate contour plots are provided in Appendix 5.

4.3.3 Fast response ozone sensor (GFAS)

Instruments must be capable of resolving the smallest scale turbulence in order to measure the turbulent characteristics of the atmosphere accurately. This is particularly true when considering the transport of a scalar quantity, because if the smallest scales contributing to transport are not resolved the resulting flux will be under-estimated (McMillen 1988). Typically, measurements in the lowest 10 metres of the atmosphere require a 1 second response time in daytime conditions and, as a result of the smaller turbulent length scales, sometimes as short as 0.1 s at night. Thus, a high frequency ozone monitor was required to measure turbulent fluctuations in ozone concentration accurately.

A light weight OS-B-2 high frequency ozonesonde manufactured by Gesellschaft fur angewandte Systemtechnick mnH & Co. (GFAS) was selected for this purpose. The GFAS was mounted at a height of 5.05 m on the 8 m tower as shown in Figure 4.7. Although the instrument was designed as a balloon-borne device for measuring high frequency fluctuations in ozone concentration in the troposphere and stratosphere, it was easily adapted to make continuous measurements from a tower. Ozone concentration is measured by passing a sample of air over a chemiluminescent target. Light is emitted from the target when ozone molecules are present, the intensity of which is directly proportional to the ozone concentration.

The instrument has an accuracy level of +/- 5% which corresponds to about 2 ppb for 45 ppb background (Gusten & Heinrich 1996). A miniature fan ensures a continuous flow rate of 100 l min^{-1} over the sensor. At this rate the sensor is considered to have a '90% response time significantly better than 0.1s and a lower detection limit of 50 ppt' (Gusten & Heinrich 1996). The effects of atmospheric reactions between ozone and the oxides of nitrogen (NO_x) on the turbulence data are expected to be minimal during the daytime, though at night these may become more important under stable conditions (Droppo 1985). However, the error is considered to be less than 10% in a non-urban environment (Gusten & Heinrich 1996).

Pre-ozonisation of the unit was required to activate the target, and this was conducted using the parent VM-K-2 unit on site. As the unit measures the relative amount of ozone in the air and the sensitivity of the dye decays with time, the unit must be calibrated continuously. This was done by recording the voltage output from the GFAS and calibrating the data with ozone concentrations recorded by the Monitor Labs 9811 ML at 5 minute intervals. Tests indicated that 30 minute calibration periods were sufficient to maintain a consistent calibration of the data. The 21 Hertz data recorded by the GFAS were recorded in 30 minute blocks using an automated program and stored in binary format on the computer.

4.3.4 Co-location of turbulence instruments

Given that two high frequency sensors were required to simultaneously measure different atmospheric variables the relative position and mounting of instruments on the boom became an important issue. Ideally trace gas sensors would occupy the same point in space. Some studies have attempted to achieve this by using a Teflon tube intake to connect the sonic anemometer with the GFAS OS-B-2 instrument located at a different site. However, this can result in the introduction of a significant time lag. For example, Gusten & Heinrich (1996) positioned a GFAS below a sonic anemometer and used a Teflon tube of 0.5 m length to connect the two sites, resulting in a 0.1 s lag.

An alternative approach is to locate the instruments close together using a configuration to minimise flow distortions. A large distance between the sensors minimises flow distortion, however, this results in a greater systematic error in flux measurement. This is particularly true for small scale turbulence and sensors mounted close to the ground (Kristensen et al. 1997; Lee & Black 1994). There is controversy in the literature over the exact impact of instrument separation on flux measurements and concerning the relative merits of vertical versus horizontal

displacement. This is largely because the effects are dependent on the height of the sensors, distance apart, shape, their orientation with respect to wind direction and the scale of the turbulence (stability) (Lee & Black 1994). For example, a 0.4 – 0.6 m separation effectively acts as a low band pass filtering system (Foken & Wichura 1996). These effects can be corrected for using cospectral analysis, although the correction may be significant for instruments mounted at heights of less than 5 m or under stable conditions (Foken & Wichura 1996).

To minimise such errors, the instruments were mounted 0.34 m apart in the horizontal plane with the top of the GFAS system located 0.1 m below the main sensor location for the sonic. As the GFAS system is 0.16 x 0.19 x 0.16 m this meant that the ratio between separation distance to the height of the sensors is within acceptable (5%) limits (Lee & Black 1994). Further, even allowing for the 'pancake' shape of eddies in the NBL (generated by strong vertical stability) the two instruments should be measuring the same eddy in most cases.

4.4 Data quality control techniques

During the field campaign, 2275 blocks of turbulence data, each 30 minutes in length, were recorded. Of these, 107 were contaminated and had to be discarded. The remaining 2145 files were subject to data quality control checks. The characteristics of the site, conditions of the field experiment and the type of data analysis determine the appropriate quality control procedures applied to turbulent data sets. To date there is no single categorical method for distinguishing between errors in the data set (caused by instrumental error or poor field design) and erratic but plausible data generated by real physical mechanisms (Vickers & Mahrt 1997). However, consistent data quality control procedures are fundamental to accurate data analysis and to facilitate inter-comparisons of results between data sets collected at different times of the day and at different places. Foken & Wichura (1996) advocate the definition of a special filter for each data set to accept and reject files. These methods require the arbitrary choice of thresholds and individual (potentially human biased) inspection of records. The values chosen for data exclusion are critical and can result in introducing further bias into the data sets. For example, the elimination of records that fail the tests may systematically exclude high pressure, low wind speed conditions and generate a bias towards strong wind cases. If left unacknowledged this can result in sampling errors, or the inappropriate sub-selection of data. Consequently, the following criteria were selected with care to ensure that the data were valid whilst minimising the introduction of human and experimental bias into the data sets.

4.4.1 Testing for instrument alignment

Taylor's hypothesis cannot be applied under heterogeneous conditions. Errors in instrument alignment and heterogeneity in the surface can result in apparent non-stationarities in the data record. Tilt errors must be minimised because these can account for 8 - 100% of the flux measurements (McMillen 1988). Given the slight variations in surface morphology, careful consideration was given to the alignment of the instruments. Mean vertical velocity values provide a good indication of instrument alignment in the horizontal plane. If the instrument is perfectly orientated with respect to the surface, then the average vertical velocity should equal zero. Analysis of the vertical velocity data throughout the field experiment showed only small deviations from zero. The mean vertical velocity for data set was -0.005 m s^{-1} with a standard deviation of 0.03 m s^{-1}. Consistent trends in the error were not detectable. Complex adjustments can be made to data sets that are not aligned with the surface angle. However, given that further errors can be incurred through the correction procedures, the slight imperfections in the data set did not warrant correction.

4.4.2 Ensuring adequate fetch

If the surface area of the footprint is heterogeneous, horizontal advection or vertical flux divergence may occur, rendering the flux measurements inaccurate. For this reason data were excluded from the analysis when the prevailing wind direction was between 140^0 – 160^0 due to the presence of buildings in the fetch. Data with wind directions from 178 - 182^0 were also excluded because the boom was mounted on the northern side of the tower and southerly winds passed through the tower before reaching the instrument. The wind was deemed to be from these directions if either the 15 minute average wind direction recorded by the wind vane or more than 6 minutes out of the 30 minutes of the sonic anemometer trace recorded winds from these directions. Of the 2145 data files 330 were eliminated due to fetch considerations. See Appendix 3 for information regarding sonic wind direction.

4.4.3 Flux calculation: length of data record

The length of the data record chosen for flux calculation represents a compromise between the need for statistically valid sampling of the eddies and the need to retain stationarity within the data record. To determine the time required to ensure that the entire flux was captured, flux calculations were compared using time intervals between 2 and 30 minutes and

verified using the Ogive function as shown in Figure 4.8 for heat flux data. This test was run using data which had been screened for non-stationarities (see 4.4.4). The results demonstrated that while there was little difference between the 15 minute and 30 minute values for the daytime data there was a small difference in the night-time case. Similar results were observed in the ozone flux data. A 30 minute interval was ultimately chosen, which facilitated comparison with a range of other studies. Periods longer than 30 minutes incur serious error as a result of the capture of non-stationarities and thus a time period longer than this was not considered for flux calculation.

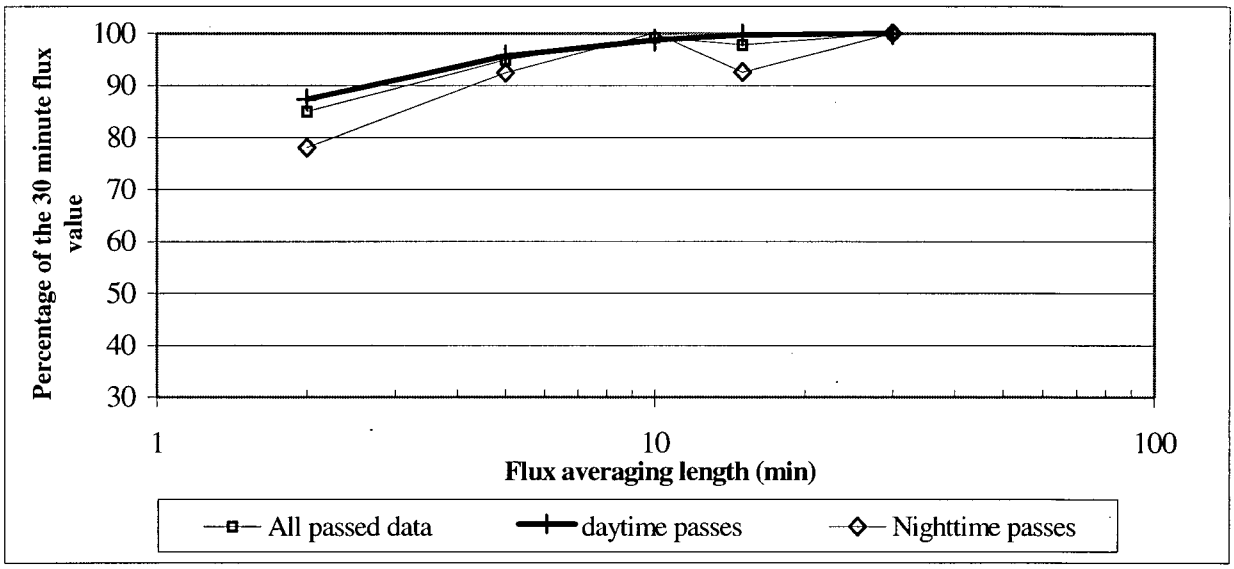

Figure 4.8 Application of the Ogive function to determine the minimum time period suitable for flux averaging

4.4.4 Testing for stationarity

Statistical stationarity of the data set was tested using both the 'runs test' proposed by Bendat & Piersol (1986) and the methodology suggested by Foken & Wichura (1996). The latter test is less statistically rigorous and more suited to data from experimental field sites where conditions are less than ideal.

The 'runs test' was conducted by dividing each 30 minute data set into 1.5 minute segments. The median value of the 20 files was then compared to the mean and variance of each 1.5 minute section. A run was accepted when successive values were consistently above or below the median value. A Chi-square statistic determined that if six or more runs occurred in

the test, the data was considered randomly distributed at the 95% confidence level. Due to the loss in sensitivity of the GFAS with time and the calibration method used, this test could not be used on the high frequency ozone data.

The test provided by Foken & Wichura (1996) involved dividing the 30 minute (~6000 data point) time series into six blocks. The covariance of these individual segments is then compared to the covariance of the 30 minute block. If there is a difference of less than 30% between the covariance determined by the two approaches then the data are considered stationary. The covariance for individual segments (N/M) = 6 is determined using Equation 4.1. The total covariance is determined using Equation 4.2 (Foken & Wichura 1996).

$$\overline{x'_i x'_j} = \frac{1}{N/M}\left[\sum_{l=1}^{N/M} \overline{x'_{il} x'_{jl}}\right] \tag{4.1}$$

$$\overline{x'_i x'_j} = \frac{1}{N-1}\left[\sum_{l=1}^{N/M}\sum_{k=1}^{M} x_{ikl} \cdot x_{jkl} - \frac{1}{N}\left(\sum_{l=1}^{N/M}\sum_{k=1}^{M} x_{ikl}\right)\cdot\left(\sum_{l=1}^{N/M}\sum_{k=1}^{M} x_{jkl}\right)\right] \tag{4.2}$$

Results of the tests (shown in Table 4.3) indicate that, as expected, the vertical velocity measurements are more stationary than the temperature data. Comparison of the two techniques shows that whilst the Foken and Wichura test allowed 245 more passes than the 'runs test', there was no substantial difference in classification between the two techniques. Not surprisingly, only 30% of the data records collected during the night-time period were classified as stationary, and more than 90% of the records collected between 1100 - 1800 PDT were viable (as shown in Figure 4.9). The total number of records collected for the ozone data was considerably lower than for the heat flux data because the GFAS was only operated during IOPs. This instrument was considerably more sensitive to external conditions which may account, in part, for the increased failure rate of the data records. Ozone concentrations (like temperature) show a marked diurnal periodicity, further accounting for the reduced stationarity of the data set.

Table 4.3 Results of the stationarity tests

	Runs test for vertical velocity	**Runs test for temperature**	**Runs test for vertical velocity and temperature**	**Foken and Wichura test on heat flux**	**Foken and Wichura test on ozone flux**
PASS	1757	1302	1145	1390	164
FAIL	388	843	1000	747	295

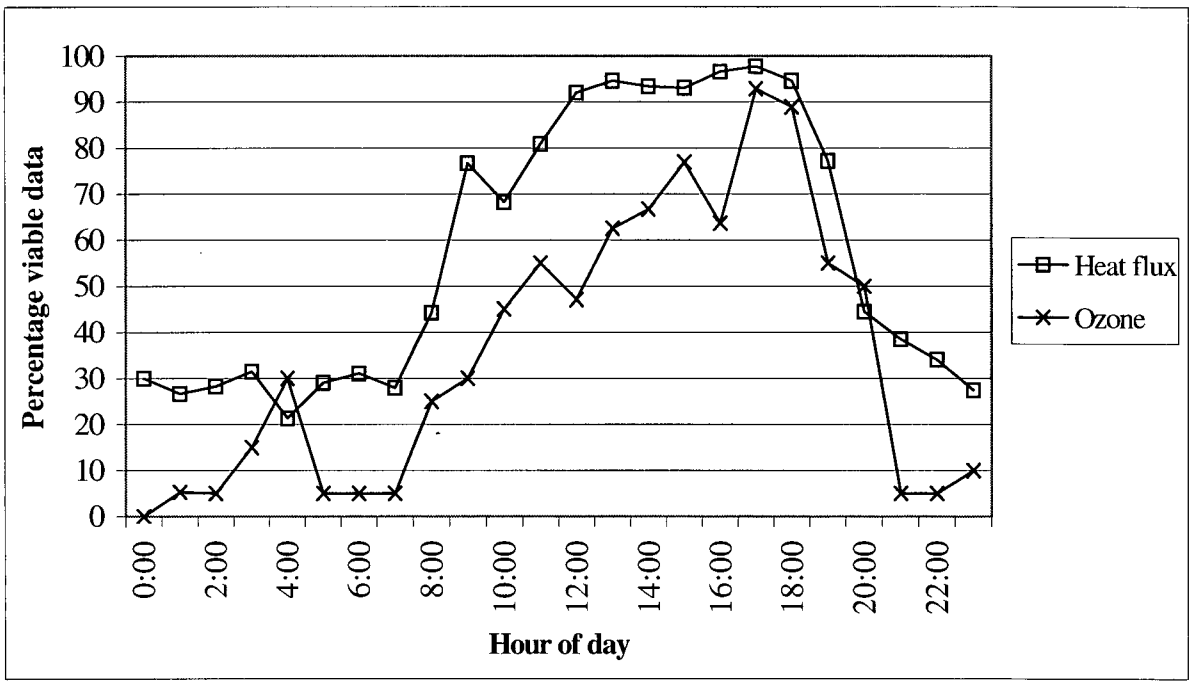

Figure 4.9 Percentage of heat flux data records that passed both wind tests, and non-stationarity tests, by hour of the day

4.4.5 Instrumental noise and lags in the data set

Noise in the data sets is most commonly associated with instrument error, although isolated physical causes such as tower movement, electrical or physical interference are also possible sources. High frequency noise is particularly a characteristic of all trace gas sensors when operated near their limits (Hicks & McMillen 1988). It is very difficult to isolate 'real' spikes from instrumental noise in the data set and this can lead to contamination of the signal. Signals with serious contamination errors cannot be processed as the data sets could not be read

by simple computer programs. These accounted for the 107 records discarded at the start. The remaining data records were checked by eye for invalid maximum or minimum values and unusual characteristics.

The sensitivity of the calculated flux to a lag time between the sonic anemometer and the scalar micrometeorological instrument can be significant (McMillen 1988). A systematic lag may result from instrumental separation or the time period required to test a sample for a particular compound, and this results in an under-estimate of fluxes (Vickers & Mahrt 1997). However, unless a systematic lag can be identified it is not possible to correct for it. The presence of a lag between the sonic and GFAS data set was tested for by identifying successive correlation coefficients between the two data sets, using an incremental offset between zero and 10 seconds.

Of the 144 files that passed the wind direction and Foken and Wichura tests, 17 demonstrated a presence of a lag in the maximum correlation coefficients between w' and O_3'. There was no consistency in the value of the lag which ranged between 0.01 seconds - 20 seconds. Further, the lag results were clustered towards the 0.01 end of the range. Thus it was deemed that the GFAS has a negligible lagtime.

4.4.6 Integral turbulence parameters

During the last five years integral turbulence statistics (based on flux-variance similarity), together with the tests outlined above, have been used to determine data quality (Foken & Wichura 1996). These statistics identify how well developed the turbulence is based on the similarity theory of turbulent fluctuations (Foken & Wichura 1996). From the results of these tests errors within the data set, associated with a range of instrumental or site difficulties (such as inhomogeneous terrain), can be identified. For example, mechanical turbulence induced by an obstacle or sensor results in increased values compared to the model. Higher values can also be associated with heterogeneity of surface temperature and moisture.

The integral characteristics of the wind are defined in Equation 4.3 and the integral temperature characteristics are defined in Equation 4.4 (Foken & Wichura 1996, 95). Values for these parameters are given in Foken & Wichura (1996) for a range of stabilities. The quality of the data is considered good if the values calculated from these equations are within 20 - 30% of the measured values.

$$\frac{\sigma_w}{u_*} = a_1 \cdot [\psi_m(z/L)]^{b_1} \tag{4.3}$$

$$\frac{\sigma_T}{T_*} = a_2 \cdot [(z/L) \cdot \psi_h(z/L)]^{b_2} \tag{4.4}$$

$$\psi_m = a(1 + 3|(z - d)/L|)^b \tag{4.5}$$

where:

L	Monin Obukhov length scale
z	height of measurement
a_x	constant
b_x	constant
σ_w	standard deviation of vertical velocity
u^*	friction velocity
σ_T	standard deviation of temperature
T^*	temperature scale
ψ_m	dimensionless wind shear
ψ_h	dimensionless temperature gradient
d	zero-plane displacement length

The statistical behaviour of vertical velocity is of particular interest here, due to the heterogeneous characteristics of the land surface morphology immediately around the tower. A commonly accepted form of the equation for the dimensionless vertical velocity wind shear is given in Equation 4.3 (Blanken et al.1998).

As shown in Figure 4.10 the data collected in this field experiment appears to correspond well with the integral statistics calculated using Equation 4.5 during both unstable and stable conditions.

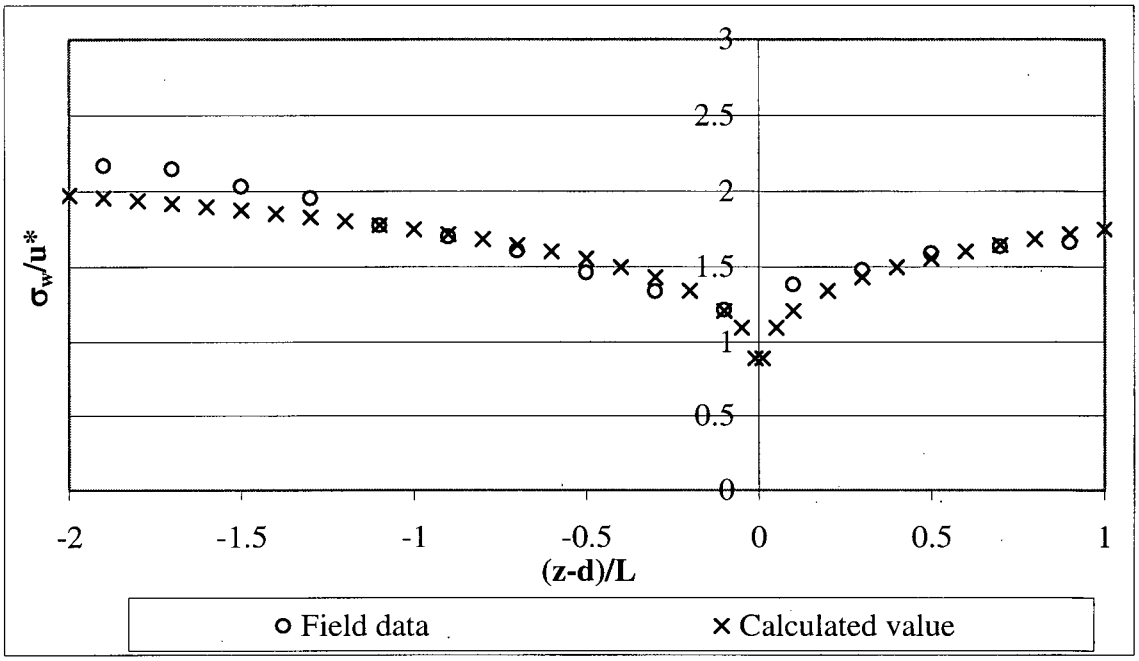

Figure 4.10 Comparison between expected and calculated integral statistics for σ_w/u^*

This suggests that measurements were primarily made at heights within the surface layer (Blanken et al. 1998). Under very stable conditions ((z-d)/L > 1.0) this is no longer likely to be true as the limits of free convection are reached and σ_w/u^* is no longer an appropriate scaling for surface layers (Blanken et al. 1998). Nevertheless these results indicate that the data are of good quality and there were no serious systematic problems in the instrument set up or data collection procedure.

4.4.7 Friction velocity

Many authors use a minimum value of friction velocity (u*) as a means of data quality control. This is because low values of u* potentially indicate that the turbulence is not fully developed, resulting in underestimation of the flux. However, the minimum u^* is dependent on the height of measurement (Blanken et al. 1998) and a variety of different criteria have been used in the literature. There is also a danger that the choice of u* value could result in eliminating significant fractions of data that represent low wind speeds, producing a biased data set. This can be avoided by calculating a critical value for u* determined by the flux associated with each value of u*. The analysis is done only based on night-time data because under-estimation can also result from low levels of available energy (Blanken et al. 1998).

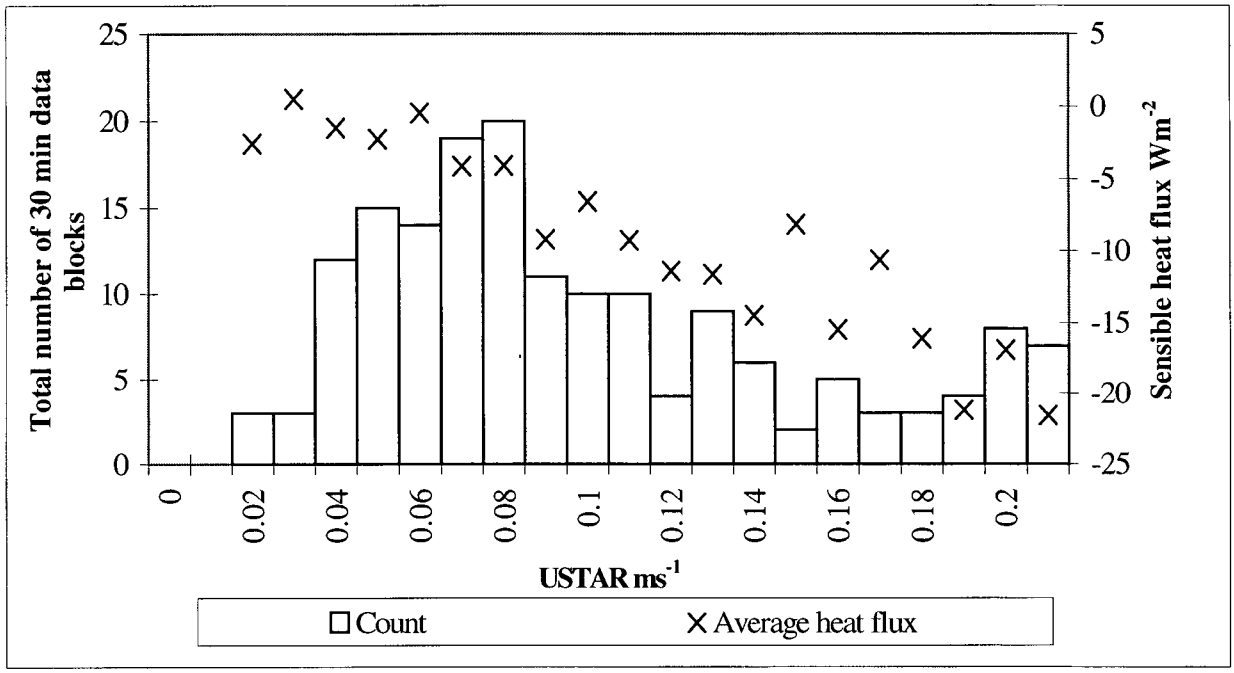

Figure 4.11 The relationship between heat flux and friction velocity for nocturnal data

As shown in Figure 4.11, it is difficult to discern a suitable cut-off value from the data set. Given that all of the data were collected during anti-cyclonic conditions and the data of primary interest are nocturnal (hence friction velocities of less than 0.2 m s^{-1} are common), this data quality check was not an appropriate tool for the field experiment.

4.5 Summary

A variety of data sets were collected at CFS Aldergrove during the summer of 1998 to provide information about the specific meteorological characteristics of the boundary layer and the three dimensional distribution of ozone. Although the location chosen was not 'ideal' in micrometeorological terms, the data are shown to be reliable within expected parameters. Data quality control tests highlight the significance of the problem of non-stationarity in nocturnal data sets, with only 30% of the original data passing standard tests for non-stationarity. These results demonstrate a pressing need for the development of alternative analytical tools, which are less sensitive to non-stationarities in the data set, to calculate reliable flux estimates in the nocturnal boundary layer. In the following analysis, only time series which fail to meet fetch requirements are excluded, however, non-stationary data sets are flagged for caution.

Chapter 5: Ozone concentrations in the nocturnal boundary layer

5.1 Introduction

This chapter provides a detailed description of the anatomy of spikes in surface ozone concentration observed at CFS Aldergrove. These are situated within the context of temporal variations of ozone concentration with height and the meteorological characteristics of the nocturnal boundary layer. The chapter commences with a discussion of the mean diurnal cycle in surface ozone concentrations observed during anti-cyclonic conditions. Temporal variations in fumigation, advection, deposition and chemical titration processes are discussed in light of the characteristics of the diurnal ozone budget. Data for individual nights are then assessed to determine the magnitude, frequency and duration of periods of increased ozone concentration ('ozone spikes') observed at the surface. A spatial context for these ozone spikes is then established through the examination of ozone data from a number of sites throughout the Lower Fraser Valley. This is primarily intended to ascertain whether this is a local or valley-wide phenomenon and to provide an insight into the temporal and spatial patterns observed during the field season. The analysis also examines the role of surface chemistry, particularly local sources of nitrogen monoxide (NO), in determining incidence and specific morphology of ozone spikes at the surface. A detailed climatology of these temporally sporadic events is beyond the scope of this thesis.

The second half of the chapter examines the hypothesis that these events result from vertical mixing processes operating in the nocturnal boundary layer. This is achieved through a detailed examination of the vertical distribution of ozone and meteorological characteristics of the nocturnal boundary layer. Several potential causes of turbulence are identified and the qualitative relationships between them and the existence of surface ozone spikes identified during the IOPs. The aim of this chapter is to provide a qualitative assessment of the characteristics and processes operating in the very stable NBL, and their relevance to observed increases in ozone concentration at the surface. A more quantitative analysis of these phenomena is provided in Chapters 6 and 7.

5.2 Temporal variations in ozone concentration

Surface ozone data collected during the 11 days of intensive field measurements show distinct diurnal cycles in concentration (Figure 5.1). This variation in ozone concentration with time is a product of the complex interplay between chemical production and titration, deposition, and vertical and horizontal mixing processes. The characteristics of the cycle identified are very similar to results from studies within the Lower Fraser Valley (Pryor & Steyn 1995) and other semi-rural locations downwind of urban areas (e.g. Kleinman et al. 1994).

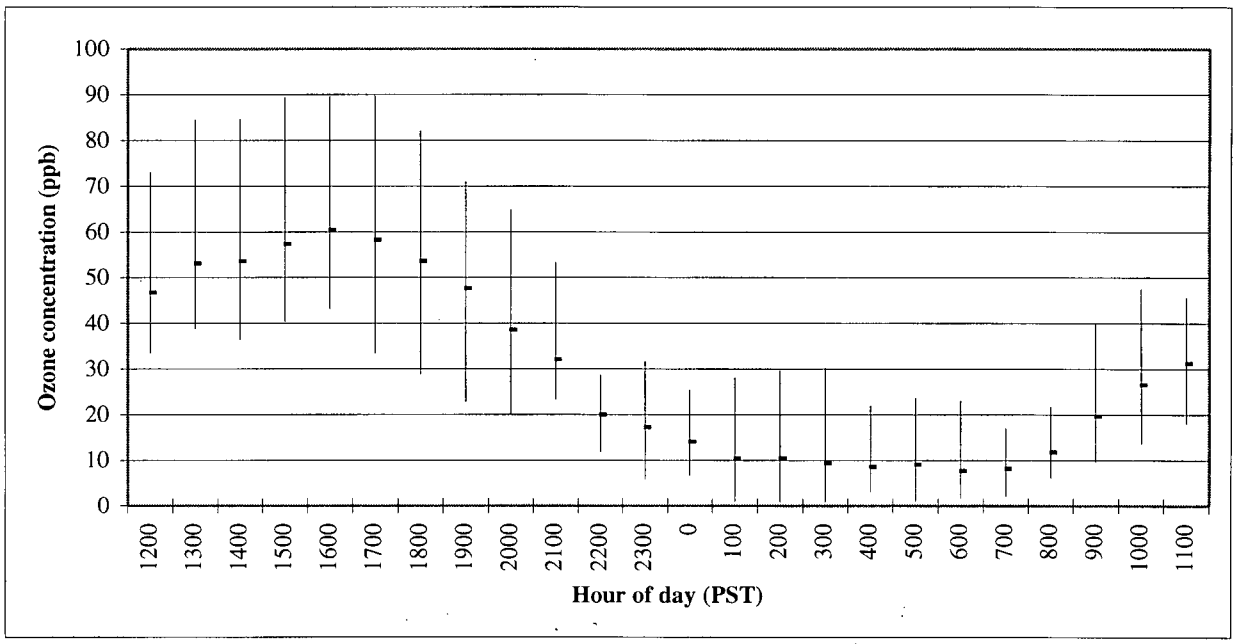

Figure 5.1 Mean diurnal cycle in ozone concentrations observed during the 11 days of intensive field studies during July and August 1998 at CFS Aldergrove (maximum and minimum recorded values also shown)

Following the onset of vertical mixing at around 0700 PDT until 1200 PDT ozone concentrations can be seen to increase steadily at a rate of 1.7 ppb h^{-1}. After 1200 PDT concentrations continue to increase but at a slower rate of 0.5 ppb h^{-1} until 1700 PDT. These increases are likely to be the product of both in-situ production of ozone and transport of ozone to the site. The increased rate of ozone accumulation observed in the early morning hours may be accounted for, at least in part, by enhanced rates of fumigation of ozone to the surface (Kleinman et al. 1994; Zhang & Rao 2000). As the depth of the mixed layer increases, ozone from the previous day(s) emissions stored in the residual layer is entrained into the growing

mixed layer and transported to the surface. At other locations, modelling exercises have shown that this process may account for more than 50% of the observed daily maximum ozone concentration (Neu et al. 1994) and have a significant impact on the diurnal ozone budget.

During the early morning phase, rates of ozone production are also likely to be comparatively high. Concentrations of NO_2 typically increase overnight as ozone reacts with local sources of NO providing a reservoir of NO_2 in the stable layer. Although the rate of photolysis may be limited for up to two hours following sunrise by lower levels of ultra-violet light and lower temperatures (compared to the early afternoon period), the reservoir of NO_2 ensures that ozone can be rapidly produced both locally and throughout the valley during the early morning hours. This effect is visible in the NO_2 data for August 31st - September 1st as shown in Figure 5.2.

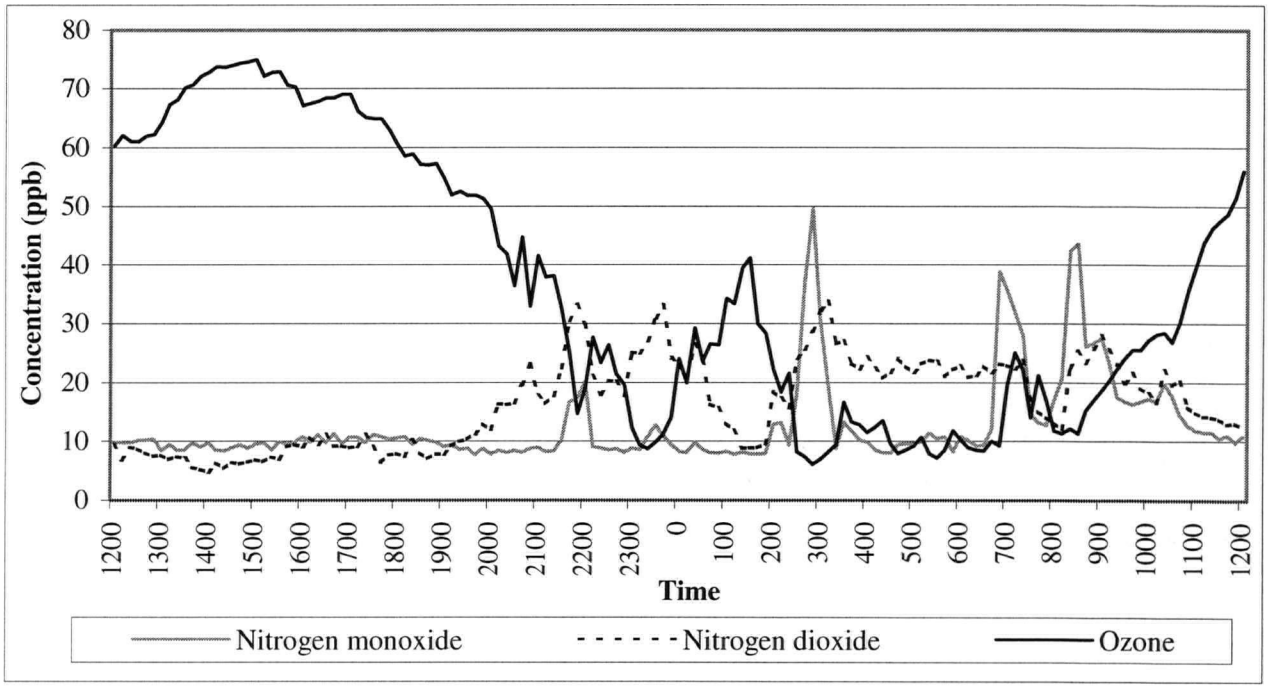

Figure 5.2 Variations in nitrogen dioxide, nitrogen monoxide and ozone concentrations with time between 1200 PDT 31st August 1998 and 1200 PDT 1st September 1998

Later in the day the rate of growth of the mixed layer is slowed considerably as the depth of the boundary layer reaches that of the previous day. When this occurs (in the absence of elevated layers of ozone in the free atmosphere (McKendry & Lundgren 2000)), lower ozone

concentrations are mixed to the surface and vertical mixing processes may become less significant in determining the ozone budget.

The peak in ozone concentrations occurs at 1700 PDT, indicating the potential importance of ozone and precursor advection at this time (Greenhut et al. 1995). Ozone, volatile organic compounds and NO_2 from the urban plume may become embedded in up-valley flows and advected to the site. Advection of ozone within mesoscale flows has been shown to play a significant role in determining local variations in diurnal ozone cycles in regions of complex terrain (Martin et al. 1991; McElroy & Smith 1986). However, the dominance of advection processes may only become apparent in the late afternoon when fumigation mechanisms have ceased and chemical production is slowed as a chemical equilibrium is reached between the oxides of nitrogen and ozone concentrations.

Advection processes may also explain the absence of an early afternoon decrease in concentrations generated by dynamic increases in boundary layer depth (and hence volume) typically observed in rural locations (Kleinman et al. 1994; Kelly et al. 1984). Alternatively, synoptic scale subsidence may inhibit boundary layer growth within the valley. This limits the volume of air with low ozone concentrations incorporated into the mixed layer, and the total volume of the mixed layer, reducing the dilution effect.

From 1800 - 0000 PDT ozone concentrations rapidly decrease at the surface at an average rate of -1.9 ppb h^{-1}. This probably reflects both the role of depositional mechanisms and chemical titration with NO (Garland & Derwent 1979; Banta et al. 1997). Between 0000 - 0600 PDT concentrations remain low, decreasing at a slower rate of -0.4 ppb h^{-1}. The lower rate of ozone decay in this latter period may be a result of lower ozone concentrations and reduced NO emissions after the evening rush hour. However, dewfall is also a common occurrence in the latter part of the night. Given that ozone has limited solubility in water this may slow deposition rates. Although CFS Aldergrove is predominantly rural (thus with minimal local sources of NO), the proximity of Highway #1 to the site may account for the intermittent increases in NO concentrations shown in Figure 5.2. This effect is particularly noticeable during the early morning rush hour when the shallow boundary layer depth and absence of ozone, and hence lack of chemical conversion to NO_2, enables the build up of NO at the surface (Berkowitz et al. 2000).

The reduced rate of ozone depletion in the latter part of the night may also be a result of the temporal averaging procedure which masks the presence of sporadic increases in ozone concentration observed in the data for each individual night (as shown in Figure 5.2 between 0000 - 0300 PDT September 1st 1998). These increases are not reflected in the average data set as the timing, frequency and magnitude of events varies significantly between nights.

Whilst insufficient data were collected during the field campaign to determine the characteristics of the diurnal cycles of NO_2 and NO, some clear patterns emerged. NO concentrations typically showed little evidence of a diurnal cycle, but were characterised by sudden peaks in concentration during the night. These spikes were out of phase with periods of increased ozone concentration (Figure 5.2). By comparison, NO_2 concentrations were typically higher during the night and lower during the day and a decrease in NO_2 concentrations was frequently observed simultaneously with periods of increased ozone concentration during the night (Figure 5.2). Given the absence of any common chemical or depositional removal mechanisms of NO_2 in the NBL, this decrease in concentration suggests that the transport process responsible for increased ozone concentrations - whether horizontal advection or vertical transport - results in the mixing of the pollutants through a larger volume of the boundary layer, diluting the concentrations of pollutants trapped within the stable layers. This is further supported by the increase in NO_2 concentrations recorded once ozone concentrations start to decrease and NO concentrations increase, as any remaining ozone is rapidly removed from the system forming NO_2.

5.3 Nocturnal spikes in ozone concentration at CFS Aldergrove

Preliminary analysis of the five minute mean ozone concentrations revealed isolated periods of increased ozone concentration which occurred well after sunset. However, the marked temporal variability of these events rendered it impossible to ascertain their significance using data sets averaged over several days. Thus each night was examined in detail to determine the magnitude, frequency and duration of ozone 'spikes' in the data set.

In order to objectively assess the presence of nocturnal increases in ozone concentration the following criteria were developed to identify ozone 'spikes' in the data set. These criteria included the observation of a (temporarily localised) minimum increase in ozone concentration of 5 ppb, sustained for at least 15 minutes and followed by a well defined decrease of at least 5 ppb at the end of the episode. This was to ensure that the increases in concentration were both

significant (given the sensitivity of the ozone analyser) and temporally localised. This definition excluded from analysis spikes that occurred during the morning and evening transition periods. These were difficult to isolate from the general trends in ozone concentration.

Figure 5.3 and Table 5.1 demonstrate the wide variety of ozone spikes recorded during the 11 nights of the IOPs. Figure 5.3 illustrates the temporal variation in ozone concentrations during four nights when the characteristics of the ozone spikes were particularly difficult to objectively isolate. These examples show that identifying the temporal boundaries of the ozone spikes was not always straight forward due to the difficulty of establishing a mean rate of ozone decay. Local variations in the spatial and temporal rates of deposition, chemical titration and surface advection result in different baseline decay rates for each night. For example, between 2130 and 2330 PDT on August 8th 1998 (Figure 5.3c), an increase in ozone concentration can be identified which could be classified as an ozone spike. However, this spike (and others like it) were not included in the analysis due to the difficulty of identifying the baseline trend in ozone concentrations during the hours immediately preceding and following the event. In this case, it could be argued that between 2000 and 2200 PDT a negative spike in ozone concentration was observed. Such a pattern is physically possible and could be the result of the either the advection or vertical mixing of air containing lower ozone concentrations (and/or higher NO concentrations to the site). In the absence of a more detailed vertical and horizontal data set it is impossible to distinguish between these two mechanisms for NO. If such a negative spike exists then the corresponding positive spike identified would represent a return to the baseline conditions, probably as a result of advection processes.

Thus it could be argued that the peaks of positive ozone spikes represent the baseline trend whilst the lower concentrations on either side (negative spikes), a deviation from the norm. This scenario is however most unlikely to occur given the prevalence of depositional profiles near the surface throughout the night in the Lower Fraser Valley, and persistence of higher ozone concentrations aloft. These surface patterns are documented throughout the LFV in section 5.4 and in the vertical domain for the field site in section 5.5.3. Further, analysis of individual time series using moving average statistics strongly supports the identification of positive rather than negative spikes.

Thus, given that this study is motivated by an interest in localised increases in ozone concentration, negative spikes in ozone concentration are not considered in detail. However, in

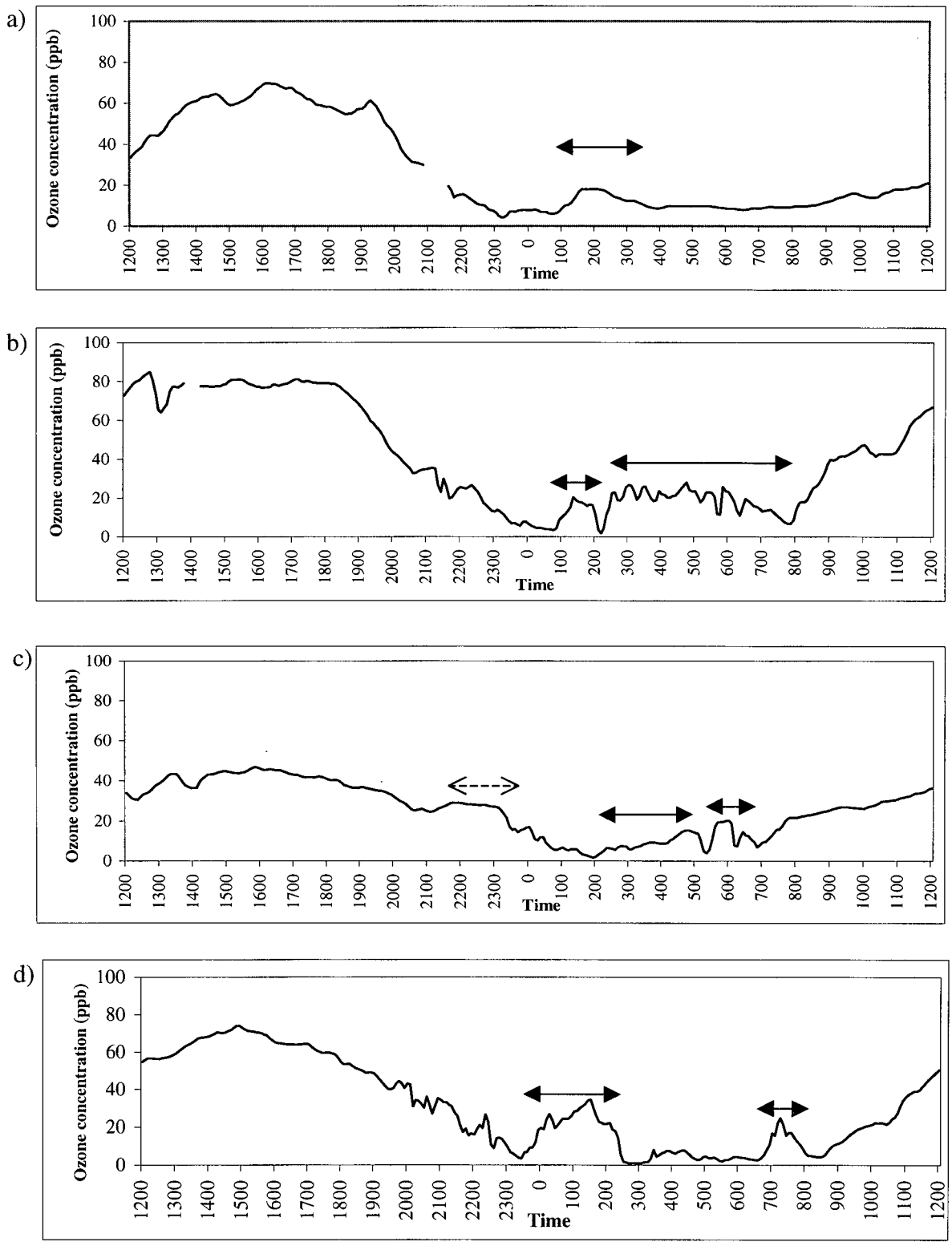

Figure 5.3 Identification of ozone spikes from surface ozone data recorded between 1200 PDT - 1200 PDT at CFS Aldergrove on a) July 22nd - 23rd 1998, b) July 26th - 27th 1998, c)August 8th - 9th 1998 and d) August 31st - September 1st 1998 (Arrows denote duration of spike identified, hash line indicates spike excluded - see text.)

Table 5.1 Summary of ozone spikes observed at CFS Aldergrove during the IOPs, 1998

Date	Number of spikes per night	Start time (PDT)	Duration	Start concentration (ppb)	Time of Max	Max concentration (ppb)	Increase in ozone (ppb)	Increase in temperature ^{0}C	Rate of temperature change ^{0}C hr^{-1}
July 21 - 22	0	-	-	-	-	-	-		
July 22 - 23	1	0100	3 hr 15 min	6	0215	18	12	-0.7	-0.56*
July 26 - 27	2	0050	1 hr 20 min	4.3	0125	18.8	14.5	-0.2	-0.34*
		0215	5 hr 45 min	5.6	0500	25.2	19.6	-0.5	-0.18*
July 27 -28	3	0050	3 hr 10 min	18.2	0135	37.1	18.9	0.9	1.20
		0445	1 hr 10 min	7.5	0500	14.5	7	0.3	1.20
		0555	1 hr 15 min	5	0645	13.2	8.2	0.6	0.65
July 28-29	3	2350	1 hr 10 min	8.2	0020	17.3	9.1	-0.1	-0.20*
		0100	30 min	4.7	0115	17.4	12.7	0.9	3.60
		0130	1 hr 45 min	3.2	0245	19.5	16.3	1	0.80
August 8 -9	2	0155	4 hr 25 min	1.7	0450	15.2	13.5	0.7	0.24
		0520	55 min	3.9	0600	20.3	16.4	1.3	1.95
August 9 -10	3	2320	1 hr 10 min	13.8	0000	20.7	6.9	1.4	2.10
		0215	1 hr 55 min	1.7	0340	12.3	10.6	1.2	0.85
		0500	1 hr	6	0535	11	5	0.3	0.51
August 12 -13	0	-	-	-	-	-	-		
August 13 -14	3	0045	1hr 35 min	5	0110	12	7	0.4	0.96
		0220	45 min	6.1	0250	16.3	10.2	-0.2	-0.40
		0310	5 hr	5.7	0440	12.4	6.7	0.6	0.40
August 30 - 31	0	-	-	-	-	-	-		
August 31 - September 1	2	2325	3 hr 20 min	3.5	0130	34.6	31.1	-0.7	-0.34
		0645	1 hr 45 min	5.3	0720	21.4	16.1	1.4	2.40
Mean	**1.9**	**0220**	**2 hr 10 min**	**6.1**	**0320**	**18.8**	**12.7**	**0. 5**	**0.8**
Maximum	**3**	**2320**	**5 hr 45 min**	**18.2**	**0000**	**37.1**	**31.1**	**1.4**	**3.6**
Minimum	**0**	**645**	**30 min**	**1.7**	**0720**	**11**	**5**	**-0.7**	**-0.6**

* Average cooling rate for between 2100 - 0200 is 1.2^{0}C and 0200 - 0600 is 0.4^{0}C. (All times in PDT.)

recognition of the sensitivity of ozone concentrations to NO concentrations, temporally localised negative spikes in ozone concentration (such as can be observed in Figure 5.3b between 0500 - 0700 PDT on July 27th and at 0620 PDT on August 9th) were not considered reliable indicators of either the start or end of an ozone spike. Such a pattern could result from either local advection of NO or vertical mixing of air parcels containing lower ozone concentrations to the surface. Further criteria of an observed decrease in ozone concentrations of at least 5 ppb to be sustained for at least 15 minutes were therefore also established.

To avoid the introduction of unwarranted subjectivity, the criteria above were strictly observed. Throughout the analysis procedure, where the data were ambiguous the spikes were excluded from further examination. If the remaining positive spikes identified are indeed 'false positives', this should become clear with the more detailed analysis of turbulence in Chapters 6 and 7.

During the course of the study 19 positive spikes in ozone were identified during 8 of the 11 nights, an average of 1.9 spikes per night. The spikes were superimposed upon a mean background concentration of 6 ppb. Although net increases in concentration of up to 31.1 ppb were recorded, the average net increase was 12.7 ppb. Spikes in ozone concentration occurred sporadically between 2320 - 0645 PDT with no obvious temporal pattern in their occurrence. Ozone spikes typically lasted for approximately two hours, although on one occasion (July 26th - 27th) a single spike lasted for 5 hours and 45 minutes.

5.4 Spatial patterns in nocturnal spikes of ozone concentration in the Lower Fraser Valley

In order to determine whether nocturnal increases in ozone concentration observed at the field site were representative of conditions throughout the Lower Fraser Valley, ozone data from 12 of the monitoring sites operated by the Greater Vancouver Regional District were evaluated for the 11 nights during the intensive measurement period. The sites chosen were located throughout the valley floor (Figure 5.4), and all demonstrated broadly similar average diurnal cycles in ozone concentration, with high concentrations recorded during the day and lower concentrations at night. This eliminated the possible influence of monitors located at higher elevations which may remain in the residual layer (Beyrich et al. 1996). Ozone data were only available at an hourly scale for these sites. This reduced the noise in the data set but resulted in a bias towards the identification of spikes of longer duration, as events of shorter duration were

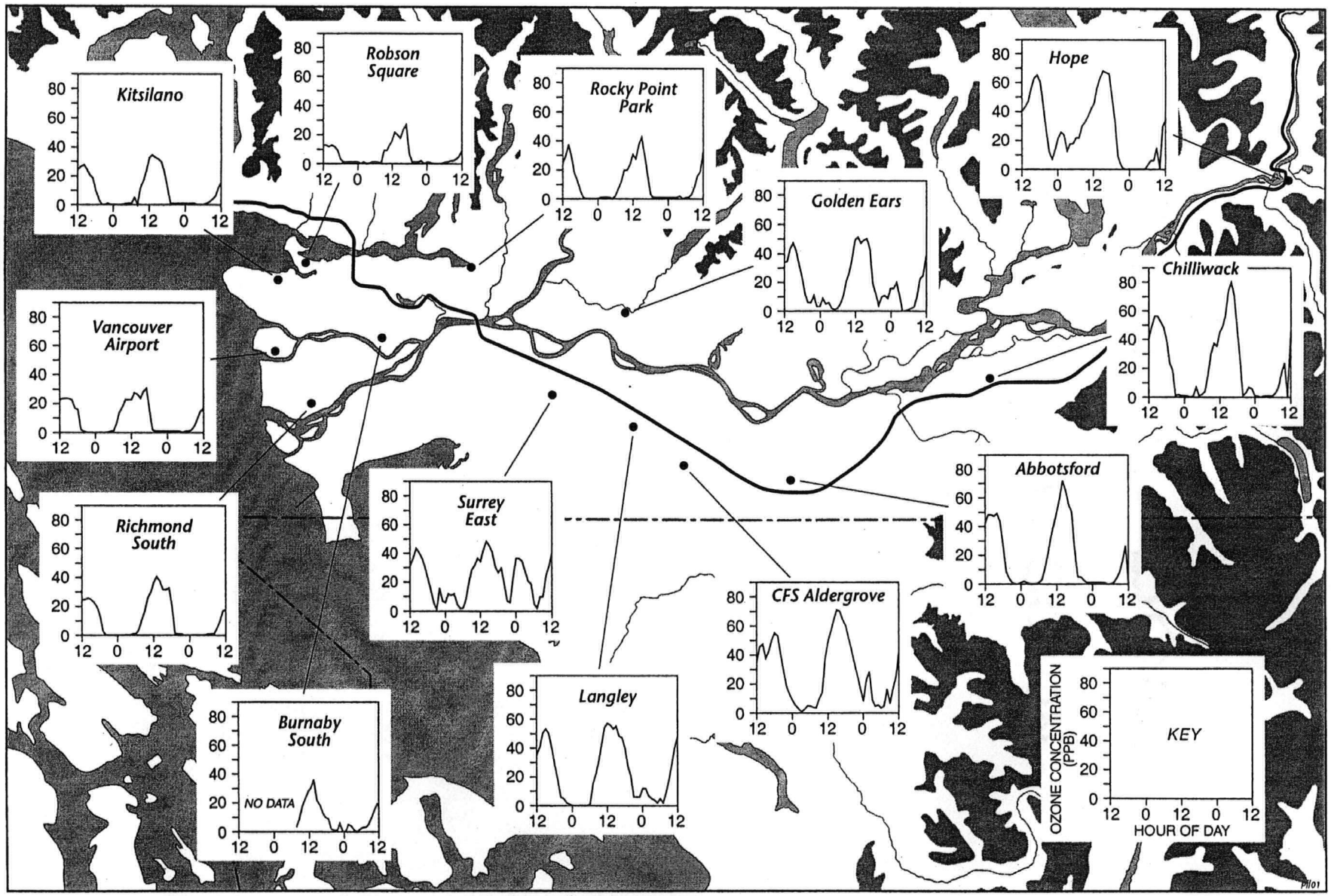

Figure 5.4 Map to show the variations in ozone concentration recorded at twelve of the Greater Vancouver Regional District ozone monitoring sites and the Aldergrove site between 1200 PST 30th August and 1200 PST 1st September 1998

masked by the averaging process. Nevertheless, the data demonstrate that nocturnal spikes in ozone concentration are a common feature of diurnal ozone cycles throughout the valley. They also provide an insight into the temporal and spatial patterns of the phenomenon.

Figure 5.4 and Figure 5.5 illustrate the diurnal cycle in ozone concentration recorded at the selected sites throughout the region between August 30th - 1st September. Distinct spatial patterns in both the timing and value of daily maximum concentrations are apparent. Lower daytime concentrations were recorded in the immediate vicinity of Vancouver City (Kitsilano & Vancouver Airport locations) where NO concentrations are highest. Higher concentrations are recorded progressively east of the city peaking first at Abbotsford, Chilliwack and finally Hope in the late afternoon. This suggests that both local chemistry and the advection of ozone and its precursors play an important role in determining the characteristics of the pollutant cycles at these sites during the day (Hastie et al. 1999; Pryor & Steyn 1995; McKendry et al. 1990).

During the night, ozone concentrations throughout the valley decrease substantially and it becomes harder to discern any spatial patterns in the cycle. However, spikes in ozone concentration occur sporadically in both time and space throughout the valley. The timing and magnitude of ozone spikes recorded throughout the LFV are provided in Table 5.2. The increase in ozone concentration associated with these events was typically of the order of 15 - 25 ppb, although values of up to 40 ppb were recorded at Surrey East (0000 PDT 27th July, 1998). The increase in concentration observed occasionally reflected values more than half the maximum recorded the previous day at that site (as shown in Figure 5.5 on August 31st at Surrey East).

Although there are no consistent temporal patterns in the incidence of spike occurrence, some spatial trends are discernible. For example it is clear from Figure 5.4 and Table 5.2 that few spikes occur at the Kitsilano site which is located at western edge of the valley. Figure 5.6 indicates high levels of NO at this site during the night. The primary sources of surface based NO in the LFV are vehicle emissions. Ozone concentrations at sites located within close proximity to urban areas or major roads may be strongly affected by local titration with NO (Vecchi & Valli 1999; Samson 1978). This is particularly true at night when surface emissions become trapped at the surface in the stable boundary layer. Thus high levels of NO may mask any trends in the advection or vertical mixing of ozone as it is rapidly titrated from the system (Samson 1978). Spikes were also not recorded at the Abbotsford site. This is probably a result of the downtown location of the monitor and associated higher levels of NO (Figure 5.6).

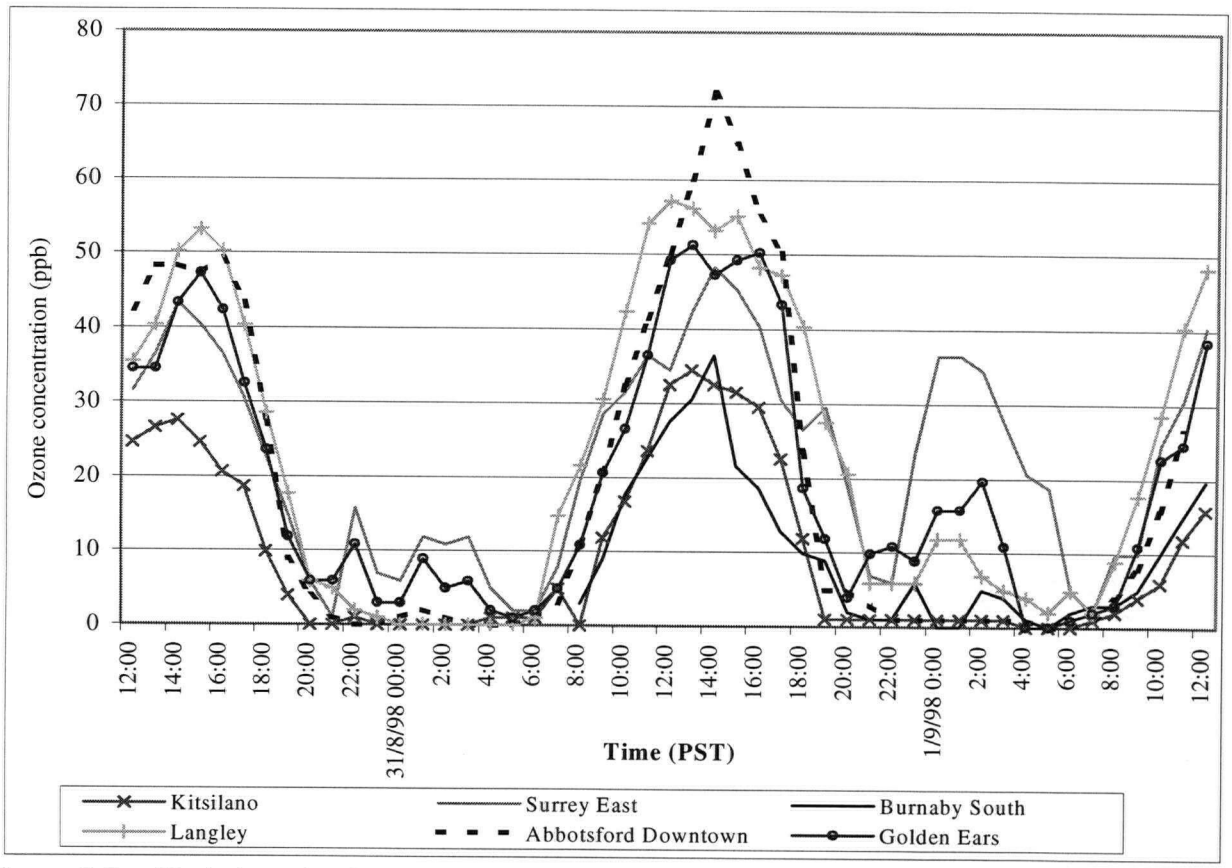

Figure 5.5 Variations in Ozone concentration recorded at sites in the Lower Fraser Valley August 30th - September 1st 1998

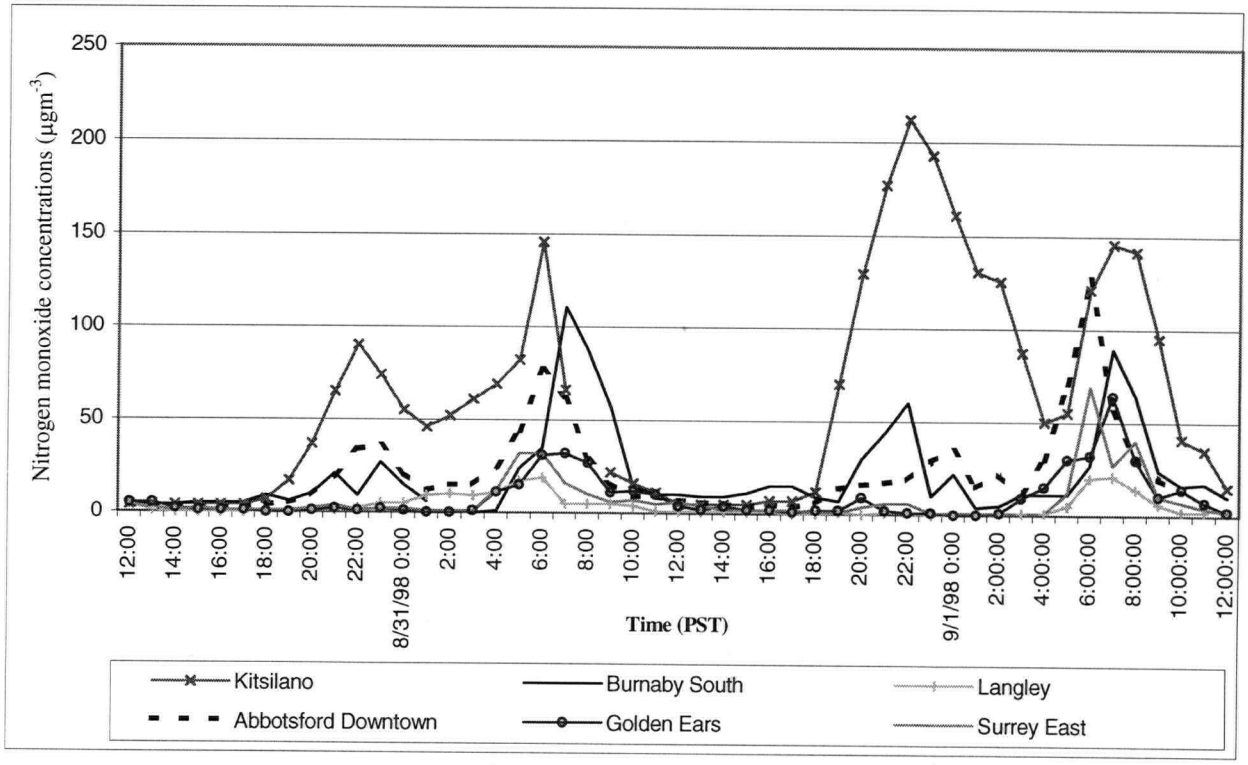

Figure 5.6 Nitrogen monoxide concentrations at selected sites in the Lower Fraser Valley during August 30th - September 1st 1998.

Ozone concentration (ppb)	Vancouver International Airport				Kitsilano				Richmond South			
	Ozone maximum	Start of spike	Time of max	End of spike	Ozone maximum	Start of spike	Time of max	End of spike	Ozone maximum	Start of spike	Time of max	End of spike
July 21 - 22	7.9	0100	0200	0300					10.8	0200	0300	0500
July 22 - 23					8.0	2200	0000	0200				
July 26 - 27												
July 27 -28	28.6 15.8	2000 2300	2200 0100	2300 0300					18.7	2300	0000	0200
July 28-29	6.9 5.9	2100 0100	2200 0300	2300 0400								
August 8 -9												
August 9 -10	12.7 9.8	2100 0200	0000 0300	0200 0600	10.8	2200	0100	0600	14. 8 12.7	2100 0300	0000 0400	0300 0600
August 12 -13	11.3	2300	0000	0300					9.8	2200	0000	0200
August 13 -14									9.8	2100	2200	0000
August 30 - 31												
August 31 - September 1												

Table 5.2 Summary of magnitude and time of onset, ozone maxima and end of ozone spikes observed during the IOPs throughout the LFV, 1998 (All times in PDT, page 1 of 3)

Ozone concentration (ppb)	Burnaby South				Surrey East				Langley			
	Ozone maximum	Start of spike	Time of max	End of spike	Ozone maximum	Start of spike	Time of max	End of spike	Ozone maximum	Start of spike	Time of max	End of spike
July 21 - 22					8.9	2200	0000	0200				
July 22 - 23					11.8	2100	2200	2300				
July 26 - 27	32.5 16.7	2300 0400	0000 0600	0300 0700	40.4	2300	0200	0500				
July 27 -28	17.7	0000	0200	0300	46.3 22.7	2200 0100	0000 0200	0100 0500				
July 28-29	14.8	0300	0400	0700	23.6 14.8	2200 0200	0000 0030	0200 0400				
August 8 -9					16.7	2200	2300	0300				
August 9 -10	8.9	0200	0300	0500	13. 8	0000	0200	0600				
August 12 -13	5.9	0000	0200	0600								
August 13 -14					8.9	2300	0300	0500				
August 30 - 31					15.8 11.8	2100 0000	2200 0030	2300 0500				
August 31 - September 1	6.0 5.9	2200 0100	2300 0200	0000 0500	36.4	2200	0000	0700	11.8	2300	0000	0500
NOTE: No spikes recorded at the Abbottsford, Rocky Point Park or Robson Square monitoring locations												

Table 5.2 Summary of magnitude and time of onset, ozone maxima and end of ozone spikes observed during the IOPs throughout the LFV, 1998 (All times in PDT, page 2 of 3... continued)

Ozone concentration (ppb)	Chilliwack Airport				Hope Airport				Golden Ears Elementary School			
	Ozone maximum	Start of spike	Time of max	End of spike	Ozone maximum	Start of spike	Time of max	End of spike	Ozone maximum	Start of spike	Time of max	End of spike
July 21 - 22					10.8	2300	0000	0300	9.8 9.8	2200 0100	2300 0300	0000 0400
July 22 - 23									9.8	2100	2300	0000
July 26 - 27									10.8	0100	0400	0500
July 27 -28												
July 28-29					7.9	0000	0300	0400	25.6	2200	2300	0300
August 8 -9									11.8	2200	2300	0200
August 9 -10									22.6	2300	0100	0500
August 12 -13	6. 9	2200	2100	2300	10.8	0000	0300	0600	13. 8	1900	2100	2200
August 13 -14												
August 30 - 31	6. 9	0300	0400	0500	25.6	2200	0100	0300	10.8 8.9	2100 0000	2200 0100	2300 0400
August 31 - September 1	6. 9	2100	2200	0100					10.8 19.7	2000 2300	2200 0200	2300 0400
Summary of mean, minimum and maximum ozone concentrations within the ozone spike												
Mean for all sites	15.0	2330	0030	0300								

Table 5.2 Summary of magnitude and time of onset, ozone maxima and end of ozone spikes observed during the IOP's throughout the LFV, 1998 (All times in PDT, page 3 of 3)

Light and variable winds in the stable layer may also have a strong influence on NO concentrations. A small change in wind direction can result in a temporary increase in NO concentrations as a roadway plume is advected over the monitoring site. This can be seen in the sporadic NO spikes at the Burnaby site. In this case, peaks in ozone concentration (shown at 2300 and 0200 PDT on August 31st in Figure 5.5) are recorded out of phase with the NO concentrations (shown at 2200 PDT and 0000 PDT in Figure 5.6).

Localised advection of NO may account for differences in ozone spike incidence between nights. For example although ozone spikes were recorded at Langley on the 31st August they were not observed during the previous night. Figure 5.6 demonstrates that NO concentrations were considerably higher during the night of August 30th - 31st. Thus it is perhaps not coincidental that a spike in ozone concentration was recorded on the night of the 31st but not the previous night.

Spikes in ozone concentration occur most frequently at the Golden Ears, Burnaby and Surrey sites. Low NO concentrations were observed during the night throughout the measurement period at these sites. In addition the Golden Ears site is located at the edge of the valley and likely to be influenced by the development of local down-valley winds which may transport ozone to the site (Banta et al. 1997).

Although temporal patterns in the incidence of ozone spikes could not be repeatedly identified in the data set, it is clear that they are an important feature of the diurnal ozone cycle throughout the LFV. Ozone spikes were observed every night (at one or more sites) during the intensive measurement periods. Local sources of NO clearly played an important role in determining both the temporal and spatial patterns of spike incidence. However, it was difficult to identify cases where ozone was transported to the site but rapidly titrated by high NO concentrations and cases where no transport occurred. In theory, an increase in NO_2 levels should have been reported in the former instance. Unfortunately the data show no clear evidence for spikes in NO_2 concentration, perhaps because the NO_2 becomes mixed into a larger volume of air during transport events. It was therefore not possible to determine from the surface data if transport mechanisms were operating ubiquitously throughout the Lower Fraser Valley, the effects of which were masked by local chemistry. However, given the substantially lower NO concentrations recorded at sites to the east of Vancouver, it seems more likely that transport processes were operating sporadically in time and space.

5.5 Vertical distribution of ozone in the nocturnal boundary layer

5.5.1 Stable layer

Clear skies and strong subsidence associated with the prevailing anticyclonic synoptic conditions during the 11 nights of intensive observations, facilitated the development of a very stable nocturnal boundary layer at CFS Aldergrove. This developed between 2100 – 2300 PDT and comprised of a shallow, very stable layer typically 50 - 150 m in depth, marked by a strong temperature inversion. This is illustrated in the vertical profile observed at 0055 PDT on July 28th, 1998 shown in Figure 5.7b. Ozone concentrations typically increased with height throughout stable layers, revealing a marked depositional profile similar to that observed by Harrison et al. (1978). During an ozone spike, the distribution of ozone typically became much more homogeneous with height through the stable layer (corresponding to an altitude of 100 m), as shown in the 0308 PDT profile in Figure 5.7a (see section 5.6.2 for further discussion).

Surface wind speeds were typically light (consistently less than 2 m s^{-1}) and variable. The top of the stable layer was marked by a wind speed maximum (shown at 0055 PDT July 28th, 1998 in Figure 5.7c), which frequently developed into a weak nocturnal low-level jet (LLJ). Once the stable layer was established, the depth appeared to oscillate with time (Figure 5.8), showing no consistent trends in growth through the latter parts of the night, similar to the definition of a type 1 SBL suggested by Beyrich (1994). However, it was often very difficult to establish the exact height of the SBL from the tethersonde data. There was little consistency between heights determined using a variety of parameters including wind speed maxima, the height of the temperature inversion and the extent of the ozone depositional profile. Although this is a recognised problem in the very stable nocturnal boundary layer (Mahrt et al. 1979; Beyrich 1994; Beyrich & Weill 1993), in this instance the difficulties were further compounded by the limited temporal resolution of the tethersonde data.

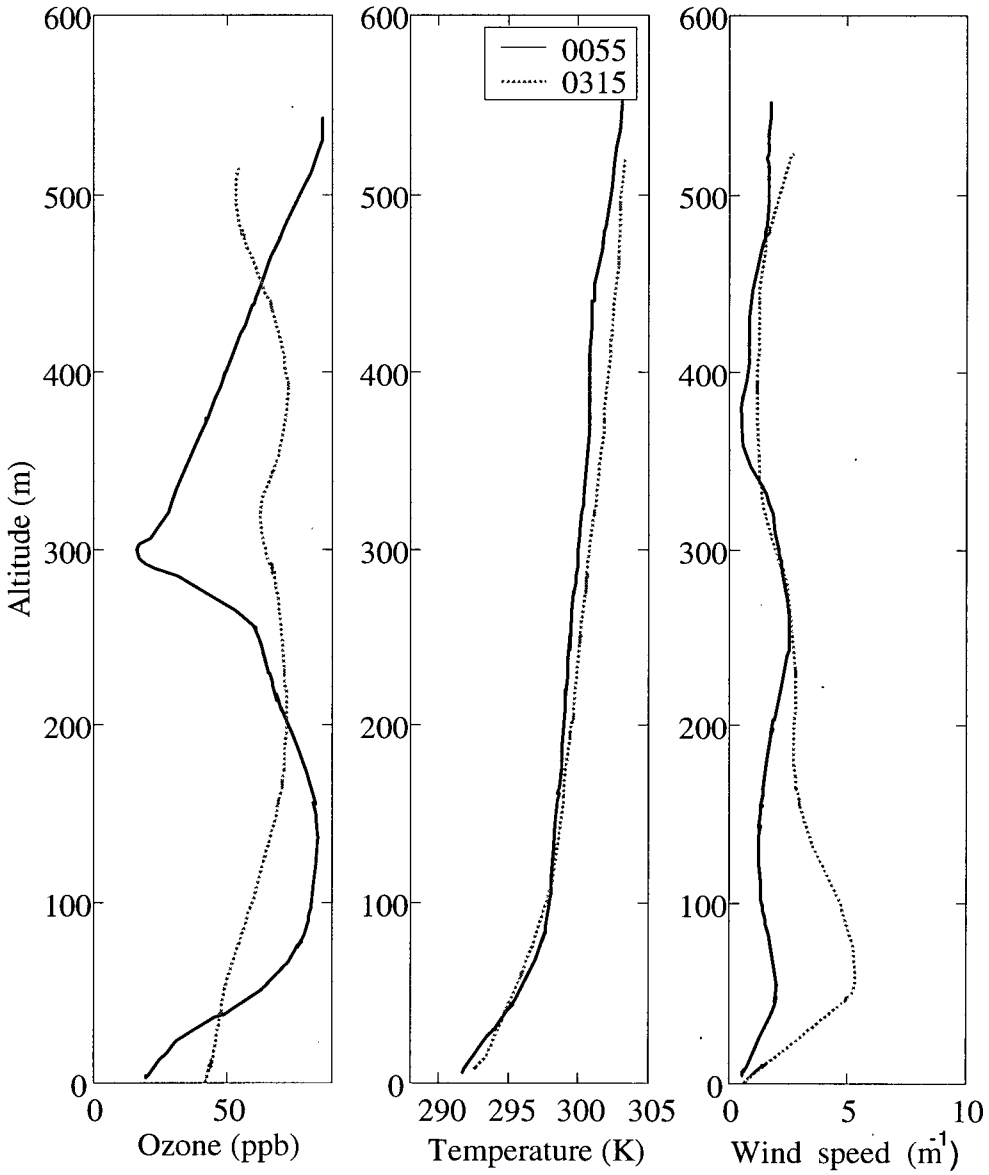

Figure 5.7 Vertical profiles through the nocturnal boundary layer immediately prior to an ozone spike at 0055 PDT and during an ozone spike at 0315 PDT on July 28th 1998

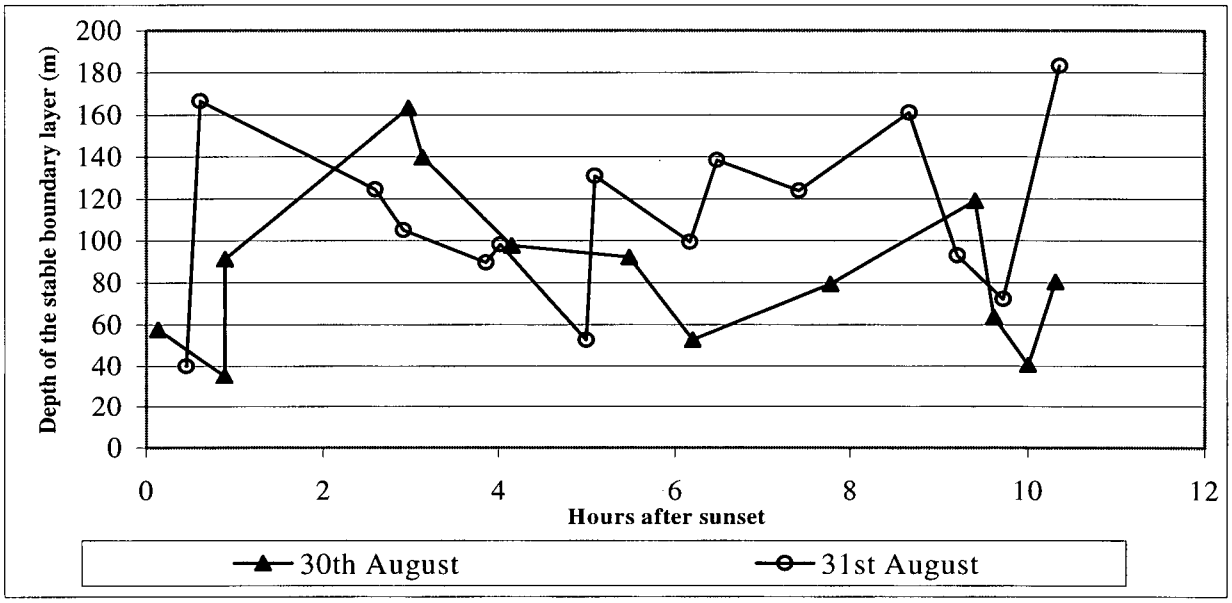

Figure 5.8 Oscillations in the depth of the stable boundary layer with time as estimated from the potential temperature data from tethersonde flights for August 30th - 31st and August 31st - September 1st 1998.

5.5.2 Nocturnal low-level jet

A nocturnal LLJ was observed at the site during every night of the IOPs. (A low level jet was defined using the criteria of a 2 m s^{-1} decrease in wind speed immediately above the localised wind speed maximum.) However, the specific characteristics of the jet continually evolved with time and were variable between nights. The LLJ typically developed at the top of the SBL between 70 - 150 m, where Richardson numbers were high and conditions very stable (as predicted by Blackadar (1957)). A second jet (separated by a distinct wind speed minimum) was also periodically observed well above the stable layer between 300 - 500 m. Figure 5.9 b and c demonstrate that while wind speeds of up to 13 m s^{-1} were recorded in the jet, more typical values ranged between 5 - 6 m s^{-1}. The prevailing direction of the LLJ was southerly, although jets from a range of directions between NE-S-NW were observed (Figure 5.9a).

Analysis of the characteristics of the LLJ suggested that jets could be classified into four different categories. The classification was based on the height and number of distinct wind speed maxima within the profile. LLJs with a single wind speed maximum above 300 metres were classified as a type 1 LLJ. Those with a single wind speed maximum below 300 meters were classified as a type 3 LLJ. Profiles indicating the presence of two distinct maxima were classified according to the height of the strongest jet (or branch). When the upper jet was stronger than the lower jet a type 2 LLJ was identified, and when the lower jet was stronger than

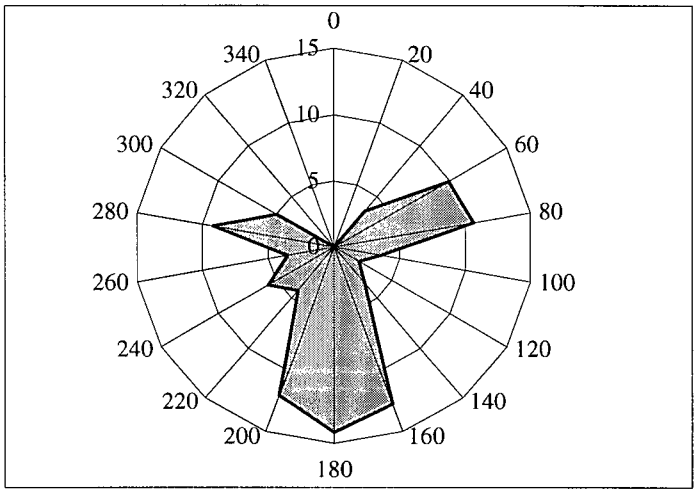

Figure 5.9a Frequency of LLJs by direction during the IOPs at CFS Aldergrove, 1998 Values given as a percentage of the total number of tethersonde observations where LLJs were recorded.

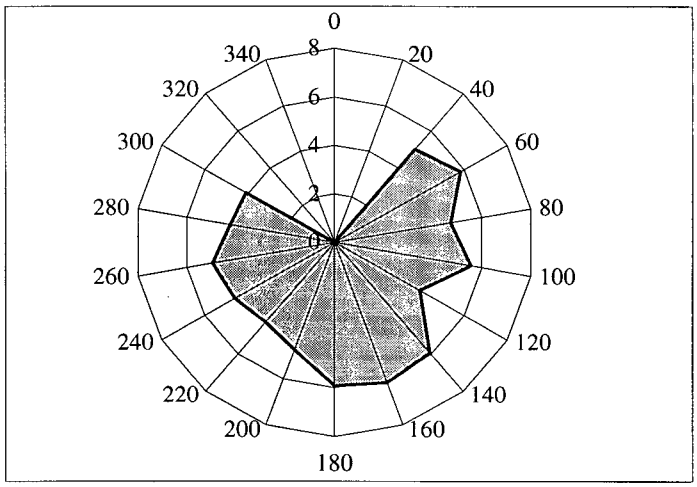

Figure 5.9b Mean wind speed (m s^{-1}) recorded in the nocturnal low level jet by direction during the IOPs at CFS Aldergrove, 1998

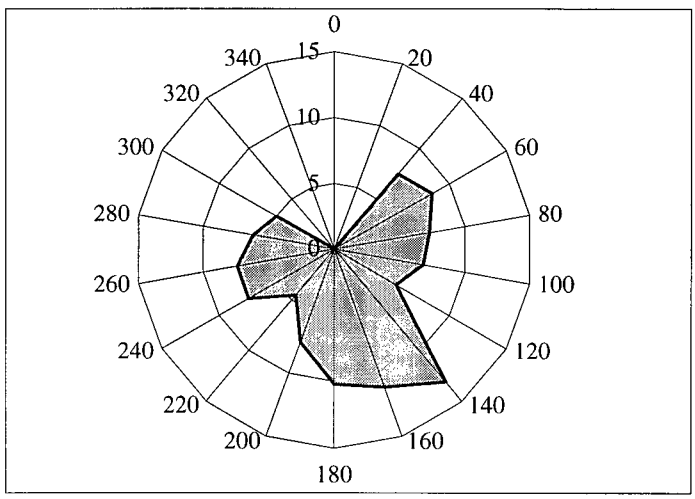

Figure 5.9c Maximum wind speed (m s^{-1}) recorded in the nocturnal low level jet by direction during the IOPs at CFS Aldergrove, 1998

the upper jet a type 4 jet identified. The idealised morphology of the four jets identified is shown in Figure 5.10 and real examples of each jet type provided in Appendix 6.

Overall 81% of the LLJs were classified as type 1 or type 3 jets, the latter being the most common, accounting for 62% of all LLJs. Although two jets appeared to co-exist on occasion, more frequently the development of the upper or lower low-level jet was preceded by the breakdown of the other branch. Buckley & Kurzeija (1997) observe a similar phenomenon during the STABLE field experiment in Savannah, South Carolina. They attribute the demise of a 'deep 6 m s^{-1} jet' and introduction of a 'shallow (~75m) jet with a 12 m s^{-1} maximum' (Buckley & Kurzeija 1997) to the passage of a land breeze front. At the Aldergrove site, jets occurring below 300 metres were predominantly southerly whilst jets above were either north-easterly or north-westerly. This suggests that two mechanisms may also be responsible for LLJ formation at the site. For example one LLJ may be the result of inertial oscillations associated with the frictional decoupling of the surface layers and driven by regional or synoptic scale forcings (resulting in a southerly jet). The second LLJ may be associated with the land breeze front (resulting in a north-west or north-easterly jet). This warrants further investigation, but is beyond the scope of this thesis.

Previous studies have also shown that the low-level jet is an effective transport mechanism introducing higher ozone concentrations to rural areas (Corsmeier et al. 1997; Kalthoff et al. 2000; Beyrich 1994). There was little evidence to support this mechanism in the data collected from the Aldergrove site. High ozone concentrations observed in the residual layer were not associated with the development of the LLJ. The average ozone concentration in the LLJ band was 46 ppb. This typically corresponded to only 70 - 80% of the value of the maximum ozone concentration recorded in each vertical profile.

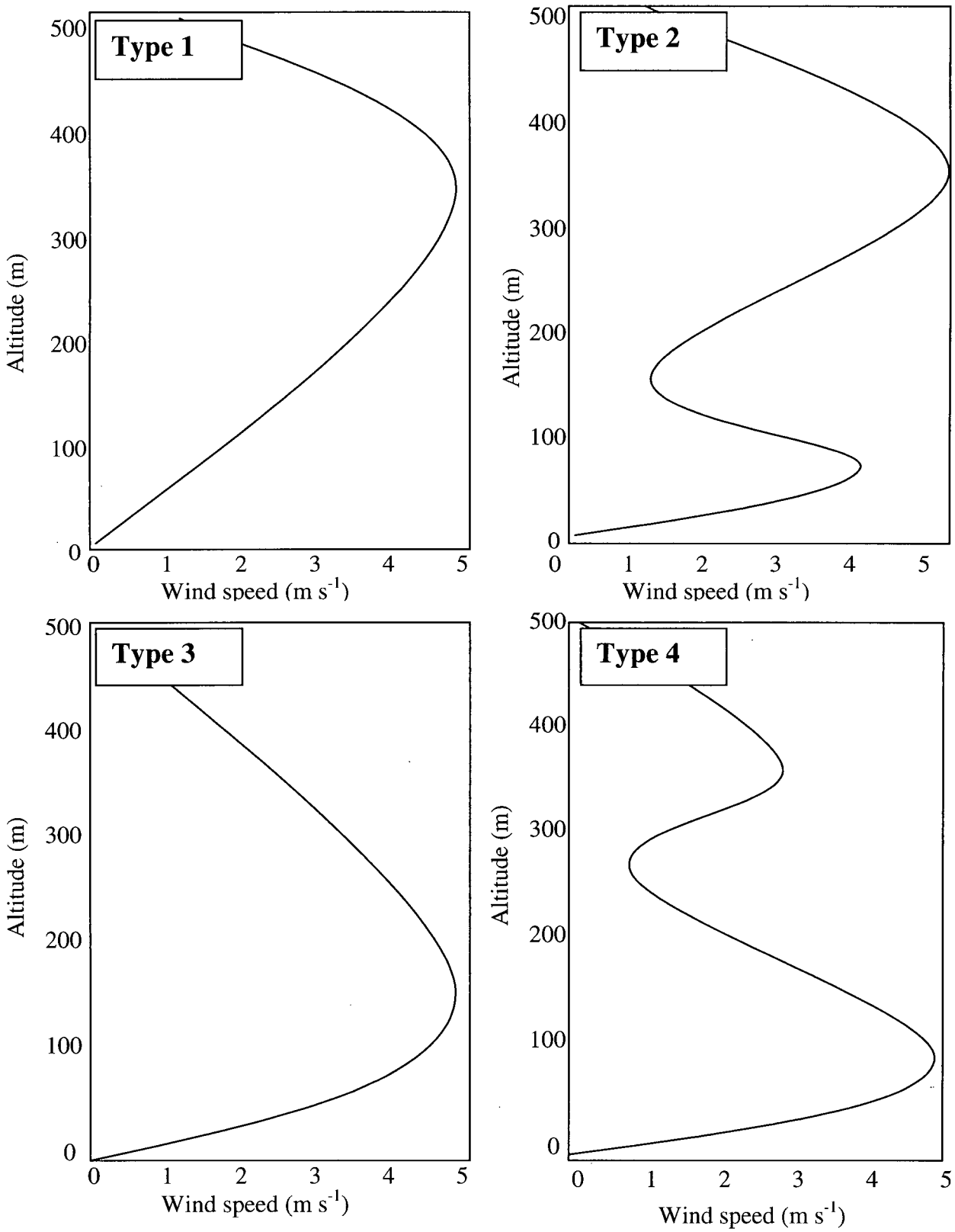

Figure 5.10 Schematic diagram to illustrate the different morphology of the four different types of LLJ identified in the data set

5.5.3 Residual layer

Counter to the common assumption within the literature that ozone concentrations are homogeneous with time and height in the residual layer (Corsmeier et al. 1997), ozone concentrations were found to be highly variable with time and height. This may reflect the complexity of the wind profile observed in the residual layer illustrated in Figure 5.11a and b. Although down-valley winds developed during 8 of the 11 nights (with winds backing from a W-SW daytime direction to a SE-NE direction), they often developed at different heights and at different times throughout the residual layer. The profile was frequently layered, with isolated bands existing in directions often counter to the prevailing wind flows. A westerly band was commonly observed between 200 - 300 m for 1 - 2 hours following wind reversal through the remainder of the profile. This can be seen between 0000 PDT and 0400 PDT in Figure 5.11a at between 200 - 300 m. During the three nights when down-valley winds failed to develop, a prevailing southerly flow was observed.

Generally, ozone concentrations in the lowest 400 m of the nocturnal boundary layer decreased with height following the development of the down-valley wind regime. Although this pattern is illustrated in Figure 5.12, it is somewhat obscured by a band of high ozone concentrations between 150 - 250 m in height observed between 0000 - 0500 PDT July 27th. (A clearer example of this is given in section 5.8 where conditions on August 30th - 31st are discussed in a case study.) Although concentrations decreased at a slower rate in the lower layers of the residual layer compared to the surface layers, this frequently blurred the expected boundary in the profiles between the top of the stable layer and the residual layer. Banta et al. (1997) also observed reduced concentrations in the lowest 500 m of the boundary layer in their study of the Lower Fraser Valley. This may be a consequence of the surrounding complex terrain. Depositional processes operating along the valley walls may act to cleanse down-valley winds as they pass through tributary valleys prior to convergence in the Lower Fraser Valley (Banta et al. 1997). Above 400 m ozone concentrations remained more stable with time, more closely representing conditions observed during the previous afternoon. This reflects the absence of depositional surfaces or primary sources of NO in the upper levels of the residual layer.

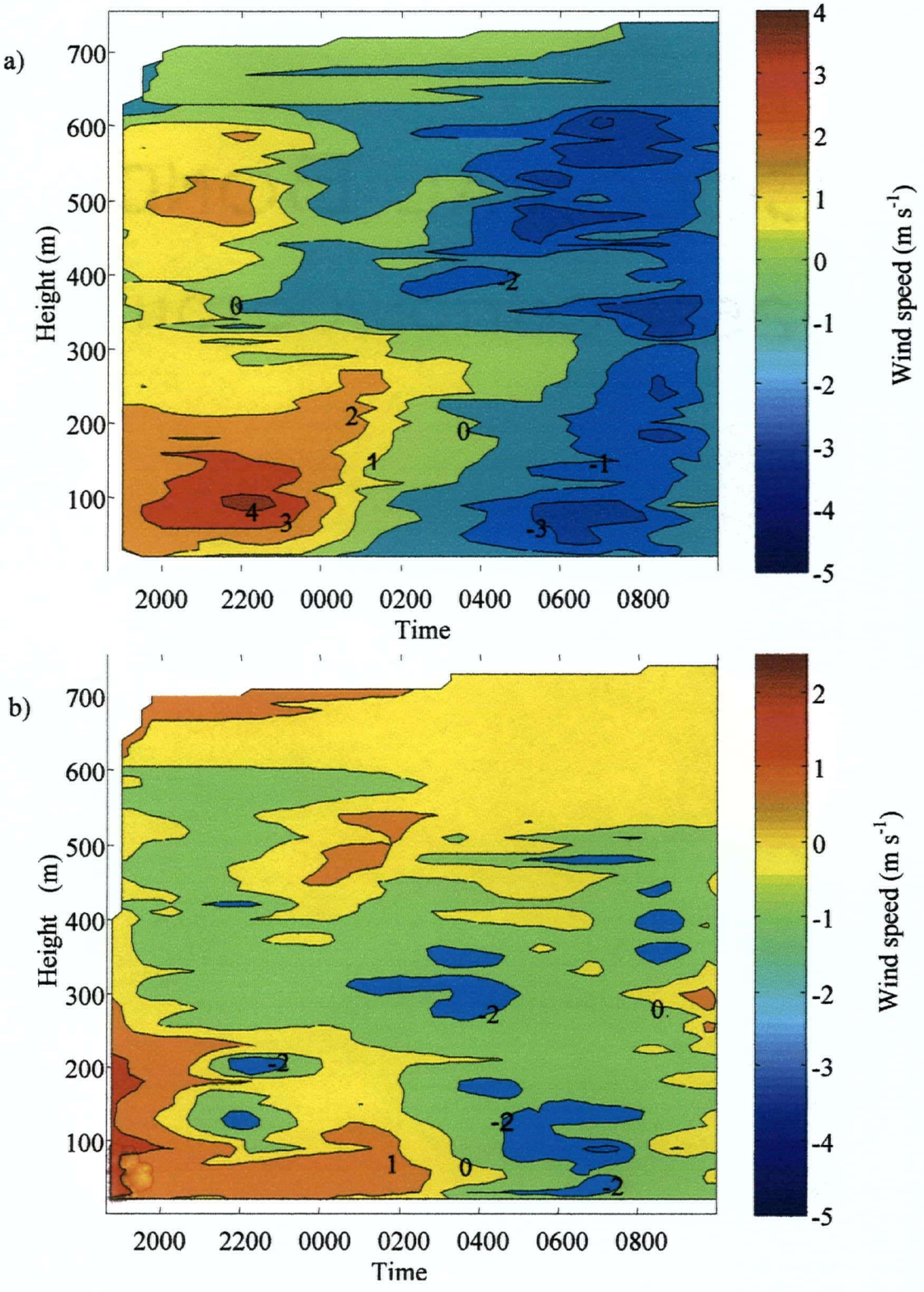

Figure 5.11 Contour plot to illustrate a) u-component of wind vector and b) v-component of wind vector for July 26th - 27th 1998 (Note: Time-height diagrams of the tethersonde data are provided in Appendix 5, for all days-nights contoured, to provide an indication of the temporal resolution of the data used to calculate contours.)

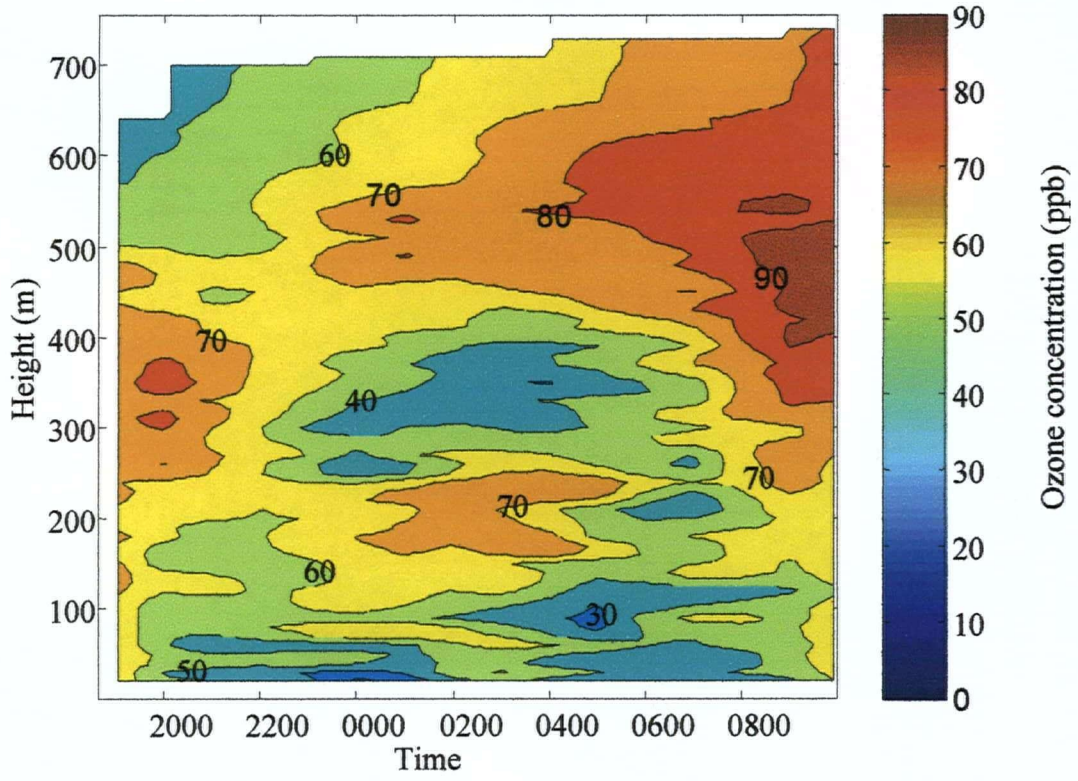

Figure 5.12 A contour plot to show ozone concentration with height on July 26th - 27th 1998 at CFS Aldergrove

Although the temporal resolution of the tethersonde observations inhibited the complete capture of changing conditions in the residual layer, the data clearly demonstrate the sporadic advection of layers containing both high and low ozone concentrations across the site (as shown in Figure 5.12). Due to the light winds and meandering motions (characteristic of flows in the residual layer) it was sometimes difficult to isolate the sources of these pockets effectively. Analysis of the tethersonde data reveals that the maximum concentration in any given profile was most likely to be associated with an ENE wind or a SSW - SSE wind. This suggests that pollutant re-circulation may be occurring within the nocturnal mesoscale flows.

However, the data also demonstrates that layers containing high concentrations of ozone can be associated with winds from a variety of directions. For example three nights saw the advection of isolated layers with ozone concentrations in excess of 80 ppb (26th - 27th July, 27th - 28th July and 31st August - 1st September). As shown in Figure 5.13d on all three occasions, the band of high ozone concentrations was observed above the stable layer but below 300 metres. On August 31st - September 1st this band was associated with a SE flow. During the other two nights the pockets of high ozone concentration were associated with the late evening westerly band which remained following the development of the down-valley wind system as shown between 0000 - 0400 PDT on July 27th 1998 in Figure 5.11a and Figure 5.12.

These patterns were not consistent. Pockets of air with low ozone concentrations were also periodically observed embedded within easterly flows and low ozone concentrations were also observed in westerly bands which developed during the early morning hours. The latter observation may be a result of the trajectories of air parcels during the early morning which coincide with urbanised regions possessing high emissions of NO. This is especially true for the Aldergrove site due to the proximity of Highway 1, located 2km north of the site. Thus this may be a reflection of high NO concentrations rather than the advection of unpolluted air.

Clearly both the timing and trajectory of the mesoscale flows play a crucial role in determining the ozone concentrations in the residual layer. Although ozone concentrations are highly variable throughout the residual layer, concentrations were consistently higher than observed at the surface. It is unlikely to be a coincidence that the three nights which recorded the highest concentrations in the residual layer were also the three nights with the largest spikes in ozone concentration observed at the surface (Figure 5.13).

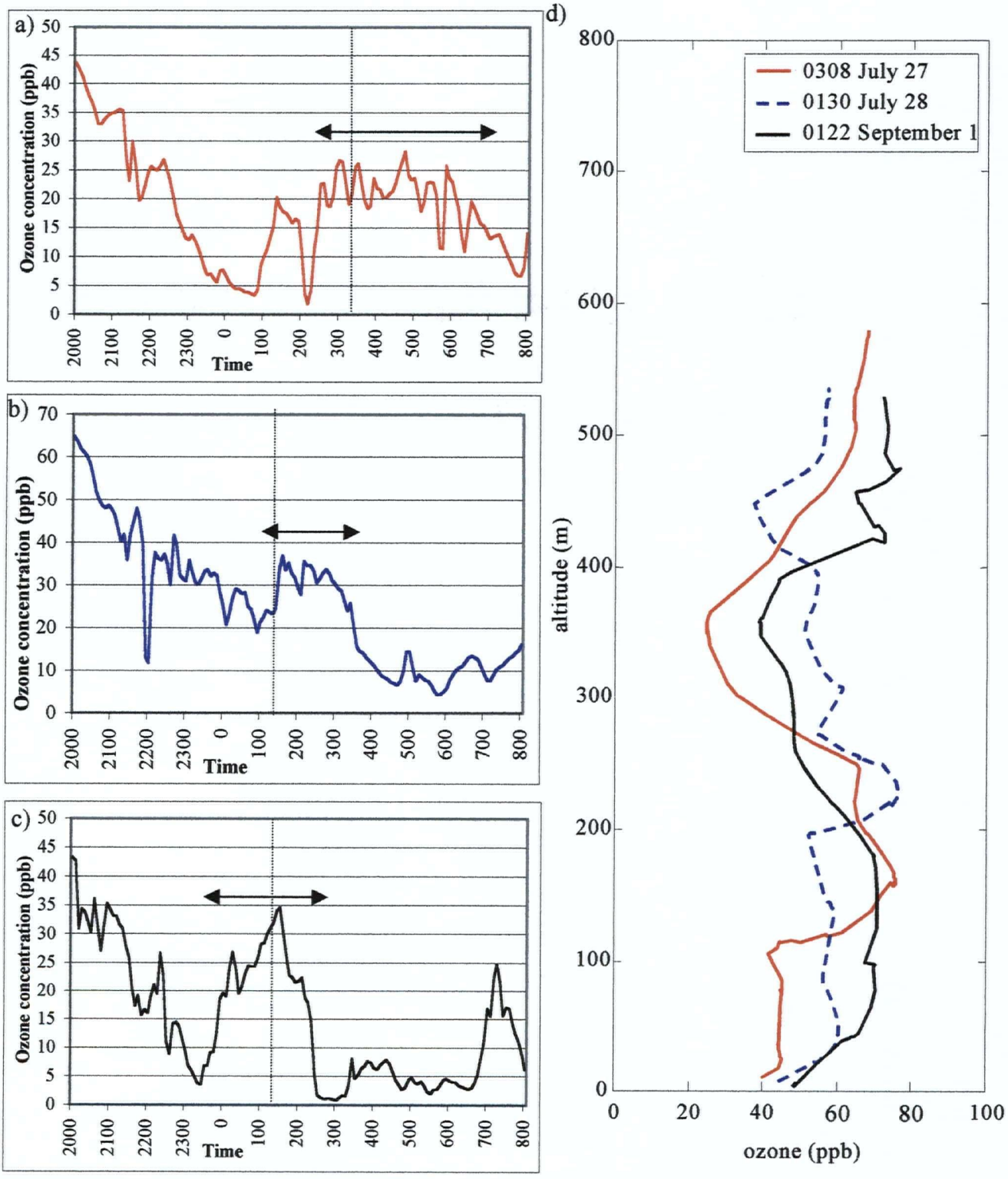

Figure 5.13 Surface ozone concentrations during the three nights with the highest recorded ozone maxima a) July 26 - 27th, b) July 27 - 28th and c) August 31st - September 1st 1998. Vertical profiles of ozone concentration through each spike are provided in part d at times indicated with the hashed line on parts a - c. Surface ozone spikes are marked with an arrow.

5.6 Vertical mixing or horizontal advection?

5.6.1 Intermittent turbulence in the very stable nocturnal boundary layer

Two mechanisms could account for increases ozone concentration at night: horizontal advection and vertical mixing. Given the dominant role of deposition and chemical titration processes, it is expected that horizontal advection of ozone may be limited in regions of homogeneous terrain (Samson 1978). In regions of complex terrain, advection patterns become more complex as air parcels, forced to rise over an obstacle, follow isentropes rather than contours. Thus it is possible that, when the prevailing wind direction forces air parcels to rise over mountain barriers, the trajectory of air parcels measured at the surface in the LFV may not have previously been in contact with the earth surface (and hence deposition and chemical removal processes will have been limited and advection of ozone could occur).

This scenario is unlikely to be a regular feature in the Lower Fraser Valley. Previous studies (e.g. Banta et al. 1997) indicate that the prevailing flow in the valley is from drainage winds which flow down the valley sides and along the valley floor. Further, the prevalence of near zero concentrations in the surface layers as observed by the GVRD suggests that deposition and chemical removal processes are active throughout the LFV. Thus whilst the horizontal advection of ozone can not be ruled out, given the prevailing wind flows and ubiquity of NO emissions particularly in the western part of the LFV, it is unlikely to be a significant source of ozone concentrations. Thus the hypothesis that 'nocturnal increases in ozone concentration recorded at the surface result from vertical mixing processes' is proposed.

To support this hypothesis, nocturnal surface temperature and wind data were examined for periods immediately prior to the onset of incidences of increased ozone concentrations recorded at the field site. Given strong radiational cooling at the surface, an increase in temperature with height is expected to be observed through the stable layers. Thus if vertical mixing mechanisms are active at (or within a close proximity to) the site, an increase in surface temperatures should be observed (Corsmeier et al. 1997). Table 5.1 demonstrates that for 13 out of the 19 cases a simultaneous increase in surface temperature and ozone concentration was recorded. Five of the remaining six examples demonstrated cooling rates considerably slower than average. (Given that all data were recorded under clear sky conditions, cooling rates may be similar.) Thus at least 18 of the spikes arguably coincided with warming trends at the surface

and are therefore potentially associated with vertical mixing. Unfortunately, the site is located in a region of complex terrain (the LFV), and thus warming may also be due to surface advection of heat therefore this observation alone does not unequivocally suggest vertical mixing.

Despite the presence of a number of GVRD monitoring locations around CFS Aldergrove it was not possible to provide a quantitative estimate of advection of ozone. This was due in part to the apparent sensitivity of the ozone data at the Abbotsford site to local NO concentrations. The presence of other sources of NO (such as Highway #1) between the monitoring locations and the field site also limits the value of these measurements.

It is equally difficult to determine whether advection processes were active from the surface wind data. As in the Corsmeier et al. (1997) study, marked changes in wind speed or direction were not typically observed at the same time as the onset of increased ozone concentrations, suggesting that increased ozone concentrations are unlikely to be the result of advection. However, given the light and variable wind patterns and meandering characteristics of wind flows in the very stable NBL, it is difficult to determine air parcel trajectories from wind speed and direction alone. Changes in wind direction occasionally coincided with the end of an ozone spike. This is shown between 0600 - 0700 PDT on July 27th 1998 (Figure 5.14), and indicates that advection of lower ozone or higher NO concentrations to the site may affect the duration and morphology of the ozone spike.

The possible existence of vertical mixing mechanisms operating in the nocturnal boundary layer can be determined using the Richardson number (Ri). Data from the 80 m tower were used to calculate Ri. As the thermocouples were located 30 m apart, the critical Richardson number could not be used to determine the exact timing of the onset of stable conditions. (As discussed in Chapter 3, it is likely that turbulence can exist at Ri > 0.25.) Nevertheless Figure 5.15 clearly demonstrates intermittent breakdowns in the stability of this layer throughout the night. These correspond well with periods of increased ozone concentration, which strongly supports the hypothesis of vertical mixing. For example between 0100 - 0200 PDT Ri drops from 4.0 at 0045 PDT to 0.4, where it remains until 0200 PDT. During this period ozone concentrations increase from 3 ppb to 20 ppb. Between 0200 and 0230 PDT stability increases and a corresponding drop in ozone concentrations is observed. At 0230 PDT stability clearly decreases and ozone concentrations once again increase. Between 0230 - 0500 PDT ozone concentrations remain high.

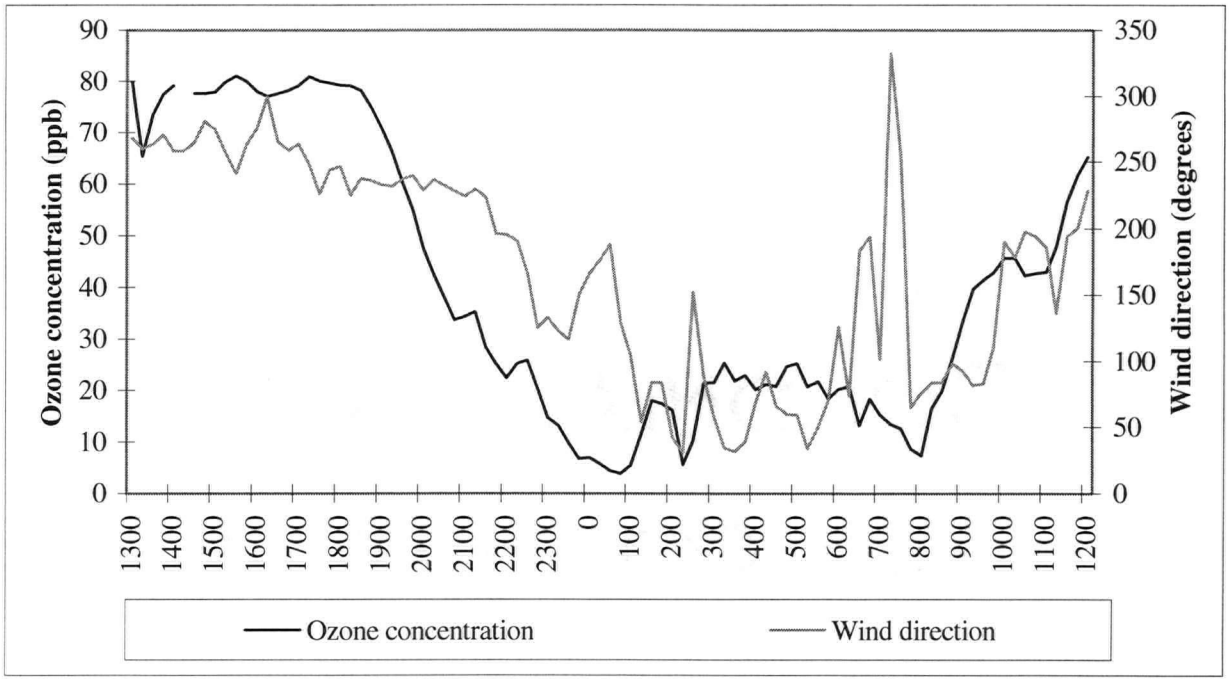

Figure 5.14 Nocturnal variations in surface wind direction and ozone concentrations observed July 26th - 27th 1998

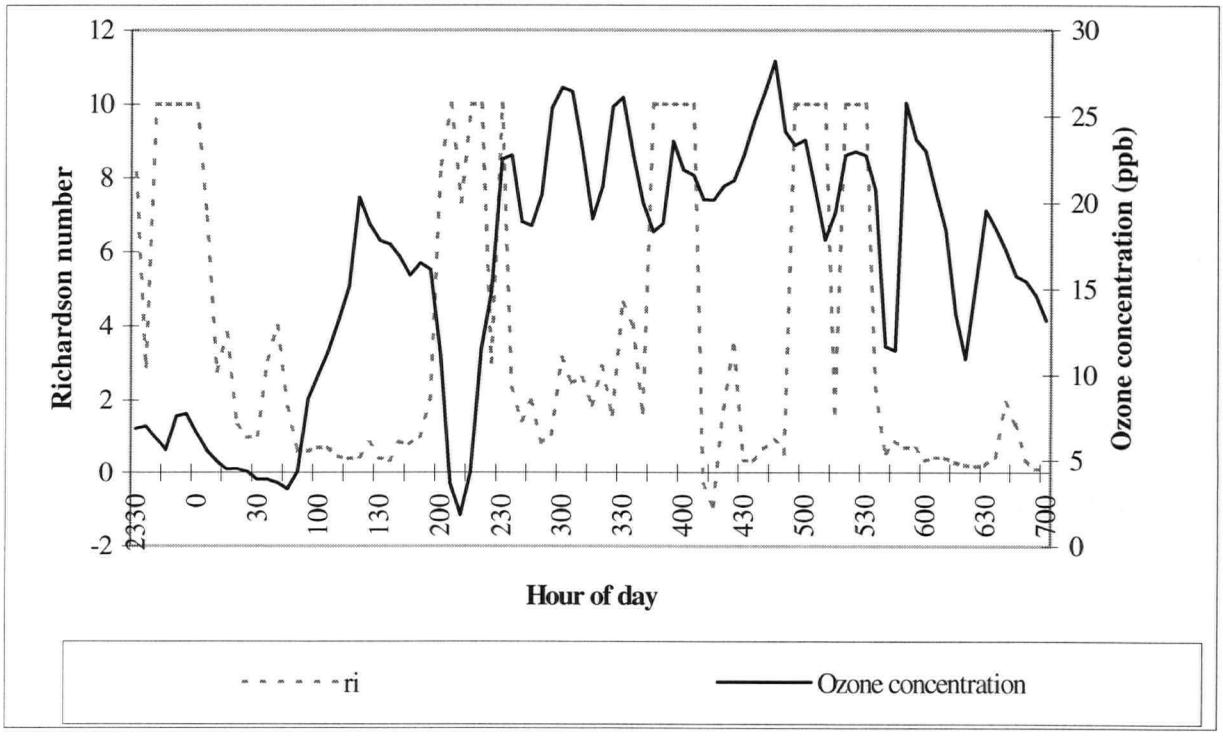

Figure 5.15 Nocturnal variations in the Richardson number calculated between 30 - 60 m and ozone concentrations measured at the surface between 2230 PDT and 0700 PDT July 26th - 27th 1998 (Note: Richardson numbers were capped at 10.0. See justification in Chapter 3.)

The Richardson number indicates the possibility of intermittent turbulence during this time period as although stability increases, it is only maintained for 15 - 30 minute intervals. Clearly either the absence of NO (unfortunately no data are available for this period) or the continued (if intermittent) vertical mixing is sufficient to maintain higher ozone concentrations at the surface during the latter part of the night. Further examples of the relationship between ozone concentrations and Ri are provided in Chapter 7.

5.6.2 Vertical profile through an ozone spike

If vertical mixing mechanisms are operating in the nocturnal boundary layer, evidence of a mixed profile should be found in other variables, such as temperature, during an ozone spike. Sections 5.5.1 - 5.5.2 paint a clear picture of a shallow, very stable boundary layer essentially decoupled from complex wind and ozone variations aloft. This, to some extent idealised understanding of the structure of the very stable NBL, must be re-examined if vertical mixing mechanisms are indeed responsible for increased ozone concentrations at the surface.

Figure 5.7 (page 95) shows vertical profiles through the ozone spike which occurred at 0308 PDT on July 27th 1998. (The temporal variations in surface ozone concentration during this period can be found in Figure 5.15, relevant contour maps for wind flow are provided in Figure 5.11a & b and vertical observations of ozone concentration shown in Figure 5.12.) The black line indicates conditions immediately prior to the start of the ozone spike. The profiles show a 80 - 90 m deep stable layer capped by a wind speed maxima. The ozone profile shows some advection in the top 20 - 30 m but the remainder of the profile through the stable layer is indicative of active deposition and titration processes. The ozone profiles indicate that by 0308 PDT mixing has occurred at least through the lowest 100 m of the profile. Although the corresponding temperature profile is not representative of a mixed layer, it does indicate warming through the layer which supports the hypothesis of vertical mixing. The changes in the wind profile are perhaps more convincing, as the wind maxima at the top of the stable layer identified at 0055 PDT is not evident at 0308 PDT.

Given the limitations of the gradient Richardson number when applied to tethersonde data (outlined in Chapter 3), the results in this section have to be interpreted with care. To minimise the depth of the layer for the calculation, a linear interpolation scheme was applied to the tethersonde data to achieve a 0.5 m resolution. Thus the critical number should be close to Ri = 0.25 but it is likely that turbulence may still exist at higher numbers.

Figure 5.16 illustrates the variations in Ri with height calculated from the tethersonde data for a) 0055 PDT and b) 0308 PDT for July 26th - 27th 1998. The data are shown in both the raw format and smoothed using a Gaussian function to facilitate comparison. Results indicate the presence of a very stable layer between 0 - 50 m immediately prior to the onset of vertical mixing. Between 50 - 100 m the Ri drops below 0.25, indicating that turbulence may be present in this layer. There is no obvious indication of this in either the wind speed or temperature profiles shown in Figure 5.7. However, the ozone profile shows a marked increase in concentrations between these heights and this corresponds to a backing of wind directions with height from NE near the surface to W at 100 m. A stable layer between 100 - 200 m isolates the surface layers from a second region of turbulence found above 200 m. The Richardson number clearly demonstrates the potential existence of isolated layers or pockets of turbulence at 0055 PDT which do not connect with the surface.

By 0308 PDT the Richardson number indicates that turbulence may exist throughout the profile. This means that ozone from heights < 500 m may be mixed to the surface. As shown in Figure 5.7, ozone concentrations peak at more than 80 ppb at 100 m. The proximity of this layer of high ozone concentrations, combined with mixing through a deep section of the boundary layer, probably accounts for the marked increase in ozone concentrations measured at the surface. The evidence from these profiles strongly suggests that the ozone spikes are at least partially a result of vertical mixing processes.

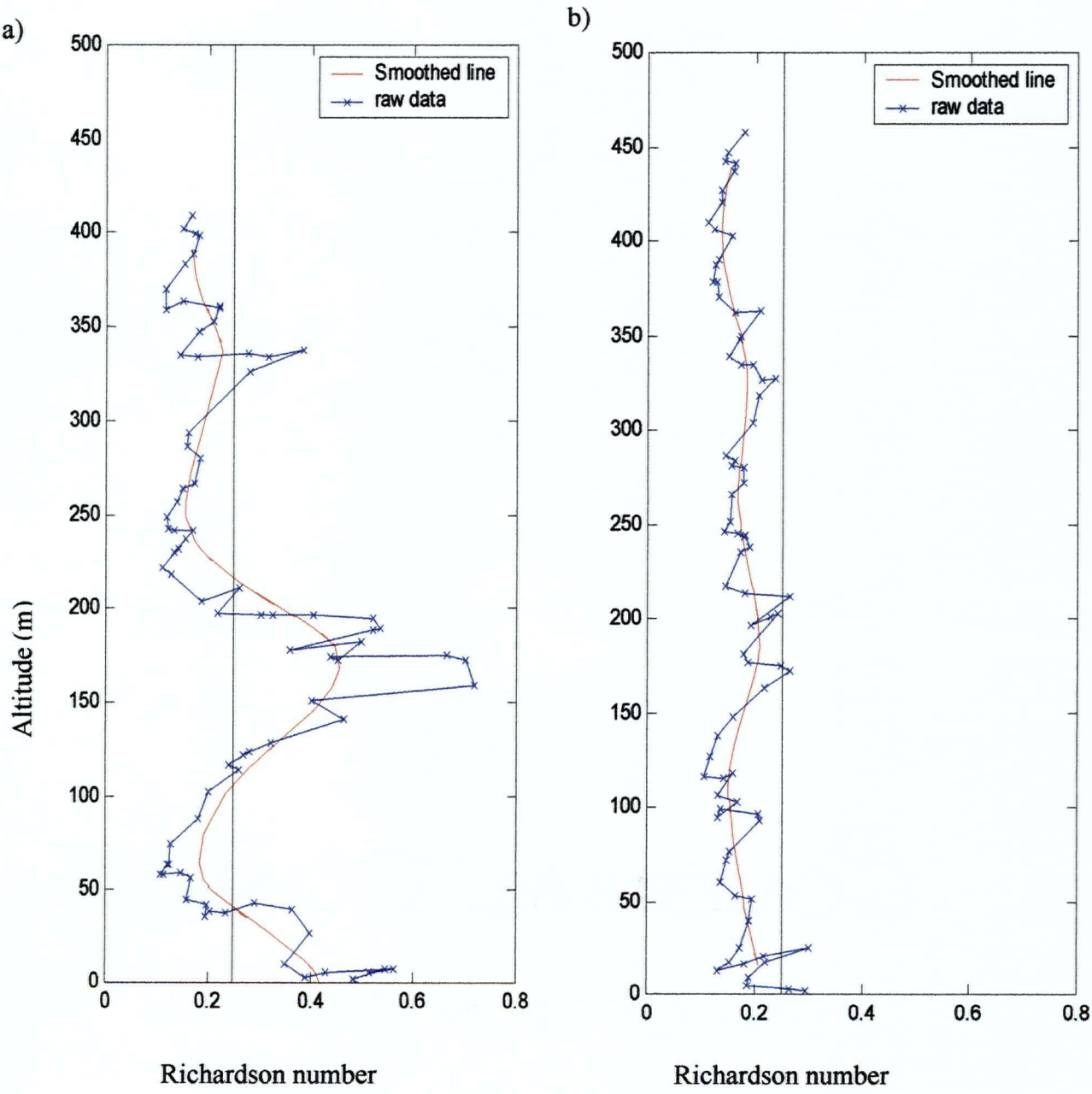

Figure 5.16 Vertical profile of Richardson numbers calculated from the tethersonde data for a) 0055 PDT and b) 0308 PDT for July 27th 1998

5.7 Causes of turbulence in the nocturnal boundary layer

5.7.1 Nocturnal low-level jet

Turbulence in the very stable nocturnal boundary layer typically results from shear associated with changes in wind velocity with height (Mahrt et al. 1998). One of the primary causes of turbulence in the very stable nocturnal boundary layer is the nocturnal low-level jet (LLJ) (Beyrich et al. 1996b). As the jet develops the resulting changes in velocity and direction with height cause localised increases in shear which may generate localised bursts of turbulence and hence vertical mixing (Corsmeier et al. 1997). Table 5.3 indicates that 8 out of the 19 nocturnal spikes in ozone concentration coincide with the presence of low-level jet above the site. A further two possible cases are identified when the jet was weakly developed, and one more when the wind speeds in the jet were too strong in the previous flight to enable continued tethersonde operation. Thus approximately half of the ozone spikes may be associated with turbulence generated by a well-developed nocturnal jet.

A relationship could not be identified between any specific characteristics of the LLJ (such as height or speed) and the magnitude, frequency or duration of ozone spikes observed at the surface. This may be in part a consequence of the temporal resolution of the tethersonde data (flights were approximately one hour apart and lasted 45 - 60 minutes). It also reflects the variability of ozone concentrations in the residual layer - as the presence of vertical mixing mechanisms in the absence of ozone aloft cannot generate increased levels at the surface.

However, using the jet classification system identified in section 5.5.2, trends in jet type and surface ozone concentration become more apparent. As shown in Figure 5.17 the largest average increase in ozone concentrations is observed with a type 3 jet. Indeed, the majority of the LLJs associated with surface ozone spikes were type 3 jets. This type of LLJ developed at the top of the stable boundary layer. Wind speeds in the type 3 jets were higher than those found in the lower branches of type 2 or type 4 jets (Figure 5.18) suggesting that this type of jet was associated with larger shear and hence more likely to cause turbulence.

Table 5.3 Summary of ozone spikes and coincident characteristics of the LLJ and wind direction through the NBL observed during the IOPs throughout the LFV, 1998 (All times in PDT)

Date	Start time	Time of max	Jet	Height m	Speed m s^{-1}	Surface winds switch to easterly	Winds aloft switch to easterly	Presence of westerly band
July 21 - 22	-	-	Yes 2300 to 0800	300 - 650	5 - 6	2100 (S) 0030 (SE)	2100 (SW) 2400 (SE)	2200-2400, (SW)
July 22 - 23	0045	0155	Yes breaking down	50 - 150	4 - 5	Does not develop 2100 (S)	2100 (SW) 0600 (S)	0100-0230, W(NW), 100/300 m, Low O_3
July 26 - 27	0050	0125	breaking down	100 - 200	2 - 3	2100 (S) 0200 (E)	0000 (S) 0200 (E)	0100 - 0500, 200/300 m, High O_3
	0215	0500	No; develops 0500					
July 27 - 28	0050	0135	No; develops 0200	50- 100	3 - 5	2100 (S) 0000 (E)	0000 (S) 0200 (E)	2300 - 0100, 200/300m, High O_3
	0445	0500	Yes (weakens @ 0530)	180 - 60	6 - 2			
	0555	0645	Yes	450	5			
July 28- 29	2350	0020	No					
	0100	0115	Yes (weak)	300	3			
	0130	0245	Yes (weak)	300	3			
August 8 - 9	0155	0450	Yes	200 - 450	6	Does not develop S flow 2000		2100 - 2300, W/NW, 400-500 m High O_3
	0520	0600	Yes	200 - 450	8 - 9			
August 9 - 10	2320	0000	Yes	200	10	Does not develop S flow		
	0215	0340	No flights					
	0500	0535	No					
August 12 - 13	-	-	Yes 0300 - 0600	300 - 500	4-7	2200 (S) 0000 (E)	2100 (S) 2300 (E)	2000, W/NW, 300 m, High O_3
August 13 - 14	0045	0110	Yes	300	7	1900 (S) 2200 (E) 0100-0400 (SW)	0200 (S) 0400 (SE) 0500 (E)	0200 - 0400, 100-150 m, High O_3
	0220	0250	Yes breaking down	300	7			
	0310	0440	Yes (2)	300/500	5/3			
August 30 - 31	-	-				1900 (S) 0100 (E)	2000 (S) 2200 (E)	2100 - 2300, 50 -100 m
August 31 - September 1	2325	0130	Yes breaking down	100	4-5	2100 (SE) 0000 (S)	2300 (S) 0100 (E)	0000 - 0300, 300 m, low O_3
	0645	0720	Yes (2)	100/400	4/3			

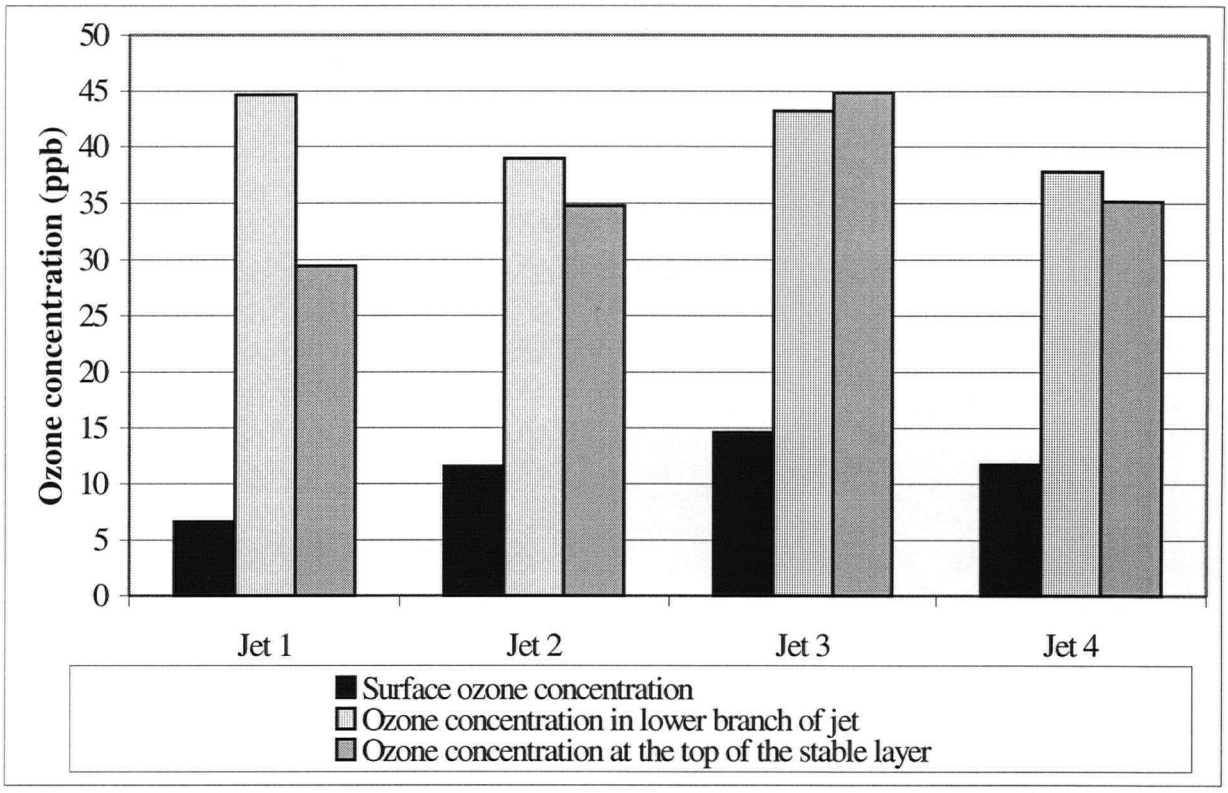

Figure 5.17 Variations in ozone concentrations at the surface, top of the stable boundary layer and within the jet core by jet type observed during the IOPs at CFS Aldergrove, 1998

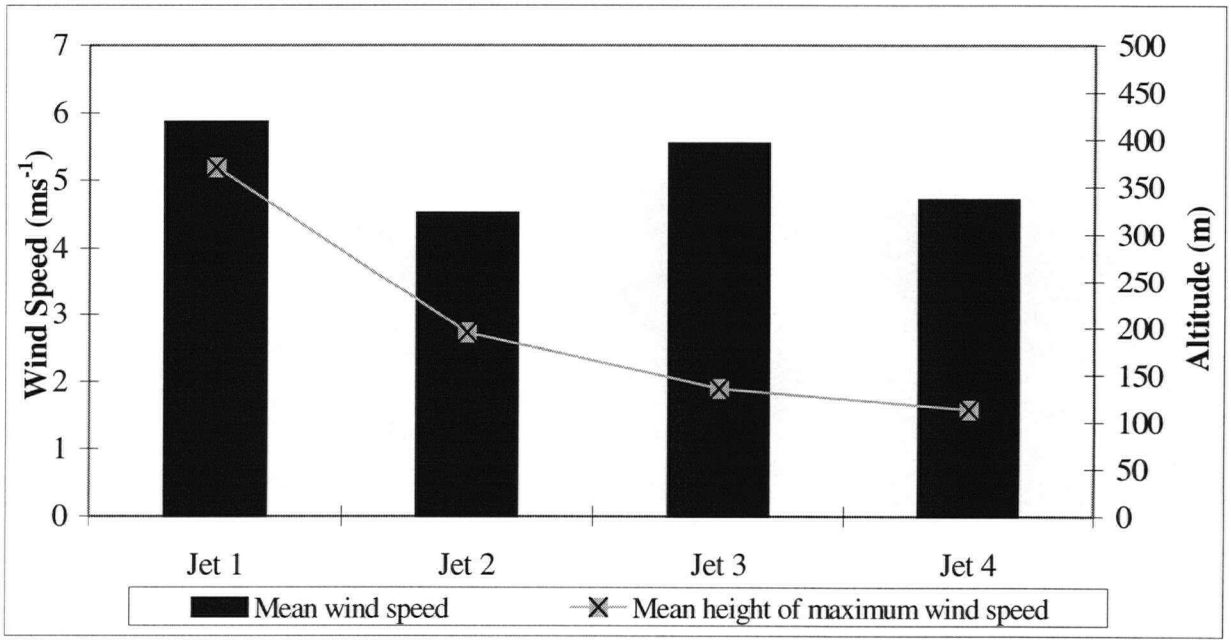

Figure 5.18 Variations in mean wind speed and height by jet type for the LLJ observed during the IOPs at CFS Aldergrove, 1998

Smedman et al. (1995) argue that the low-level jet can act to prevent turbulence from other sources (such as breaking gravity waves) from reaching the stable surface layers. This is partly because any turbulence should be dissipated in the layers with high Ri where the jet develops. Type 1 LLJs were associated with considerably lower ozone concentrations at the surface. This suggests that although type 1 jets may generate mixing through a deeper layer, this is less efficient than the mixing resulting from type 3 jets through a shallow layer. It is also possible that type 1 jets may limit the penetration of turbulence generated by other processes into the surface layers. However, due to the temporal resolution of the tethersonde data, it is very difficult to establish whether the LLJ affects the characteristics of turbulence or whether reduced concentrations of ozone in the residual layer account for the observed trends.

Observations revealed that the characteristics of the jet were continually evolving throughout the night as it sporadically broke down and re-developed at different heights and speeds. This is consistent with other studies of the nocturnal LLJ. Finnigan (1999) and Derbyshire (1999) suggest that the jet exists in an 'uneasy' equilibrium. If the shear associated with the jet becomes too great, a breakdown in stability may occur which disrupts jet formation. This typically results in significant vertical mixing, and the temporary coupling of residual and surface layers. Once the jet has disappeared, the stability in the stable layer may be restored enabling the low-level jet to re-develop and cycle again through the stages.

Incidents of the break-up of the LLJ were classified when it was present and then absent in two consecutive profiles. A further 6 out of the 19 ozone spikes identified occurred when the jet was breaking-down. This suggests that turbulence associated with the break-down of the jet is a further cause of vertical mixing in the nocturnal boundary layer. However, given that a number of examples demonstrate continued increase in concentrations following the break-down of the jet (sometimes for up to four hours), it is likely that the turbulence is attributable to an external factor rather than the jet cycle suggested by Finnigan (1999) and Derbyshire (1999). This is further supported by the failure of the LLJ to re-establish during ozone spikes coincident with this phenomenon.

5.7.2 Mesoscale wind regimes

Wind shear generated by mesoscale wind systems is an important source of turbulence in regions of complex terrain. Mesoscale wind systems have been shown to cause sufficient turbulence to initiate the breakdown of the LLJ (Haeger-Eugensson 1999; Buckley & Kurzeija 1997). This mechanism has the potential to mix a higher concentration of ozone to the surface, since the turbulence is more prolonged and mixing can occur through a greater depth of the boundary layer.

The complexity of the profile renders it difficult to determine the time of onset of down-valley winds. This was hindered further by the temporal resolution of the tethersonde flights. Although development of down-valley winds aloft was frequently preceded by changes in surface wind direction, the complexity of the profile was also reflected in the surface data. The expected wind reversal generated by thermo-topographic wind systems typically occurred over a period of several hours at the surface and did not demonstrate a clear jump in direction, as has been observed in other valley locations (Loffler-Mang et al. 1997; Kalthoff et al. 2000). This limits the accuracy with which the relationship between mesoscale wind systems and ozone spikes can be assessed. Nevertheless, the development of the down-valley wind regime was frequently associated with an ozone spike at the surface. This appears to be particularly true at the Aldergrove site when a westerly band persists at 200 - 300 m after the remainder of the profile has turned easterly. Seven out of the 19 spikes occurred when westerly bands remained aloft.

An example of vertical mixing resulting from shear generated by mesoscale wind regimes can be seen by examining the u and v components of the wind field for 26th - 27th July 1998 in Figure 5.11a & b and wind speed data for the same night in Figure 5.19. Figure 5.19 shows a weak, shallow (100 m) LLJ located at the top of the SBL between 2100 - 2330 PDT. As down-valley winds become established between midnight and 0200 PDT, the jet disappears. However, a westerly band persisted at 200 - 300 m until 0500 PDT. From 0215 - 0500 PDT an increase in ozone concentration was recorded at the surface. The Richardson number indicates that turbulence, perhaps generated from the wind shear extended between 300 - 500 m, enabled mixing throughout the layer (illustrated at 0308 PDT in Figure 5.16). As the westerly band weakens the LLJ starts to re-establish at the top of the SBL in the hour before dawn. This

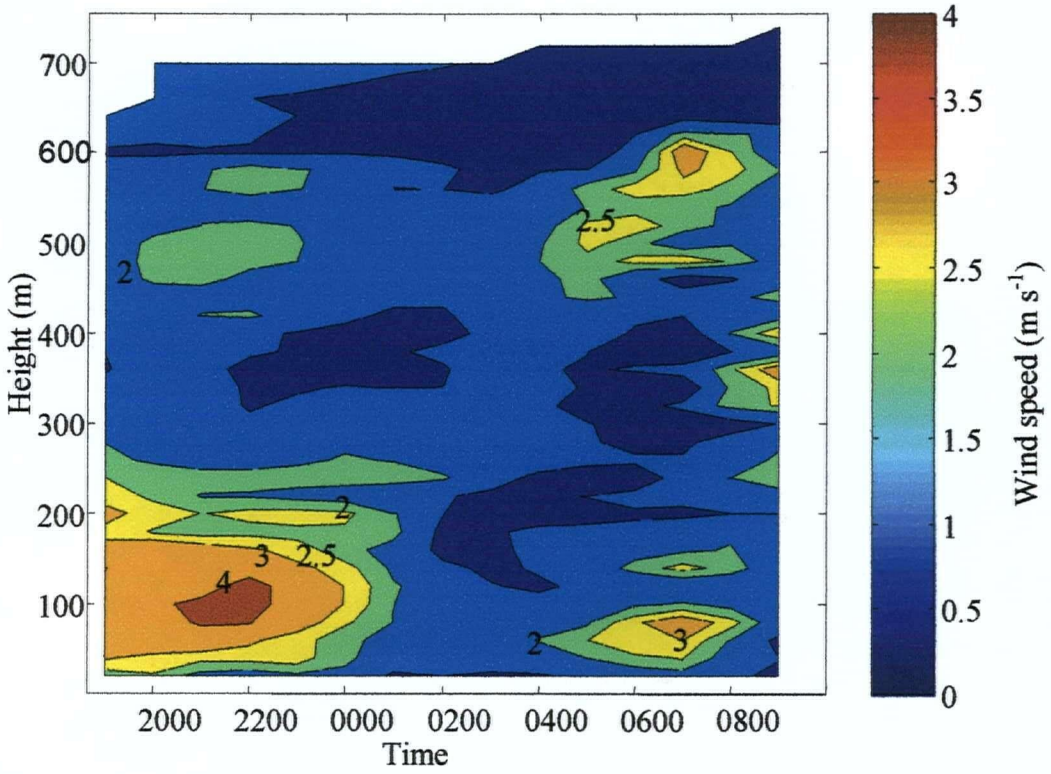

Figure 5.19 A contour plot to show wind speed with height on July 26th - 27th 1998 at CFS Aldergrove

suggests there was sufficient generation of turbulence from the changing mesoscale wind regime to disrupt the development of the jet.

In this example, presence of the LLJ was not well correlated with increases in surface ozone concentration. Instead, once the jet had disappeared (strongly suggesting a turbulent disturbance in the boundary layer), ozone concentrations increased at the surface. This example suggests that a shallow, weakly developed type 3 jet may generate insufficient shear to facilitate vertical mixing. However, it is very hard to establish whether reduced turbulence or lower ozone concentrations aloft (or indeed high NO concentrations at the surface) account for this observation.

Three spikes in ozone concentration could not be linked either to the presence or breakdown of a LLJ or to the development of mesoscale wind flow regimes. A possible further source of turbulence in regions of complex terrain is the breaking of gravity waves (Finnigan 1999). This mechanism may generate sufficient turbulence to disrupt the formation of the LLJ (Coulter 1990). Evidence from micro-barographs placed at the site did not conclusively support the existence of gravity waves at the site. Thus, although gravity waves may prove fundamental to our understanding of turbulence in the NBL, it was not possible to objectively identify them from the data analysed here. (This issue is explored further in Chapter 6 using turbulence data.) Thus the cause of turbulence for these three ozone spikes could not be identified.

Given the variability of ozone concentration with both height and time, it is not surprising that it is difficult to determine any correlation between specific characteristics of the jet (such as height speed or direction) and surface ozone concentrations. However, both the presence of the LLJ and especially its periodic break-down play a significant role in the local generation of vertical mixing. Mesoscale wind systems, particularly the prevalence of a westerly band aloft, also represent a significant source of turbulence in the nocturnal boundary layer. Sixteen out of the nineteen ozone spikes were correlated with variations in the mesoscale wind regime, the presence of a nocturnal LLJ, or its subsequent demise.

5.8 Case Study: August 30th - 1st September 1998

The general trends outlined above can be illustrated with reference to a specific case study. Two consecutive nights were chosen for analysis: August 30th - 31st (night 1) and August 31st - 1st September 1998 (night 2). There were minimal variations in the overall synoptic

situation between these nights. The variation in surface ozone concentration between the two nights, however, was considerable. As shown in Figure 5.20, ozone concentrations remained low throughout the night on August 30th - 31st, while two spikes were recorded on August 31st - 1st, one of which exceeded 40 ppb.

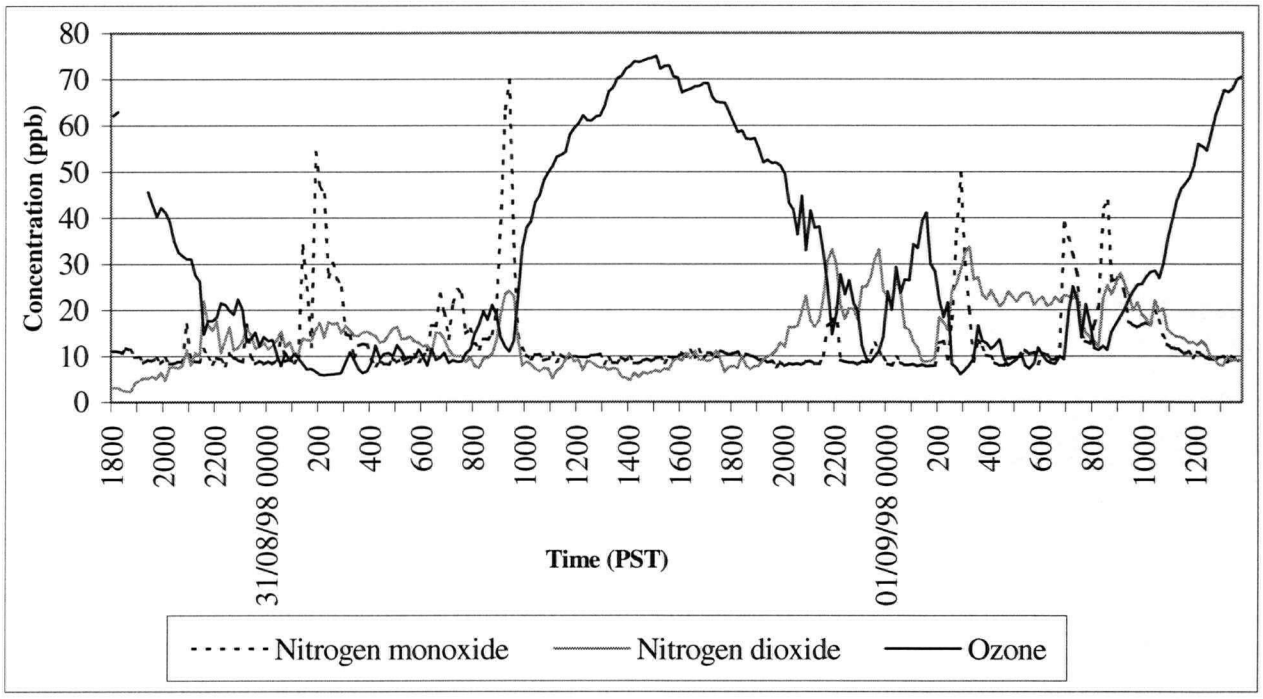

Figure 5.20 Ozone, nitrogen monoxide and nitrogen dioxide concentrations for 30th August - 1st September 1998

Figure 5.4 and Figure 5.5 illustrate that spikes in ozone concentration occurred throughout the valley during both nights. Thus the absence of ozone spikes at CFS Aldergrove on August 30th - 31st indicates that local factors may be affecting surface ozone concentration on this night. Analysis of the surface concentrations of NO shows that although spikes in NO concentration were recorded on both nights, background concentrations were consistently low, around 9 ppb. Thus it is unlikely that increased NO concentrations can account for the absence of ozone spikes on the first night. This is further supported by the incidence of increased NO_2 concentrations during night 2. (If chemical titration had been active enough to disguise the presence of vertical mixing, higher concentrations of NO_2 would have been expected during the first night.)

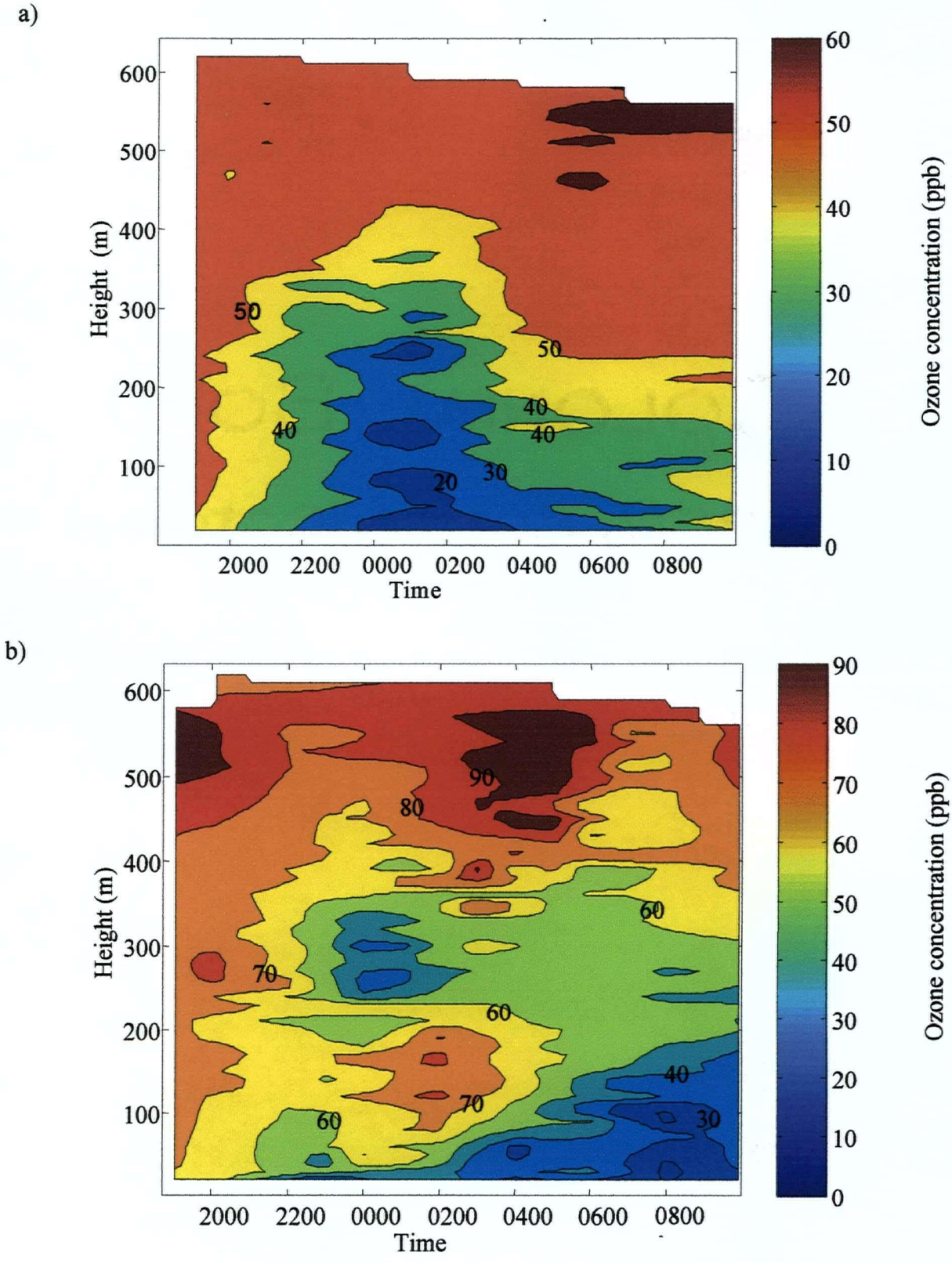

Figure 5.21 Contour plots of ozone concentration for the nights of a) August 30th - August 31st b) August 31st - September 1st 1998

Thus the differences between the two nights must be accounted for either by variations in stability, or in the concentrations of ozone in the residual layer aloft. Figure 5.21 illustrates the marked differences in ozone concentration between the two nights. Ozone concentrations are significantly lower throughout the RL between 0 - 300 m on the first night. During the first night deposition appears to dominate through the profile to 400 m and there is no evidence for the advection of air parcels containing high ozone concentrations. During the second night, although there is evidence for deposition later in the night (from 0300 PDT onwards), a layer containing high ozone concentrations is evident between 150 - 200 m at 0100 PDT.

Figure 5.22 demonstrates that considerably higher wind speeds throughout the residual layer were observed particularly during the latter part of the night (6 - 9 m s^{-1} compared to less than 2 m s^{-1}), and the development of a strong type 1 LLJ between 0300 - 0600 PDT at 300 m, on August 30th - 31st. Although a wind speed maximum can be identified at the top of the stable layer between 2200 - 0300 PDT during night 2, this only weakly resembled a type 3 LLJ. Down-valley winds could be identified in the residual layer on both nights (Figure 5.23). However, on the first night there is a marked difference between surface wind direction and wind profiles in the residual layer, indicating that the stable layer may be decoupled from the wind regime aloft.

Despite the increased wind speeds prevalent in the residual layer during night 1, Figure 5.24 indicates that much of the profile is dominated by high Ri particularly between 2300 - 0500 PDT. The strong stability of the residual and surface layers suggests that vertical mixing is likely to be minimal throughout most of the night. Although intermittent turbulence may have been generated by the type 1 LLJ between 0400 - 0600 PDT (suggested by the isolated region of increased Ri between 0 - 100 m) this was not captured by the tethersonde flights, and due to the absence of ozone in the profile, there was no evidence of increased concentrations at the surface.

The Ri is smaller throughout the profile on the 31st - 1st September. This is particularly apparent between 0000 PDT and 0100 PDT when the Ri remains small throughout the profile, indicating that vertical mixing could occur through to 500 m. Figure 5.23 and Figure 5.25 indicate that the wind direction was changing throughout the boundary layer at this time (generating shear and hence turbulence) as the mesoscale down-valley wind system develops. This time period coincides with the increase in ozone concentrations associated with the first ozone spike at the surface. Evidence in support of vertical mixing can be found in temperature contours which show a marked flattening throughout the boundary layer during this time period

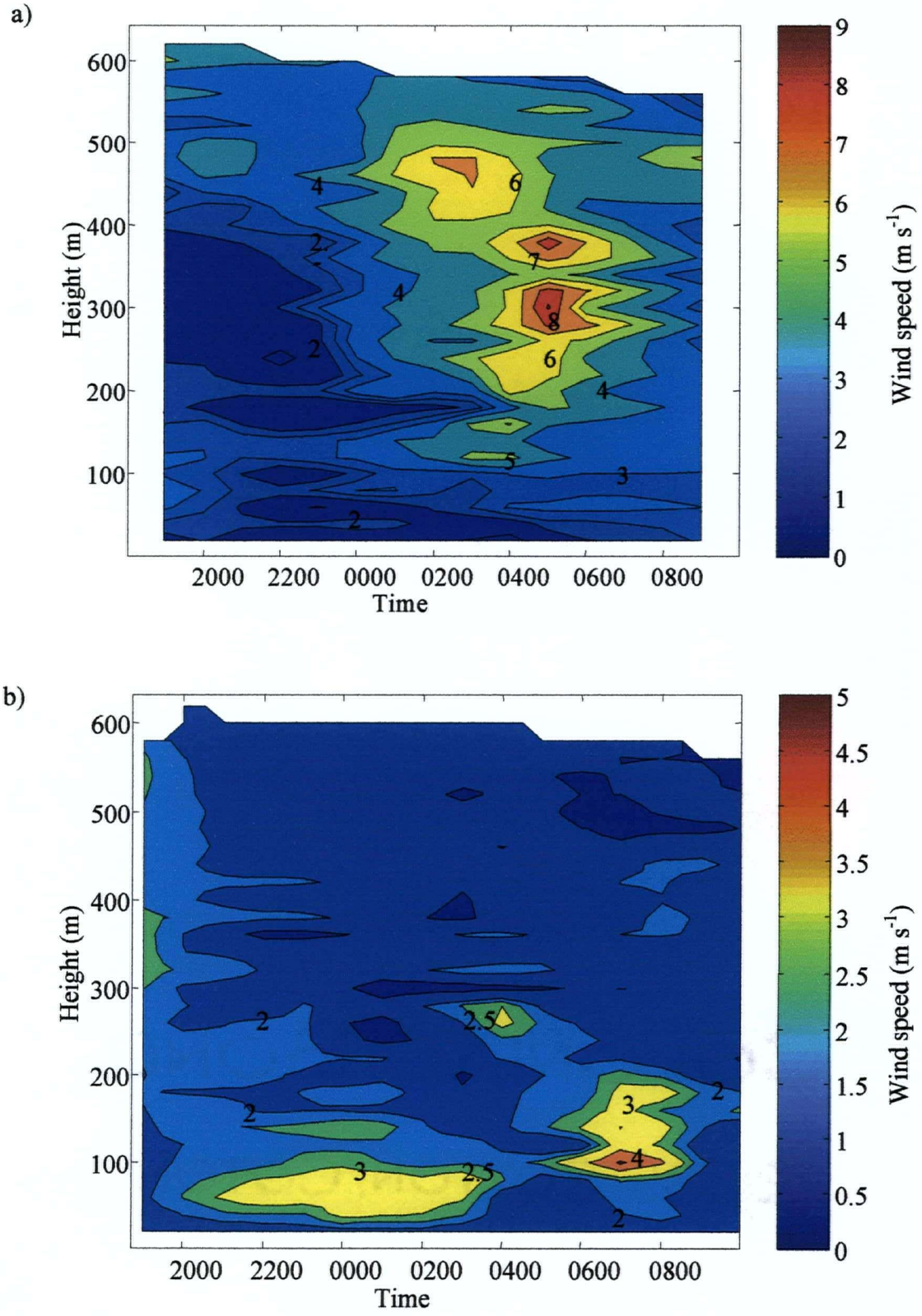

Figure 5.22 Contour plots of wind speed for the nights of a) August 30th - August 31st and b) August 31st - September 1st 1998

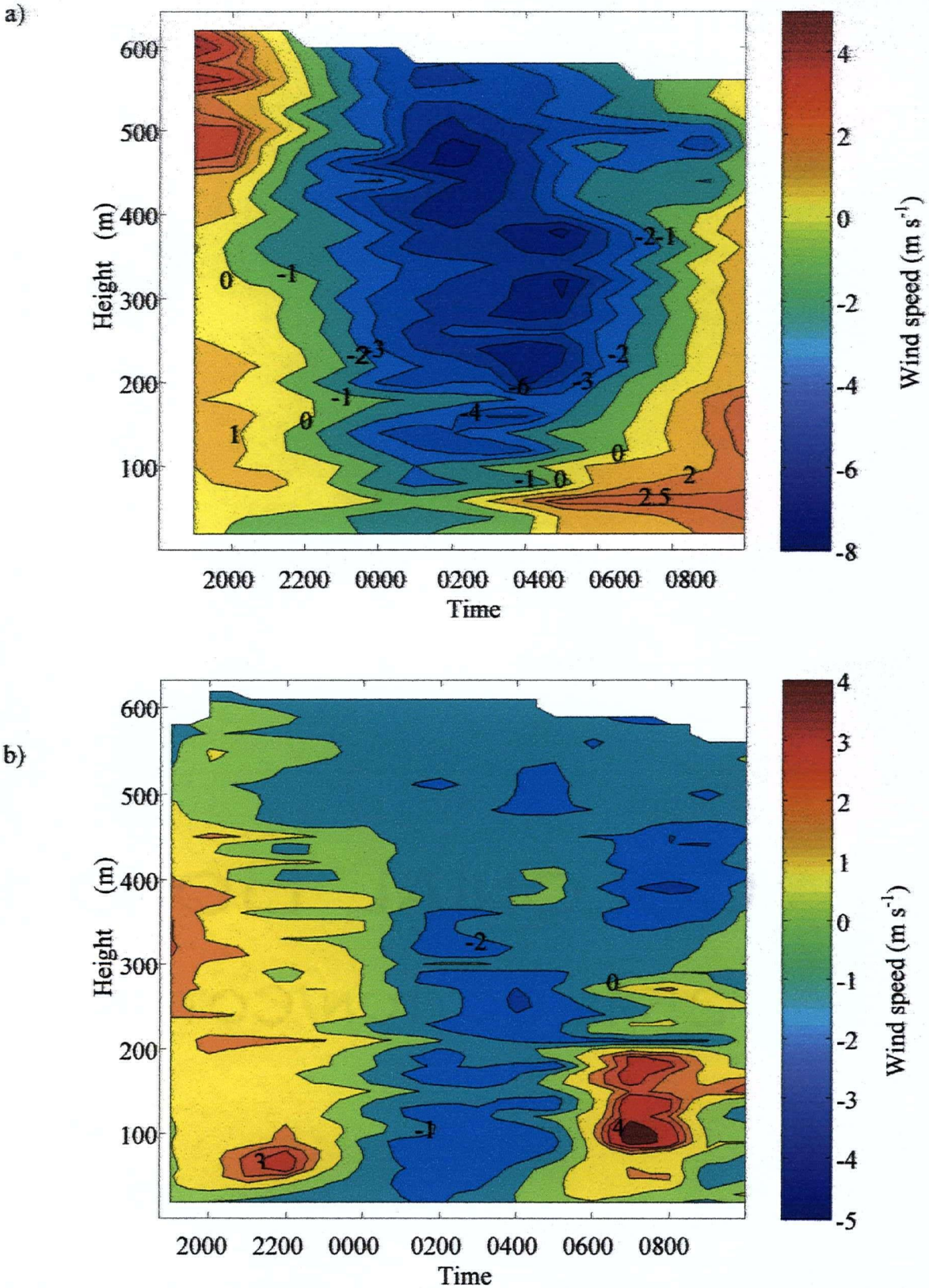

Figure 5.23 Contour plots for u-component of the wind vector for the nights of a) August 30th - August 31st and b) August 31st - September 1st 1998

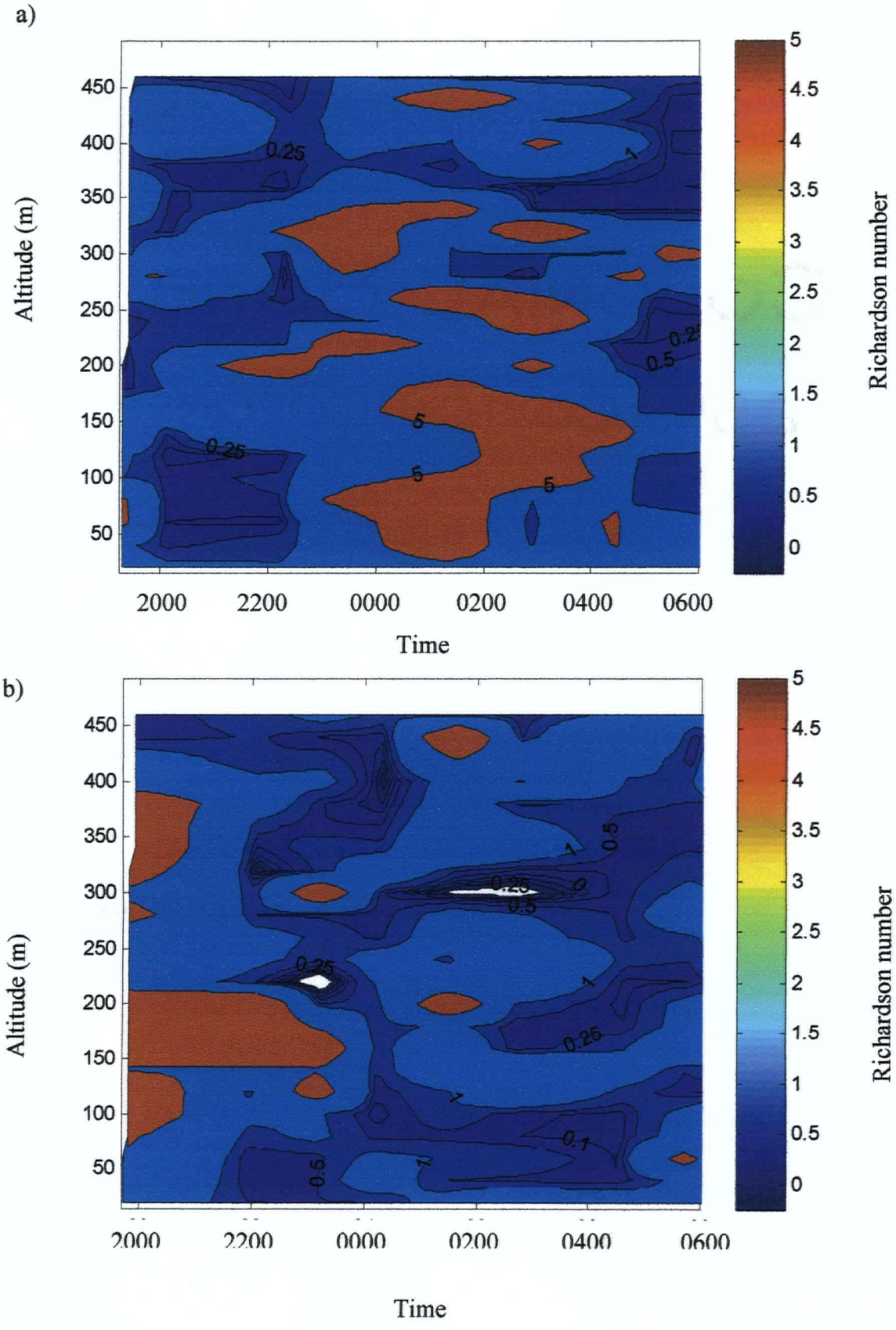

Figure 5.24 Comparison of contour plot to show changes in Richardson number with height for a) August 30th - 31st and b) August 31st - September 1st 1998 at CFS Aldergrove. (Note areas of white in the contour plot represent values of the Richardson number which were negative and thus very likely to support turbulence.)

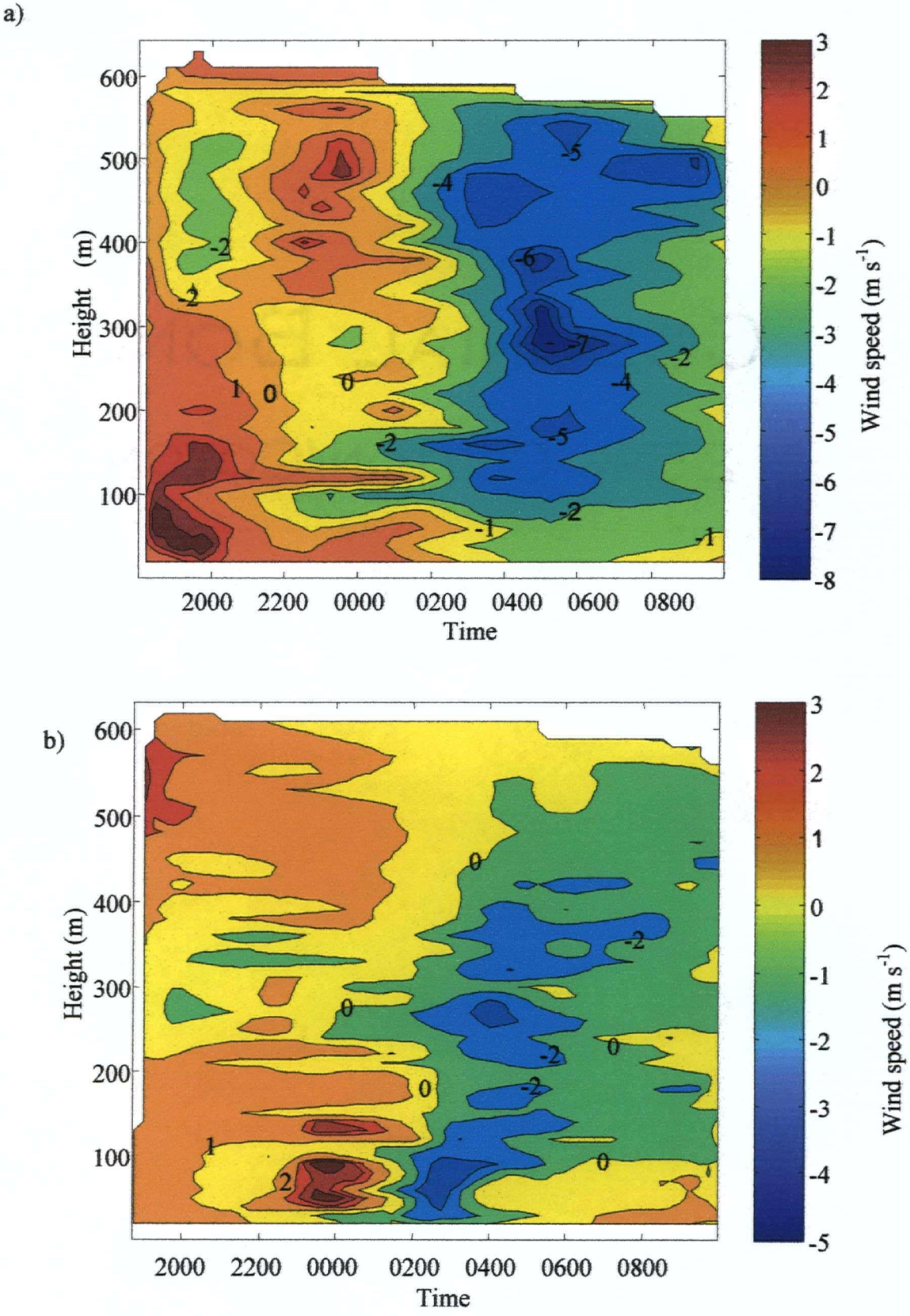

Figure 5.25 Contour plots of v-component of the wind vector for the nights of a) August 30th - August 31st and b) August 31st - September 1st 1998

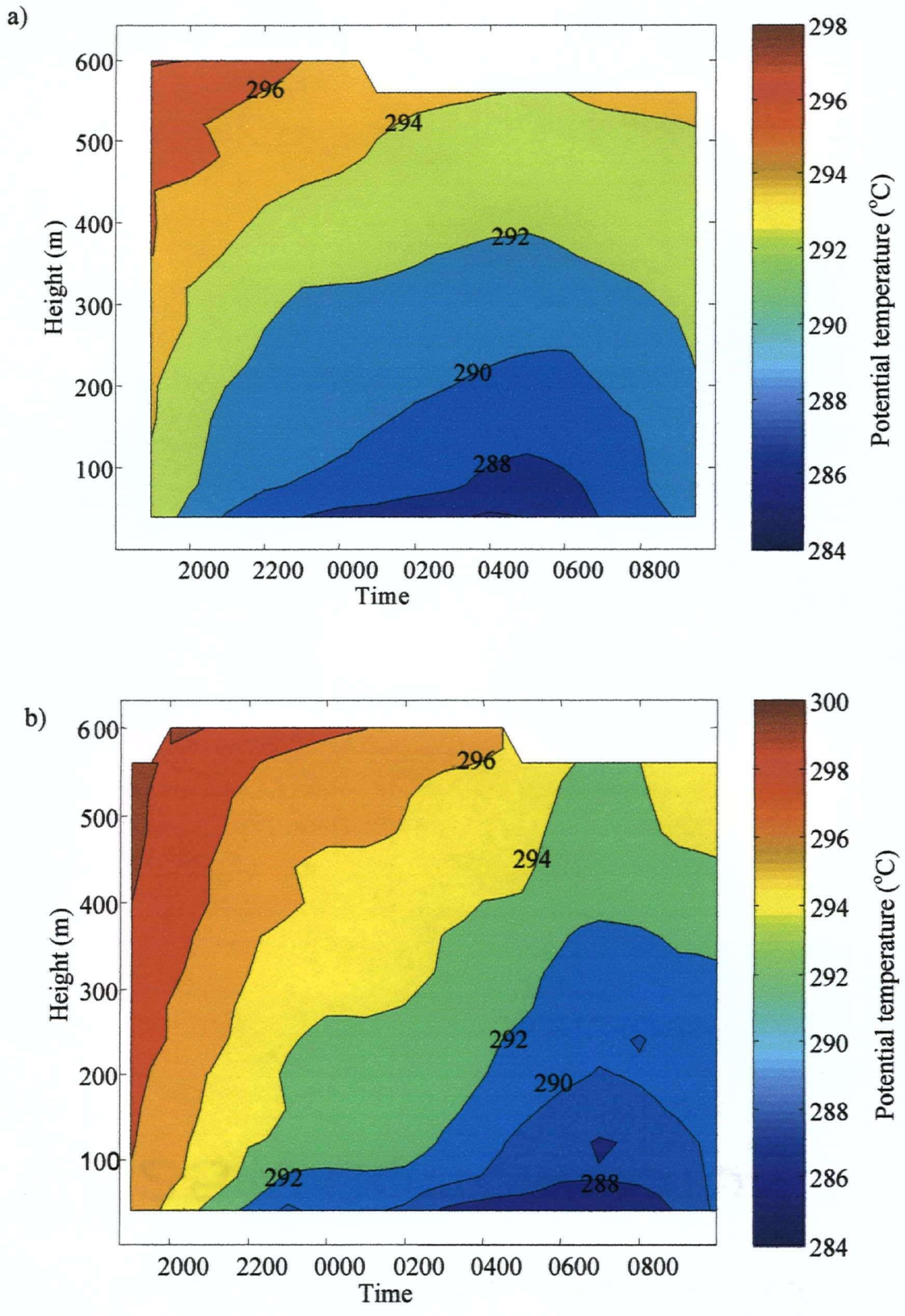

Figure 5.26 Contour plots of temperature for the nights of a) August 30th - August 31st and b) August 31st - September 1st 1998

(Figure 5.26). Evidence for vertical mixing throughout the 500 m layer is harder to identify as high concentrations aloft and between 150 - 200 m are interspersed with lower concentrations between 250 - 400 m. It is therefore likely that a combination of vertical mixing processes, which occurred simultaneously with the advection of high ozone concentrations over the site, account for the marked increase at the surface.

Two other periods of marked instability are particularly noticeable during night 2: between 200 - 250 m (2200 - 2400 PDT) and at 300 m (0200 - 0400 PDT) (Figure 5.24). Increased ozone concentrations at the surface were observed between 2200 - 2400 PDT. However, a decrease in ozone concentration was initially observed at 0200 PDT, despite the fact that high ozone concentration remain aloft and Ri through much of the boundary layer below 300 metres were low enough to indicate the continued existence of turbulence. Surface data show an increase in both NO and NO_2 concentrations during this time period. Thus it is probable that there is continued mixing of ozone to the surface, but that chemical titration is masking the evidence and hence there is no recorded ozone spike.

Surface chemistry is also likely to play an important role in accounting for the morphology of the second ozone spike which occurred between 0600 - 0800 PDT on September 1st 1998. Here, ozone concentrations and NO concentrations increase simultaneously, suggesting either the coincidental advection of NO to the site or vertical mixing of a NO plume to the surface. Evidence in Figure 5.21 suggests the presence of a low altitude band at 100 m with low ozone concentrations during this time period. This provides circumstantial evidence for the presence of NO aloft. However, further information is required to confirm this hypothesis.

In summary, the combined effect of comparatively low ozone concentrations in the residual layer, and the strong stability of both the surface and residual layers, account for the absence of ozone spikes during the night of August 30th - 31st. Increased surface ozone concentrations observed on the night of August 31st - September 1st likely resulted from the advection of a plume of high ozone concentrations over the site, combined with a period of vertical mixing throughout the boundary layer. In this instance the turbulence appears to be the result of the development of mesoscale down-valley flows which were sufficient to destroy the weakly developed LLJ. However, surface chemistry was an important factor in determining the local impact of the mixing process.

5.9 Summary

A marked diurnal cycle can be identified in surface ozone concentrations throughout the LFV. Specific characteristics of the cycle are dependent on the complex interactions between advection, fumigation, chemical production, deposition and titration processes operating at each site. Although deposition and titration processes dominate in the stable surface layers during the night, localised increases in ozone concentration are a common feature of diurnal ozone cycles throughout the Lower Fraser Valley. These spikes in ozone concentration occur sporadically in both time and space. Local concentrations of NO appear to be an important factor in determining the timing, frequency and duration of ozone spikes.

Ozone concentrations in the residual layer were highly variable with both time and height. Plumes of high ozone concentrations were intermittently advected over the site from a variety of different directions. Examination of the vertical profiles of temperature and wind speed and direction suggests the primary cause of ozone spikes is vertical mixing. This was supported by the relationship between increased ozone concentrations at the surface and low Richardson numbers in both the tethersonde profiles and surface layer. Using this parameter, turbulence was seen to be intermittent and to exist in isolated layers within the nocturnal boundary layer.

The primary cause of vertical mixing was wind shear resulting from the presence or break-down of the nocturnal LLJ or associated with the development of mesoscale down-valley winds. Largest increases in ozone concentrations recorded at the surface were coincident with shear from mesoscale wind reversals. This is a result both of the mixing through a deeper section of the boundary layer (compared to turbulence generated by a shallow LLJ) and advection of high concentrations of ozone in the westerly flow. The timing of turbulence with respect to advection of ozone aloft was critical to the vertical mixing of high ozone concentrations to the surface.

Chapter 6: Wavelet analysis of turbulence in the nocturnal boundary layer

6.1 Introduction

In Chapter 5 the Richardson number was used to identify dynamically unstable layers in the NBL. On occasion, these potentially turbulent layers were shown to extend through the NBL to the surface. The near-surface layers were also shown to be characterised by temporal variability in stability. This strongly suggested the existence of turbulence in the very stable NBL. The aim of this chapter is to provide a detailed analysis of the characteristics of near-surface turbulence during the IOPs using high frequency turbulence data.

The weak, intermittent nature of turbulence in the NBL hinders quantitative analysis using traditional analytical tools such as the Fourier Transform. In this chapter a comparatively new analytical tool - wavelet analysis - is used to evaluate the characteristics of turbulence in the very stable NBL. A 2-dimensional plot of the calculated wavelet coefficients (a scalogram) is used to localise high frequency fluctuations associated with turbulent activity and to ascertain the characteristics of larger scale (and perhaps more wave-like) motions in the NBL. An original technique (based on wavelet analysis) is then developed to objectively isolate intermittent turbulent 'bursts' or events within the time series. This permits a quantitative description of the characteristics and global intermittency of the turbulence observed in the signal.

This technique is used to assess the frequency, duration and strength of intermittent turbulence observed during the IOPs. The characteristics of the turbulence observed at the surface associated with two of the potential causes of such activity identified in Chapter 5 - the nocturnal LLJ and mesoscale wind regimes - are then examined. Given the correlation identified between these disturbances and ozone spikes at the surface, the hypothesis that these disturbances result in increased turbulence in the surface layers is examined.

The turbulent characteristics of the boundary layer associated with the spikes in ozone concentration, which could not have been generated by either a LLJ or mesoscale disturbance in the NBL, are also analysed. Wavelet analysis is used to probe the characteristics of the turbulence data to determine whether breaking gravity waves may also cause vertical mixing. Finally, the implications of these results are discussed within the context of vertical mixing processes and the observations made in Chapter 5.

6.2 Intermittent turbulence in the very stable nocturnal boundary layer: analysis techniques

Turbulence is very difficult to quantify in the very stable nocturnal boundary layer. The turbulence data utilised in this chapter were collected at a temporal resolution of 21 Hertz and are characterised by rapid fluctuations in turbulence intensity. Figure 6.1 compares the characteristics of four 30 minute series of vertical velocity. The data recorded between 1130 - 1200 PDT August 31st are compared with three nocturnal time series observed between 2330 - 0100 PDT August 31st - 1st September 1998. Note the different resolution on the y-axis between the daytime and night-time scenarios. The first series represents conditions in a fully developed convective boundary layer, the latter three series are representative of conditions in the NBL where turbulence is likely to be primarily driven by shear. The turbulence observed in the NBL was typically more than an order of magnitude smaller than that observed during the day. Thus measurements were often made close to the resolution limit of the instruments. The nocturnal traces clearly show three periods of marked increase in vertical velocity between 2353 PDT and 0108 PDT which likely correspond to turbulent 'bursts'. They are representative of intermittent turbulence in the NBL. These isolated events in the time series are of primary interest here since they represent the more turbulent portion of the time series.

Many different attempts have been made to quantify the intermittent behaviour of natural systems (Hagelberg & Gamage 1994). Qualitatively, intermittency refers to the behaviour of a process or system which can be classified into two polar opposite categories such as on and off. A process would be described as intermittent if it showed non-periodic, temporally irregular fluctuations between these two states over a defined period of time. Intermittent behaviour can then be quantified as a ratio between the time when the process was turned on (or off) and the total length of the time series. This ratio is commonly called the intermittence factor. The precise time the system or process changed state, the time interval between changes and the number of changes per time period may also be of interest in studying intermittency.

In the case of atmospheric turbulence a turbulent 'event' or burst may be identified when an increase in turbulence is observed above a certain threshold. For the convective boundary layer these bursts are sometimes described as coherent events, referring to the physically coherent structure of the turbulent eddy isolated from the time series (Hagelberg & Gamage 1994). Two types of intermittency can then be identified with regards to turbulence: local

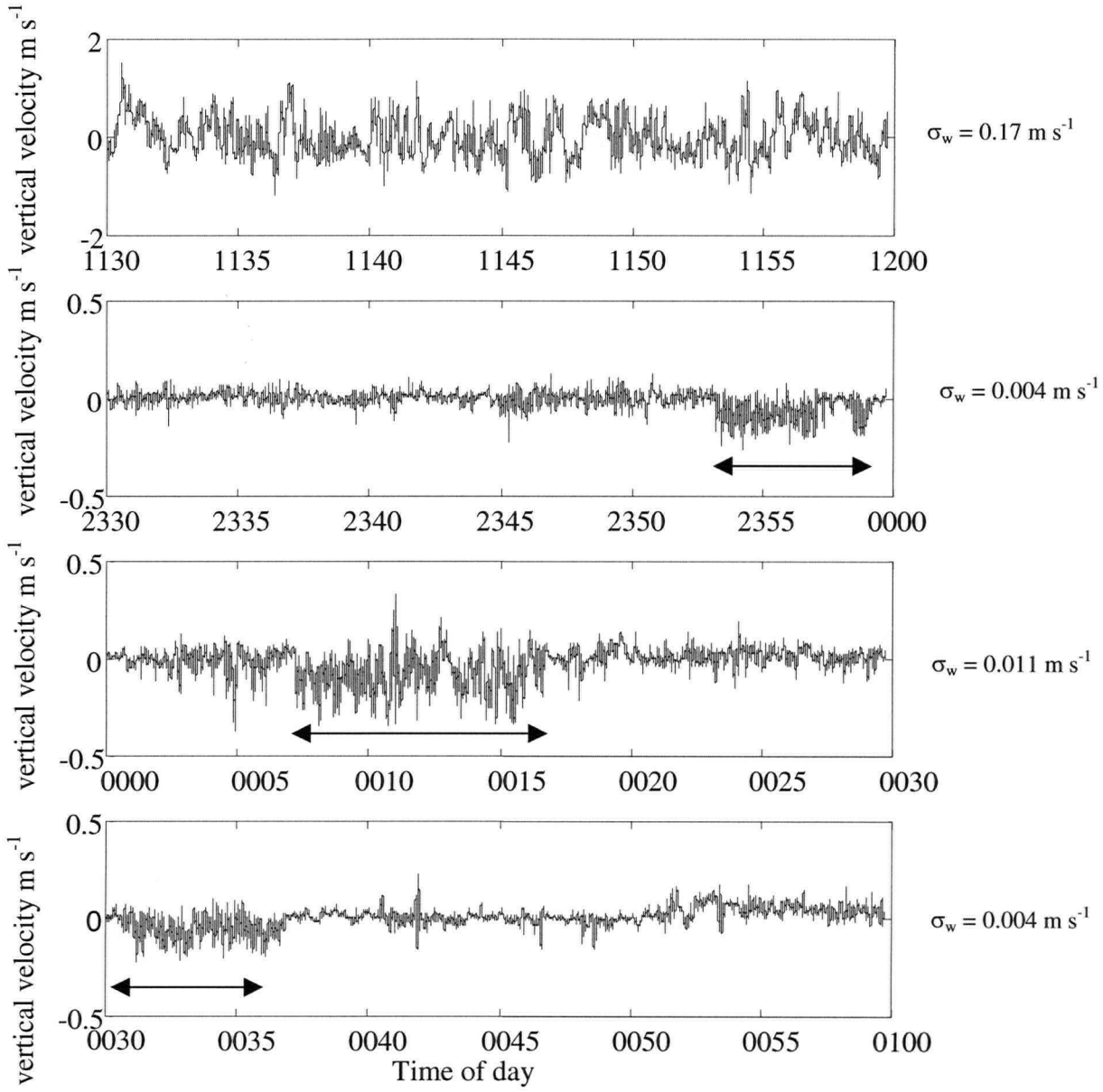

Figure 6.1 Variations in vertical velocity observed during four 30 minute time series ending at:

a) 1200 PDT August 31st 1998 (Day-time - convective boundary layer- conditions)

b) 0000 PDT September 1st 1998 (Night-time conditions)

c) 0030 PDT September 1st 1998 (Night-time conditions)

d) 0100 PDT September 1st 1998 (Night-time conditions)

(Note the different resolution of the y-axis between day-time and night-time scenarios. Arrows indicate approximate limits of three turbulent bursts.)

intermittency, which refers to variation within a turbulent eddy, and global intermittency (of interest in this chapter), which refers to the separation of clusters of turbulent eddies in time or space (Mahrt 1989).

One of the particular challenges facing the quantitative definitions of intermittency with regards to atmospheric turbulence, is that a threshold must be selected to separate the time series into two components. This may be done visually, based on the magnitude of a particular feature in physical space or the selection of a frequency threshold (Hagelberg & Gamage 1994). Although it is increasingly recognised that a significant portion of vertical flux transport in the very stable nocturnal boundary layer occurs as a result of intermittent bursts of turbulent activity (Mahrt et al. 1998; Weber & Kurzeja 1991; Coulter 1990), there is little consensus in the literature as to the most appropriate method for identifying thresholds or quantifying intermittency within this context. As a result quantitative indices of intermittency range from a) the ratio of flux time (structure or event component) to time series length (Hagelberg & Gamage 1994), to b) the ratio between the standard deviation of 5 minute fluxes to the total flux of the time series (Mahrt et al. 1998). However, neither of these definitions describe the individual or relative temporal placement between turbulent events.

The aim of this chapter is to develop an objective, statistically robust threshold to identify periods of the time series when turbulence is active. Using wavelet analysis, the number of these events, their temporal placement and duration are identified within each 30 minute time series. The primary interest of this study is to identify the relationship between intermittent turbulent events and local increases in surface ozone concentration. Thus no further attempts are made to describe the statistical properties of intermittency within or between time series using functions such as the Hurst exponent, commonly used in hydrology or engineering applications.

6.2.1 Fourier transform

It is very difficult to effectively analyse the large volume of data generated by turbulence measurements without the use of quantitative tools to summarise and describe the data. As demonstrated in Chapter 3, the most common analytical tool used to quantitatively analyse turbulence data is the Fourier transform. This has been successfully used in the convective boundary layer to describe turbulence, quantify scalar transport and elucidate information from the turbulent trace about the characteristics of the underlying processes. However, due to the global nature of the transform and intermittent characteristics of the signal, this tool provides

only a very limited insight into the nature and characteristics of turbulence in the very stable NBL.

For example, Figure 6.2 illustrates the energy spectra calculated using the FFT for the four 30 minute time series in Figure 6.1. Comparison of the day-time and night-time spectra illustrates marked differences between the characteristics of the turbulence during the two regimes. Although both periods show the expected –5/3 gradient in the inertial subrange characteristic of turbulent activity, this can only be found in wave numbers above 0.6 m^{-1} in the nocturnal data. At longer scales, the nocturnal spectra become noisy and difficult to decipher. The technique also identifies the increased net energy content of the 0030 PDT trace compared to the other night-time time series. However, it is difficult to distinguish between the 0000 PDT and 0100 PDT data sets in Figure 6.2 even though visual analysis of the raw time series (Figure 6.1) indicates considerable differences between the two data sets. All the information in the signal regarding the timing, duration or strength of the individual turbulent bursts is hidden within the global characteristics of the transform. Further, due to the absence of a clear spectral gap in the turbulent time series, it is also not possible to identify the range of frequencies generated by the intermittent turbulent bursts from the non-turbulent ('noise') component of the remainder of the time series.

Clearly, using the FT as the primary analytical tool limits the quantitative evaluation of important turbulent characteristics such as intermittency, duration and local positioning of turbulence within the time series. Furthermore, the characteristic frequencies of turbulent bursts become obscured as a global characteristic of data sets. These details are, however, crucial to understanding turbulent transport of scalar quantities in the NBL. Although some of these details could be obtained by a thorough visual assessment of data sets, it is very difficult to effectively analyse large amounts of data. Further, this time consuming procedure is subject to personal bias and inconsistencies. It can be very hard to isolate and identify trends or patterns in the data set or even undertake basic quality control procedures by eye. Thus an alternative analytical tool was sought to quantitatively evaluate the characteristics of turbulence in the very stable NBL.

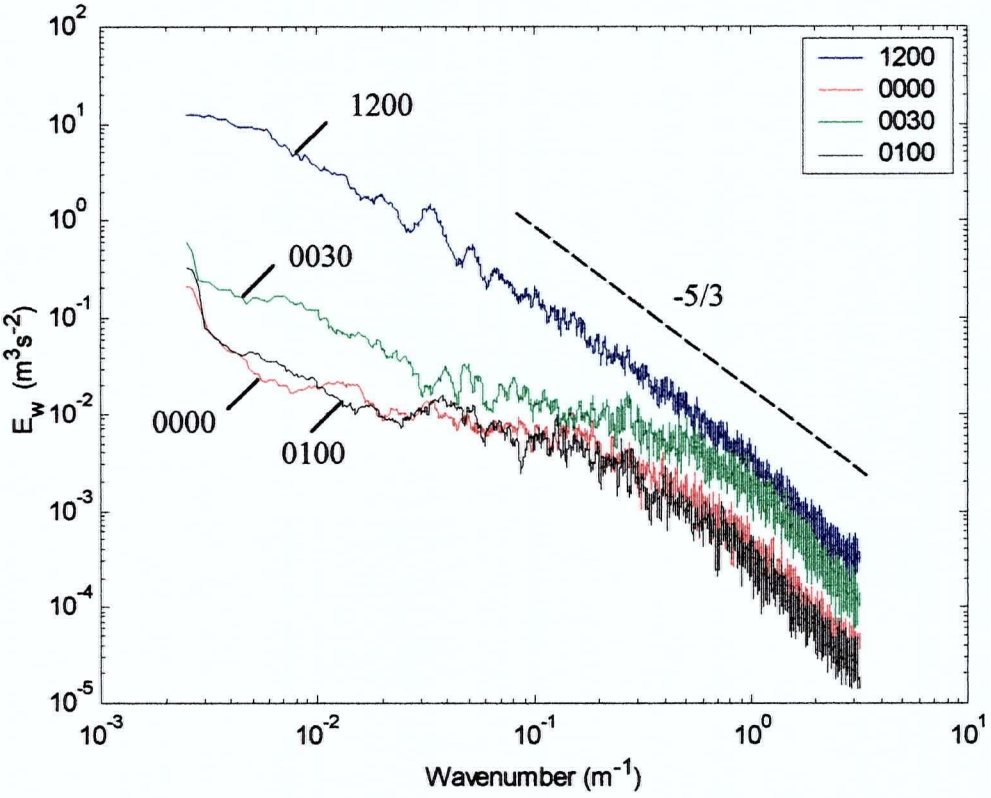

Figure 6.2 The energy spectra calculated using the FFT for four 30 minute time series ending at1200 PDT August 31st and 0000 PDT, 0030 PDT, and 0100 PDT September 1st 1998

6.2.2 Wavelet analysis

Wavelet analysis offers an alternative approach for analysing nocturnal time series. It is a local, 2-dimensional transform that facilitates the retention of information about the temporal location of frequencies within the data set. This is most easily visualised using a scalogram. A scalogram is a 2-dimensional plot of the square of wavelet coefficients. This can be easily compared with the original time signal to determine whether the chosen wavelet base has detected the characteristics of interest within the signal, acting as an effective first step in an analysis procedure. (See Torrence and Compo (1998) for detailed discussion on interpreting the wavelet coefficients from the scalogram.)

Although an increasing number of papers use wavelet analysis to analyse turbulent time series (Collineau & Brunet 1993; Hagelberg & Gamage 1994; Trevino & Andreas 1996; Jordan et al. 1997; Howell & Mahrt 1997; Katul & Parlange 1995; Katul et al. 1996; Farge 1992; Mayer et al. 1994), few exploit the details available from a scalogram. This may be a result of the perceived qualitative nature of the presentation. This can be overcome through the application of rigorous statistical tests as suggested by Torrence and Compo (1998). Using this methodology, Galmarini & Attie (2000) demonstrate that wavelet analysis and specifically the scalogram can be used to provide a clear insight into spatial variations of turbulent transport processes.

As demonstrated in Chapter 3 a variety of different wavelet bases can be defined. For the purposes of this chapter, two different wavelets are utilised. The first is the Haar wavelet, which efficiently detects breaks or jumps in data sets and is well localised in the temporal domain. It has a very simple morphology, minimising contamination of the coefficients with too much information about the wavelet. This was used in the initial stages of analysis (section 6.3) as it has been previously applied to turbulent signals with good results (Howell & Mahrt 1997; Howell & Sun 1999; Katul & Parlange 1995). Given that the discrete orthogonal form of the Haar wavelet transform satisfies the requirements of Parseval's theorem, this wavelet was also used to calculate variances, energy spectra and to reconstruct the original signal at different scales.

The remainder of the analysis uses the Morlet wavelet (section 6.4). Use of a second wavelet reduces the probability that the trends observed above are a product of the wavelet rather than the innate characteristics of the time series. The Morlet wavelet is a symmetrical wavelet with a shape more akin to that of the phenomenon of interest. Lau & Weng (1995) argue

that, in the absence of other criteria, the choice of a wavelet with a 'reasonable resemblance' between the shape of the wavelet and the signal is the best basis upon which to select the analysing wavelet. Symmetric wavelets are coherent at the edge of a transition and effectively define the start of the change in conditions (Hagelberg & Gamage 1994). This enabled efficient identification of the start and end points of turbulent periods. It is also a compact wavelet and is well defined in Fourier space. Good resolution in the frequency domain is important if a scale separation between turbulent fluctuations and other longer scale motions is to be achieved. It also enables fast calculation of the wavelet coefficients in Fourier space. This wavelet is a complex wavelet which enabled the definition of cross-spectra and phase used in section 6.7.

6.3 Identifying temporal variations in dominant frequencies

In this section wavelet analysis is used to identify temporal variations of different scales of motion within the data set. The continuous form of the Haar wavelet was used to calculate the wavelet coefficients for the scalograms. This ensures that all the information about the energy characteristics is represented and enables effective tracking of changes with time (Farge 1992). The redundancy of information associated with a high density of scales in the continuous form of the transform acts to reinforce jumps or breaks in the data set (Collineau & Brunet 1993).

In practise, analysis of any signal using a truly continuous scale is not practical. Scales have to be chosen within the context of the resolution of the signal, the characteristics of interest and the computational resources available (in this case a Pentium-2 computer processor with 200 Mb of RAM). Following initial testing of a range of different resolutions, 90 scales were chosen for analysis using the Haar wavelet, each separated by 10-second intervals.

Wavelet coefficients effectively represent the correlation between wavelet and signal. Warm colours in the scalogram indicate a high degree of correlation between the wavelet and the time series. Thus, for the Haar wavelet, warm colours represent a jump or break in the signal. This may be the product of a change in the characteristics of the turbulent signal, perhaps associated with the onset or cessation of turbulent activity. Cool colours in the scalogram, which indicate a poor degree of correlation, indicate a more flat-line signal.

Further information about the characteristics of the signal can be obtained by analysing the scales at which the activity is detected. For example warm colours found only at small scales indicate jumps in the data set at high frequencies that may be indicative of turbulent activity. Thus if turbulence exists in the nocturnal boundary layer, and it is truly intermittent, then

clusters of warm colours should be identified at high frequencies throughout the data set. Warm colours at large scales are representative of jumps occurring at longer scales in the time series which are perhaps representative of a more wavelike processes. However, if a low frequency jump is present in the data set, wavelets of all sizes will show a good correlation with the time series. Thus under these conditions it is not possible to determine whether turbulent scale processes are operating simultaneously with larger scale processes.

Scalograms for the 30 minute time series observed between 0000 - 0030 PDT September 1st 1998 (shown in Figure 6.1c) are plotted in Figure 6.3. Turbulent scale activity shown in the scalogram for vertical velocity (Figure 6.3a) does appear to be temporally isolated between 0005 – 0017 PDT in the scalogram and corresponds well with the period of increased variance observed in Figure 6.1c. This activity is superimposed on a background of a few larger scale motions which do not always correlate with the turbulent scale motions. A lag can be observed in the first part of the scalogram between these low frequency structures in the vertical velocity time series and the corresponding change in the temperature time series. This suggests that the two variables are initially out of phase with each other and may indicate the presence of waves within the NBL.

From 0012 PDT there is a higher degree of correlation between the timing of jumps detected in the temperature and vertical velocity traces. This is particularly evident at the smaller time scales, suggestive of turbulent activity across a range of frequencies within the signal. The cross-scalogram shows a marked 'burst' of colour across the scales between 0015 PDT and 0016 PDT indicating coherence between the vertical velocity and temperature time series and the wavelet. This pattern is also suggestive of turbulent activity. Although a clear gap (which would correspond to the spectral gap in the time series) cannot be identified between small and large scale patterns in the scalogram, the technique does suggest the presence of intermittent activity at turbulent scales within the nocturnal boundary layer. Flashes of warm colours are visible at the start and end of the scalogram in Figure 6.3b. These are artefacts of the wavelet transform resulting from analysis of a time series of a finite length. Like Fourier analysis, wavelet analysis is sensitive to the length of the time series. They are particularly noticeable in the scalogram of temperature due to the marked non-stationarity of the time series.

For comparison, scalograms and the cross-scalogram for vertical velocity and temperature representative of conditions in the convective daytime boundary layer observed between 1130 - 1200 PDT August 31st (shown in Figure 6.1a) are given in Figure 6.4.

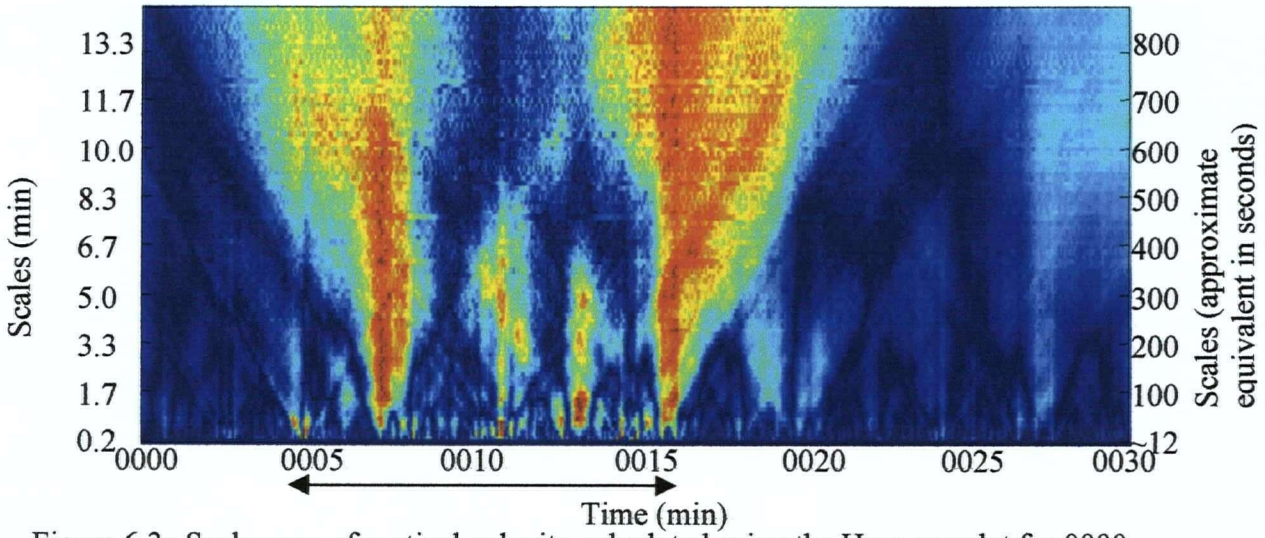

Figure 6.3a Scalogram of vertical velocity calculated using the Haar wavelet for 0000 - 0030 PDT September 1st 1998 (Arrows indicate period of dominant turbulent activity)

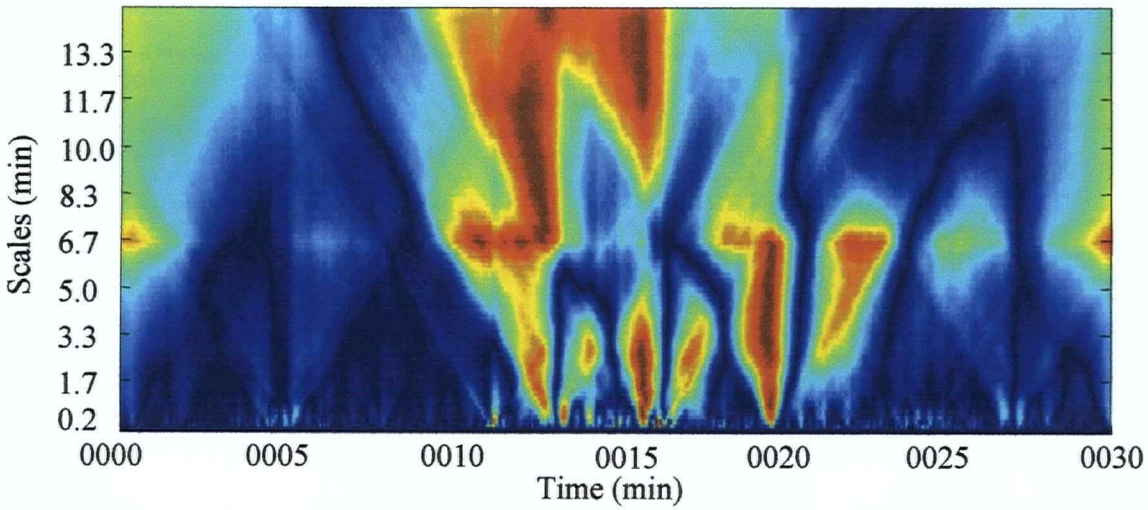

Figure 6.3b Scalogram of temperature calculated using the Haar wavelet for 0000 - 0030 PDT September 1st 1998

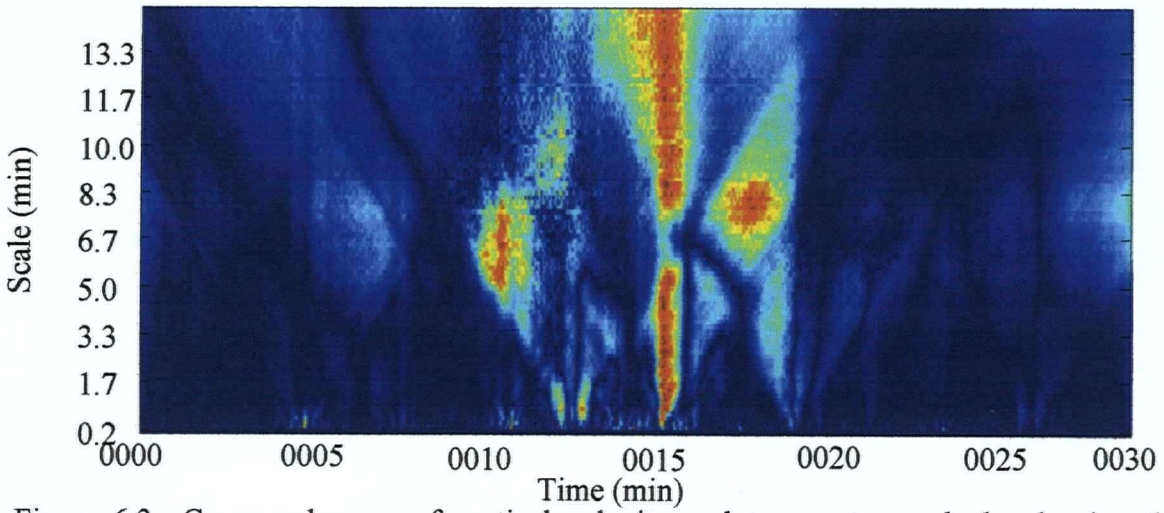

Figure 6.3c Cross-scalogram of vertical velocity and temperature calculated using the Haar wavelet for 0000 - 0030 PDT September 1st 1998

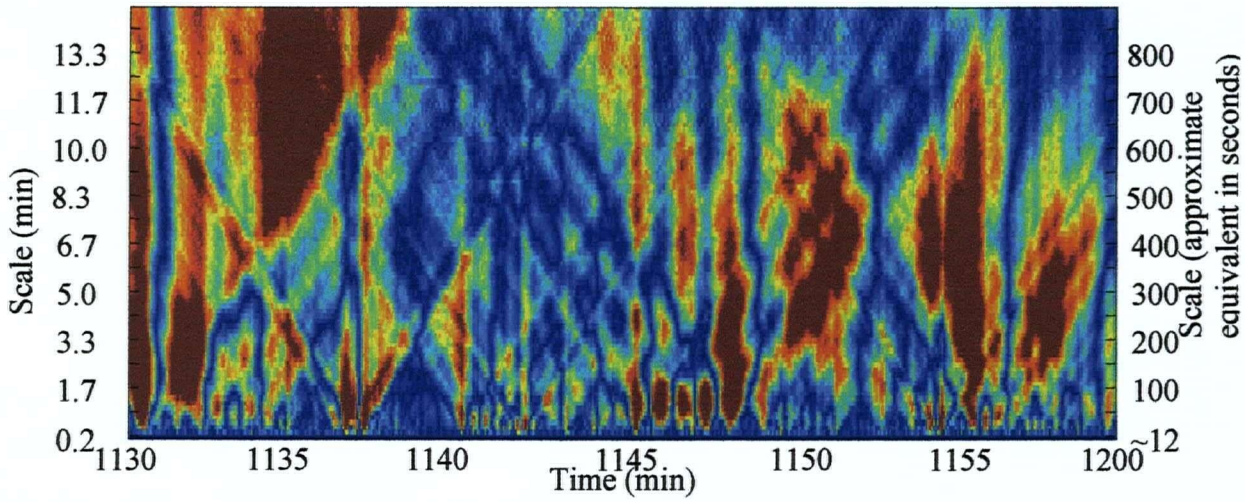

Figure 6.4a Scalogram of vertical velocity calculated using the Haar wavelet for 1130 - 1200 PDT August 31st 1998

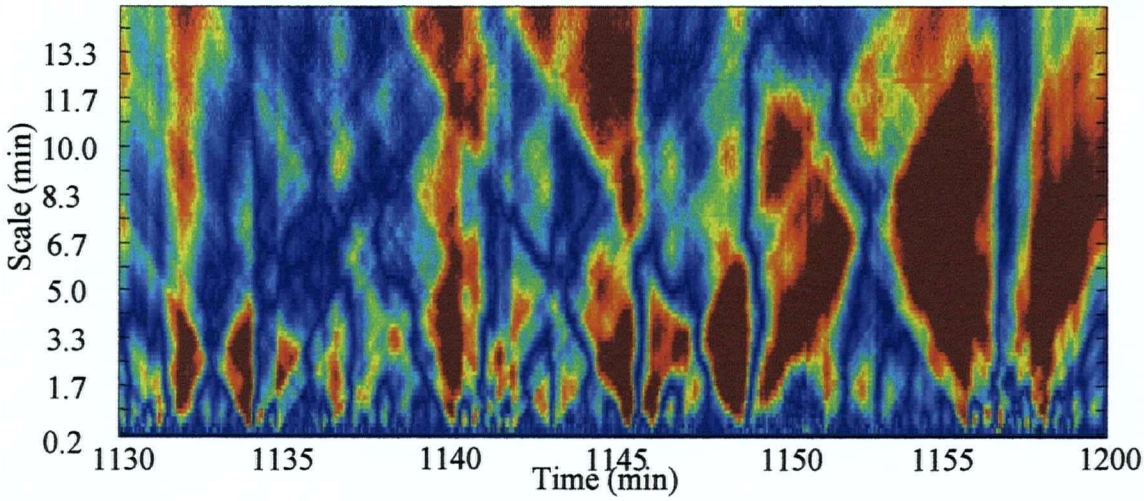

Figure 6.4b Scalogram of temperature calculated using the Haar wavelet for 1130 - 1200 PDT August 31st 1998

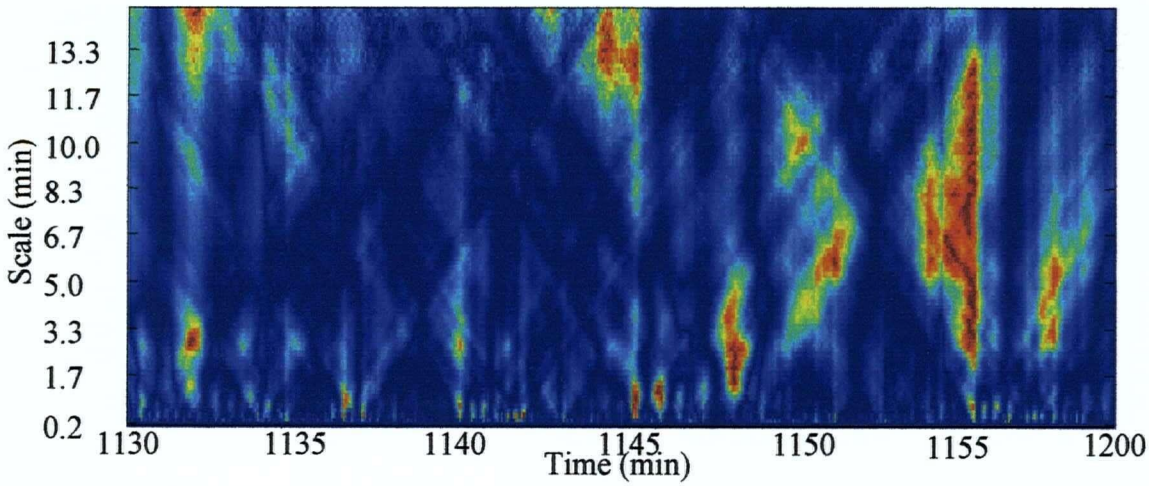

Figure 6.4c Cross-scalogram of vertical velocity and temperature calculated using the Haar wavelet for 1130 - 1200 PDT August 31st 1998

Comparison of Figure 6.3 and Figure 6.4 illustrates marked differences in the frequency component of the time series between the convective and nocturnal boundary layers. Small scale turbulent activity is evident throughout the morning trace (Figure 6.4) whilst in the nocturnal time series (Figure 6.3) it is more intermittent and localised in time. A large number of coherent eddies are easily identified in Figure 6.4 as turbulent structures appear well developed across a range of scales in the morning trace. There is also a much stronger correlation between the timing of structures present in the vertical velocity and temperature scalograms, indicating effective transport of the scalar variable within well-developed thermals.

6.4 Quantification of global intermittency using wavelet analysis

Wavelet analysis provides an insight into changes in the dominant frequencies with time present in a turbulent time series. This property can be exploited to locate and quantitatively analyse the turbulent component of time series. In this section, an original technique is proposed to objectively isolate turbulent sections of the time series for further analysis. This technique also permits the quantitative description of the frequency and duration (global intermittency) of turbulent bursts.

A discretised version of the continuous form of the Morlet wavelet is applied to the 30 minute turbulent time series using scales $2^{j/dj}$ where j = 1:14 (a scale of 2^{14} is approximately equivalent to 26 minutes) and dj = 0.5 (which is equal to the allocation of 2 scales (sub-octaves) per octave (2^j)). This approach increased the speed of the calculations and enabled clear identification of the jumps in the data set whilst incurring minimal loss of resolution at high frequencies. The code for the basic Morlet wavelet transform (including primary graphical output) and statistical tests were modified from that compiled by Torrence and Compo (1998) and which is available on the world-wide-web (http://paos.colorado.edu/research/wavelets/ - see Appendix 4). In order to avoid misinterpretation of the data contaminated as a result of the finite length of the signal, a region known as the 'cone of influence' (COI) was defined. This broadly encompasses the sides (edges) of the transform and the bottom or longest wavelengths and is represented by area under the white line in Figure 6.5b. The size of the COI is determined by scale and the shape of the wavelet. (Note scales on the y-axis are reversed in Figure 6.5 compared to Figure 6.3.)

Figure 6.5b shows an example of the scalogram obtained using the Morlet wavelet for 0000 – 0030 PDT 1st September 1998. Figure 6.5b can be loosely compared to Figure 6.3a to

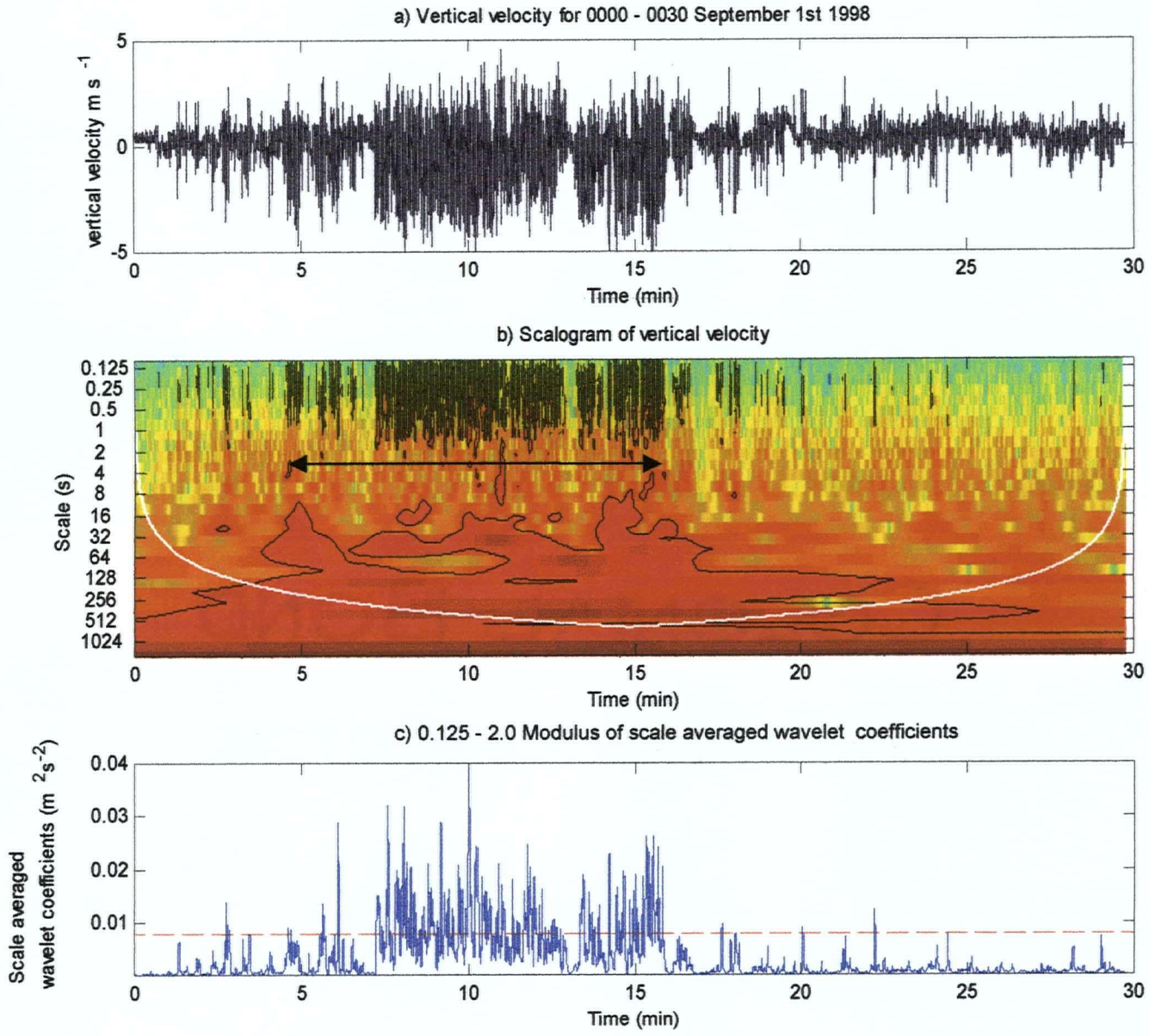

Figure 6.5 a) Variations in vertical velocity recorded between 0000 - 0030 PDT 1st September 1998 b) Scalogram of vertical velocity calculated using a discrete form of the Morlet wavelet for 0000 - 0030 PDT 1st September 1998. (Black circles/lines indicate regions where the values are significantly different compared to those expected due to red noise; white line indicates cone of influence.) c) Composite wavelet coefficients for scales 0.125 - 2.0

↔ Arrow indicates region of dominant turbulent activity identified in

illustrate the influence of different wavelets on the patterns identified in the scalogram. However it is important to note that the scalogram in Figure 6.5b is plotted using a logarithmic y-axis in order to gain more detailed information about wavelet coefficients at smaller scales. Comparison of the two figures reveals that despite the change in wavelet base and increased resolution of the signal, the broad characteristics of the scalograms are very similar. In both figures discrete clusters of activity are identified at small scales. The reduced temporal resolution of the Morlet wavelet (a necessary trade-off to gain increased resolution in the frequency domain) compared to the Haar wavelet is not apparent at smaller scales (which are of primary interest in the analysis of the turbulent component of the time series).

The data were normalised by dividing each time series by its variance prior to analysis. This is equivalent to removing white noise from the scalogram (Torrence & Compo 1998). White noise is random, background noise in the signal and typically results from instrument errors or disturbances. Red noise, which results from the presence of trends (non-stationarities) operating at longer time scales than the measuring period, can also be determined. Tests for red noise have been developed for a range of wavelet bases by Torrence and Compo (1998) and successfully applied by other authors such as Galmarini & Attie (2000). The tests are wavelet specific and use the auto-correlation at lag = -1 of the time series to generate a theoretical red noise spectrum specific to each time series as shown in Equation 6.5 (Torrence & Compo 1998).

$$P_k = \frac{1-\alpha^2}{1+\alpha^2-2\alpha\cos\left(2\pi k/N\right)} \tag{6.5}$$

where:

α lag –1 auto-correlation of the signal

k k = 0 … N/2 frequency index

N total number of data points

P_k red noise spectrum

This test was originally developed for stationary signals and is based on an underlying assumption that the variance and covariance of the data set have a Chi-squared distribution. Although this is almost certainly violated for turbulence data (especially from the NBL) judicious choice of the significance level enables application of the tests in a wider range of circumstances. For example Galmarini & Attie (2000) successfully apply the test to assess non-stationary data using the 95% significance level. The areas of the scalogram surrounded by black circles on the scalogram indicate regions where the scalogram is significantly different (at the 95% level) to that expected due to red noise. As a result of the high temporal resolution of the scalogram in Figure 6.5 the circles appear to resemble black lines.

Analysis of the scalogram shown in Figure 6.5 reveals intermittent periods when the high frequency coefficients (scales 2 seconds and smaller) are significantly different from the red noise spectrum. These correspond well with the periods of increased variance shown in the original data set (Figure 6.5a). A second area of the scalogram where the wavelet coefficients are significantly different to the red noise spectrum is identifiable at scales 16 - 32 seconds and longer. The enhanced resolution of the Morlet wavelet compared to the Haar wavelet in frequency space, combined with the use of a smaller number of scales of analysis, facilitates the identification of a clearer gap between the portions of the high frequency data set (which are significantly different to the red noise spectrum) and the lower frequency motions in the data set (which are significantly different to the red noise spectrum).

Given typical observed depths of the stable boundary layer of between 50 – 150 m (see Chapter 5 for justification) and mean wind speeds of 2 m s^{-1} or less in the stable boundary layer, the small scale activity may be considered within the range expected for shear induced turbulence. Although it is likely that turbulent activity extends through larger scale motions in the boundary layer, it becomes increasingly difficult to separate turbulence from more wave-like motions. (As shown in section 6.7 gravity waves are shown to exist with wave periods as small as 20 seconds.) However, by focussing initially on just these smallest scales, this technique appears to provide a clear scale separation between the high frequency turbulent activity and lower frequency patterns (which are perhaps more wave-like).

The relationship between the small scale wavelet coefficients and the red noise spectrum can be used to accurately and objectively identify periods when turbulence was active (the signal was significantly different to that expected due to red noise) at the surface in the NBL. This was done by taking the mean modulus of the wavelet coefficients at scales between 0.125 and 2.0

seconds (Equation 6.6) as illustrated in Figure 6.5c. The dashed line represents the 95% level for red noise for wavelet coefficients at these scales (white noise has already been removed from the variance). Coefficients are considered to be significantly different (at the 95% level) to that expected by red noise when the variance is greater than the dashed line.

$$\overline{W}_n^2 = \frac{\delta j \delta t}{C_\delta} \sum_{j=j_1}^{j2} \frac{|W_n(S_j)|^2}{S_j} \tag{6.6}$$

Where :

s scale

W_n wavelet coefficient

δj number of sub-intervals per octave

C_δ scale independent constant for wavelet

j scale number

In order to determine the global intermittence of turbulence, the variance was smoothed using a 30-second running mean (Figure 6.6). This removes isolated spikes from the signal which are more likely to result from noise in the signal than to be indicative of turbulent activity. For the purposes of this analysis, a turbulent burst was defined by the length of time the signal remained greater than the 95% red noise significance level. Time periods of less than 0.01 minutes in duration were excluded from analysis as these typically corresponded to isolated spikes in the signal. Figure 6.6a illustrates that four coherent turbulent periods have been identified by the technique for the 30-minute vertical velocity trace observed between 0000 - 0030 PDT September 1st 1998. The duration (total and average), frequency and intermittency (flux time/total time) were then calculated for each 30 minute turbulent time series collected between 2130 - 0630 PDT during the IOPs. This time period was chosen since it represented the time period when daytime convective turbulence was no longer likely to be active and a stable boundary layer had at least begun to develop near the surface.

This method is similar to previous attempts to isolate the local intermittence of convective turbulence using wavelet analysis (Gao & Li 1993; Hagelberg & Gamage 1994; Collineau & Brunet 1993). These studies rely on the identification of a key scale or choice of

a)

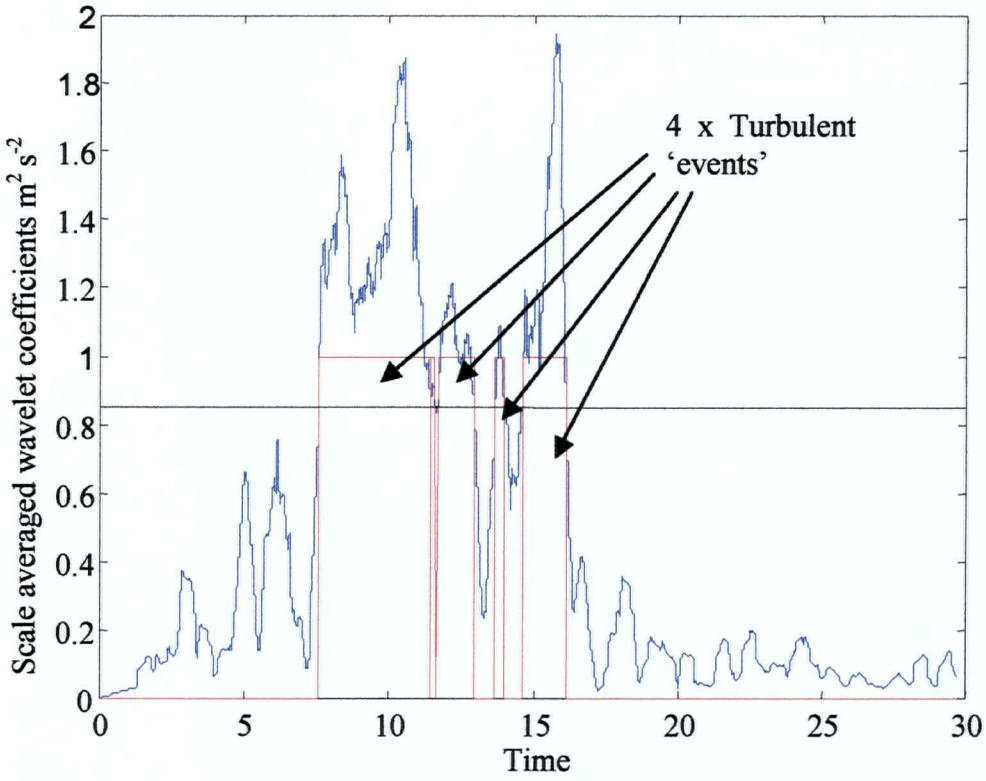

b)

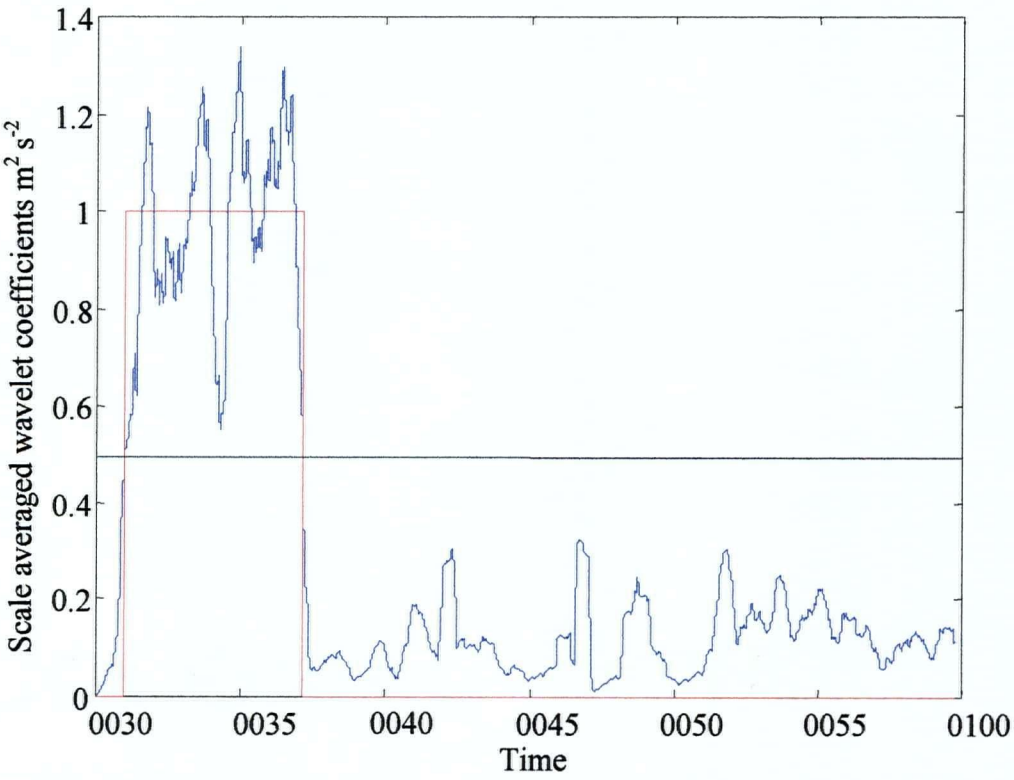

Figure 6.6 Smoothed average wavelet coefficients for scales 0.125 - 2.0 (blue line), red noise significance level (black line) and identification of turbulent events (red line = 1) for a) 0000 - 0030 PDT 1st September 1998 and b) 0030 - 0100 PDT 1st September 1998

specific criteria to isolate the coherent turbulent structures of interest. However, the characteristics of the turbulence in the very stable nocturnal boundary layer make it very difficult to identify a consistent structure associated with nocturnal turbulent activity. Thus the advantage of the methodology proposed is that not only does it provide an objective means of isolating the turbulence from more wave-like activity which can be applied consistently between data sets, it is also based on a statistically rigorous technique used to distinguish between the signal and noise in the time series.

Hagelberg and Gamage (1994) illustrate the success of their technique by demonstrating that the structure (or turbulent) component of their time series has a -5/3 gradient in the inertial subrange whilst the non-structure component has a -1 gradient. This exercise was repeated on the nocturnal data sets for CFS Aldergrove. Whilst the turbulent component of the time series repeatedly demonstrated the presence of a -5/3 gradient in the inertial subrange, it was harder to identify the presence of the -1 gradient identified by Hagelberg and Gamage (1994) (Figure 6.7). This is largely due to wave activity in the time series. However, as a -5/3 gradient could also not be identified in the non-turbulent component of the time series, it is likely that the technique successfully isolates most of the turbulent component of the time series.

6.5 Mechanisms responsible for intermittent turbulence in the very stable nocturnal boundary layer

The technique developed in section 6.4 was applied to the nocturnal turbulence data collected between 2130 PDT - 0630 PDT during all IOPs. The results (summarised in the first row of Table 6.1) indicate that turbulent conditions typically prevail for a total of less than three minutes of each 30 minute data set. Typically three to four individual turbulent bursts or events, each lasting less than a minute, account for this mean total duration (Table 6.1). This supports the underlying assumption made in Chapter 5 that the surface layers can be classified as 'very stable'. These results are comparable to other studies of turbulence in the very stable nocturnal boundary layer. For example, Howell and Sun (1998) define a flux intermittency factor for their field experiment over grasslands in Kansas, which suggests that during very stable conditions turbulence persists for 1.25 - 4.0 minutes out of every eight minute data set.

However, these figures are strongly weighted by the skewed distribution of the data points resulting from a large number of data files recording near zero values. Thus, despite the prevailing stability, a wide range in turbulent conditions were observed (as reflected in the large

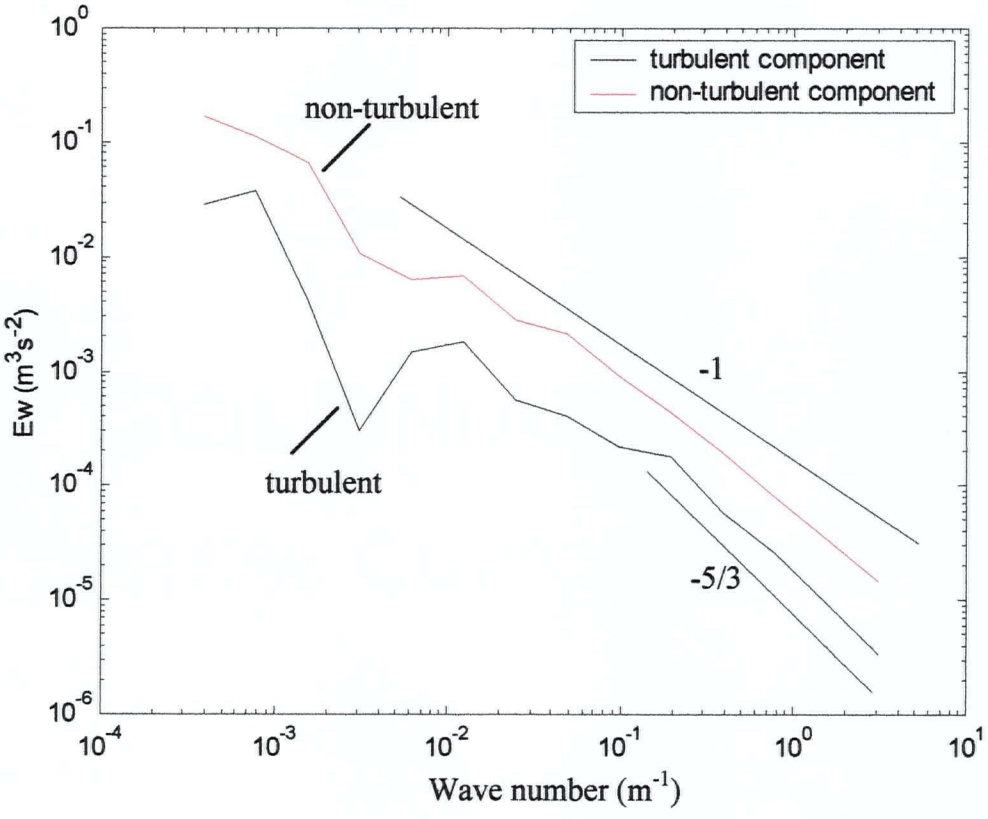

Figure 6.7 Energy spectra calculated from the turbulent and non-turbulent components of the time series for 0130 PDT September 1st 1998

standard deviation of the data set (Table 6.1)), with turbulence persisting on several occasions for more than eight (of the total 30) minutes of the time series).

In Chapter 5 three processes were identified as possible sources of turbulence in the NBL: the nocturnal LLJ, the development of down-valley winds, and breaking gravity waves. However, low temporal resolution of tethersonde data (flights lasted 45 – 60 minutes with typically one hour between flights) only provided a limited insight into the relationship between potential causes of turbulence and the resulting vertical mixing of ozone to the surface. For example, in Chapter 5 evidence for a good correlation between type 3 nocturnal LLJs and increased ozone concentrations at the surface was presented. However, it was not possible to determine whether this was the result of turbulence associated with this type of LLJ. Using the technique developed in section 6.4 it is possible to examine the relationship between processes operating in the NBL and the resulting turbulence in more detail.

Using information from the tethersonde data, the 30 minute turbulent data sets were classified according to the potential source of turbulence aloft. Initially the data were subdivided into two categories: time series associated with a LLJ aloft and those without. The former category was then further subdivided into the 4 different jet types identified in Chapter 5. Given that a significant proportion of the ozone spikes identified in Chapter 5 coincided with the break-down of the LLJ, the characteristics of the turbulence during this phase were also analysed. Time series associated with this type of phenomenon were only included when data from two consecutive tethersonde flights confirmed the presence and then absence of the LLJ. Finally, the remaining data not associated with LLJ activity were classified according to the nature of the mesoscale wind regime. The results from this classification are summarised in Table 6.1.

Table 6.1 The characteristics of intermittent turbulence associated with the nocturnal low level jet and development of mesoscale wind systems and in the very stable NBL during IOPs at CFS Aldergrove, 1998 (Classification described in text.)

	Number of cases (N)	**Average duration of turbulent burst (min)**	**Mean duration of turbulence in each 30 minute time series (min)**	**Standard deviation of mean turbulence duration in each 30 minute time series (min)**	**Maximum recorded duration of turbulence in 30 minute time series (min)**	**Intermittency (Flux time / non-flux time)**	**Standard deviation of vertical velocity in turbulent bursts (m s^{-1})**
All 30 minute nocturnal time series collected during IOP's	193	0.94	2.9	2.37	8.8	0.12	0.05
Low level jet present aloft	91	0.98	3.0	2.43	8.8	0.12	0.05
Low level jet absent aloft	102	0.92	2.8	2.36	8.0	0.11	0.04
Jet Type 1	18	0.86	2.6	2.95	8.5	0.11	0.02
Jet Type 2	9	0.90	2.5	2.08	4.8	0.10	0.03
Jet Type 3	56	1.06	3.2	2.42	8.8	0.13	0.06
Jet Type 4	8	0.74	2.4	1.61	4.7	0.09	0.05
Jet break-down (see text for explanation)	37	1.25	3.1	2.50	8.0	0.13	0.05
Development of down-valley winds	45	0.60	2.2	2.29	7.3	0.09	0.08
Presence of westerly band aloft	35	0.81	2.4	2.43	8.5	0.10	0.04

In this table the mean duration of each turbulent burst, total duration of turbulence and intermittency of the flux are documented. The standard deviation of vertical velocity during turbulent bursts is included as a measure of the strength of the turbulence. As a result of the temporal variability of the mechanisms expected to generate turbulence (particularly the evolution of the LLJ), intermittency of the resulting turbulence and the resolution of the turbulence data, it was not possible to determine whether any given mechanism persisted throughout the 30 minute data sets. The inadvertent inclusion of periods not associated with disturbances may have skewed the data affecting mean values and magnitudes of the difference observed between categories. Further, due to the plethora of different processes operating in the NBL (and especially the prevalence of gravity waves identified in section 6.7) it was very difficult to isolate the influences of individual disturbances on the turbulent characteristics of the boundary layer. It was also very difficult to isolate a 'typical' or baseline level of turbulence (other than zero) for comparison. Thus the analysis presented here is relative rather than absolute.

6.5.1 Nocturnal low-level jet

Table 6.1 (rows 2 and 3) illustrate that the presence of a LLJ aloft had little influence on the characteristics of the turbulence observed at the surface in the NBL. Although a small increase in both the average and total duration of turbulence was recorded at the surface when a LLJ was present in the NBL, differences between the two groups were not found to be significant using an independent samples T-test or a one-way ANOVA analysis. This may be a product of a number of different factors. For example the nocturnal LLJ is only one possible source of turbulence in the NBL. Although periods when the mesoscale wind regime was changing were removed from the data set, it was not possible to isolate time periods when the only influence on the turbulent characteristics of the data set was the presence or absence of the jet. Thus both the sample group representing conditions with a LLJ and the sample group representing conditions without a LLJ may be contaminated by turbulence generated by other processes.

Further, in Chapter 5 two disparate effects of the LLJ were identified. Beyrich (1994) suggests that the presence of the LLJ aloft generates sufficient shear to enhance turbulence in the near-surface layers, whilst Smedman et al. (1995) argues that the LLJ only develops in regions of very strong stability, which limits the penetration of turbulence through to the surface layers.

Thus it is possible that the different morphology of the LLJ observed in the NBL result in different turbulent responses in the surface layers.

The characteristics of turbulence associated with each of the different LLJ types identified in Chapter 5 were analysed. As shown in rows four to seven of Table 6.1, differences were found between the jet types. Unfortunately the large range in sample sizes between groups, and the temporal dependence of the observations, hindered accurate testing for the statistical significance of the difference between each group.

The longest duration of both an individual turbulent event and the total turbulent component of the 30 minute time series were observed with type 3 LLJ (Table 6.1). This jet type is associated with a single wind speed maximum of 5.5 m s^{-1} located at a mean height of 136 m (Table 6.2). The turbulence associated with this type of jet also exhibits the largest standard deviation of vertical velocity observed within the turbulent periods (indicating the strongest turbulence). By comparison the shortest mean and total duration of turbulent conditions within the 30 minute time series are observed with type 4 LLJ (Table 6.1). This jet is characterised by two wind speed maxima, the stronger of which is the lower jet (or branch) at 4.7 m s^{-1} and located at a mean height of 117 m (Figure 5.18 and Table 6.2).

Despite the reduced duration of the turbulence associated with a type 2 LLJ, the turbulence itself was comparatively strong (Table 6.1). The weakest turbulence was associated with a relative increase in turbulence duration time generated by type 1 LLJs. This jet type had the highest mean wind speed (5.9 m s^{-1}) but the wind speed maxima was located at an increased altitude of 371 m. These results suggest that whilst jet height is an important determinant of the intensity of the turbulence, jet speed plays an important role in determining the duration of the turbulence.

However, when the data sets for all categories of LLJ were examined as a whole, there was a poor correlation between the turbulence strength and duration and jet height or speed. This can be accounted for in part by the co-dependence between the two variables (a stronger jet at a lower height generates more turbulence than the same jet located higher in the NBL). This effect

Table 6.2 Variations in ozone concentration throughout the NBL associated with different sources of turbulence observed during IOPs at CFS Aldergrove, 1998 (Classification described in text. For N see table 6.1)

	Surface ozone concentration (ppb)	Maximum ozone concentration in profile (ppb)	Height max ozone (m)	Ozone concentration at top of the SBL (ppb)	Mean height of SBL (m)	Speed of jet ($m\ s^{-1}$)	Height of jet (m)	Ozone concentration in jet (ppb)
All nocturnal time series collected during IOPs	12.4	57.1	448	40.2	106	N/A	N/A	N/A
Low level jet present aloft	12.3	65.0	383	49.6	101	N/A	N/A	N/A
Low level jet absent aloft	6.6	54.6	538	29.4	99	5.9	371	44.7
Jet Type 1	11.5	56.0	489	34.8	88	4.5	195	38.9
Jet Type 2	14.6	59.0	414	44.9	93	5.5	136	43.2
Jet Type 3	11.7	50.6	435	35.1	119	4.7	114	37.8
Jet Type 4	11.2	60.8	443	42.9	107	N/A	N/A	N/A
Jet break-down (see text for explanation)	17.6	68.3	400	43.5	103	N/A	N/A	N/A
Development of down-valley winds	17.5	71.7	436	52.2	106	N/A	N/A	N/A
Presence of westerly band aloft	17.2	68.2	442	50.0	112	N/A	N/A	N/A

is less apparent once the data have been sorted by jet type as the classification technique effectively stratifies the data set by the altitude of the lowest wind speed maxima as shown in Figure 5.18.

To avoid the difficulties introduced by the co-dependence of LLJ height and speed, the mean average vertical shear between the top of the LLJ and the surface was also calculated. Although a stronger correlation between this variable and turbulence intensity was observed (r^2 = 0.4) the correlation was not significant given the large number of samples analysed. This may be due to the different temporal scales of analysis (between the tethersonde measurements and the turbulence measurements) and the depth of the layer examined (turbulence conditions were measured at 5 m whilst the shear was averaged over a layer more than 100 m deep).

The results in Table 6.1 indicate that the break-up of the LLJ was associated with stronger turbulence and increased duration times compared to the turbulence associated with the LLJ types. Clearly the break-up of the nocturnal LLJ, whether a result of its own evolutionary cycle or other disturbances in the NBL, is an important indication of increased turbulence in the NBL.

6.5.2 Mesoscale wind reversals: Development of down-valley winds

A second source of turbulence identified in Chapter 5 was the shear resulting from the wind reversal generated by mesoscale thermo-topographical wind systems. Table 6.1 indicates that the characteristics of intermittent turbulence associated with the development of down-valley winds are different to those generated by the LLJ. The turbulence is characterised by several short bursts of strong turbulence, each averaging 36 seconds in duration. The total duration of the turbulence within each 30 minute data block is also considerably lower than that observed in association with the LLJ, at an average of 2.2 minutes per 30 minute time series (Table 6.1). However, the turbulence is stronger than that associated with the LLJ with a mean standard deviation of the event vertical velocity of 0.08 m s^{-1} compared to 0.05 m s^{-1}. Table 6.1 indicates that slightly longer turbulent events were observed with the presence of a westerly band aloft. The turbulence was comparatively weak with a low total duration of 2.4 minutes. However, due to the high standard deviation of the data sets, the differences observed in the characteristics of the turbulence between data sets were not statistically significant.

In summary the characteristics of turbulence at the surface were seen to vary with the different disturbances identified. A clear relationship could not be found between the duration and the strength of the turbulence. Both categories were therefore used to determine increased turbulent activity in the NBL. Thus far, three regimes can be identified as associated with the most active turbulence in the NBL: the presence of a type 3 LLJ, the break up of a LLJ, and the development of mesoscale down-valley winds.

6.5.3 Gravity waves

The relationship between enhanced turbulence at the surface and the characteristics of the LLJ and mesoscale wind regimes strongly supports the hypothesis presented in Chapter 5 that increased ozone concentrations recorded at the surface are the result of vertical mixing processes. However, three ozone spikes were identified in Chapter 5 could not be associated with either the LLJ or changing mesoscale wind regimes. Using the method identified in section 6.4 it is possible to determine the characteristics of the intermittent turbulence associated with two of these periods: July 28th (0050 PDT - 0135 PDT) and August 10th (0500 PDT - 0535 PDT). Unfortunately turbulence data was unavailable for the third ozone spike which occurred on July 28th - July 29th between 2350 PDT - 0020 PDT. During these periods, increased surface ozone concentrations were associated with increased turbulent activity (as determined by a mean total duration time of the turbulence of 4.1 minutes). This strongly suggests that these ozone spikes are also the result of vertical mixing processes.

A third possible source of turbulence identified in Chapter 5 was breaking gravity waves. It was suggested that turbulence resulting from this process might explain the three remaining ozone spikes. The maximum frequency of gravity wave activity supported by the conditions in the NBL can be estimated using the Brunt-Vaisala frequency. A Brunt-Vaisala frequency of zero is expected when conditions are unstable and the boundary layer cannot support the development of gravity waves. Figure 6.8 illustrates the Brunt-Vaisala frequencies calculated throughout the NBL from the tethersonde data for the flights commencing on the 28th July at 0005 PDT (observed immediately prior to the mixing event) and 0130 PDT (observed immediately after the event). Both profiles indicate the possible existence of gravity waves throughout the profile with frequencies in excess of 0.3 s^{-1} (equivalent to a period of 20 seconds) at the surface. Data from a tethersonde profile on August 10th at 0544 PDT (taken immediately after the second ozone spike)

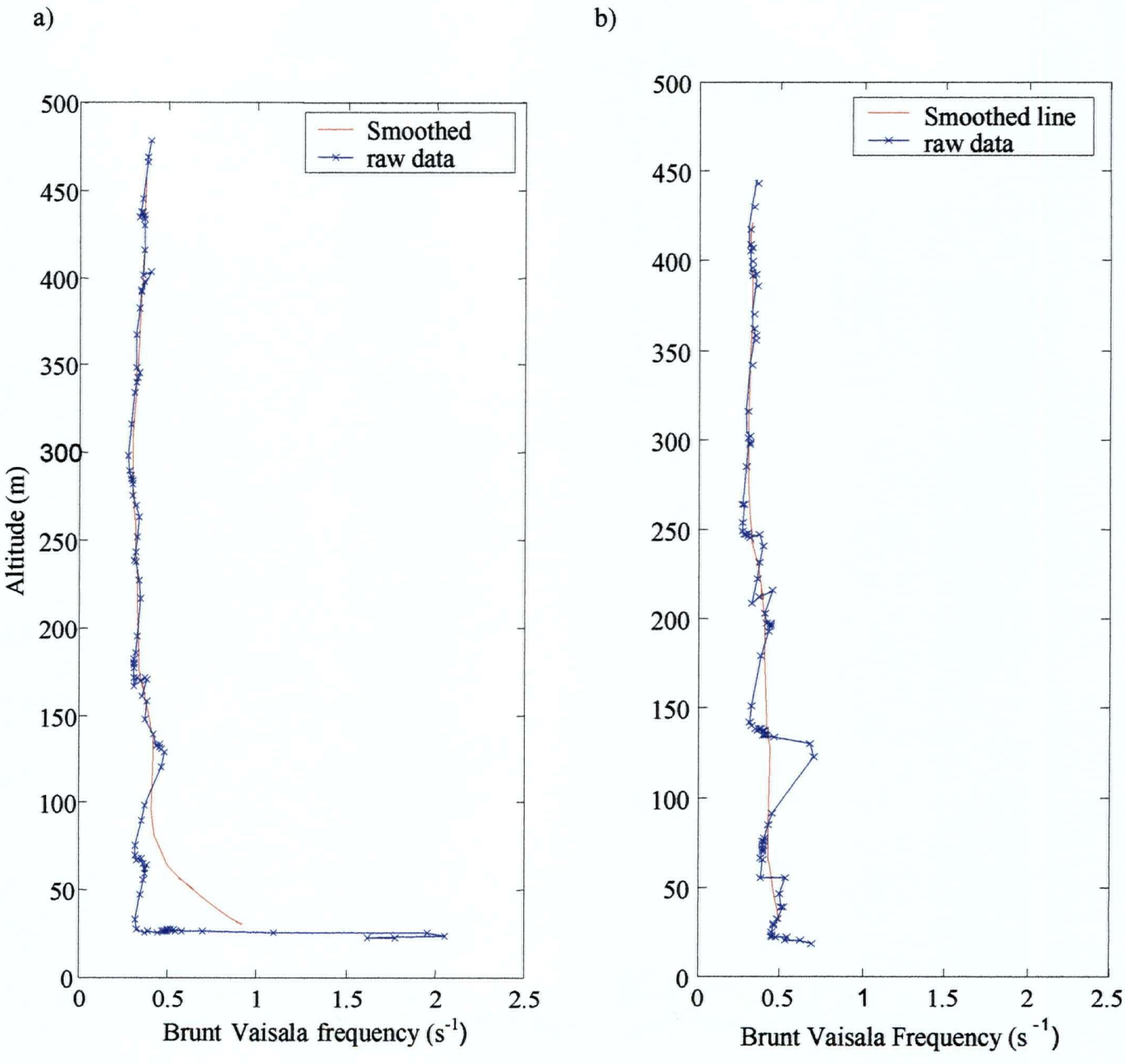

Figure 6.8 Brunt Vaisala frequencies as calculated from the tethersonde data for flights at a) 0005 PDT 28th July and b) 0130 PDT 28th July 1998

also indicated that gravity wave activity could be supported at frequencies of 0.33 s^{-1} at the surface and 0.55 s^{-1} at 500 m. Thus gravity waves could have been present during these two ozone spikes. However, the Brunt-Vaisala frequencies calculated on all the nocturnal flights indicated that gravity waves may have been present throughout the night. This is probably a consequence of the limited temporal resolution of the flights (45 - 60 minutes in length and separated by approximately one hour). Given the intermittency and time scales of the turbulence it is unlikely that the tethersonde captured a mixing event as it occurred and thus zero Brunt-Vaisala frequencies were not observed even in the near-surface layer.

Detection of gravity waves by wavelet variance

Traditionally Fourier analysis has been used to identify the presence of gravity waves in turbulence spectra (for example see Rees et al. (2001)). Although Fourier analysis is arguably well suited to the identification and analysis of gravity waves (since the function itself is based on the wavelike patterns of sine and cosine functions), the technique does not facilitate the identification or delimitation of the timing of intermittent periods of wave activity. Wavelet analysis offers an alternative technique which can be used to gain a more detailed insight into the presence of gravity waves in the frequency data. The advantages of this technique are further expanded in Chapter 3. Given that wavelet analysis offers the potential to gain specific information about the temporal placement of wave activity, it can be used to analyse time series longer than 30 minutes without loss of detail. This is important since gravity wave activity may occur with wave periods longer than 15 minutes (the maximum resolvable wave period given a 30 minute data set) or occur intermittently, crossing the artificially constructed 30 minute time periods. Thus, where appropriate, longer data sets were utilised to examine the characteristics of gravity wave activity.

The discrete form of the Haar wavelet transform (which satisfies energy preservation requirements) is used to calculate variance and energy spectra in this section. Using a plot of wavelet variance, dominant scales in the time series can be identified. Figure 6.9 and Figure 6.10 illustrate the variance of vertical velocity observed for four 30 minute periods immediately prior to, during and immediately following, the mixing events for July 28th and August 10th respectively. These were calculated using the Haar wavelet for orthogonal scales between 2^1 (0.01 second) to 2^{14} (13 minutes). The figures demonstrate the marked increase in variance at

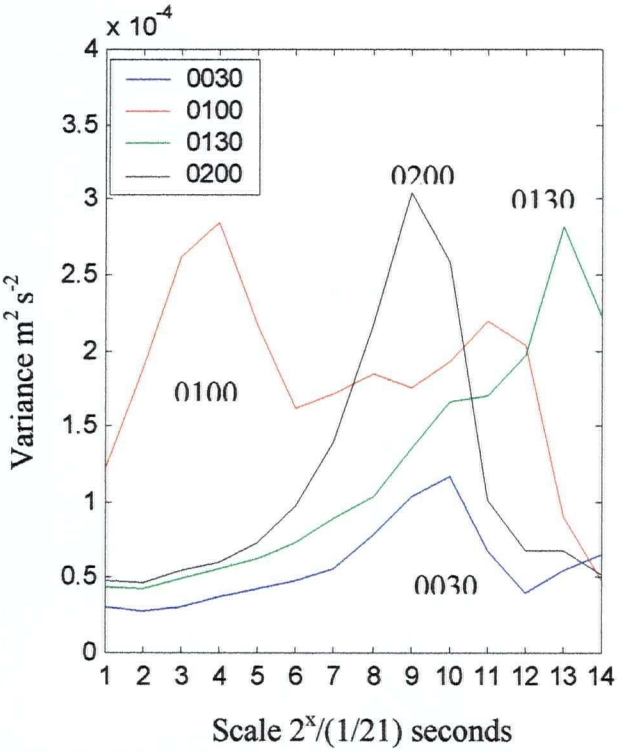

Figure 6.9 Variance of vertical velocity as calculated using the Haar wavelet for 30 minute periods ending 0200 PDT on July 28th 1998

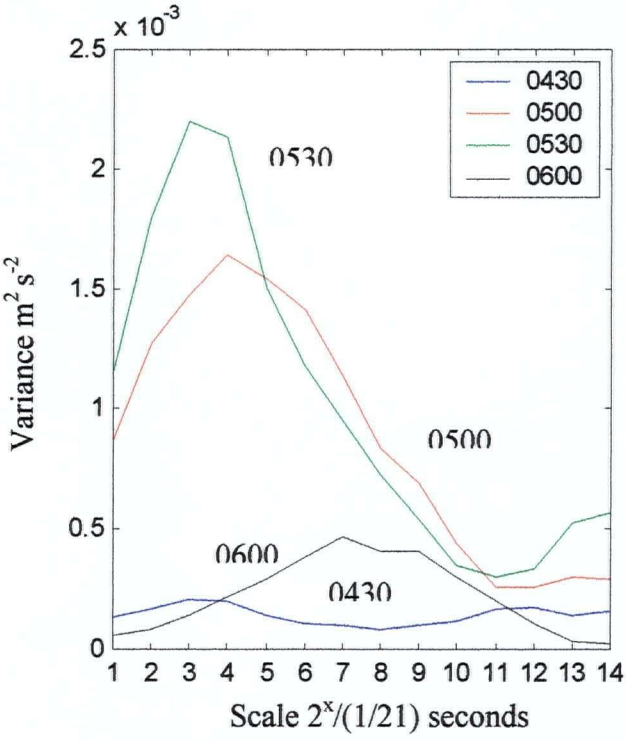

Figure 6.10 Variance of vertical velocity calculated using the Haar wavelet for 30 minute periods ending 0600 PDT on August 10th 1998

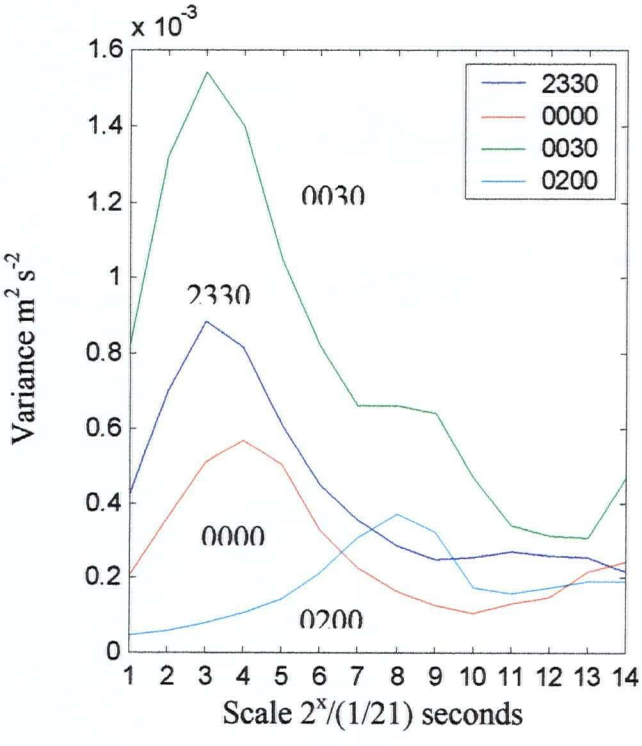

Figure 6.11 Variance of vertical velocity as calculated using the Haar wavelet for 30 minute periods ending 0200 PDT on September 1st, 1998

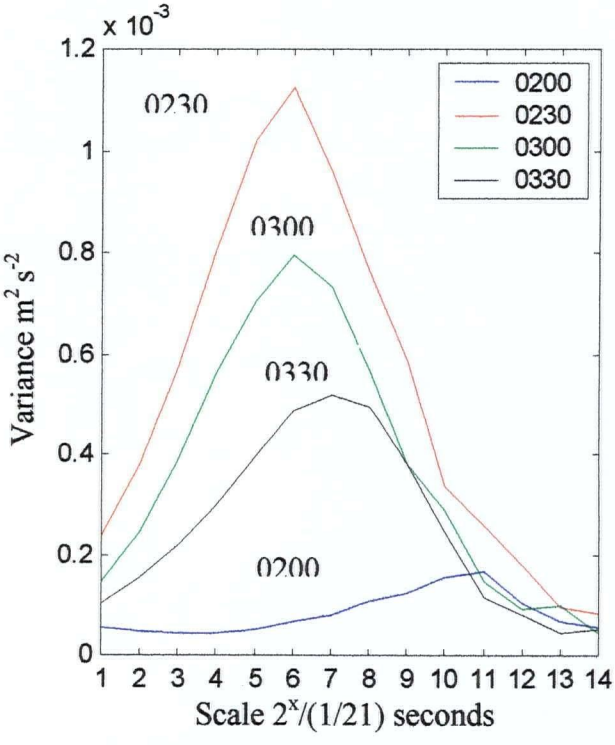

Figure 6.12 Variance of vertical velocity calculated using the Haar wavelet for 30 minute periods ending 0330 PDT on August 9th 1998

NOTE: Scale 5 is equivalent to 1.5 seconds whilst scale 10 is equivalent to 48 s and scale 14 equivalent to 13 min.

small (turbulent) scales (2^3 - 2^4 which are approximately equal to 0.4 - 0.8 seconds respectively) during the 30 minute periods when increased ozone concentrations were observed at the surface. The variances are also characterised by a second peak at larger scales (2^{12} - 2^{14} or 3.25 - 13 minutes). This suggests the presence of two scales of activity, one that may be turbulent, and another larger scale that is perhaps more wave-like. This is particularly evident in the variance calculated for 0100 PDT July 28th in Figure 6.9 where the second peak is almost of the same magnitude as the peak at turbulent scales. In the absence of turbulent activity the variances are dominated by maxima at these longer scales 2^9 - 2^{13} (scales approximately equivalent to 24 seconds - 6.5 minutes respectively). This is evident immediately before and after the ozone spikes for 0030 and 0200 PDT on July 28th and 0430 and 0600 PDT on August 10th. This suggests that longer scale motions dominate in the very stable nocturnal boundary layer.

Increased variance at small scales was a key characteristic of the variances calculated during the ozone spikes and confirms the presence of turbulent scale activity within the data set. This is illustrated in Figure 6.11 and Figure 6.12 by the variances calculated during two ozone spikes associated with vertical mixing resulting from two different sources of turbulence. The first represents a case when the vertical mixing was thought to be generated primarily by turbulence resulting from increased wind shear from mesoscale flows (2330, 0000 and 0030 PDT August 31st - September 1st). The second represents a case when the turbulence was thought to originate primarily from a type 3 nocturnal LLJ located at an altitude of 200 m with wind speeds in excess of 6.5 m s^{-1} (for 0230, 0300, 0330 PDT August 9th). In this latter example there is no evidence for a second peak in variance during the mixing period. In the former example where the turbulence is likely to result from mesoscale wind shear there is some evidence of a second peak in variance suggesting the dominance of a second scale motion in the atmosphere. Thus, whilst the presence of a peak in small scale activity is a consistent feature of periods associated with an ozone spike, the presence of a second peak in variance is not limited to examples of vertical mixing where there was no identifiable disturbance. Further, the presence of a second peak in the variance alone is insufficient to confirm gravity wave activity.

Detection of gravity waves by wavelet energy spectra

Analysis of the energy spectra for each 30 minute data set can provide further information about the presence of gravity waves and turbulence within the nocturnal boundary layer. Wavelet analysis can be used to calculate energy spectra as shown in Chapter 3. To

determine the presence of turbulence, a gradient of -5/3 should be found in the inertial subrange. If gravity waves are also present then a gradient of -3 should be found at longer scales (Stull, 1988). Figure 6.13 demonstrates the compatibility of the wavelet and Fourier methods at longer wave numbers. It also illustrates the considerable advantage of the technique in this application due to the enhanced resolution of the technique at longer wave lengths. Errors and subjectivity introduced due to the averaging of data points (and choice of bin sizes) are also avoided. This makes it much easier to establish the presence of -3 slope indicative of gravity waves.

Figure 6.14 shows the presence of a -3 slope in the spectra immediately before (0030 PDT) and immediately following (0200 PDT) the ozone spike on July 28th 1998. These spectra also illustrate the dip between the buoyancy subrange and the inertial subrange characteristic of nocturnal spectra with gravity wave activity (Stull, 1988). The -3 slope is not present in the 0100 PDT profile. Due to the noise in the spectra at smaller wave numbers (which are representative of longer wave lengths) a -3 slope was only identified when three or more points formed a straight line with this gradient. The absence of the -3 slope between 0100 - 0130 PDT, when ozone concentrations were increasing, suggests that the NBL may have become too unstable to support gravity wave activity for at least part of the 30 minute time series. The flattening of the slope at smaller wave numbers suggest that it is unlikely that gravity waves and turbulence were interacting at this time. A steeper gradient of between -5/3 and -3 could be expected if interaction between gravity waves and turbulent scales of motion occurred. Figure 6.15 indicates the presence of gravity waves between 0500 - 0530 PDT (during the ozone spike on August 10th), but not prior to it between either 0400 - 0430 PDT or 0430 - 0500 PDT. The slope of the spectra of the former of these two periods at low wave numbers is between -3 and -5/3 which suggests that gravity wave - turbulence interaction may have occurred during this period. Thus gravity wave activity could be identified during both of the ozone spikes of interest in this section.

Gravity waves can result from a variety of different processes from the interaction of large scale flows with complex terrain, to features such the nocturnal LLJ. Not surprisingly therefore, gravity waves were not limited to periods when other turbulent scale forcings were absent. One of the clearest examples of gravity wave activity generated by the presence of a LLJ was observed during the night of August 30th - 31st (Figure 6.16). On this occasion gravity wave activity was observed to commence at 0130 PDT with the development and persistence of a type 1 LLJ at 400 m with associated wind speeds of 6.0 m s^{-1} and higher (see Chapter 5). Only weak

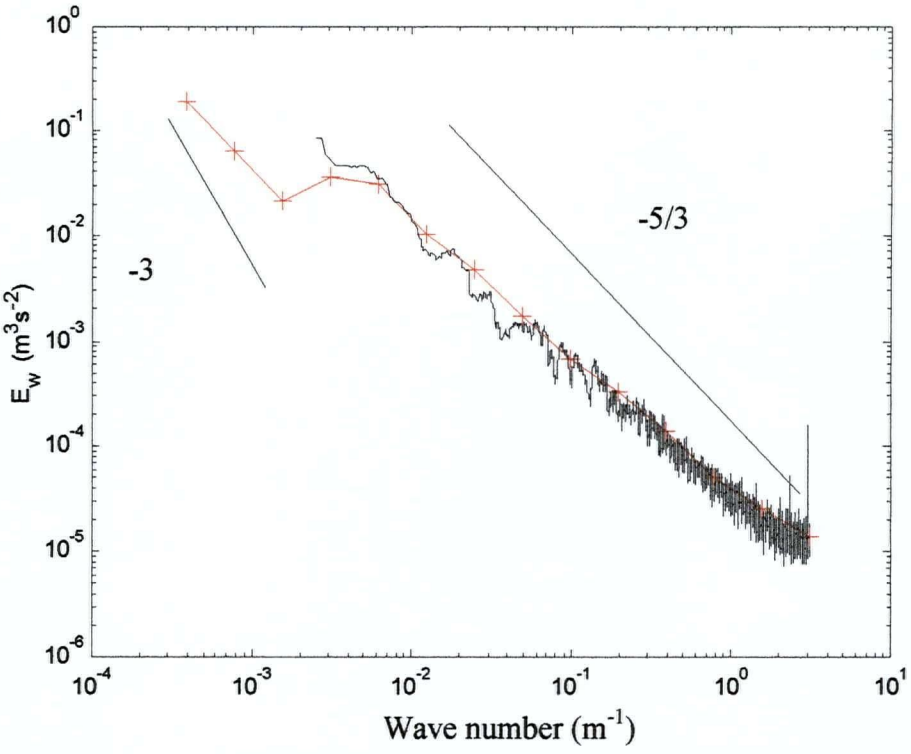

Figure 6.13 Spectra as calculated by FFT (black line) and the Haar wavelet transform (red line) for vertical velocity between 0000 - 0030 PDT July 28th 1998

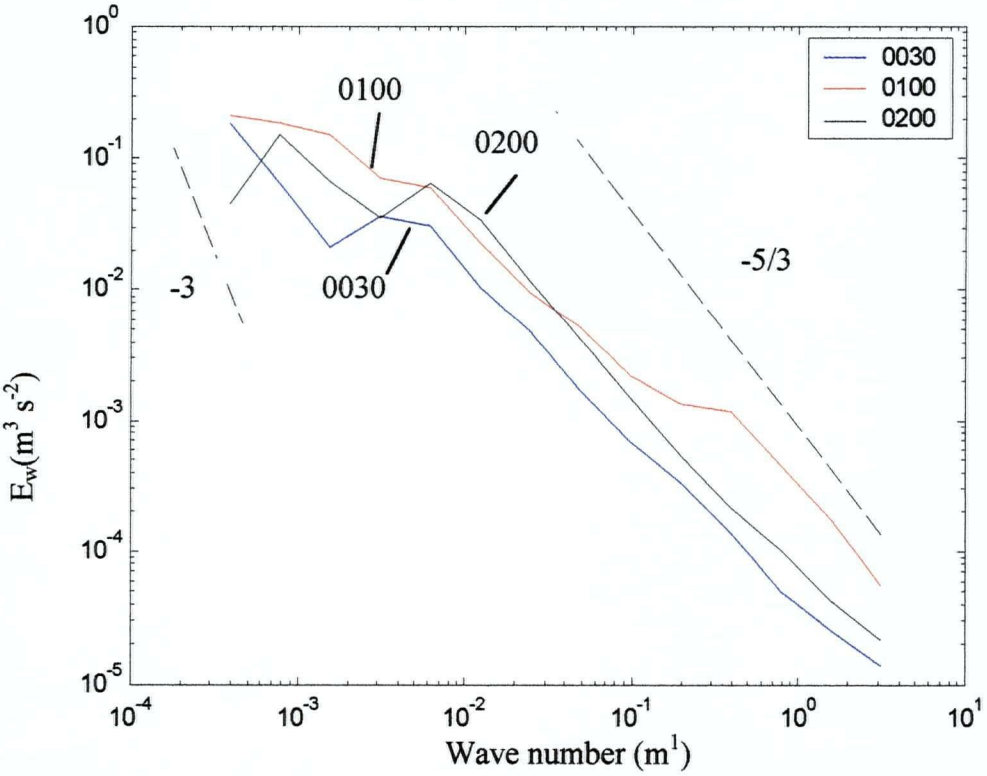

Figure 6.14 Spectra as calculated using the Haar wavelet transform for vertical velocity at 0030 PDT, 0100 PDT, and 0200 PDT July 28th 1998

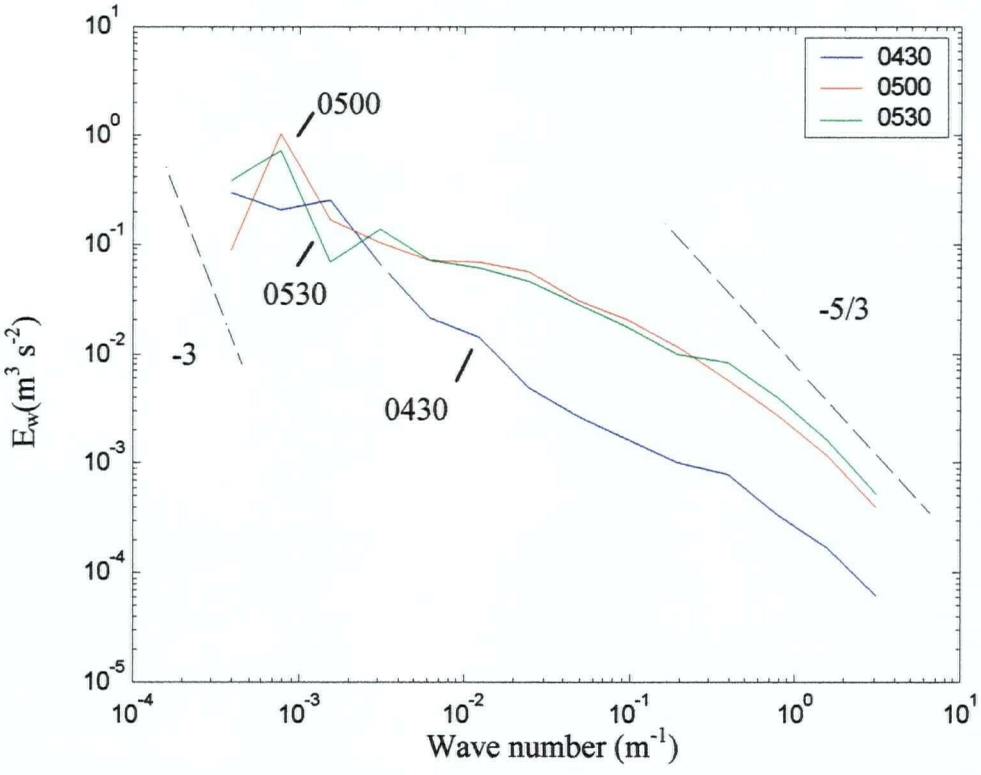

Figure 6.15 Spectra as calculated using the Haar wavelet transform for vertical velocity at 0430 PDT, 0500 PDT, and 0530 PDT August 10th 1998

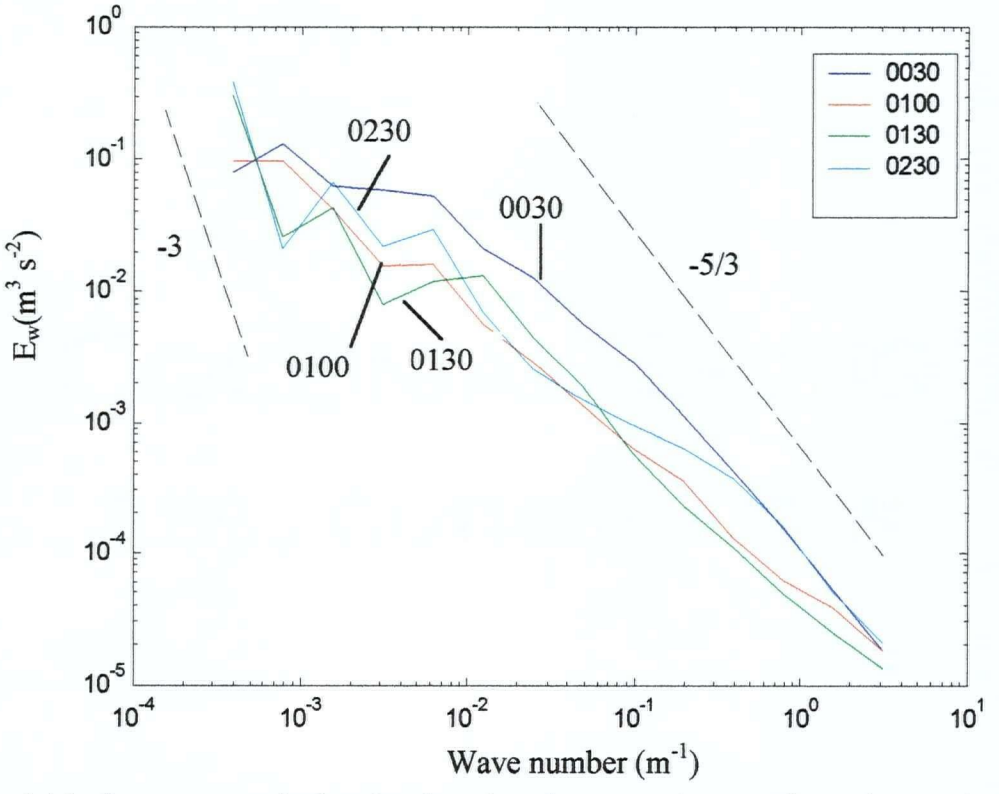

Figure 6.16 Spectra as calculated using the Haar wavelet transform for vertical velocity at 0000 PDT, 0030 PDT, and 0200 PDT August 31st 1998

turbulence prevailed at the surface during this time.

Gravity waves were also detected during some, but not all, of the periods of vertical mixing associated with spikes in ozone concentration at the surface. For example Figure 6.13 illustrates the spectra for 0000 - 0030 PDT which suggests that gravity wave activity may have been present. During this time period increased ozone concentrations at the surface were attributed to turbulent activity resulting from mesoscale changes in the wind regime. Clearly, whilst gravity wave - turbulence interaction may obscure the evidence for gravity waves during periods of increased turbulence, due in part to their intermittency, they are not always absent from time series which also illustrate the -5/3 slope characteristic of turbulent activity.

Indeed gravity waves were detected throughout the data sets collected during the 11 nights and it was harder to isolate periods when they were continually absent than to detect their presence. The only clear example in the data set for the consistent absence of gravity wave activity occurred on August 9th (Figure 6.17a). Although the Brunt-Vaisala frequencies during this period are close to zero, the values do not indicate that gravity wave formation is inhibited by the characteristics of the NBL (Figure 6.17 b and c). On this occasion a type 3 LLJ became established at 150 m above the surface with wind speeds between 5.5 - 8.3 m s^{-1}. Unusually the jet did not appear to evolve with time and remained a consistent presence throughout the night. Further, a down-valley wind regime did not develop in the NBL with southerly winds recorded at the surface and aloft. The turbulent activity recorded at the surface throughout this period was not atypical of the characteristics expected for this type of LLJ. Given that gravity waves have been detected in association with other examples of this type of jet it is unlikely (though possible perhaps due to the consistency of the jet characteristics) that this supports Smedman's (1998) argument that the LLJ limits the transmission of gravity wave activity to the surface. It is further unlikely that the atmosphere was too turbulent to support gravity wave activity. Thus it is possible that no gravity waves were present in the atmosphere on this occasion, though given that the LLJ itself may cause gravity waves this remains a conundrum.

Detecting breaking gravity waves: Phase and signal reconstruction

Presence of gravity waves alone does not support the hypothesis that turbulence observed in the surface layers is the result of breaking gravity waves. In order to try and establish differences between the nature of breaking gravity waves associated with turbulent activity and those occurring during stable conditions a more detailed analysis using a complex wavelet (the

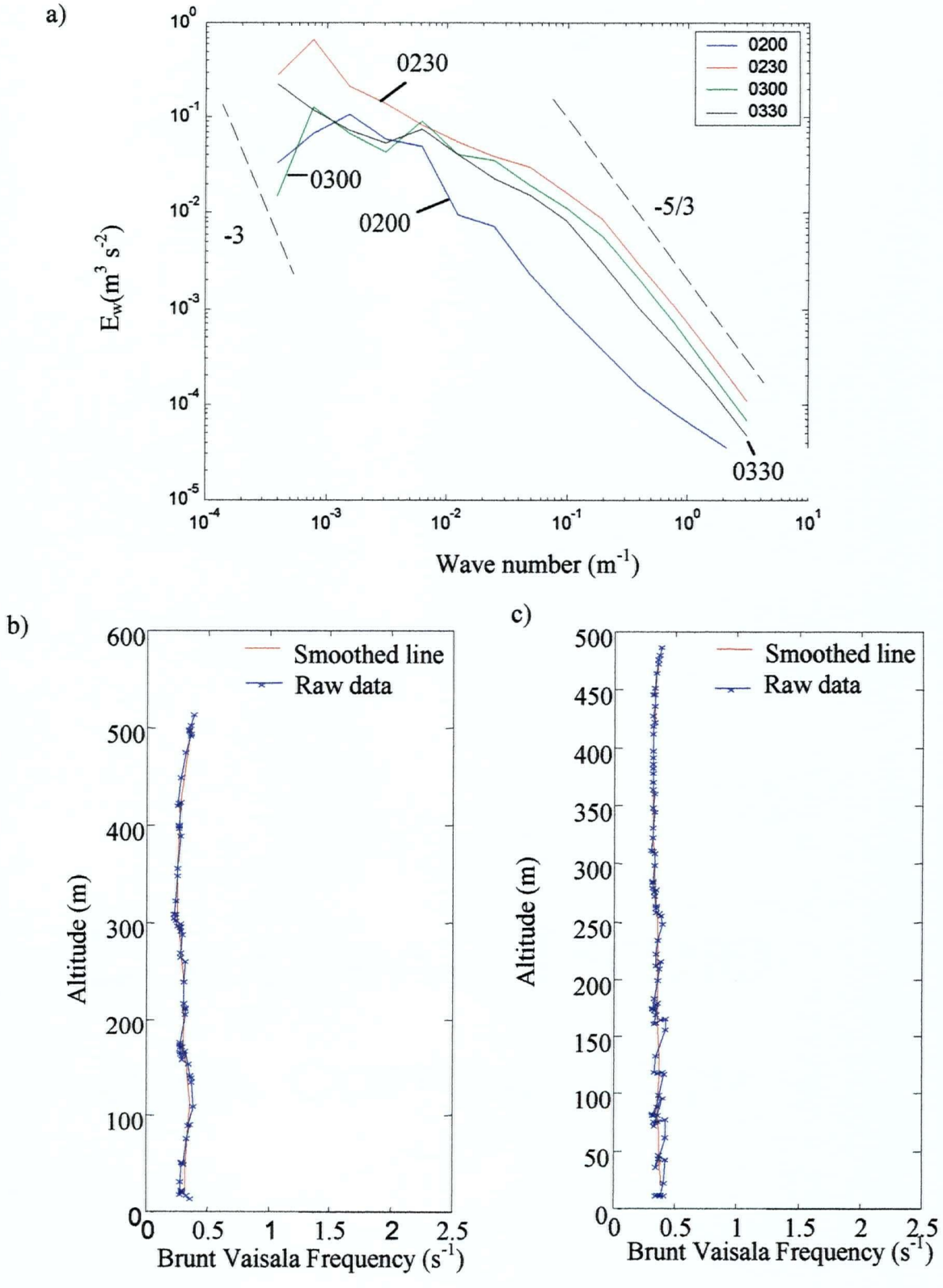

Figure 6.17 a) Spectra as calculated using the Haar wavelet transform for vertical velocity for 0200 PDT, 0230 PDT, 0300 PDT and 0330 PDT August 9th 1998, and Brunt Vaisala frequencies as calculated from the tethersonde data for the ascending limbs of flights at b) 0111 PDT August 9th 1998 and c) 0229 PDT August 9th 1998

Morlet wavelet used in section 6.4) was undertaken. The aim of this technique was to identify the phase between vertical velocity and temperature time series at each scale of analysis. A 90^0 offset between the two time series is expected if gravity waves are present whilst a 180^0 offset is expected if the nocturnal time series are turbulently coupled. However, a great deal of scatter was observed in the time series. Figure 6.18 illustrates the results for the two remaining ozone spikes of primary interest. The results indicate that whilst at larger scales both time series show a marked deviation from 180^0 the phases identified are not offset by 90^0. Although this result does not support the case that the waves observed are indeed gravity waves, this may be a consequence of the intermittent presence of gravity waves within the time series and the choice of 30 minute data blocks.

Wavelet analysis can also be used to reconstruct time series at individual scales. This is similar to filtering the time series to expose only information at the scales of interest and can be used to take a more detailed look at timing of wave activity and the covariation between temperature and vertical velocity. Evidence from the Brunt-Vaisala frequencies demonstrates that the NBL frequently supports gravity waves with periods longer than 20 seconds near the surface. Thus the signal was reconstructed at scales ranging from $2^9 - 2^{14}$ (equivalent to 24 seconds – 13 minutes) for the time series. (The wavelet coefficients for scales longer than 13 minutes showed no cyclical patterns when analysed at an hourly scale.)

Figure 6.19 shows the reconstructed temperature and vertical velocity time series at these scales for 0030 - 0130 PDT on July 28^{th}. (The Brunt-Vaisala frequency for this period is given in Figure 6.8b.) Although it is difficult to determine exactly the temporal location of waves with a 90^0 offset, Figure 6.19 suggests that gravity waves may have been present between 0050 - 0110 PDT at scale 2^{11}. This section of the time series is enlarged in Figure 6.20 which illustrates that both variables have an average wave period of approximately 5 minutes, and that the two variables are offset by approximately 90^0. This is further confirmed in Figure 6.21 where the lagged correlation between the two variables cycles at approximately 5 minute intervals between $r^2 = 0.3$ and $r^2 = -0.4$ as the two time series are alternately positively and negatively correlated. Although this is a weak correlation, the data do suggest that gravity waves may have been present intermittently at this time. Given that gravity waves were detected in the time series for 0000 PDT - 0030 PDT, it is possible that the first part of the 0030 PDT - 0100 PDT time series represents a period when the gravity waves were breaking. Whilst it is not possible to determine whether they broke as a result of internal dynamics or an external disturbance this does support

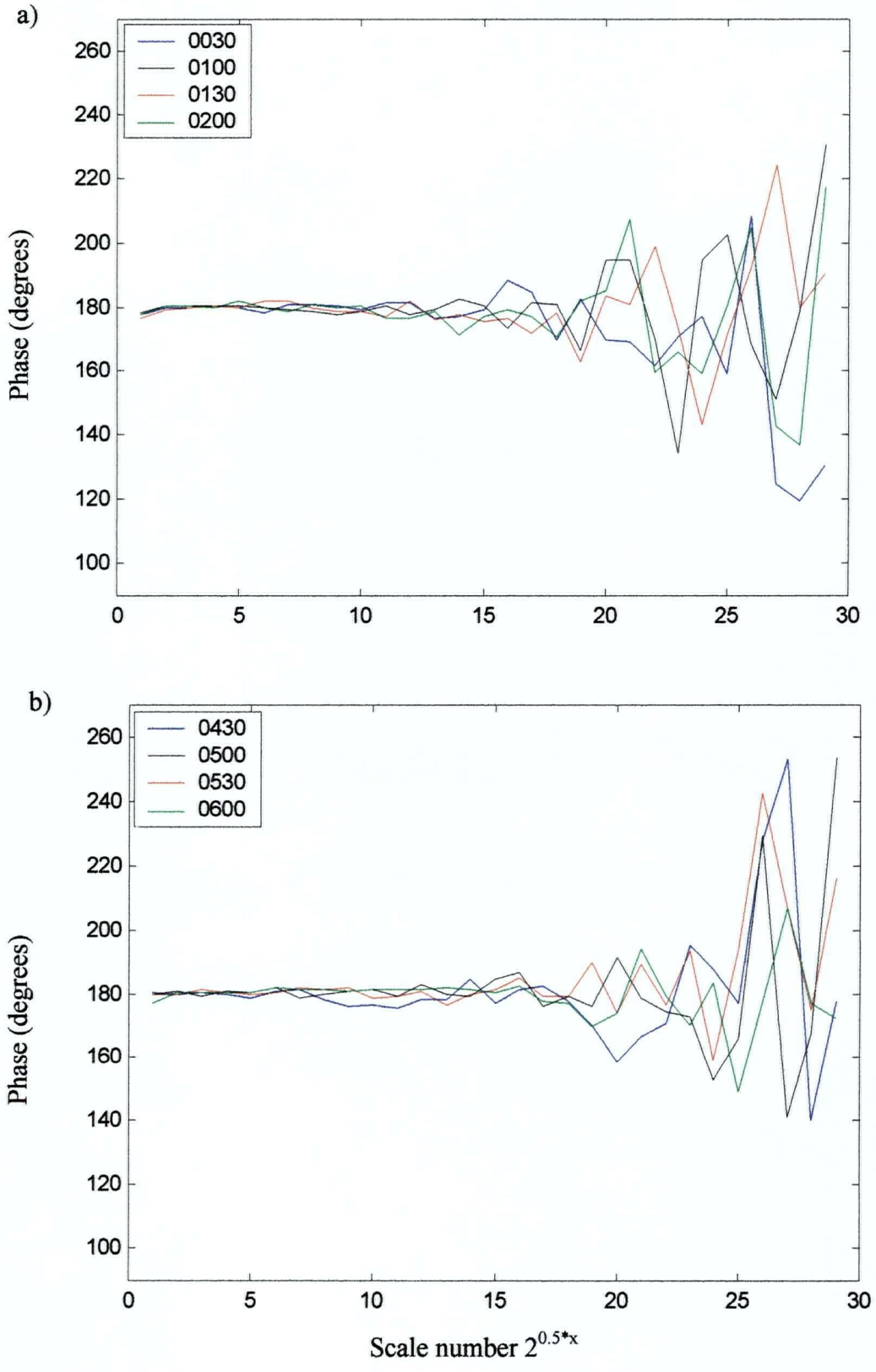

Figure 6.18 Phase between vertical velocity and temperature times series as observed for a) 0030, 0100, 0130 and 0200 PDT July 28th 1998 and b) 0430, 0500, 0530 and 0600 PDT August 10th 1998

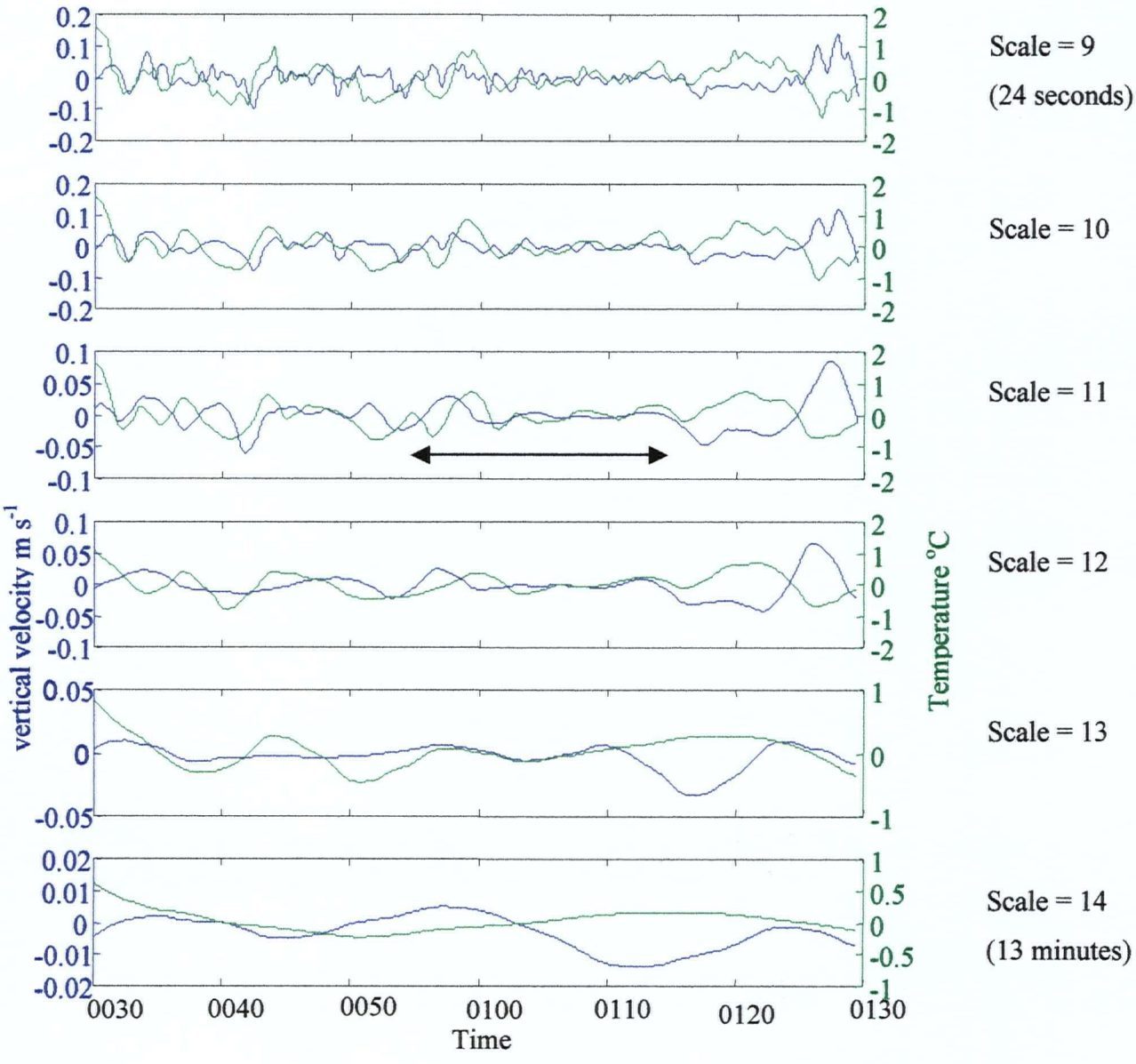

Figure 6.19 Reconstruction of the vertical velocity and temperature time series observed between 0030 - 0130 PDT 28th July1998 at scales 9 - 14. (Arrow indicates region of possible gravity wave activity)

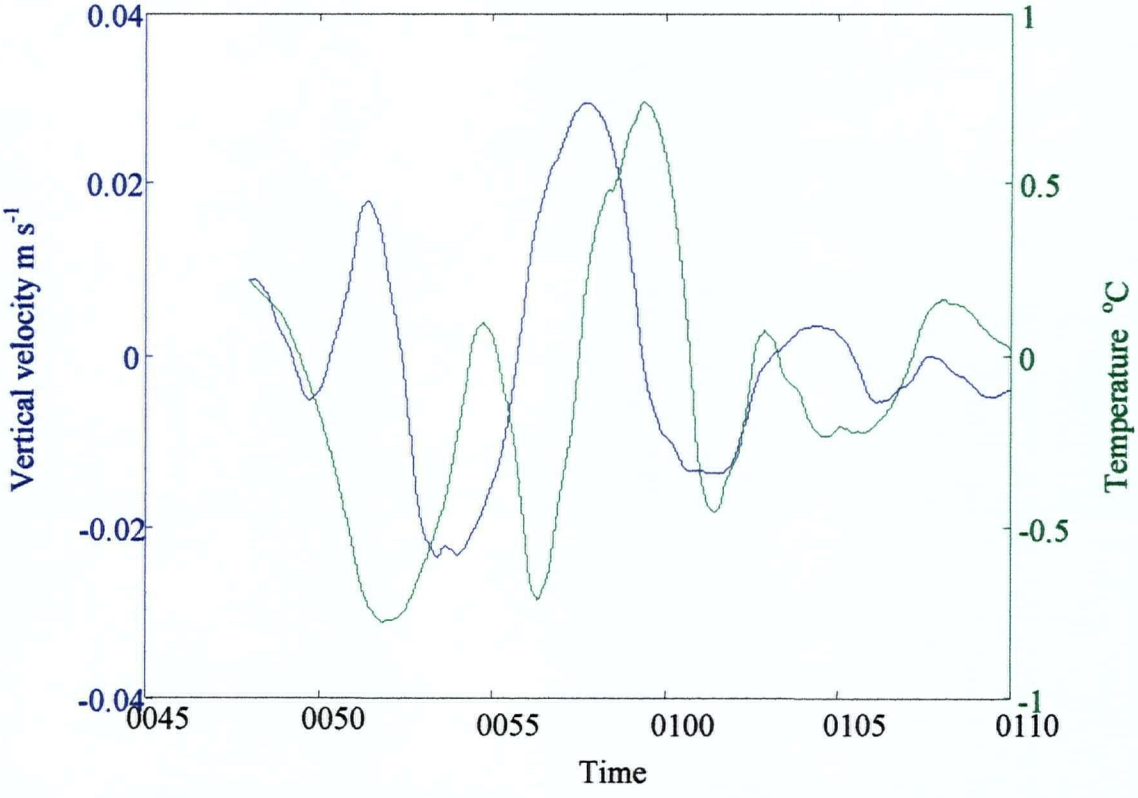

Figure 6.20 Reconstruction of the vertical velocity and temperature time series observed between 0045 and 0110 PDT 28th July 1998 at scale 11

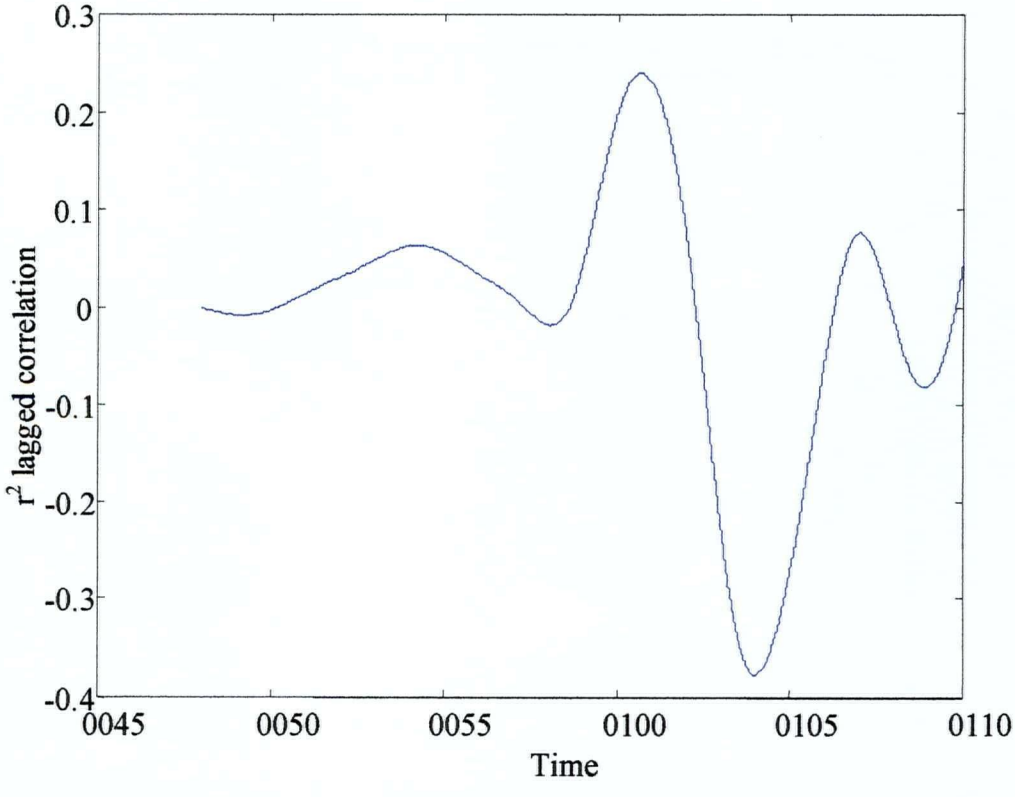

Figure 6.21 Changes in the lagged correlation between vertical velocity and temperature time series observed with time 0045 - 0110 PDT 28th July1998 at scale 11

the hypothesis that breaking gravity waves may at least be associated with increased turbulence (and hence vertical mixing) at the surface.

Temporal intermittence of gravity waves was a common feature of turbulent time series where significant turbulent activity was also reported. For example gravity wave activity was also identified in the time series for 0030 PDT on September 1st (scale 14, Figure 6.22). (This was the example used in the earlier sections since it represented turbulence associated primarily with the development of a down-valley wind regime.) Using this technique it is possible to demonstrate that gravity wave activity was also present in time series and may have contributed to turbulence generation at the surface. Interestingly, when the reconstructed signals are evaluated for nights when gravity wave activity was only associated with weak turbulence at the surface, the gravity waves are much easier to identify and remain consistently throughout the measurement period, as shown between 0100 PDT - 0130 PDT on September 1st 1998 in Figure 6.22. This further supports the idea that the intermittent presence of gravity waves is an indication of breaking gravity waves.

The evidence for intermittent gravity waves throughout the observation period accounts for the absence of 90^0 phase observed in Figure 6.18 and periods when the -3 gradient was not perfectly identified. If only half of the individual 30 minute time series contain gravity waves, then the expected phase or gradient will be not be observed. It also highlights the importance of applying a local rather than global transform when analysing data from the very stable nocturnal boundary layer.

In summary, the results indicate that turbulent processes were active during the two remaining ozone spikes under examination: 0050 PDT - 0135 PDT July 18th 1998 and 0500 PDT - 0535 PDT August 10th 1998. Using wavelet analysis it was possible to identify the presence of intermittent gravity wave activity and gravity wave - turbulence interaction during these periods. However, these characteristics were also identified in other examples of vertical mixing periods which had previously been attributed to mesoscale disturbances in the NBL. It was therefore not possible to determine whether the gravity waves were destroyed as a result of internal dynamics or external forces. Given that no external factors could be identified within the context of the temporal resolution of the tethersonde data set, there is at least circumstantial support for the notion that breaking gravity waves may account for the turbulence and hence vertical mixing associated with the observed increase in ozone concentration at the surface during these periods.

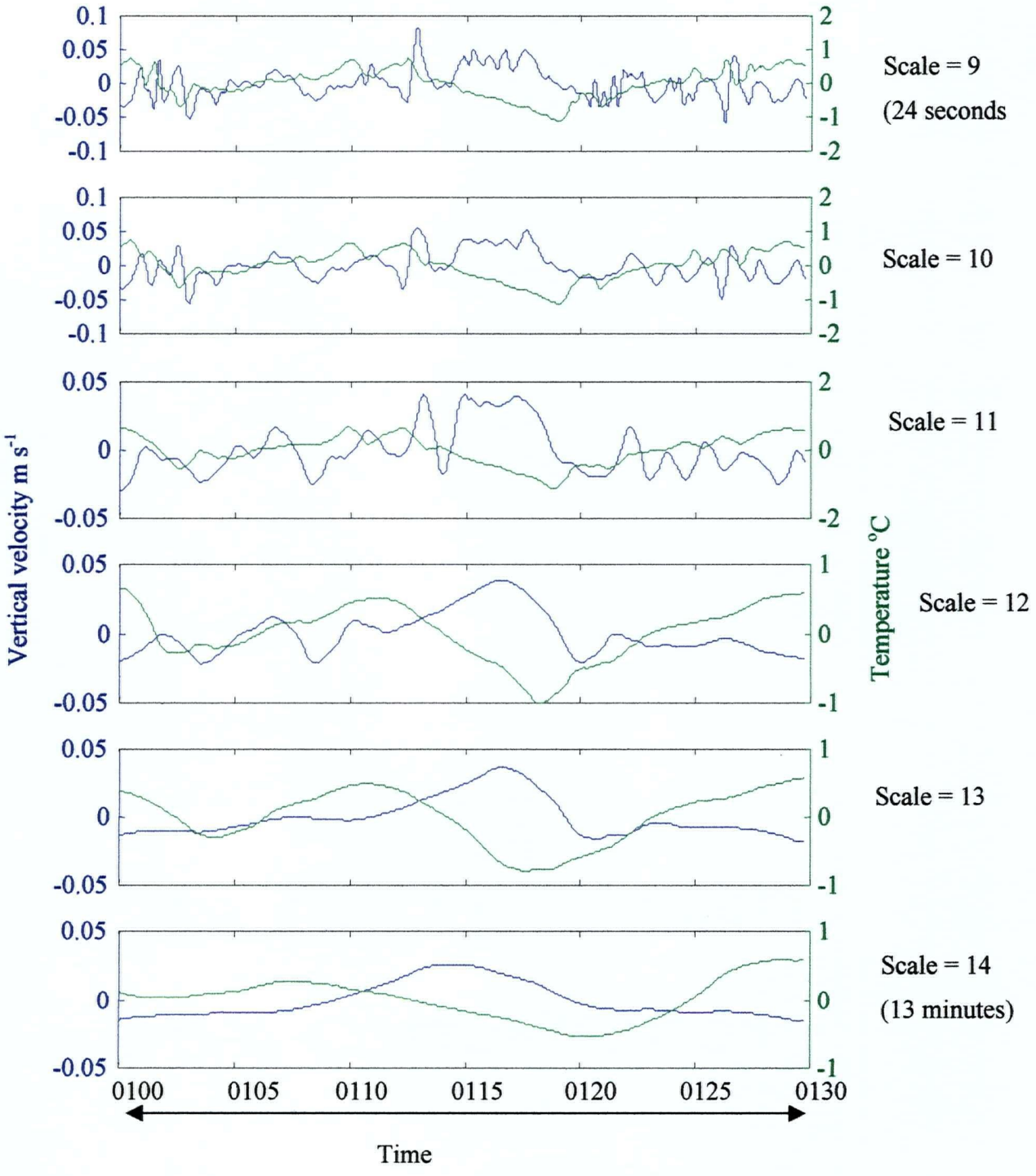

Figure 6.22 Reconstruction of the vertical velocity and temperature time series observed between 0100 - 0130 PDT 1st September 1998 at scales 9 - 14. (Arrow indicates period of possible gravity wave activity)

6.6 Intermittent turbulence and the vertical mixing of ozone

Having established a technique to quantitatively evaluate the turbulent characteristics of the NBL, an attempt can be made to ascertain whether the nature of the turbulence provides an insight into the characteristics of vertical mixing of ozone to the surface. Comparison of turbulence during nights when ozone spikes were observed at the surface with those nights when spikes did not occur, reveals a small increase in the strength (as measured by the standard deviation) and total duration of the turbulent periods during nights when ozone spikes were present (Table 6.3). However, these differences are not statistically significant (assessed using standard measures based on independent samples t-Test and ANOVA statistical tests) and may be accounted for in part by the reduced concentration of ozone throughout the profile during non-mixing nights. Thus periods of increased turbulence may have been observed during nights when ozone spikes were absent due to low ozone concentrations aloft rather than the dynamic efficiency of the mixing process.

To reduce the influence of ozone availability, time series collected when increasing ozone concentrations were recorded at the surface (the ascending limbs of ozone spikes) were compared with time series from the same nights when ozone concentrations were decreasing (descending limbs of ozone spikes) or remained consistently low. As shown in Table 6.3 the mean maximum available ozone concentrations in the two categories are now very similar (63.9 ppb compared to 64.3 ppb). The results demonstrate that increases in duration of the turbulent component of the time series is reported when ozone concentrations are increasing at the surface, whilst the strength of the turbulence is comparatively reduced. This suggests that longer duration of the turbulence is more important than strength in determining the effectiveness of the vertical mixing process.

However, this relationship is also not statistically significant. This is in part a consequence of the high variance of the data sets. However, as identified in Chapter 5 one of the important influences on surface concentration of ozone is NO. Prolonged periods of turbulence may therefore not result in increased surface ozone concentrations if high NO concentrations are observed at the surface. Thus while the data do indicate a correlation between increased turbulence at the surface and the incidence of ozone spikes, the relationship may be mitigated both by ozone availability within the NBL and local variations in surface based chemistry.

Table 6.3 The characteristics of turbulence associated with mixing and non-mixing events during IOPs

	Number of 30 minute time series considered (N)	**Average duration of turbulent 'bursts' (min)**	**Total duration of turbulence in the 30 minute time series (min)**	**Standard deviation of vertical velocity of turbulent bursts ($m\ s^{-1}$)**	**Mean ozone concentration at the surface (ppb) (and height measured)**	**Mean ozone concentration at the top of the SBL (ppb) (and mean height measured)**
Nights with ozone spikes	138	0.91	3.01	0.052	14.2 (2 m)	46.4 (88 m)
Nights with no ozone spikes	58	1.04	2.53	0.035	7.8 (2 m)	29.7 (108 m)
Periods when ozone concentration increasing at the surface	41	0.96	3.38	0.045	13.5 (2 m)	44.7 (100 m)
Periods when ozone concentration decreasing at the surface	155	0.88	2.85	0.056	14.5 (2 m)	47.1 (113 m)

Despite the difficulties identified previously in establishing a generalised relationship between the characteristics of turbulence and increased ozone concentration, analysis of ozone spikes on individual nights reveals a good correlation between the characteristics of the turbulence and increased ozone concentrations at the surface. For example, Figure 6.23 demonstrates that on August 8th - 9th ozone concentrations decrease at the surface between 2300 PDT and 0200 PDT. The drop in ozone concentrations coincides initially with a decrease in strength (Figure 6.24) and latterly with a decrease in duration of turbulence (Figure 6.23). The strength and duration of the turbulence are therefore important determinants of surface mixing. These results clearly support the hypothesis that increased ozone concentrations at the surface are the result of vertical mixing processes.

This technique can also be used to determine whether the correlation established in Chapter 5 between increased surface ozone concentrations and the type of LLJ, the break-up of the LLJs and mesoscale disturbances in the NBL are a product of the characteristics of the turbulence at the surface. The results in section 6.6 suggest that of the four different types of LLJs, type 3 was associated with the strongest, longest duration of turbulence at the surface. This type of LLJ was identified in Chapter 5 and in Table 6.2 as the jet associated with the highest concentrations of ozone at the top of the SBL and at the surface. Given that there is only a small difference between the mean maximum ozone concentrations associated with the different jet profiles, this suggests that the characteristics of turbulence play an important role in the enhanced vertical mixing of ozone through the profile.

The results also suggest that the strength of the turbulence is an important determinant of vertical mixing. For example, despite the short duration of the turbulence generated by type 4 LLJs (event = 0.74 minutes and total = 2.4 minutes), these jets are associated with the second highest ozone concentrations both at the top of the SBL and at the surface. The strength of the turbulence may also be significant in explaining the reduced vertical mixing of ozone associated with type 1 LLJs. Although the average duration of the turbulence is very similar to type 2 LLJs (event = 0.86 minutes and total = 2.6 minutes) the standard deviation is considerably smaller at 0.02 m s^{-1}.

This example suggests that the strength of the turbulence rather than the height of the disturbance is critical in determining the distribution of ozone through the boundary layer. Type 1 LLJs are located at approximately 100 metres above the mean of the other jet. However,

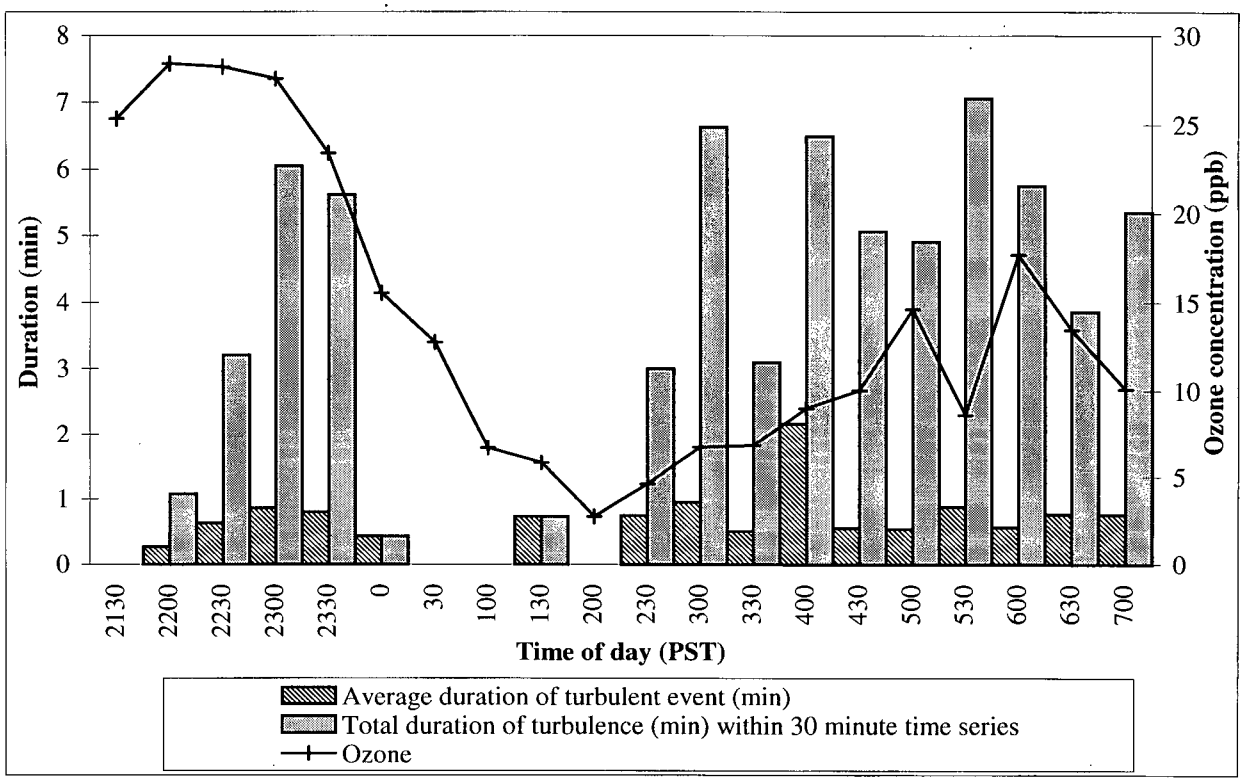

Figure 6.23 The relationship between average duration and total duration of turbulence and surface ozone concentrations August 8th - 9th 1998

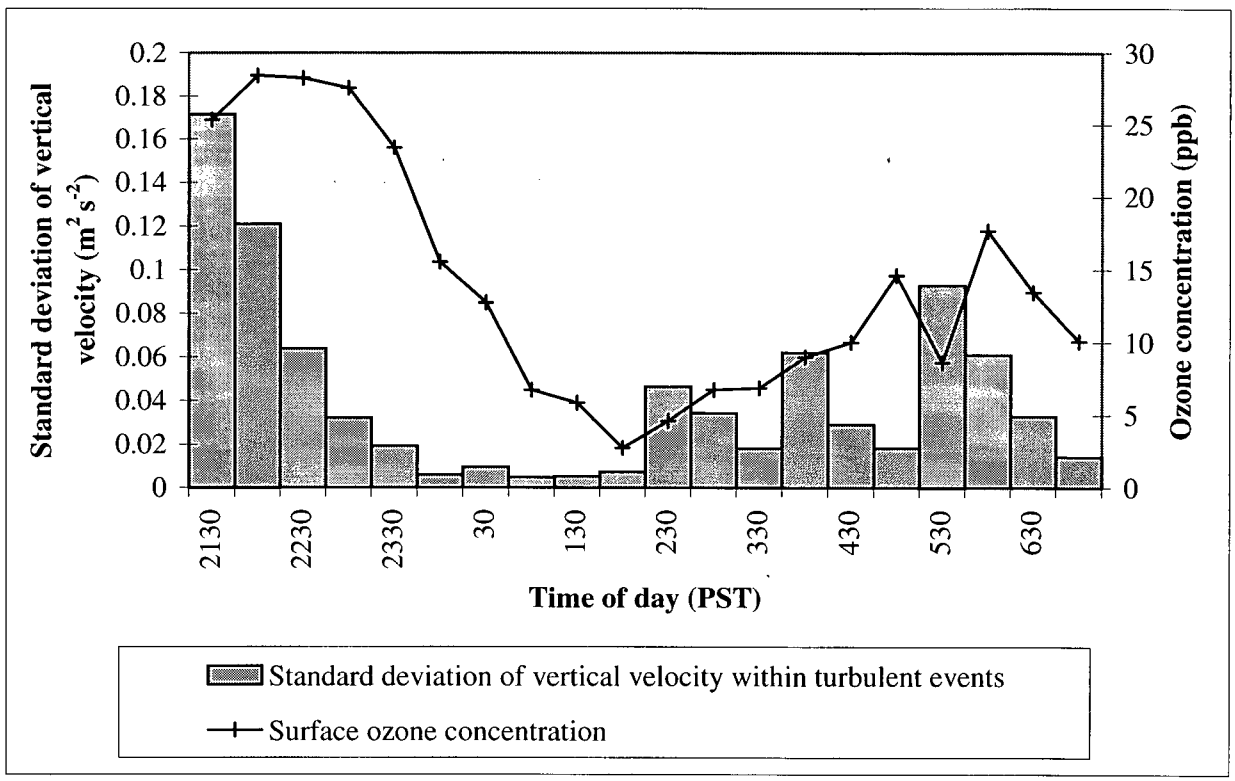

Figure 6.24 The relationship between standard deviation of mean vertical velocity of the turbulent component of the time series and surface ozone concentrations August 8th - 9th 1998

despite the similarity of the mean maximum ozone concentrations in profiles between the jet types, ozone concentrations at the top of the SBL and at the surface are considerably lower for type 1 LLJs (Table 6.2). In this example it is clear that the characteristics of turbulence limit vertical mixing of ozone throughout the profile.

The notion that the strength of the turbulence is key to the efficiency of vertical mixing of ozone to the surface is further supported by the characteristics of the turbulence associated with the development of a down-valley wind regime (Table 6.1). Although the duration of the turbulence associated with this disturbance is small, it is very strong (0.08 m s^{-1}). Ozone concentrations through the profiles associated with mesoscale disturbances are also considerably higher compared to those associated with the LLJ. Thus while increased ozone concentrations at the surface may be the result of increased concentrations through the profile, these results also suggest that the strength of the turbulence may enable effective mixing through a greater depth of the NBL, enabling higher ozone concentrations to be mixed down from the residual layer.

Interestingly, large increases in ozone concentration are also observed at the surface associated with the prevalence of the westerly band (identified as a common feature in the residual layer in Chapter 5) despite weaker turbulence of short duration. This supports the suggestion that ozone availability plays a key role in determining vertical mixing.

The absence of a clear relationship between turbulent characteristics of the boundary layer during periods of increased surface concentrations does not undermine the hypothesis that these events are the result of vertical mixing processes. It merely reinforces the importance of a complete understanding of the chemical and meteorological processes operating in the NBL. Clearly, local surface chemistry and concentrations of ozone aloft play as important a role as the characteristics of turbulence in determining the sustained vertical mixing of ozone to the surface.

6.7 Case study: August 30th - September 1st 1998

The ideas presented in section 6.6 can be summarised efficiently by returning to the case study presented at the end of Chapter 5. This involves the analysis of data from two consecutive nights the first (August 30th - 31st) demonstrating no evidence of increased ozone concentrations at the surface and the latter (August 31st - September 1st) exhibiting two periods of marked increase in ozone concentrations at the surface.

Analysis of conditions during the second night shown in Figure 6.25 illustrates the relationship between increased duration of turbulence and increased ozone concentrations at the surface. Between 2330 - 0100 the duration of the turbulence increases as a down-valley wind regime starts to develop throughout the NBL, destroying a weak type 3 LLJ that preceded it. As the duration of the turbulence increases so too does the ozone concentration at the surface. Between 0130 - 0300 ozone concentrations remain low as the stability at the surface increases. From 0330 the presence of a westerly band at 300 m is correlated with increasing turbulence at the surface and once again ozone concentrations can be seen to increase at the surface. Although the turbulence is stronger (Figure 6.26) and more prolonged during this period, ozone concentrations only increase by a small amount. However, despite a simultaneous decrease in ozone concentrations is observed during this period aloft, levels are high enough at the top of the SBL to enable the transport of ozone to the surface if turbulence mechanisms are active. Thus it is unlikely that the absence of ozone in the profile is limiting vertical mixing. At this point in time it becomes clear that the turbulence is no longer the driving factor determining increased ozone concentrations.

As demonstrated in Chapter 5 and Figure 6.27, an increase in NO concentrations is observed immediately prior to the second period of increased ozone concentrations. Concentrations of NO are typically out of phase with periods of increased turbulence at the surface. Given that NO is primarily emitted from surface-based sources, increased surface stability enables concentrations to build up in the stable layers. This increase in NO concentrations observed immediately prior to the mixing event is likely to limit the total increase in ozone surface concentrations, as ozone mixed to the surface is initially titrated from the system until levels of nitrogen monoxide are reduced. Interestingly a lag is observed between the decrease in surface concentrations and the subsequent decrease in ozone concentrations aloft. Indeed, concentrations aloft only decline following a period of increased turbulence at the surface. Thus it is possible that the decrease in concentrations at the top of the SBL is a consequence of the vertical mixing of NO upwards at this time.

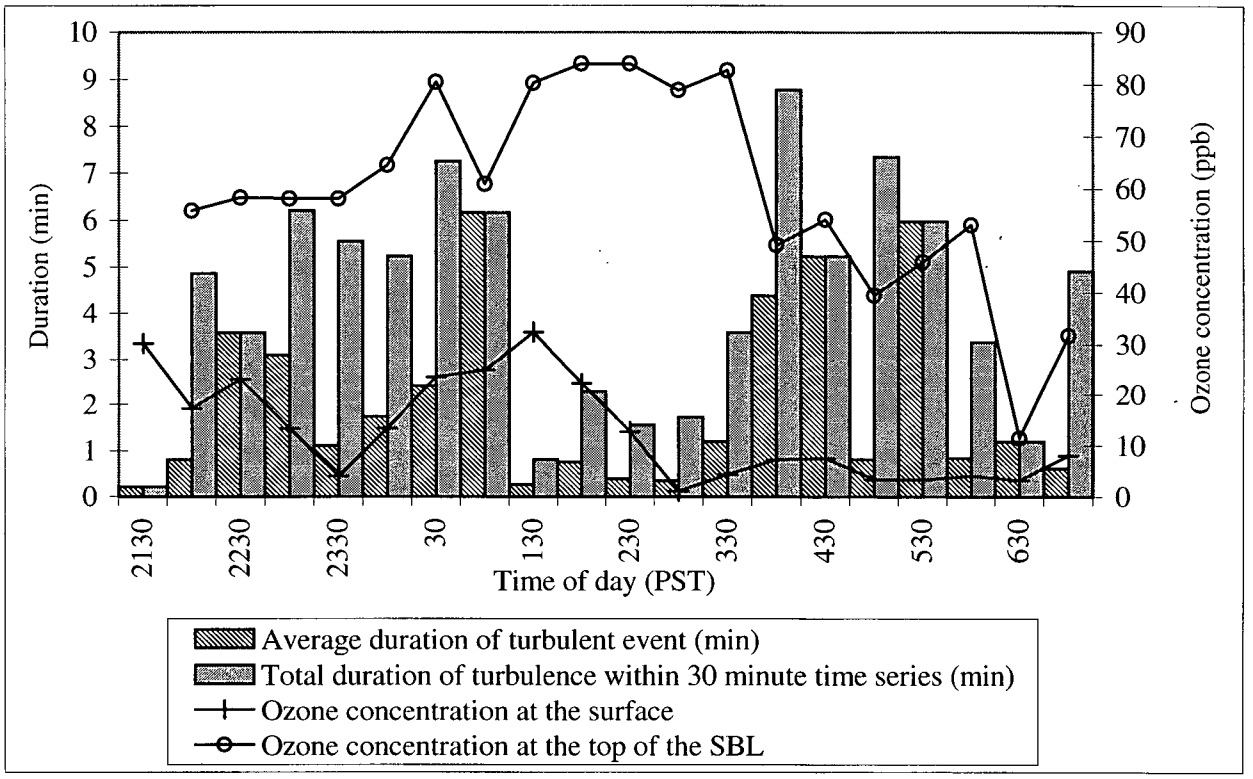

Figure 6.25 The total and individual event duration of turbulence and ozone concentrations observed at the surface and top of the stable boundary layer at CFS Aldergrove between 2130 PDT August 31st - 0700 PDT September 1st 1998

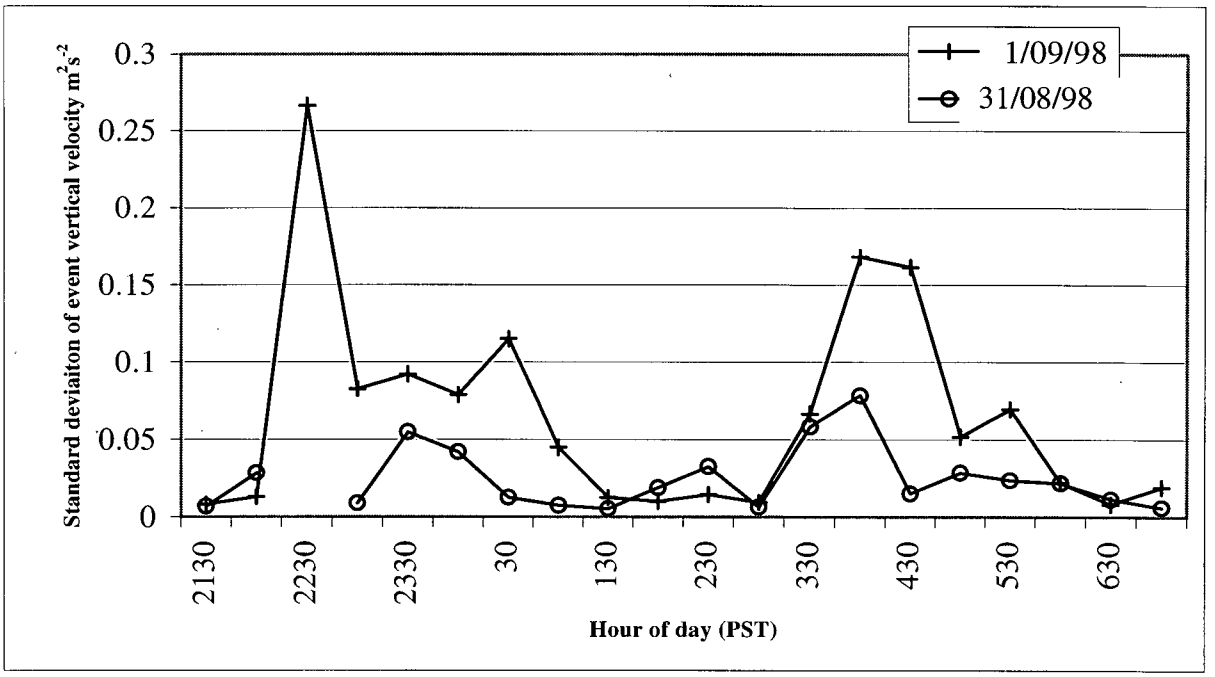

Figure 6.26 Comparison of the standard deviation of the turbulent component of the time series between 2130 PDT - 0700 PDT on August 30th - 31st and August 31st - 1st September, 1998

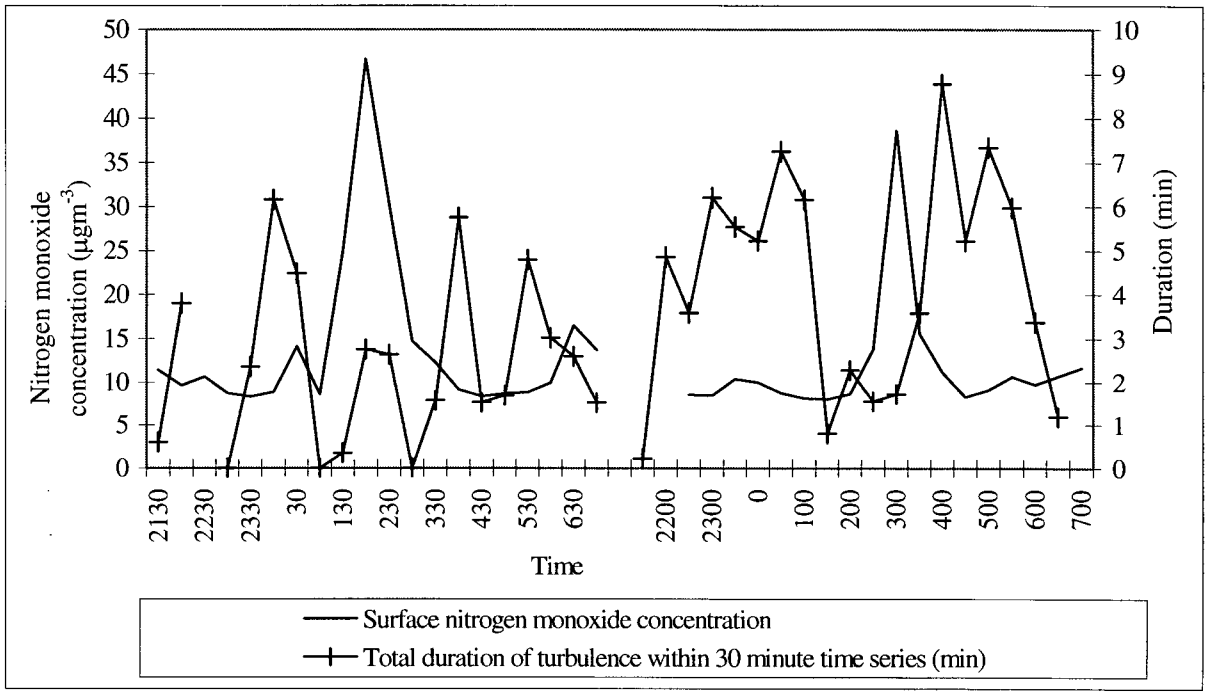

Figure 6.27 Comparison of nitrogen monoxide concentration and turbulence duration for 2130 PDT - 0700 PDT August 31st - 1st September, 1998

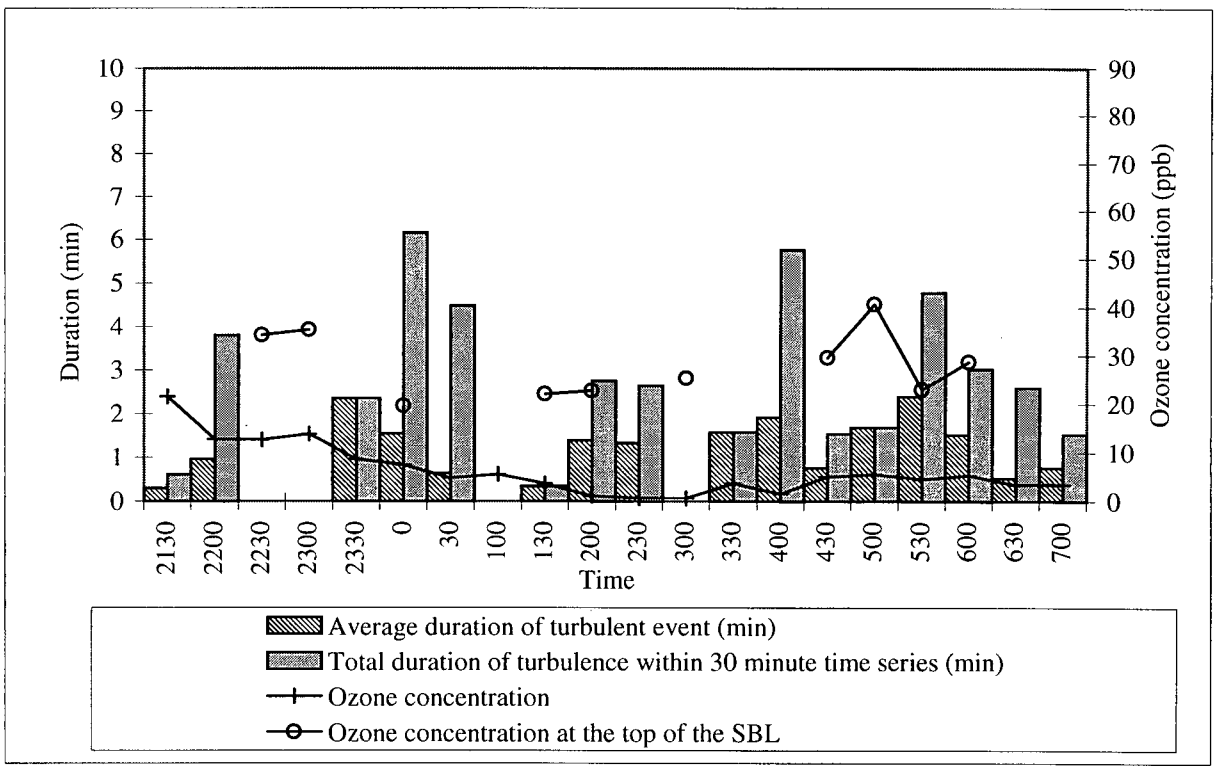

Figure 6.28 The total and individual event duration of turbulence and ozone concentrations observed at the surface and top of the stable boundary layer at CFS Aldergrove between 2130 PDT August 30th - 0700 PDT August 31st 1998

Comparison of the two nights shown in Figures 6.25 - 6.28 demonstrates the marked decrease in the duration and strength of turbulence throughout the night of the 30th -31st August compared to the following night. This supports the observation made in Chapter 5 (based on the contours of the Richardson number) that enhanced stability on the first night limits vertical mixing. Although there are periods of turbulence associated with the presence of a westerly band aloft (2330 PDT - 0030 PDT), a type 1 LLJ (0130 PDT - 0230 PDT) and a type 2 LLJ (0330 PDT - 0630 PDT), several time series record no turbulent activity at all. The mean duration of individual bursts of turbulence remains below 3 minutes on the 30th - 31st compared to a range of 0.25 - 6 minutes on the second night. It is likely that the characteristics of the turbulence are not the only factor limiting vertical mixing of ozone to the surface on this night, given that concentrations throughout the boundary layer remain low. This is supported by the observation that between 0000 - 0030 PDT and at 0400 PDT the total duration of turbulence reach 6 minutes, values not unlike those observed on the second night. However, even if a plume of 90 ppb had been advected over the site at either 0100 or 0300 PDT, an increase in ozone concentrations is unlikely to have been recorded at the surface due to the absence of turbulent activity. Thus whilst the characteristics of the turbulence clearly do play an important role, other factors such as the concentration of ozone within the profile and local surface concentrations of NO also determine the vertical mixing of ozone to the surface.

6.8 Summary

Despite the prevailing stability of very stable nocturnal boundary layer, wavelet analysis reveals the presence of intermittent turbulence throughout the measurement period. The turbulent component was efficiently and objectively isolated from a background of larger scale motions facilitating quantitative analysis of the characteristics of the turbulent component of the time series.

The characteristics of the turbulence (as determined by the duration of turbulent bursts or events, the total duration of the turbulence and the standard deviation of the vertical velocity during the turbulent periods) varied with the different type of disturbances. Increased turbulence was associated with the break-down of the nocturnal LLJ, presence of a type 3 LLJ, and the development of a down-valley wind regime. Given that 16 of the 19 ozone spikes identified in Chapter 5 occurred simultaneously with one or more of these disturbances, and a further two were identified with periods of increased turbulence (possibly associated with breaking gravity

waves), this strongly supports the hypothesis that ozone spikes are a result of vertical mixing processes.

A clear relationship could not be identified between the characteristics of the turbulence and the resulting vertical mixing at the surface. This is a result of the duality of the causal processes. For vertical mixing of ozone to occur, ozone must be available within the profile and there must be turbulent activity to mix the ozone to the surface. In the absence of other limiting factors the strength and duration of the turbulence appear to be important determinants of the concentration of ozone mixed to the surface.

Clearly a larger data set is required to fully elucidate the relationship between the processes operating in the nocturnal boundary layer and the characteristics of the resulting turbulence in the surface layers. However, this chapter has demonstrated the potential of wavelet analysis as a quantitative analytical tool, which can provide powerful insights into the characteristics of the processes operating in the nocturnal boundary layer. The technique overcomes some of the limitations of Fourier analysis, providing a tool which efficiently decomposes the signal into its time localised frequency components. The level of detailed analysis afforded by the wavelet transform renders it particularly useful in elucidating the relationship between gravity waves and turbulence. Given that wavelet analysis is well suited to non-stationary signals pre-processing of the data is not required, thus reducing the danger of contaminating the spectra by unwanted or introduced signals.

Chapter 7: Wavelet analysis of intermittent turbulent fluxes in the very stable nocturnal boundary layer

7.1 Introduction

Chapter 6 demonstrated an association between turbulence in the very stable NBL and periods of increased ozone concentration at the surface. However, in order to quantitatively analyse the importance of vertical mixing processes in determining near surface ozone concentrations, evidence from turbulent fluxes must be also examined. Due to the intermittent nature of turbulence (established in Chapter 6), it is very difficult to calculate reliable estimates of scalar fluxes in the very stable NBL. The aim of this chapter is to use wavelet analysis to develop an objective conditional sampling technique to isolate the turbulent flux component of the time series. This is used to examine the characteristics of turbulent fluxes in the very stable nocturnal boundary layer.

Although wavelet analysis has been previously applied to convective turbulent time series, little is known about the benefits of the technique or value of different wavelet bases when applied to the poorly developed, intermittent turbulence characteristic of the NBL. This gap in the literature is addressed in the first part of the chapter. Sensible heat flux data are used here to illustrate difficulties associated with flux calculation in the NBL and the potential benefits afforded by the use of wavelet-based methodologies.

The technique developed in Chapter 6 is then used to isolate periods of intermittent turbulence in each 30 minute time series, and to provide a revised estimate of the flux associated with only those parts of the time series which are turbulent. As a result of the comparatively long time scales of non-stationary processes operating in the NBL, it is likely that these still contaminate the revised flux estimates. However, due to the absence of a clear spectral gap, it is very difficult to isolate the turbulent signal using scale analysis. Thus the characteristics of the non-turbulent component of the signal were examined for each 30 minute data set. Using this information, it was then possible to isolate the 'true' turbulence signal for each time series. The validity of this technique is explored using a range of surface based variables for a specific case study. The technique is then applied to the ozone flux time series observed between 2130 PDT - 0630 PDT throughout the IOPs.

7.2 Turbulent flux measurement and calculation in the very stable nocturnal boundary layer

Measurement of turbulent fluxes in the very stable NBL represents a considerable challenge to researchers. The turbulence itself is typically weak, and measurements are frequently made at or near instrument limits. This problem is further compounded in the case of turbulent ozone fluxes due to the dominance of removal mechanisms in the NBL. The resulting low background concentrations are often below the resolution of instruments. Thus, whilst ozone is one of a limited number photochemical species for which high frequency analysers are available, their use in the nocturnal boundary is limited. The instrument used in this experiment (a GFAS - see Chapter 4) showed good sensitivity to low concentrations immediately after it was prepared for use, but this declined with time. Due to the practical difficulties associated with the measurement of high frequency fluctuations in ozone concentrations in the nocturnal boundary layer, a consecutive temporal record of events is not available. For this reason, sensible heat flux data is used as the basis for comparison of the analytical techniques and for some of the following data analysis.

Calculation of scalar fluxes in the very stable NBL is also fraught with uncertainty. Conditions in the very stable NBL are inherently non-stationary. This limits the validity of the traditional analytical tools that use the mean of the data set as the basis from which to extract information about the turbulent component of the time series. Wavelet analysis, however, effectively uses a local, un-weighted moving average to identify the turbulent component of the flux. The size of the non-over lapping averaging windows varies according to the scale of the daughter wavelet, enabling the turbulent components of two signals to be compared at the same resolution. Judicious choice of the wavelet base can also reduce the impact of non-stationaritites on the flux calculations. This avoids some of the problems associated with calculating turbulent fluxes when conditions are non-stationary (such as in the very stable NBL).

Despite the potential of this technique, particularly when applied to the very stable NBL, it has been used by only a limited number of authors in the NBL (Howell & Sun 1999; Howell & Mahrt 1997). Further, little is known about the benefits (or otherwise) of using different wavelets to calculate fluxes. However, the characteristics of turbulence in the very stable NBL hinders both the application of theories (developed primarily for the convective mixed layer) and standard analytical tools. Thus it is difficult to establish a sound basis for comparison of

analytical techniques. Due to the absence of an absolute reference point against which to assess the accuracy of each technique, the data are compared initially to each other and then in section 7.5 examined for consistency in the light of other surface based variables.

Standard sign convention is used for all fluxes calculations: negative values represent fluxes towards the surface and positive flux values represent away from the surface. Due to the dominance of chemical titration and surface deposition mechanisms in the near surface layers, radiational cooling and the development of a stable thermodynamic profile, negative fluxes of both ozone and sensible heat dominate in the NBL. If there is sufficient wind shear aloft to generate forced convection in the surface layer, negative heat and ozone fluxes are expected at the surface. This is representative of warm, ozone rich air being mixed to the surface. Positive sensible heat fluxes are only expected in rural areas such as the Aldergrove site if non-local transport mechanisms (such as horizontal advection) transport cool air parcels over the surface.

7.3 Using Wavelet analysis to calculate turbulent fluxes

The three wavelets chosen for comparison were the Haar wavelet (as proposed by Howell & Mahrt (1997)), the 'Daubechies 4' (db4) wavelet and the 'La16' wavelet. The 'db4' wavelet is an orthogonal wavelet and can be calculated using a previously developed (and widely available) fast algorithm. It has a longer filter length than the Haar wavelet and thus any polynomial trends present in the data set (resulting from non-stationarities) should not contaminate the validity of the flux estimates (Whitcher 2000, pers. comm.). The 'La16' wavelet is also an orthogonal wavelet, but it has a longer filter length than the 'db4' so is potentially even less sensitive to non-stationarities in the data set.

The maximal-overlap form of the discrete wavelet transform (MODWT) is used to calculate turbulent fluxes. This form of the wavelet transform (although not strictly orthogonal) is considered to be energy preserving and has been shown to be an effective tool in time series analysis (Percival & Walden 2000). The MODWT involves analysis of the signal at a range of different scales and positions in time. Wavelet coefficients are then statistically sampled and averaged to generate the final output. This provides a more complete analysis of the signal compared to the discrete form of the wavelet transform, whilst avoiding the problems of redundancy present in the continuous wavelet transform. The resulting variances and covariances have been rigorously tested and the mathematical justification of the technique demonstrated (Percival & Walden 2000).

The spectra calculated using the MODWT are less sensitive to the starting point of the time series. When calculating spectra using the discrete form of the Haar wavelet the contribution of any given event to the flux is dependent on its position relative to the boundaries of non-overlapping windows and limited by the choice of scales. This results in small and large scale aliasing which may become a source of error when filtering the signal by scale. The MODWT can also be applied to any length of time series. This avoids the difficulties associated with padding the time series that become particularly apparent if a large component of the flux is located at the end of the time series.

The code used to calculate the MODWT in this section was developed by Whitcher (1999) and is available on the world-wide-web (http://www.cgd.ucar.edu/~whitcher/software/ - see Appendix 4).

7.4 Comparison of different flux calculation techniques

This section uses data collected between 1130 PDT August 31st - 1200 PDT September 1st in order to explore the differences between fluxes calculated using standard eddy-correlation methods, Fast Fourier Transform (FFT) and three different wavelet bases. This time period was chosen due to the comparatively enhanced reliability of ozone flux data and the availability of measurements of NO and NO_2. Further, a pronounced ozone spike was observed at the surface during this period. Data processed using the FFT is included here to provide an alternative basis for comparison. The FFT has been widely applied to data sets collected in the convective boundary layer and shown to be an effective tool for manipulating the data set.

Comparison of sensible heat fluxes calculated using eddy-correlation and FFT techniques reveals only small difference between the magnitude of fluxes calculated for the convective boundary layer. These differences, which are accentuated at night as shown in Figure 7.1, can be largely accounted for by the presence of non-stationarities in the time series. (Time series must be detrended prior to analysis using the FFT.) Typically only the magnitude of the flux is affected by non-stationarities in the data sets, however occasionally the impact may be large enough to change the over-all direction of the flux as shown at 0230 PDT on September 1st 1998. Clearly, non-stationarities in the data set can have a significant impact on flux calculations in the very stable NBL.

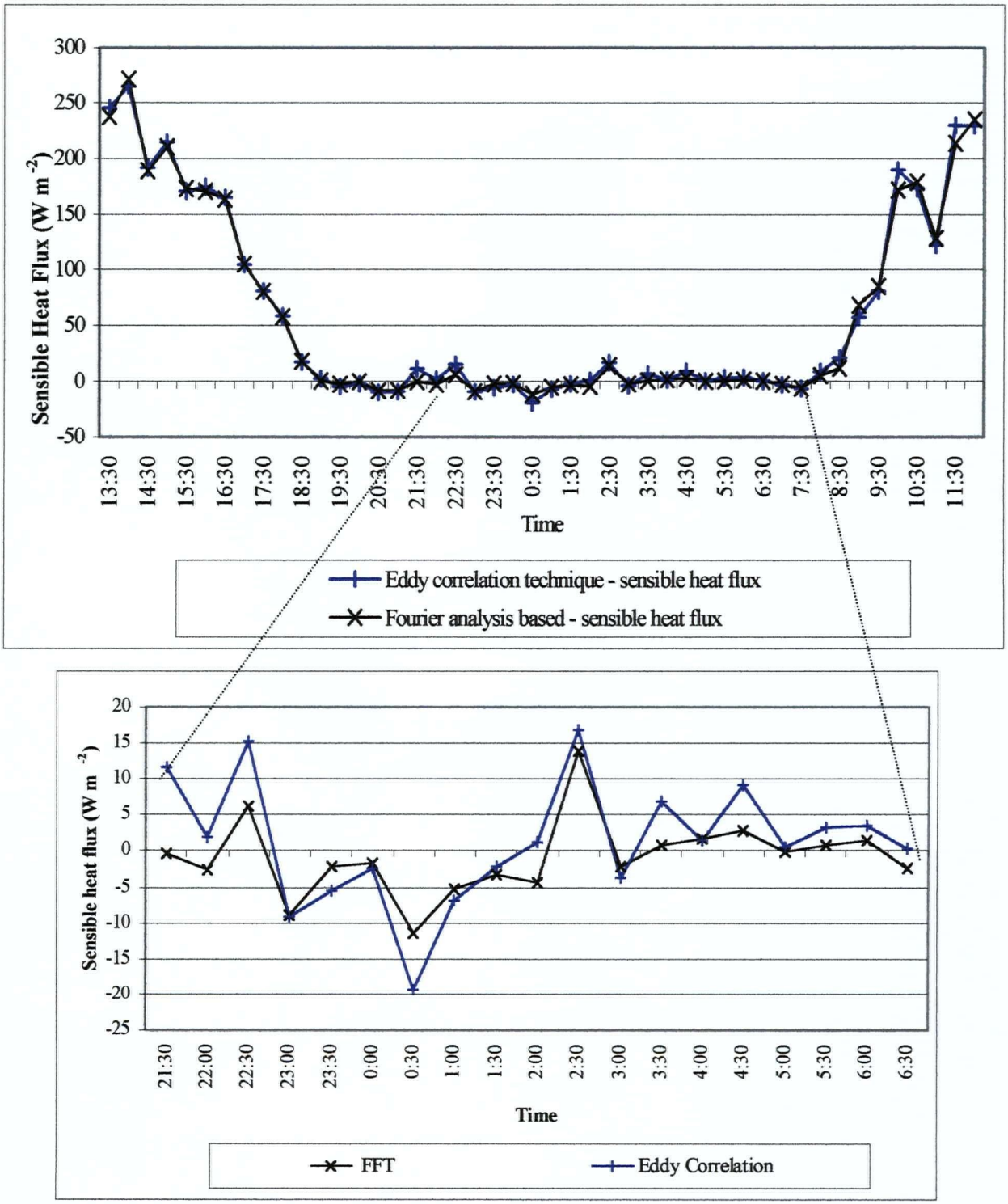

Figure 7.1 Comparison of the 30 minute average sensible heat fluxes calculated between 1330 PDT 31st August - 1200 1st September 1998 (inset plotted at enlarged scale for 2130 - 0630 PDT 31st August - 1st September 1998) using standard eddy correlation and Fourier techniques.

In order to compare fluxes calculated using the wavelet transform with fluxes from the FFT, linear detrending was also applied to the time series prior to analysis using the wavelet transform. The results shown in Figure 7.2 illustrate that there are differences of less than 0.003% between the fluxes calculated using the wavelet methodology and the fluxes calculated from the Fourier transform. The differences were consistent throughout the 24-hour period. Further the fluxes calculated by the three different wavelets were identical to three decimal places throughout the 24-hour period.

Thus these errors are very small compared to the random errors incurred due to flux sampling procedures in the very stable NBL. These are incurred as a result of the small number of eddies passing the sensor when turbulence is weakly developed and wind speeds are less than 2 m s^{-1}. These errors can be estimated based on the integral length and time scales using techniques suggested by Kaimal and Finnigan (1994): in neutral or near neutral conditions they may be as high as 20% of the total flux. Although it is very difficult to define these scales accurately for the NBL these errors are likely to be higher under very stable conditions. Mahrt (1998) suggests that a 'more practical, less rigorous' attempt to quantify random errors is to compare the sub-record flux with the total record flux. This is similar to the quality control methods suggested by Foken & Wichura (1996) and used to verify data in Chapter 5. Thus the random errors in the data sets used here may be as large as 30%. Thus these results confirm that wavelet analysis can be used to reliably calculate turbulent fluxes throughout the diurnal cycle without introducing significant sources of error. However, the results also suggest that there is little advantage to calculating fluxes using wavelet methods unless the data are to be filtered by scale or processed further using the transform.

7.4.1 Filtering the data set

Figure 7.3 illustrates the variance calculated for vertical velocity using the Haar, db4 and La16 forms of the MODWT for the 30-minute time series between 1130 - 1200 PDT 31st August 1998. The results indicate that the variances and covariances at each scale differ slightly in magnitude at different scales but present the same over-all morphology. This is a consequence of the resolution of each wavelet base in frequency space; thus the total variance and covariance calculated using each method are equal, hence the identical flux estimates. Differences between the wavelet bases however do become apparent when the data sets are filtered by scale. Due to

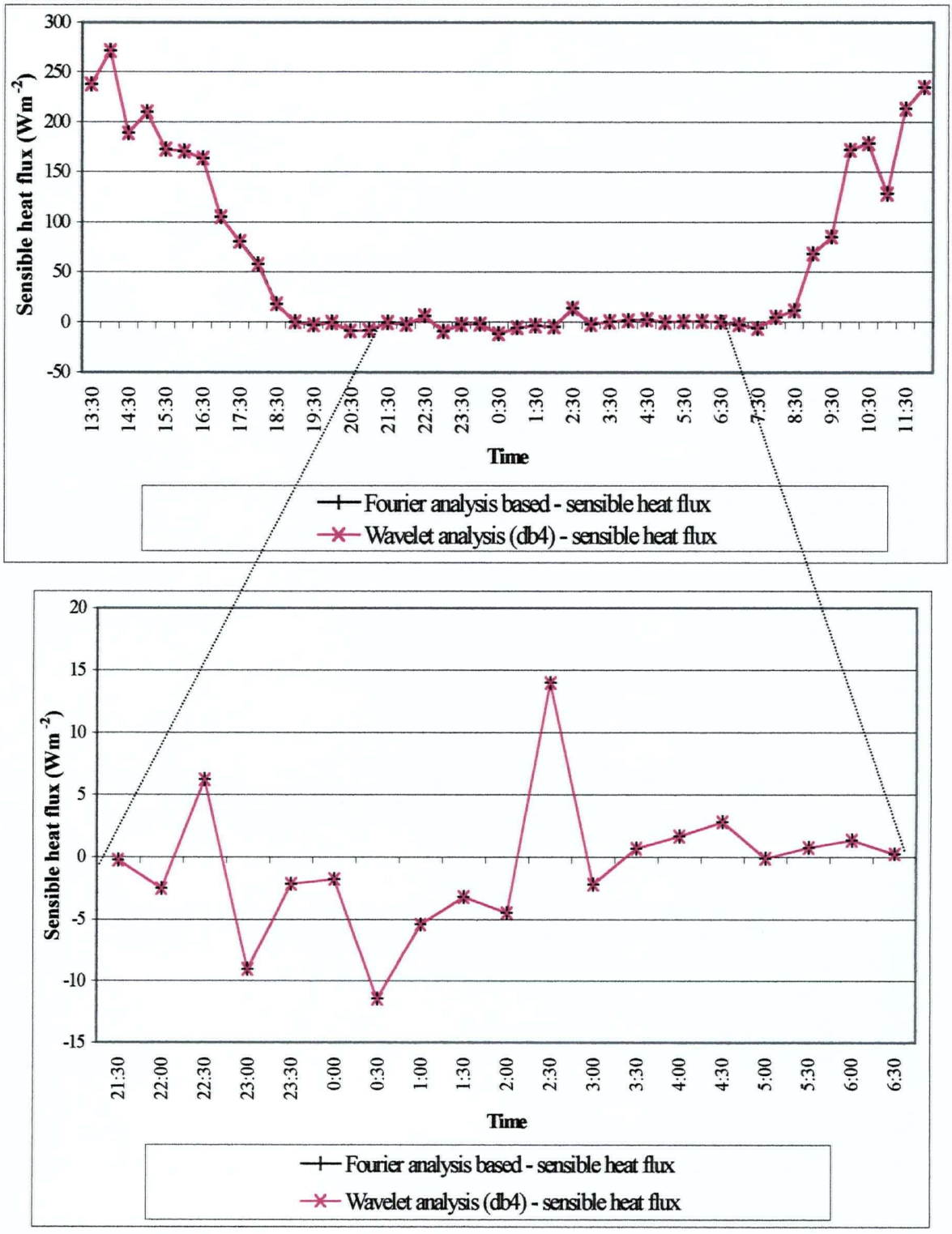

Figure 7.2 Comparison of 30 minute average fluxes calculated using Fast Fourier Transform and the db4 wavelet transform for between 1330 PDT 31st August - 1200 1st September 1998 (inset plotted at enlarged scale for PDT 2130 - 0630 31st August - 1st September 1998)

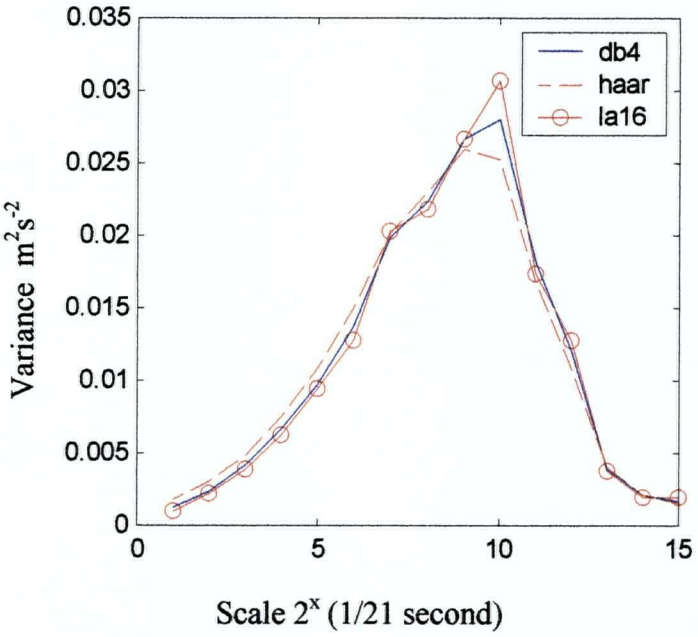

Figure 7.3 Variance calculated by MODWT form of the wavelet transform using haar, db4 and La16 wavelets for 1130 PDT -1200 PDT 31st August 1998

the enhanced resolution of the db4 wavelet in frequency space, low sensitivity of the wavelet to non-stationarities and availability of efficient computation routines, this wavelet is used in the following analysis.

Linear detrending

Although use of higher order wavelets as a basis for analysis was expected to facilitate the calculation of turbulent fluxes without the previous application of detrending programs, results did not confirm this. If the time series were not previously detrended calculation of wavelet coefficients revealed wildly distorted flux estimates for some time series, regardless of the wavelet base chosen. Analysis of the variance of these data sets revealed occasional spikes in the data set at larger scales. These were particularly evident in the temperature data, which showed the highest degree of non-stationarity.

Once linear trends were removed from the time series, spikes also disappeared. This was unexpected as the db4 and La16 wavelets should not have been sensitive to linear trends in the original data set (Whitcher 2000, pers. comm.). It is possible that the linear detrending routines sufficiently distort another non-stationary trend in the data set such that the non-stationarities no longer contaminate wavelet coefficients. These unexpected increases in variance appear to be a common feature of the nocturnal boundary layer and are visible in data published by Howell & Sun (1999), although they do not comment on it. Although beyond the scope of this study, these observations warrant further investigation. However, in light of these results the following flux calculations were made using time series that had been linearly detrended prior to wavelet analysis.

Cone of influence

Given the impact of non-stationarities in the time series care was also taken to remove the 'cone of influence' (COI) from flux calculations. The cone of influence represents the wavelet coefficients at longer scales and the edges of the transform where (due to the size of the wavelet and the length of the time series) the analysis was either incomplete or the scale was represented by a very small number wavelet coefficients. Thus removing the COI from the data set primarily isolates and removes large scale trends and edge artefacts from the flux calculation.

Perhaps not surprisingly, differences between flux estimates resulting from the removal of the COI are magnified in the nocturnal data sets, especially at low frequencies. As shown in

Figure 7.4, comparison of wavelet fluxes (COI removed) with FFT based fluxes shows a small but variable difference between the two calculations. The differences are particularly marked during the evening and morning transition periods when conditions are expected to be highly non-stationary as shown in Figure 7.5. This suggests that during these periods trends generated by non-stationarities and large scale motions within the boundary layer are affecting turbulence calculations when the COI is not removed. Unfortunately there is no method available to verify this assumption, however the results do justify removal of the COI from flux calculations.

7.4.2 Conditional sampling of the turbulent component of the time series

Given the intermittence of turbulence in the nocturnal boundary layer it is appropriate to exploit the potential of wavelet analysis in order to isolate the characteristics of the fluxes associated with only that part of the time series that is turbulent. In Chapter 6 an effective technique was developed to objectively identify time periods when turbulence was active. Using this information, the wavelet coefficients of the turbulent sections of the time series were isolated, and the corresponding flux calculated, to generate a type of ensemble average for each 30 minute time series. A schematic diagram of this is shown in Figure 7.6, where the blue hashed line represents the 95% significance level for red noise calculated for each 30 minute data block based on the auto-correlation of the time series (see Chapter 6). Information from all scales of analysis was included.

The signature of the remaining non-turbulent portions of the signal (trend component) was then characterised. Given that the signal present in the trend component is likely to have been generated by processes operating at time scales of several minutes or longer, it is likely that the non-turbulent signal can also be identified under-lying the signature of the turbulence. To obtain the 'true flux' generated by turbulence, the underlying non-turbulent component was subtracted from the turbulent part of the time series.

The technique outlined in this section avoids the need to subjectively identify and isolate turbulent scales of motion. Although this can be successfully done using wavelet analysis for turbulence in the convective boundary layer (Hagelberg & Gamage 1994), it is very difficult to apply a similar methodology in the nocturnal boundary layer due to the absence of a spectral gap. Their technique further requires identification and choice of thresholds which introduces an element of subjectivity avoided here.

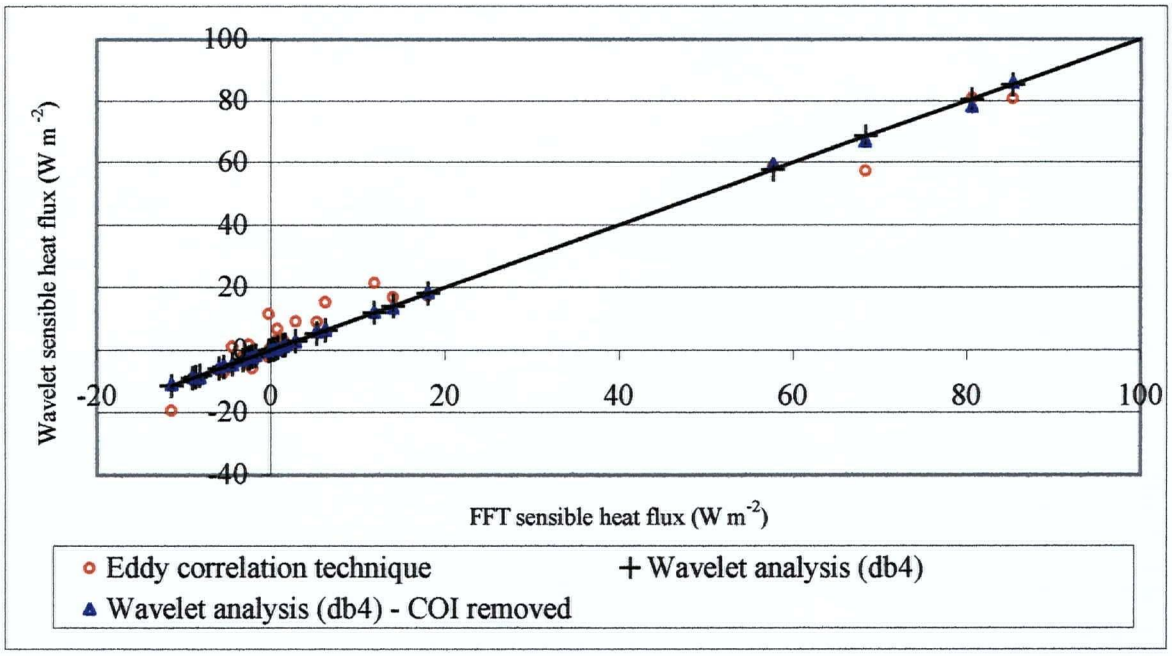

Figure 7.4 Comparison of the sensible heat flux calculated using Fourier analysis between 2130 - 0630 31st August - 1st September 1998 with standard eddy correlation, wavelet analysis and wavelet analysis with the COI removed techniques

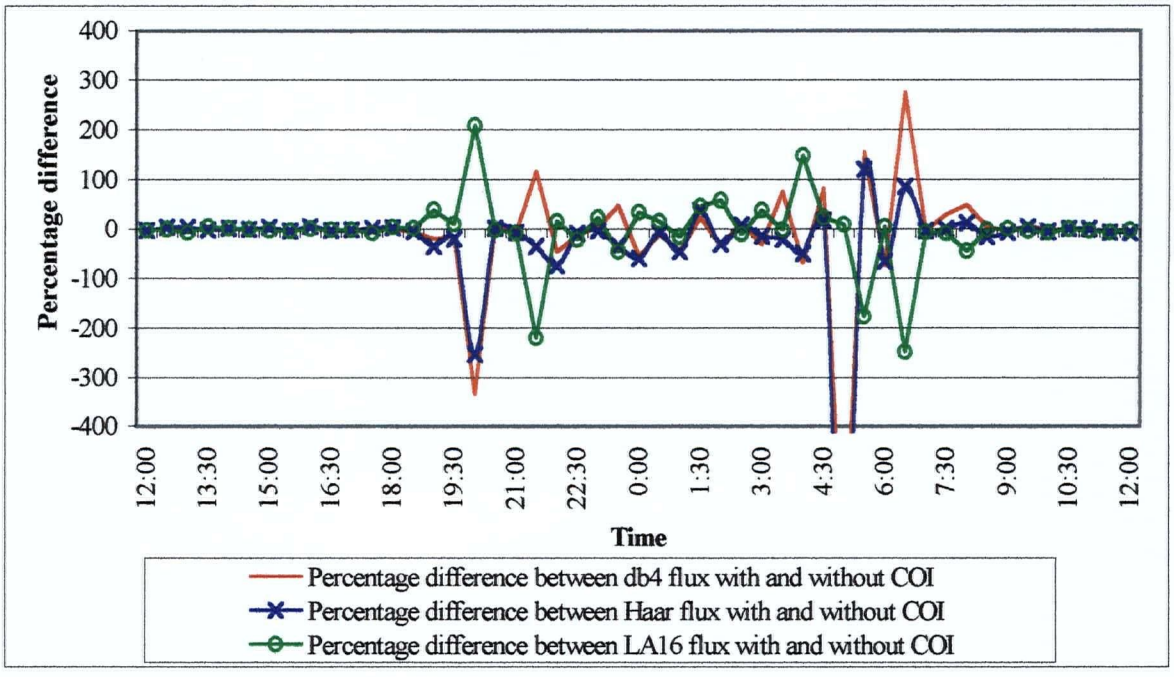

Figure 7.5 The percentage difference between the fluxes calculated using the db4, Haar and La16 wavelets with and without the COI

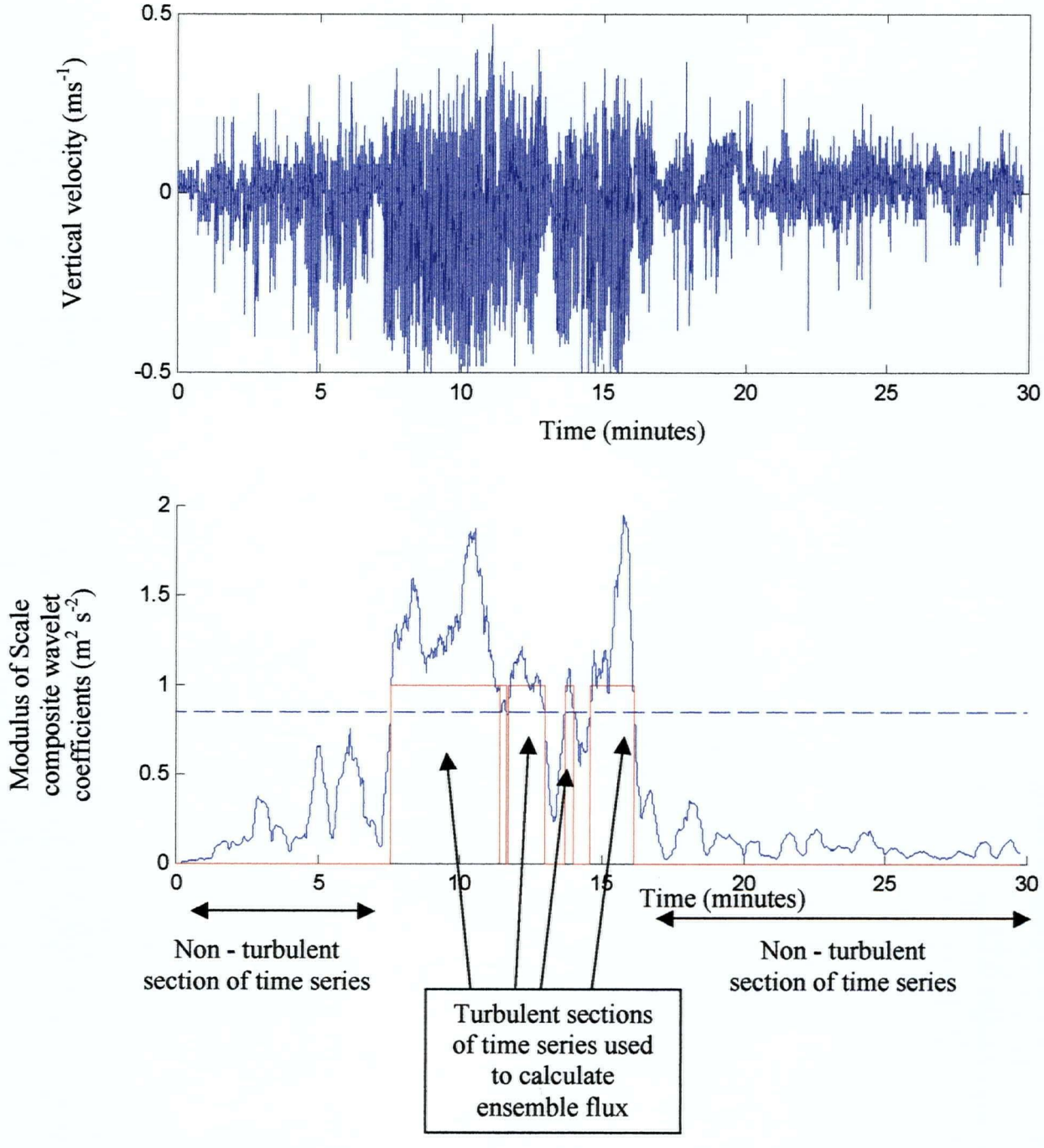

Figure 7.6 Diagram to illustrate the parts of the time series used to calculate the ensemble fluxes associated with the turbulent and non-turbulent component of the time series. (Blue dashed line is the 95% significance level for red noise, red line = 1.0 indicates the part of the time series identified as turbulent.)

Trend and turbulent flux components of the time series are compared to the original flux calculations in Figure 7.7. Results show that the trend component has very similar characteristics to the flux of the complete time series. The turbulent component however may be substantially different, with values even indicating net fluxes in a counter direction to that of the 30 minute time series. This suggests that the sensible heat fluxes calculated for the 30 minute time series are strongly influenced by the non-turbulent component of the time series.

This has significant implications for the analysis of vertical mixing processes. For example, if a large negative or positive flux is recorded in the 30 minute flux but a near zero value is observed in the flux calculated using conditional sampling of the turbulent components, then it is likely that non-turbulent processes are dominant in the boundary layer. Alternatively if the 30 minute flux is near zero but the composite flux is large, then it is likely that a short burst of intense turbulent mixing occurred. Given that the flux values for both 30 minute and composite fluxes are of the same order of magnitude, the composite fluxes may make a considerable contribution to vertical transport processes despite the short duration of the turbulence within the time series.

During periods when the duration of the turbulence is very small the resulting values are probably not representative of a 30 minute 'flux'. Studies have shown that flux averaging periods of less than 1 minute typically under-estimate the magnitude of the flux (Mahrt et al. 1996). This is confirmed in Figure 4.5 (Chapter 4) that illustrates the Ogive function for the nocturnal time series analysed here. This shows that if a flux averaging length of three minutes is used, a flux capture of less than 85% can be expected. However, the Ogive function was calculated using the 30 minute data set and thus included information about longer scale processes which would not be captured in a three minute segment. It is therefore very difficult to establish whether the flux component has been truly isolated. This problem becomes less serious as the duration of the turbulence increases.

It is also likely that only a very small number of eddies have been sampled. Thus the revised flux calculated is not representative of the whole 30 minute period but only those time periods when the signal was turbulent. However, while data from several time series could have been analysed together to produce composite flux based on longer time periods, this results in the loss of temporal information about the positioning of the turbulence. This is a considerable

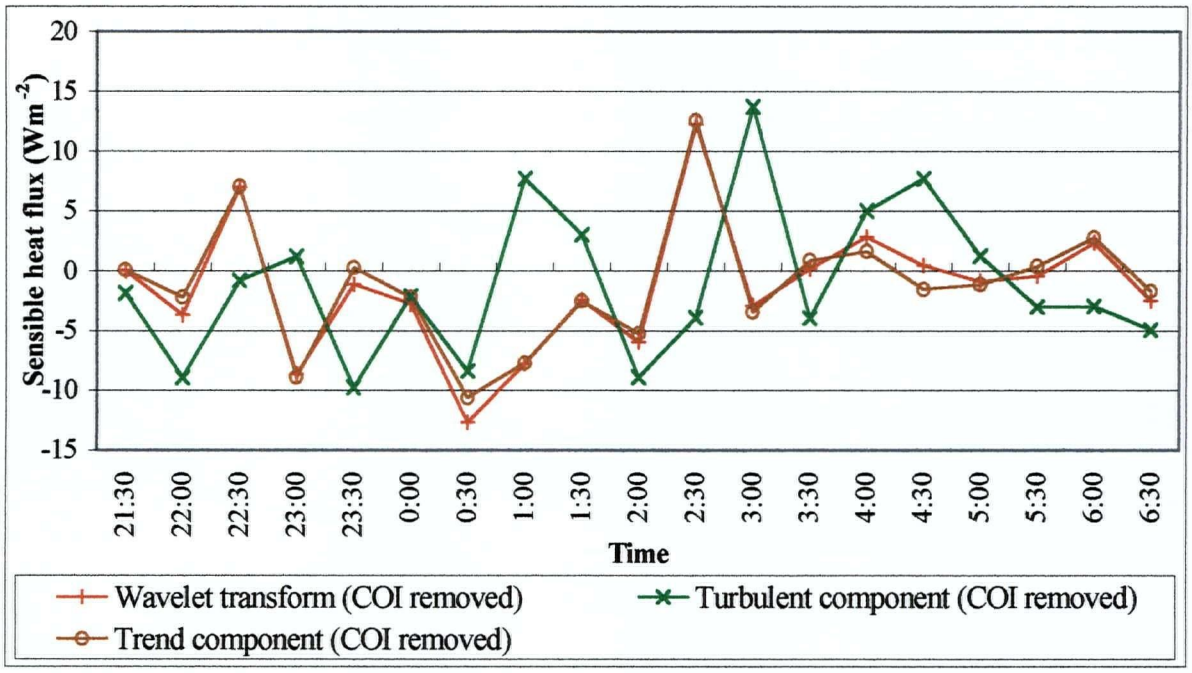

Figure 7.7 Comparison of the turbulent (ensemble average of turbulent 'events') and trend components (remainder) of the time series with the original flux calculated using the db4 wavelet with the COI removed for 2130 - 0630 PDT 31st August - 1st September

limitation (given the variability of ozone concentrations aloft demonstrated in Chapter 5) when determining the vertical mixing of ozone.

Given that mean vertical velocities associated with turbulent periods are considerably less than 10 cm s^{-1}, this suggests that the sampling errors are minimal. Thus even if the magnitude of the flux is under-estimated the direction should be correct. Given the difficulties associated with the intermittence of the turbulence, this method provides an objective technique to quantitatively analyse the vertical mixing associated with turbulence in the NBL.

7.5 Verification of flux estimates

In the absence of a reference value with which to verify the reliability of fluxes calculated using this technique, the data are analysed within the context of other surface variables in order to determine the consistency of the results. Figure 7.8 compares the temporal variations in the sensible heat flux calculated using FFT and wavelet based methods for the 30 minute time series and the composite flux calculated between 2130 PDT and 0630 PDT on August 31st - September 1st 1998. Changes in surface air temperature and ozone concentrations are also indicated. Figure 7.9 illustrates the corresponding changes in surface variables of a) temperature (at 30 m) and temperature gradient (between 30 - 60 m), b) ozone concentrations (4 m) and temperature gradient (between 30 - 60 m), c) wind direction and standard deviation of vertical velocity (recorded at 60 m) and d) nitrogen monoxide, nitrogen dioxide and ozone gradient between 4 - 2 m observed between 2100 PDT August 31st - 0630 PDT September 1st 1998. Wind direction, NO and NO_2, and difference in ozone concentrations were observed every 10 minutes, the remaining variables in Figure 7.9 were recorded at a 5 minute resolution.

The data in Figure 7.9 clearly indicate the presence of small structures in the surface variables that last 5 - 15 minutes in duration. For example, between 0000 PDT - 0015 PDT a small jump in ozone concentration (representative of a local increase of 8 ppb) and temperature (increase of 0.7 ^{o}C at 30 m) can be observed. Coincident decreases in both the temperature gradient between 30 - 60 m and ozone gradient between 2 - 4 m were also observed. Figure 7.10 indicates that these changes correspond well with the sections of the time series identified as turbulent by the wavelet technique developed in Chapter 6. This supports the observations made in Chapter 6 that turbulence observed in this field experiment occurs in bursts which have a total duration of less than 10 minutes. Thus the technique is likely to provide a reliable basis from

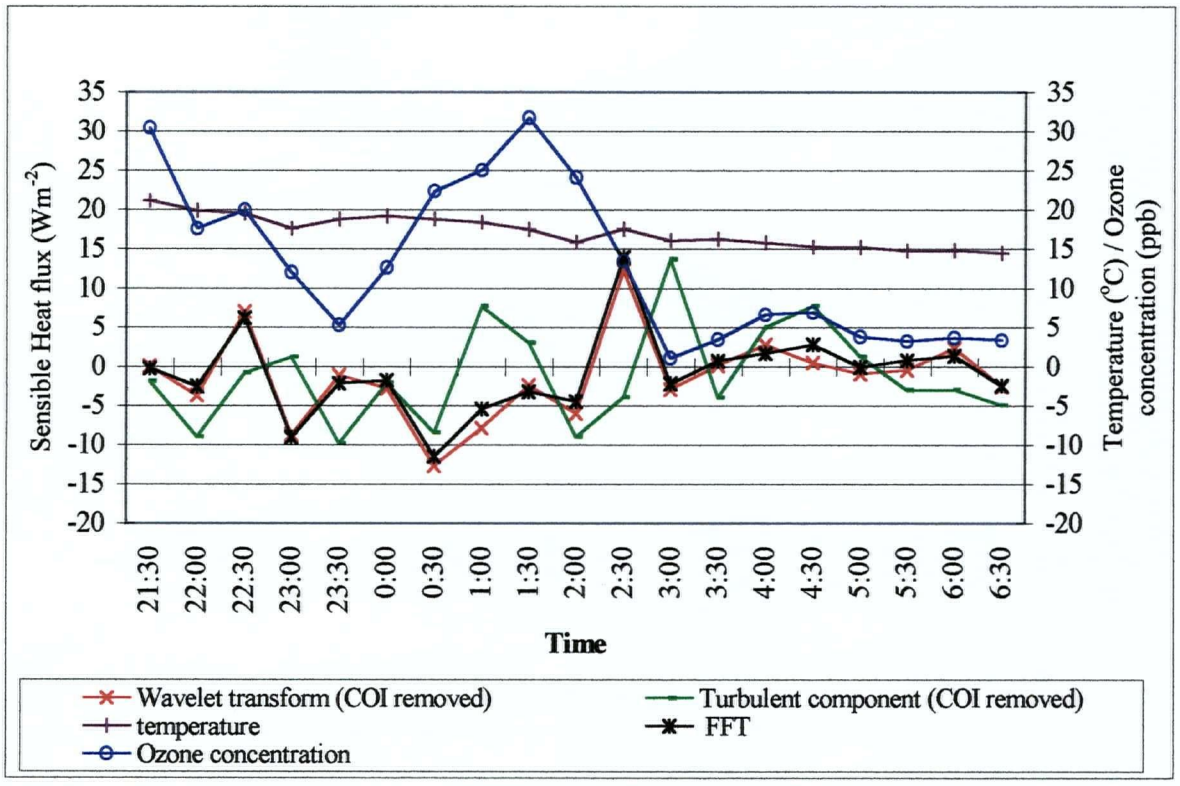

Figure 7.8 Temporal variations in the sensible heat flux as calculated using the wavelet transform and FFT methods for the 30 minute data set and using the wavelet transform to isolate the 'flux' associated with the turbulent component (ensemble average of turbulent periods) in the time series between 2130 - 0630 PDT August 31st - September 1st 1998

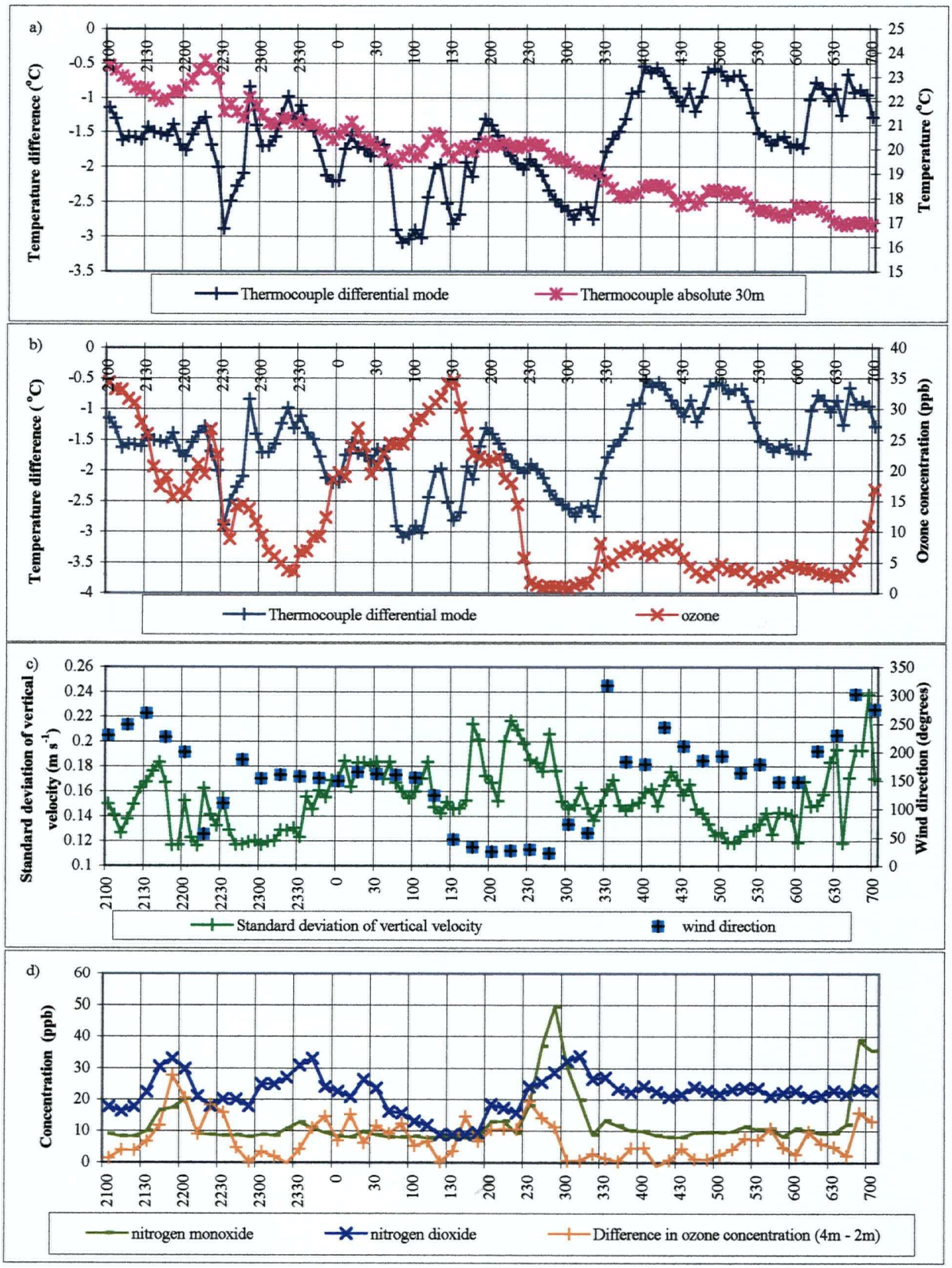

Figure 7.9 Temporal variations in a) temperature (at 30m), difference in temperature (between 30-60m), b) ozone concentrations (4m), difference in temperature (between 30-60m) c) wind direction, standard deviation in vertical velocity, d) nitrogen monoxide, nitrogen dioxide and the difference in ozone concentration between 4-2m observed between 2100 PDT August 31st - 0700 PDT September 1st 1998.

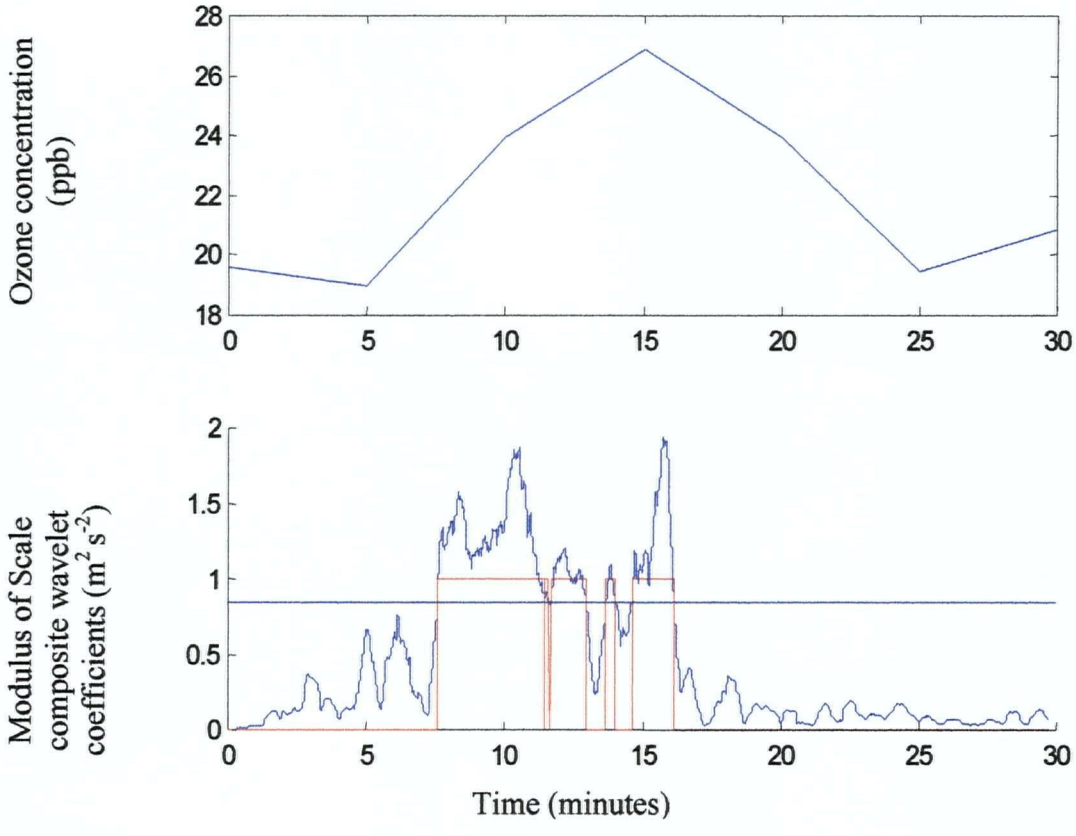

Figure 7.10 Comparison of surface ozone concentrations as recorded at 4m by the ML 9811 ozone analyser with periods of turbulent activity recorded by the sonic anemometer and identified using wavelet analysis between 0000 PDT - 0030 PDT September 1st 1998

which to isolate the component of the 30 minute fluxes which are truly associated with turbulent activity.

7.5.1 Identifying advection in the time series

Between 2130 PDT and 0630 PDT 31st August - 1st September positive heat fluxes calculated using the 30 minute time series were observed at 2230 PDT and 0230 PDT (Figure 7.8). A positive heat flux is only likely to occur in rural areas during the night when non-local transport of cooler air occurs over a warmer surface. Given that between 2200 - 2230 PDT a net increase in temperature of 0.3 °C was observed at 30 metres and between 0200 - 0230 PDT a net increase in temperature of 0.1 °C was observed this seems a little unlikely. Thus it is possible that the 30 minute fluxes calculated during this period are strongly affected by non-turbulent motions and not representative of turbulent scale activity.

This assumption is further supported by a more detailed analysis of the data in Figure 7.9 during this period. Data indicate that between 2200 PDT - 2215 PDT and 2215 PDT - 2230 PDT two different processes are dominant. Between 2200 PDT - 2215 PDT there is strong evidence to suggest turbulent activity in the near surface layers. A decrease in the temperature gradient between 30 - 60 metres of 0.5 °C indicates that vertical mixing may have occurred (Figure 7.9a). A net increase in temperature of 1.1 °C is also observed, combined with a net increase in ozone concentration of more than 10 ppb (Figure 7.9b). Further a corresponding drop in NO and NO_2 concentrations is observed (Figure 7.9d) indicating that these surface based pollutants have been mixed through a deeper layer. A dramatic decrease in the difference in ozone concentrations between 2 - 4m of 19 ppb was also observed. However, this may be partially accounted for by the sequential measurement of ozone at each height during a period of marked increase in ozone concentrations (and hence highly non-stationary conditions). These variables together indicate that turbulent conditions prevailed through this time. However, there is no direct evidence to support the presence of a positive heat flux.

The remaining 15 minutes of the time series however show marked evidence of advection. For example, a cooling of 2.2 °C is observed in the 30 m temperature time series and a 1.6 °C increase in the temperature gradient observed. Further at 2220 PDT the wind direction changed from 240^0 - 50^0 strongly suggesting that an air mass with a different trajectory (and hence different characteristics) may account for changes in surface variables. A decrease in the standard deviation of vertical velocity is also apparent during this time period. Thus, in this

example, non-stationarity induced by a period of marked advection with the airmass may have been sufficient to contaminate the 30 minute turbulent flux calculation.

By comparison the ensemble flux for the turbulent component of the time series for the 2200 - 2230 PDT time period indicates the presence of a weak negative flux (Figure 7.8). Detailed analysis of the time periods used in the composite calculation indicates several short burst of turbulent activity were identified between 2200 - 2220 PDT. The last 10 minutes of this time period (2210 PDT - 2220 PDT) coincided with the most turbulent activity and the greatest increase in ozone concentration at the surface. This suggests that the techniques developed in Chapter 6 and 7 to identify the turbulence and calculate composite fluxes identify the timing and direction of the fluxes more accurately. However, in this instance, given the magnitude of the changes in temperature observed at 30 m it is likely that either the magnitude of the flux is under-estimated or surface advection processes also account for changes in surface parameters.

Between 0200 PDT - 0230 PDT there is less evidence of advection in the time series illustrated in Figure 7.9. However, the absence of any apparent cooling immediately prior to, or during the time period suggests that a positive flux is unlikely. Again during this time period the composite flux is negative (Figure 7.8). The presence of turbulent activity during this period is supported by the absence of cooling at 30 m and a large standard deviation in vertical velocity. Although ozone concentrations do not increase during this period, NO_2 concentrations increase by 9 ppb. This suggests that NO may have been transported to the site at this time, accounting for the decrease in ozone concentrations as any ozone mixed to the surface would rapidly react with NO to form NO_2. A coincident increase in NO is not necessarily expected if the rate of chemical titration exceeds the rate of transport.

These two examples suggest that while non-stationarities in the time series combined with the intermittent characteristics of the turbulence limit the validity of turbulent fluxes calculated using the 30 minute times, the composite flux appears to provide a more reliable flux estimate.

7.5.2 Existence of positive fluxes in the nocturnal boundary layer

Positive composite fluxes were reported several times during the observation period. Given the difficulties associated with verifying the presence of a positive 30 minute flux, these cases were examined in detail. The first incidence occurred at 2300 PDT (Figure 7.8). During this time period the data in Figure 7.9 indicate that from 2240 PDT the standard deviations in

vertical velocity are very small, suggesting the absence of vertical mixing processes. Thus turbulent activity was limited throughout the time series. This was confirmed using the wavelet-based technique which identified a 2.5 minute turbulent burst between 2230 - 2233 PDT August 31st 1998 (Figure 7.11). A second 4 minute burst was also identified at the end of the time series (Figure 7.11), during both these periods the heat flux was positive. Immediately prior to 2230 PDT a period of marked advection had been identified at the surface, and this was coincident with an abrupt period of atmospheric cooling at 30 m. Thus it is possible that cool air advection resulted in a weak positive flux between 2230 - 2240 PDT. At 2240 PDT there is a marked change in wind direction suggesting advection may account for the changes in surface variables during the remainder of the time series. This is further supported by the small standard deviations of vertical velocity. Thus non-stationarities in the data may account for the negative value of the heat flux for the 30 minute time series.

A second occurrence of a positive composite flux occurred at 0100 PDT 1st September 1998. Turbulent time series for ozone, vertical velocity and temperature observed between 0030 - 0100 PDT are illustrated in Figure 7.12. Although the ozone data are incomplete, these data suggest that a strong burst of turbulence occurred during the first ten minutes of the time period. This is further supported by the standard deviation of vertical velocity shown in Figure 7.9. This time period was preceded by and coincided with a period of marked cooling at the surface (0015 PDT and 0045 PDT). Evidence in the turbulent temperature time series indicates the presence of convective mixing of warm and cold eddies during the first 7 minutes of the time series. Thus it is possible that cold air advection either at the surface or aloft (and subsequently mixed to the surface) accounts for the positive heat flux.

Evidence to support this theory can also be found in the turbulent time series for temperature observed between 0000 PDT and 0030 PDT shown in Figure 7.13. This shows three distinct cool spikes in the time series. These could be caused by the advection (and subsequent vertical mixing) of pockets of cool air aloft. However, this could not be detected in the tethersonde data (perhaps a consequence of the temporal resolution of flights). Given that these cool spikes coincide with periods of reduced fluctuations in vertical velocity, it is possible that either the turbulence is patchy (thus isolated pockets of cool air remain localised at the surface) or surface advection of cold air is occurring. Similar examples of this can be identified in the time series for 0130 PDT and 0300 PDT. Thus, whatever the cause, the identification of patches

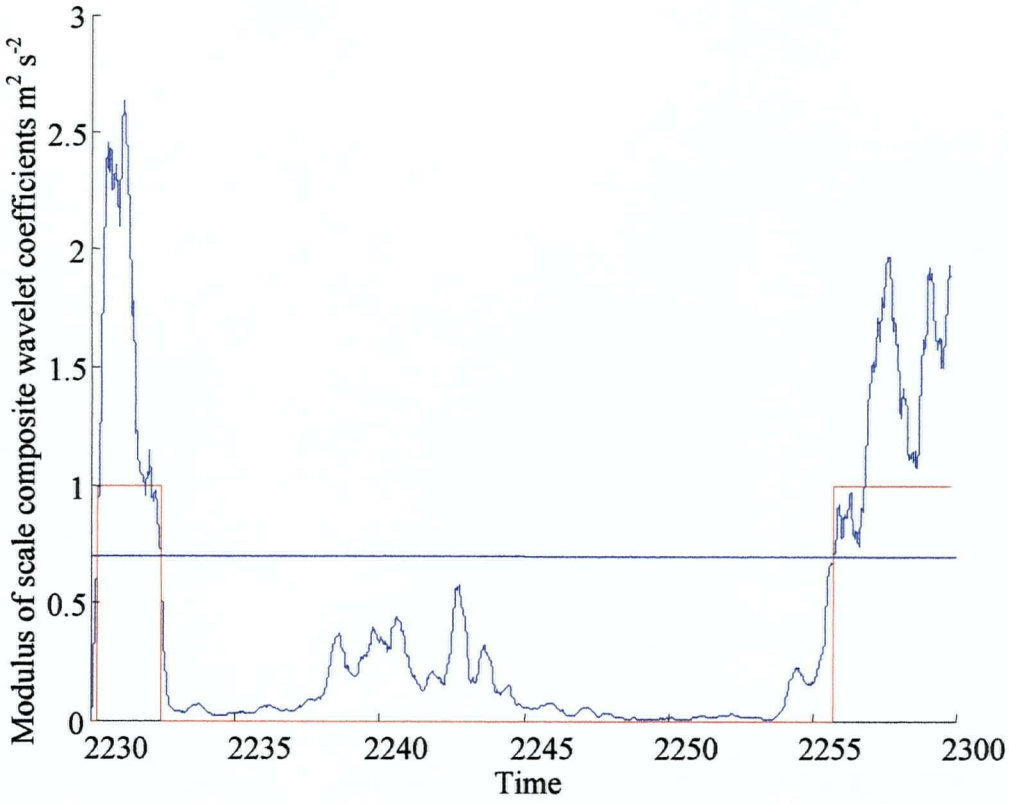

Figure 7.11 Identification of periods of turbulent activity identified from the vertical velocity data recorded by the sonic anemometer using wavelet analysis between 2230 PDT - 2300 PDT August 31st 1998

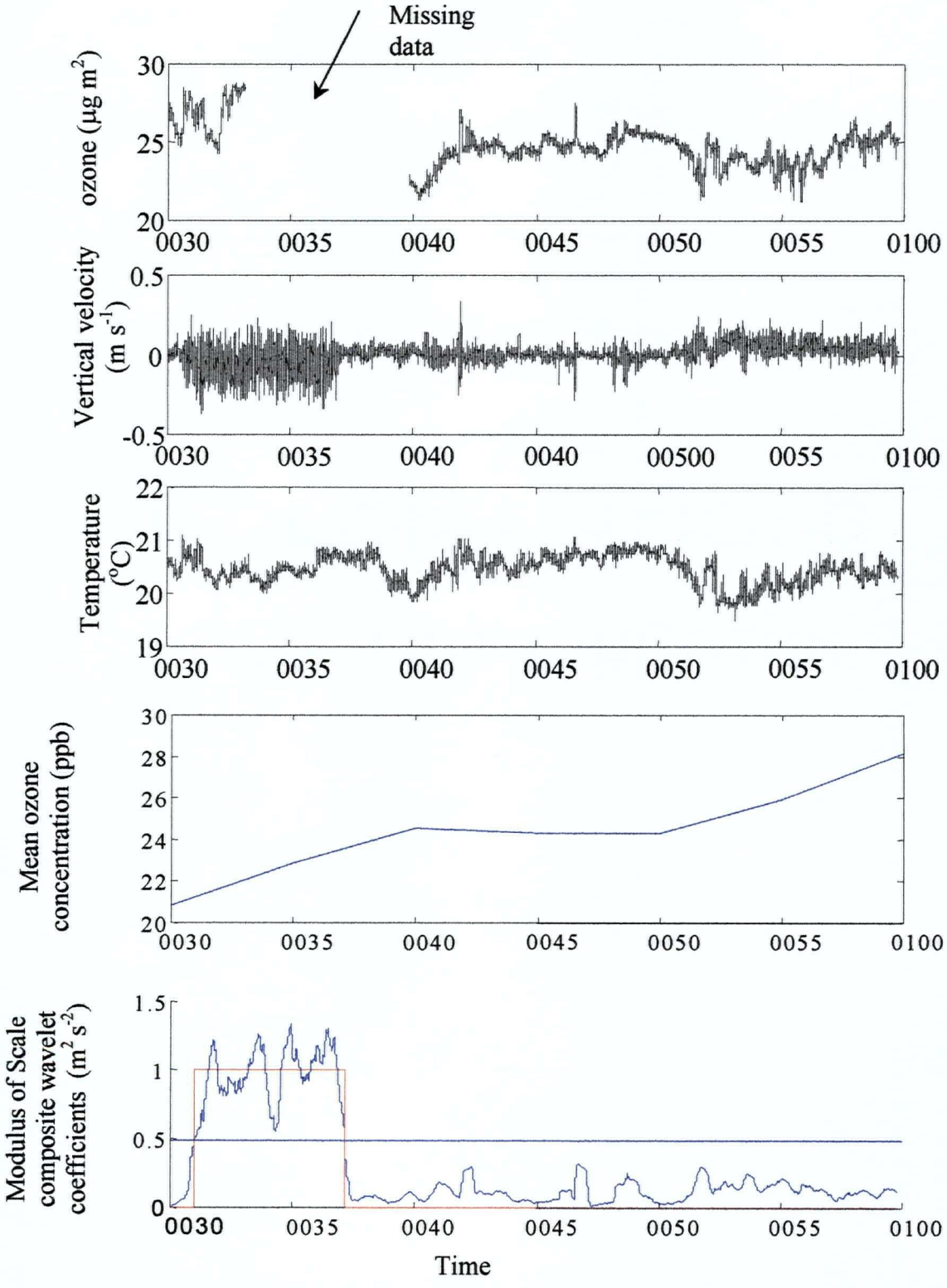

Figure 7.12 Turbulent time series of ozone, vertical velocity and temperature, and corresponding surface ozone concentrations as recorded at 4m by the ML 9811 ozone analyser and periods of turbulent activity recorded by the sonic anemometer and identified using wavelet analysis between 0030 - 0100 PDT September 1st 1998

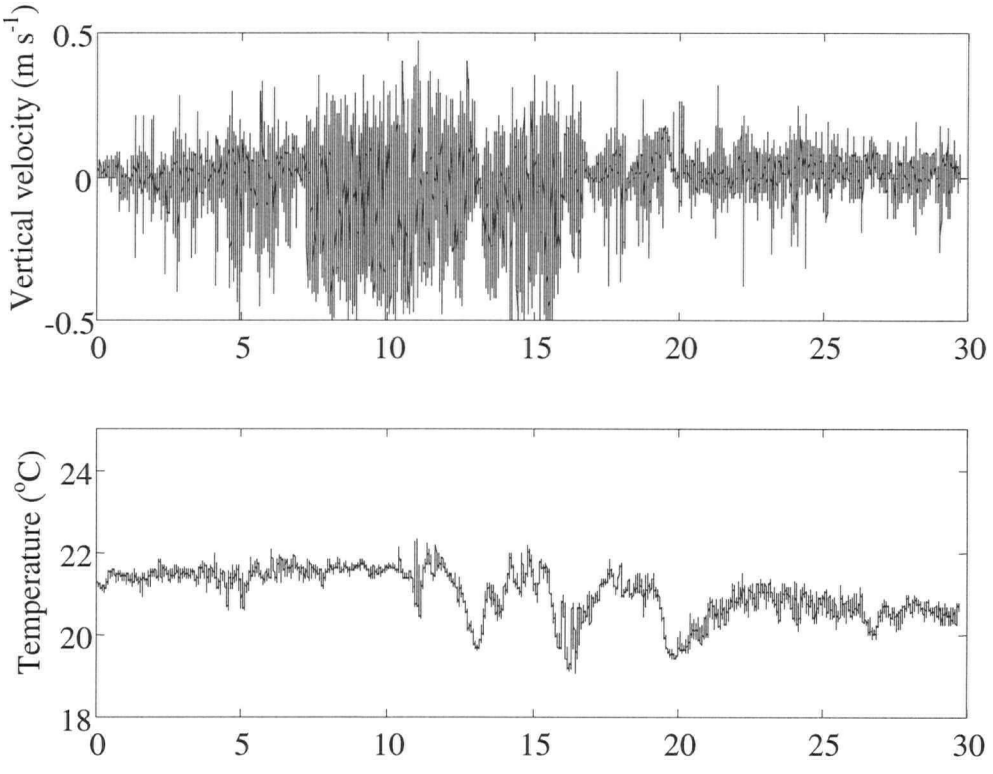

Figure 7.13 Turbulent time series of vertical velocity and temperature for 0000 -0030 PDT September 1st 1998

of cool air, combined with a net surface cooling, suggests that the composite flux may be correctly identifying positive heat fluxes in the surface layer.

7.5.3 Ozone fluxes in the nocturnal boundary layer

The results in section 7.5.1 and 7.5.2 suggest that the composite flux estimates do provide a reliable indication of the vertical mixing resulting from turbulence in the atmosphere. Thus the technique was also applied to the ozone flux data. Due to difficulties with the sensor, only 38 hours of ozone flux data were available from throughout the IOPs. These rarely coincided with periods of increased ozone concentrations at the surface. However, no attempt was made to supplement these data with flux estimates calculated using the gradient method based on temperature and ozone data from the 8m tower. This is due to errors associated with the use of a 10 minute ozone sampling regime at alternate rather than coincident heights. Whilst this measurement regime would have provided adequate data during stationary conditions, the presence of marked jumps in ozone concentration at time scales of 5 minutes or less limited the validity of the gradient method when applied to this data set.

During the night of August 31st - September 1st ozone fluxes are only available between 2130 - 2200 PDT and 0130 - 0400 PDT as shown in Figure 7.14. Observations between 0130 - 0230 PDT coincide with the end of the ozone spike observed at the surface. During this time period, the composite fluxes are negative, indicating a net transport of ozone to the surface. Despite this, a net decrease in ozone concentrations is observed at the surface. This can be accounted for by deposition processes and a coincident increase in NO and NO_2 concentrations observed at the surface (Figure 7.9d). Thus it is likely that although there is a net flux to the surface, it is insufficient to exceed the removal rates and a net decrease in concentration is observed. This suggests that in the absence of increased NO concentrations, ozone concentrations may have continued to increase until 0230 PDT.

Between 0300 PDT - 0400 PDT a net positive flux is observed at the surface. This could only occur if a decrease in ozone concentrations was observed aloft. Neu et al. (1994) suggest that the rate of chemical titration with NO is very similar to the rate of increase in ozone concentration expected due to turbulent mixing in the convective boundary layer. Thus given that a peak in NO concentrations of 50 ppb was observed at 0300 PDT, chemical titration processes may have a strong influence over the fluxes calculated. Although a tethersonde observation is not

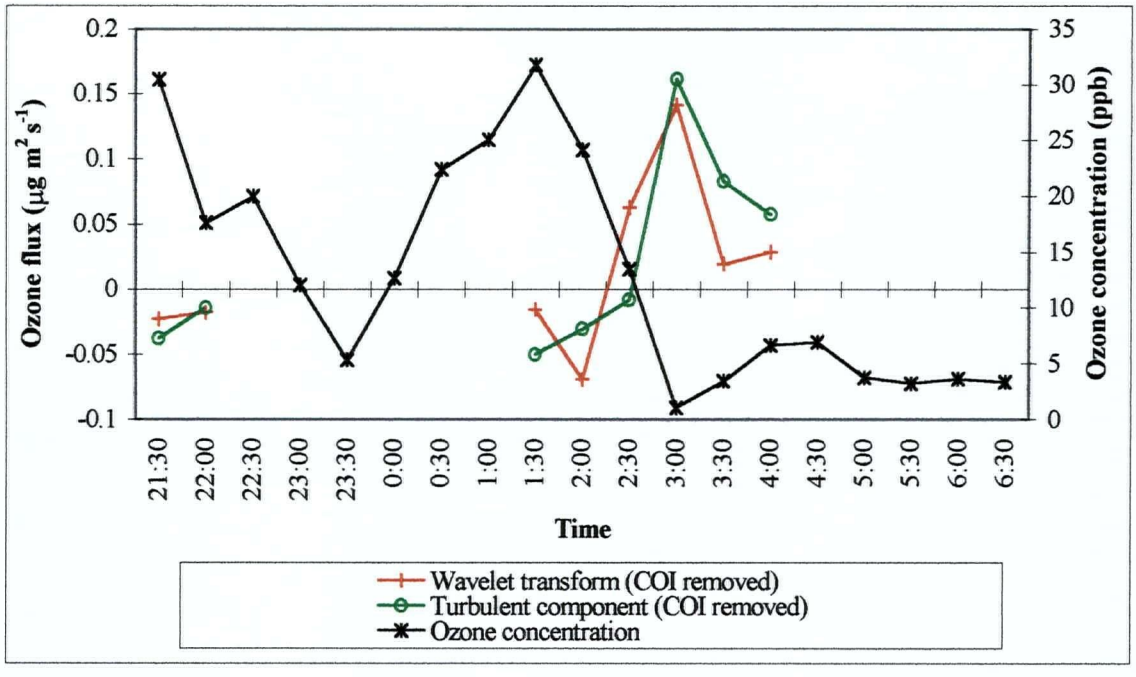

Figure 7.14 Temporal variations in the ozone flux (where data available) as calculated using the wavelet transform and FFT methodologies for the 30 minute data set and using the wavelet transform to isolate the 'flux' associated with the turbulent component between 2130 PDT and 0630 PDT August 31st -September 1st 1998. Surface ozone data are also shown

available for this period, it is possible that either a plume of NO rich or low ozone concentrations existed aloft.

Despite the sparsity of the ozone data, the techniques developed in Chapter 6 and 7 can be used to provide further insights into the data set. For example, detailed analysis of the 30 minute time series for 0030 PDT and 0100 PDT reveals that there is a good correlation between significant increases in surface ozone concentration and the turbulent component of the time series (illustrated in Figure 7.10 and Figure 7.12). This supports the notion that turbulent vertical mixing processes are active and are likely to account for at least some of the observed increases in ozone concentration at the surface.

However, increased ozone concentrations were also observed during periods when there was very little evidence of turbulent activity in the time series. This is evident between 0050 PDT - 0100 PDT in Figure 7.12. In this instance data from Figure 7.9 indicate that it is unlikely that the technique has 'missed' a burst of turbulence. A decrease in the standard deviation of the vertical velocity and an increase in the temperature gradient between 30 - 60 m indicate that the stability is increasing at the surface between 0050 - 0100 PDT. Thus it is likely that some of the increase in ozone concentrations observed during this time period is due to advection.

Surface advection of ozone in the stable NBL is very difficult to quantify due to meandering wind profiles and the sparsity of the monitoring network. Variations in local surface chemistry (resulting from NO emissions) can have a significant impact on measurements at monitoring sites making it difficult to identify trends in advection between monitors. Further, vertical mixing processes may occur sporadically between locations resulting in local advection that is not detected by monitoring sites. Thus, despite the domination of removal processes in the NBL and the absence of a marked change in wind speed or direction, it is very difficult to rule out advection processes as a transport mechanism.

The data in Figure 7.9 further support the observation that advection and vertical mixing processes are important in determining the concentrations of ozone observed at the surface. Using the wind direction data three distinct regimes can be identified during the night of August 31st - September 1st: 1) 2300 - 0130 PDT the prevailing wind is south-easterly, 2) 0130 PDT - 0330 PDT when the prevailing winds are north-easterly and 3) 0330 - 0500 PDT when the winds are south-westerly. Significant increases in ozone concentrations at the surface are observed only during the first regime. However, although the wind direction changes at 2300 PDT increased

ozone concentrations do not occur until 2330 PDT when the standard deviation of vertical velocity increases, indicating that turbulence becomes more active. This suggests that the characteristics of the airmass combined with the onset of vertical mixing play an important role in determining surface concentrations.

During the second regime, ozone concentrations decrease at the surface and NO concentrations increase. Although this period is characterised by larger fluctuations in the standard deviation of vertical velocity, the different chemistry of the air mass accounts for the reduction in ozone concentrations. During the third regime the turbulence is weaker and there is little evidence of any significant vertical mixing of ozone to the surface. Although the turbulent characteristics may account in part for the reduction in ozone concentrations, it is also likely that the absence of ozone in the layers immediately above the surface (as suggested by the positive ozone flux) limit vertical mixing processes further.

7.5.4 Summary of flux analysis

The analysis in section 7.5 demonstrates a marked temporal variability in the dominant processes operating in the NBL. Thus unlike the convective boundary layer, the non-stationarity in the characteristics (and occurrence) of the weak turbulence combined with the interaction between surface parameters makes it very difficult to draw generalisations from the data set. However, analysis of the conditions and fluxes observed during other nights in the IOPs indicated that the trends outlined above are consistent features of the nocturnal boundary layer. Thus this time period may be considered representative of other nights in the IOPs.

Detailed analysis of the turbulent fluxes calculated using the 30 minute time series reveals that values may be strongly influenced by the intermittent nature of turbulence and non-stationarity of the nocturnal boundary layer. However, composite flux calculations appear to provide a more reliable insight into the presence or absence of vertical mixing processes in the very stable NBL.

Using this technique it is possible to determine that vertical mixing processes were active during periods of increased ozone concentration at the surface. Thus increases in ozone concentration observed during the ozone spike between 2330 PDT and 0130 PDT on August 31st - September 1st are at least partially attributable to vertical mixing processes. The technique also highlights the importance of surface advection despite the dominance of removal processes in the very stable NBL. The data also indicate that NO concentrations exert a strong influence on

surface ozone concentrations in the NBL. In the absence of increased NO concentrations, surface ozone concentrations may have been increased further and sustained for longer periods due to vertical mixing processes in the near surface layers.

7.6 Implications for vertical mixing

Vertical mixing processes clearly play an important role in determining near surface ozone concentrations. However, the results in section 7.5 indicate that despite the dominance of removal processes in the surface layer, advection processes may also be an important source of ozone transport in the surface layer. Further, there is evidence to suggest that advection occurs both independently of and coincident to vertical mixing in the NBL. In order to establish the relative importance of each of these pathways it is therefore necessary to quantify the increase in surface ozone concentrations associated with each process.

An estimate of the contribution of vertical mixing processes can be obtained for each 30 minute period by multiplying the composite ozone flux with the duration of the turbulence. This technique enabled a quantitative estimate of the increase in surface concentration associated with the turbulent mixing alone. Given the magnitude and time scales of the ozone fluxes (5 - 10 minutes in duration) it is likely that deposition processes account for only a minor portion of the flux estimate, particularly once dew has formed at the earth surface given the insolubility of ozone in water. Thus whilst this technique is likely to over-estimate the contribution of vertical mixing processes due to surface chemistry, the error due to surface deposition processes should be minimal.

Figure 7.15 compares the net change in ozone concentration (ozone concentration at time t = t - 1 minus ozone concentration at time t = t) observed at the surface with the net change in ozone concentration expected due to turbulent mixing processes during times when flux data was available on August 30th - 31st and August 31st - September 1st. It is clear that during both nights the increased in ozone concentration due to turbulent mixing as predicted using this technique are higher than the actual observed increases. However, the data demonstrate the importance of NO in determining the degree of over-prediction resulting from the calculations. NO concentrations peaked at 38 ppb at 0300 PDT on September 1st, whilst concentrations of 8 ppb were typical on the 31st August.

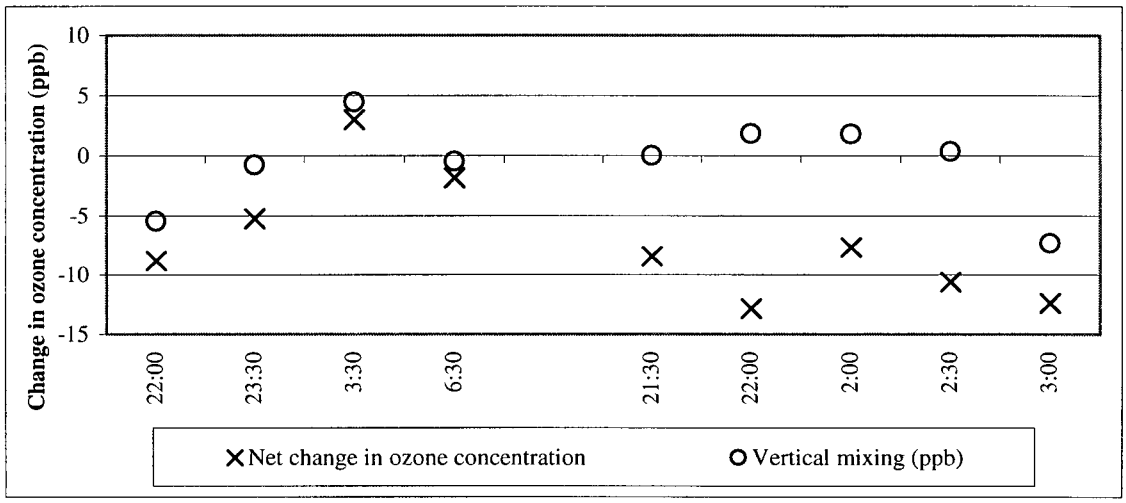

Figure 7.15 Comparison of net increase in ozone concentrations observed with increases expected due to turbulent vertical mixing processes for periods when ozone flux data were available on August 30th - August 31st and August 31st -September 1st 1998

Analysing the 38 hours of ozone flux data in this way it is possible to determine whether the net increases in concentration at the surface from turbulent processes consistently over-estimates the net increase. The results indicate that for 21% of the 30 minute time periods examined the net change in ozone concentration due to vertical mixing processes was under-estimated using this technique. In these cases it is likely that advection processes played a significant role in determining near surface ozone concentrations. Conversely for 35% of the 30 minute time periods the technique over-estimated the net change in ozone concentration at the surface. In these cases vertical mixing processes combined with surface chemistry and deposition processes (and possibly horizontal advection) played a significant role in determining near surface ozone concentrations. Overall, the net change in surface ozone concentration predicted due to the ozone flux was within +/- 2 ppb of the observed values for 44% of the total 76 (30 minute) time series.

Obviously, given the plethora of horizontal and vertical transport processes operating at a variety of different scales in the NBL, even in this scenario it is unlikely that the vertical mixing processes alone account for the observed net changes in ozone concentration. However the results do demonstrate that the order of magnitude of vertical mixing due to turbulent processes is significant enough to result in a net change in surface ozone concentrations.

7.7 Summary

The calculation of fluxes in the very stable NBL is fraught with difficulties. The weak, intermittent and non-stationary characteristics of the time series limits the validity of the fluxes calculated. Despite the theoretical advantages of the wavelet transform, little difference was detected between the 30 minute flux values calculated using the transform and those from a traditional FFT. The advantages of wavelet analysis become apparent when the data sets are manipulated.

Exploiting the local characteristics of the transform, a new conditional sampling technique was developed to isolate the turbulent component of the time series and provide a revised estimate for the turbulent 'flux'. The validity of the results from this technique were examined in the light of surface-based data for consistency. The results suggest that the 30 minute flux values may be strongly influenced by the non-turbulent component of the time series and provide a poor estimation of vertical transport generated by turbulence. The flux isolation technique provided a reliable indication of the presence and direction of fluxes in the NBL.

The results show that turbulent transport of ozone from aloft to the surface plays a significant role in determining local changes in surface ozone concentration. However, despite the dominance of removal processes in the surface layer of the NBL, increases in ozone concentration were also observed due to advection processes. The results again highlighted the importance of surface chemistry and in particular NO concentrations, in determining the timing, duration and magnitude of ozone concentrations observed at the surface.

Chapter 8: Conclusions

8.1 Summary

The mean and turbulent characteristics of the boundary layer play an important role in determining near surface ozone concentrations in the very stable nocturnal boundary layer. This study has demonstrated that localised nocturnal increases in surface ozone concentration are a common feature of diurnal cycles throughout the Lower Fraser Valley. Despite the overall dominance of chemical titration and depositional processes in the NBL, significant increases in ozone concentration were observed in the Lower Fraser Valley during every night of the intensive observation periods (IOPs). These periods were characterised by rapid increases in concentration of up to 31.1 ppb. The increases were typically sustained for at least two hours and followed by a rapid decrease in concentrations. These events were termed ozone 'spikes'.

The occurrence of ozone 'spikes' was demonstrated to be highly variable in time and space. However, analysis of data from the GVRD monitoring network showed a consistent sensitivity of increased ozone concentrations to NO concentrations. Fewer spikes were reported at the western end of the valley where higher NO concentrations were consistently observed. Further, localised spikes in NO concentration were frequently observed coincident with (and may have been significant in determining) the end of the ozone spike.

Observations of the characteristics of the NBL during the IOPs revealed the consistent development of a shallow very stable boundary layer. Due to the prevalence of chemical titration and depositional processes, a gradient in ozone concentrations was observed in the surface layers. The stable boundary layer was frequently capped by a nocturnal LLJ. Observations of the LLJ demonstrated that it continually evolved through the night, breaking-down and often re-establishing at different heights, speeds and directions. Four types of jet were identified on the basis of the height, and number, of wind speed maxima present in the profile.

Above the stable layer, winds in the residual layer were light and variable. Down-valley wind systems developed during the majority of nights observed. However, a westerly band was frequently observed at 300 m following wind reversals in the remainder of the profile. Ozone concentrations were also highly variable in the residual layer. The timing and trajectory of mesoscale flows were shown to have an important impact on ozone concentrations. High concentrations of ozone were observed embedded within the westerly band observed in the late

evening, whilst westerly bands located at the same height in the early morning hours were characterised by very low ozone concentrations. Low ozone concentrations were also observed in down-valley flows, supporting Banta et al. (1997) hypothesis of the operation of nocturnal cleansing mechanisms on valley side walls. However, pulses of ozone rich air embedded in down-valley winds were also captured by the tethersonde system. Despite the variability, ozone concentrations in the residual layer were consistently higher than in the surface layers, reflecting the absence of removal mechanisms.

Vertical profiles through the NBL during individual ozone spikes supported the hypothesis that these events were the result of vertical mixing processes. The ozone profiles in the stable layer were more similar to profiles observed in the daytime mixed layer than the vertical profiles recorded both prior to and following ozone spikes. Despite the prevailing stability of the NBL, Richardson numbers calculated from tethersonde data revealed isolated patches of instability, which occasionally extended through to the surface layers.

Analysis of the turbulence data demonstrated the presence of intermittent turbulence in the surface layers. A new wavelet-based technique was developed to facilitate the quantitative description of intermittent turbulence. Turbulence was found to be weak (standard deviation of the vertical velocity was 0.05m s^{-1}). Up to nine turbulent bursts were observed in the 30 minute data sets, each typically one minute in duration. The characteristics of turbulence varied with different potential causes of turbulence identified aloft. Given that a clear relationship could not be established between the strength and duration of turbulence, both attributes were used to describe the characteristics of the turbulence. Increased turbulence was found in association with 'type 3' LLJ (presence of a single low altitude wind speed maxima), the break-down of any LLJ, and the development of down-valley winds.

Turbulent activity was superimposed upon a background of larger scale, more wavelike motions. Gravity waves were a common feature of the turbulent time series collected in the very stable NBL. Wavelet analysis was shown to be an effective tool to identify their presence and temporal location within the 30 minute data sets. Circumstantial evidence suggests that breaking gravity waves may be an additional source of turbulence in the NBL. The results also suggest that gravity waves are not present in the stable layer when a strong low altitude LLJ is present in the NBL.

Despite the prevalence of intermittent turbulence throughout the IOPs it was very difficult to determine the relationship between the characteristics of the turbulence and increased ozone concentrations at the surface. This is a probably a result of the complexity introduced by the variability in ozone concentrations aloft and localised increases in NO concentration at the surface. Nevertheless, 16 out of the 19 ozone spikes observed at CFS Aldergrove occurred during periods when a type 3 LLJ was present aloft, during the break-down of any LLJ or when the down-valley wind system was developing. These were the three mechanisms associated with increased turbulence in the surface layers. In the absence of other factors, increased strength of the turbulence appeared to be an important determinant of increased concentrations throughout the profile.

There was no evidence to suggest that increased height of the LLJ resulted in increased mixing to the surface. This is probably due to the absence of a clear gradient in ozone concentrations with height in the residual layer. Therefore, while it is clear that turbulence may occur at the surface without a coincident increase in ozone concentrations, it is probably no coincidence that ozone concentrations in excess of 80 ppb were recorded in the residual layer during the three nights when the largest increases in ozone concentrations were recorded at the surface.

Quantifying the amount of ozone mixed to the surface as a result of vertical mixing processes proved to be a considerable challenge. The measurement and calculation of turbulent fluxes (particularly of ozone) in the very stable NBL was fraught with difficulty. Wavelet analysis was shown to be a robust technique suitable for the calculation of turbulent fluxes in the NBL. Comparison of the fluxes calculated using eddy-correlation, FFT and wavelet methodologies revealed a marked sensitivity of the fluxes to non-stationarities in the data sets. Using a new technique to isolate turbulent events in the time series, the flux associated with the turbulent component of the time series was compared to the 30 minute flux. Using a variety of surface-based variables to validate the results, the ensemble averaging technique was shown to accurately detect periods of vertical mixing in the NBL.

Detailed analysis of the turbulent characteristics, flux data and surface parameters during the night of August 31st - September 1st 1998 revealed a good correlation between increased ozone concentrations and periods of increased turbulence in the surface layers. However, while vertical mixing processes accounted for part of the observed increase in ozone concentrations associated with the ozone spike observed, it is likely that horizontal advection or non-local

transport mechanisms also played an important role in determining the marked increase in surface concentrations.

Advection of ozone is however very difficult to quantify due to the sparsity of monitoring networks and the strong influence of surface chemistry. Thus, given the light and variable wind field in the NBL localised measurements may not be representative of advection processes throughout the valley. Further, vertical mixing processes may transport ozone to the surface between monitoring sites resulting in localised advection. This makes it difficult to estimate the overall contribution of vertical mixing processes to diurnal ozone budgets throughout the valley. Nevertheless, the results indicate that vertical mixing processes do contribute to nocturnal increases in ozone concentrations observed at the surface. The increase in ozone concentrations observed at any given site is dependent on the complex interactions between the characteristics of the turbulence aloft, the concentration of ozone in the residual layer and the concentration of NO in the surface layers.

8.2 Discussion

The results discussed in this thesis largely concur with the increasing number of studies that identify nocturnal, temporally localised, increases in surface ozone concentration in regions of complex terrain (Corsmeier et al. 1997; Loffler-Mang et al. 1997; Kalthoff et al. 2000). The balance of evidence supports their conclusions that these 'spikes' in ozone concentration are primarily the result of isolated periods of vertical mixing (caused predominantly by turbulence resulting from wind shear) in an otherwise very stable NBL. As in their studies, surface ozone concentrations during ozone spikes rarely exceed 50 ppb, well below the Maximum Acceptable National Ambient Air Quality Objective (NAAQO) hourly average of 82 ppb. Thus vertical mixing processes are unlikely to pose a significant health threat to local populations.

Unlike previous studies, this thesis highlights the importance of NO concentrations to a comprehensive understanding of the presence and characteristics of ozone spikes at the surface. The results suggest that, in the absence of NO concentrations, increases in ozone concentration due to vertical mixing processes may be significantly larger than typically observed. Given that ozone concentrations in the residual layer occasionally exceeded the NAAQO, it is possible that in remote areas where NO concentrations are reduced, vertical mixing processes may have a greater impact on local air quality.

This thesis also highlights the heterogeneity of different processes operating in the NBL, and emphasises the need to consider changes in mesoscale wind regimes and breaking gravity waves, as well as the LLJ as potential causes of vertical mixing. For example, Corsmeier et al. (1997) and Beyrich (1994) focus on the relationship between the LLJ and increased pollutant concentrations at the surface. Although this study supports the broad relationship they identify, the specific morphology of the jet is also shown be an important determinant of the characteristics of the resulting turbulence and the probability that an ozone spike will occur. Further, as suggested (but not established) by Beyrich (1994), the break-up of the LLJ was well correlated with increased turbulence at the surface and coincident surface ozone spikes. Attempts were also made to address the conflicting results of Smedman (1995), which suggest that the LLJ may act to inhibit the transfer of turbulence from the residual layer to the surface layers. Although the characteristics of the data collected in this experiment prevented conclusive testing of this idea, the results point towards the importance of an understanding of the height and speed of the individual LLJ in determining the relationship between the presence of the LLJ and characteristics of turbulence near the surface.

One of the key observations in this thesis is the variability of ozone concentrations in the residual layer, which strongly refutes the common assumption that concentrations of ozone remain constant in the residual layer. This has significant implications, not only for nocturnal surface ozone concentration, but also for the temporal auto-correlation of ozone concentrations at a daily scale. For example, advection may account for the mixed results of semi-empirical models designed to estimate the contribution of ozone stored in the residual layer to the maximum ozone concentration the following day (Teichmann et al. 1997; Neu 1995). While the light wind speeds and meandering characteristics of wind flow patterns in the residual layer render it difficult to determine pollutant trajectories, advection processes cannot be ignored from modelling studies.

The thesis has also demonstrated the potential of wavelet analysis as a technique suitable for analysing the characteristics of turbulence and wave-like motions in the very stable NBL. Although turbulence is shown to be weak, poorly developed and intermittent, the advantages of wavelet analysis (compared to traditional analytical tools such as the FFT) were exploited to develop a new method to objectively and quantitatively isolate turbulent bursts in the time series. The technique was then utilised to calculate revised estimates of turbulence fluxes in the NBL. Whilst previous attempts have been made to both calculate scalar fluxes using wavelet analysis

(Howell & Mahrt 1994; Howell & Sun 1999), and to conditionally sample coherent eddies (Hagelberg & Gamage 1994) this is the first time a technique has been developed for, and applied directly to, turbulence and turbulent fluxes in the NBL. The results illustrate that the technique effectively isolates turbulent periods and provides reliable estimates of scalar fluxes. Although only a limited data set was available, the potential of this technique as a method for quantitatively determining the relative amount of ozone transported due to vertical mixing processes was illustrated.

Using wavelet based techniques it was possible to demonstrate that vertical mixing processes play an important role in determining the localised timing of increased ozone concentrations during the nocturnal component of the diurnal ozone cycle. However due to the strong influence of NO on the data set, it is unlikely that turbulent mixing of ozone to the surface acts as a significant net sink of ozone concentrations in the residual layer, at least at the scale of the pollution budget for the LFV airshed. Ozone transported to the surface is likely to be react with NO to form NO_2 which remains in the stable layers until the following morning. As levels of ultra-violet radiation increase, photolysis of NO_2 occurs and ozone is re-formed at the surface. Thus, in the absence of any complex chemical reactions, or a change in the equilibrium between NO, NO_2, and ozone, neither a net increase nor net decrease in ozone concentrations within the airshed is likely to occur. However, given that advection processes are considerably more limited in the surface layers compared to the residual layer, this process may account for localised differences in the timing and gradient of increased ozone concentrations observed at the surface throughout the LFV. Thus whilst vertical mixing processes operating in the NBL may have a negligible effect on the diurnal ozone budget of the LFV airshed, they may have a significant impact on the characteristics of the ozone budget at a local scale.

8.3 Future directions

Definition of the characteristics of the boundary layer and an understanding of the dispersion processes operating in coastal environments are fundamental to the development of enhanced air quality models and pollutant abatement strategies (McElroy & Smith 1991). There is clearly a need for a more detailed study of the processes determining pollutant transport in the very stable nocturnal boundary layer, particularly in urbanised regions of complex coastal terrain. This study highlights the difficulty of observation-based investigations of mesoscale systems within the atmosphere. The transient nature of thermo-topographical systems hinders

climatological analysis and makes it difficult to develop 'snap-shots' of mesoscale phenomena that do not involve assumptions of stationarity. This has resulted in bias towards theoretical rather than observational based investigations (Atkinson 1981).

Nevertheless, observation-based studies form an important part of the continued development of our understanding of these complex systems and are fundamental to continued model development and validation exercises. This study highlights the need for a larger and more detailed field experiment to study the characteristics of vertical mixing in the very stable NBL in regions of complex coastal terrain. Intermittent vertical mixing processes are active throughout the night and can have a significant impact on pollutant concentrations at the surface. This has significant implications for pollutant budgets at a diurnal scale.

Thus a field experiment that includes increased temporal and spatial resolution of vertical profiles, perhaps using a range of sensors from tethersondes to sodars and lidar, is justified in the NBL. Such a regime would provide a greater insight into the temporal variability of the horizontal and vertical transport processes operating in the NBL. Further, an enhanced surface network of ozone and NO sensors located immediately around the primary site would enable a more detailed quantitative analysis of advection. Improved measurements of turbulent fluctuations of both ozone and NO_2 are also fundamental to the quantitative analysis of the importance of vertical mixing processes in determining pollutant distribution throughout the NBL.

However, the techniques and analysis developed and applied in this thesis demonstrate the potential of wavelet analysis to make a considerable contribution to the study of turbulence in the very stable NBL. This technique, combined with a more complete data set, has the potential to provide an un-paralleled insight into the vertical mixing of pollutants to the surface in the very stable NBL. This technique could be successfully used to analyse the characteristics of surface ozone data and facilitate the development of a more detailed climatology of the occurrence of ozone spikes. Further the technique could be applied to explore the characteristics of gravity waves in the NBL in more detail.

In many ways this study has raised more questions than answers and has demonstrated the complexity of the NBL. Nevertheless, vertical mixing processes have important implications for local ozone pollutant budgets and thus it is likely that these processes are equally important for a range of other pollutants in the boundary layer. The techniques developed in this thesis

have the potential to make a significant contribution to the analysis of turbulent processes in the NBL. When they are applied to a more comprehensive data set, clearer insights may be gained into temporal and spatial trends of the characteristics of vertical mixing processes and their implications for vertical mixing of pollutants particularly, in regions of complex coastal terrain.

Reference List

Altshuller A.P. (1986) "The role of nitrogen oxides in nonurban ozone formation in the planetary boundary layer over N. America, W. Europe and adjacent areas of ocean", *Atmospheric Environment* **20**, 245-268.

Andreas E.L. & Trevino G. (1997) "Using wavelets to detect trends", *Journal of Atmospheric and Oceanic Technology* **14**, 554-564.

Atkinson B.W. (1981) *Meso-scale Atmospheric Circulations*, 1st edn., Academic Press, London, pp. 1-495.

Bader D.C., McKee T.B., & Tripoli G.J. (1987) "Mesoscale boundary layer evolution over complex terrain. Part 1: Numerical simulation of the diurnal cycle", *Journal of Atmospheric Science* **44**, 2823-2838.

Baldsley B.B., Birks J.W., Jensen M.L., Knapp, K.G., Williams,J. B., Tyrrell,G.W. (1994) "Ozone profiling using kites", *Nature* **369**, 23.

Bange J. & Roth R. (1999) "Helicopter-borne flux measurements in the nocturnal boundary layer over land - A case study", *Boundary-Layer Meteorology* **92**, 295-325.

Banta R.M., Senff C.J., White A.B. Trainer, M., McNider, R.T., Valente, R.J., Mayor, S.D., Alvarez, R.J., Hardesty, R.M., Parish, D. Fehsenfeld, F.C. (1998) "Daytime buildup and night-time transport of urban ozone in the boundary layer during a stagnation episode", *Journal of Geophysical Research* **103**, 22519-22544.

Banta R.M., Shepson P.B., Bottenheim J.W. *et al.* (1997) "Nocturnal cleansing flows in a tributary valley", *Atmospheric Environment* **31**, 2147-2162.

Bendat J.S. & Piersol A.G. (1986) *Random data : analysis and measurement procedures*, Wiley-Interscience, pp.1-566.

Berkowitz C.M., Fast J.D., & Easter R.C. (2000) "Boundary layer vertical exchange processes and the mass budget of ozone: observations and model results", *Journal of Geophysical Research* **105**, 14789-14805.

Berkowitz C.M. & Shaw W.J. (1997) "Airborne measurements of boundary layer chemistry during the Southern Oxidant study: A case study", *Journal of Geophysical Research* **102**, 12795-12804.

Beyrich F. & Weill A. (1993) "Some aspects of determining the stable boundary-layer depth from sodar data", *Boundary-Layer Meteorology* **63**, 97-116.

Beyrich F. (1994) "Sodar observations of the stable boundary layer height in relation to the nocturnal low-level jet", *Meteorologische Zeitschrift* **3**, 29-34.

Beyrich F., Acker K., Kalab D., Klemm, O., Moller, D., Schaller, E., Werhahn, J., Weisensee, U. (1996a) "Boundary layer structure and photochemical pollution in the Harz Mountains - An observational study", *Atmospheric Environment* **30**, 1271-1281.

Beyrich F., Weisensee U., Sprung D., & Gusten H. (1996b) "Comparative analysis of sodar and ozone profile measurements in a complex structured boundary layer and implications for mixing height estimation", *Boundary-Layer Meteorology* **81**, 1-9.

Bigler-Engler V. & Brown H.W. (2000) "Analysis of an ozone episode during the San Diego air quality study: The significance of transport aloft", *Journal of Applied Meteorology* **34**, 1863-1877.

Blanken P.D., Black T.A., Neumann H.H., Den Hartog, G., Yang, P.C., Nesic, Z., Staebler, R.M., Chen, W., Novak, M.D. (1998) "Turbulent flux measurements above and below the overstory of a boreal aspen forest", *Boundary-Layer Meteorology* **89**, 109-140.

Bottenheim J.W., Brickell P., Dann T.F., Wang, D.K., Hopper, F., Gallant, A.J., Anlauf, K.G., Wiebe, H.A. (1997) "Non-methane hydrocarbons and CO during Pacific '93", *Atmospheric Environment* **31**, 2079-2088.

Bowen B.M., Baars J.A., & Stone G.L. (2000) "Nocturnal wind shear direction shear and its potential impact on pollutant transport", *Journal of Applied Meteorology* **39**, 437-445.

Broder B. & Gygax H.A. (1985) "The influence of locally induced wind systems on the effectiveness of nocturnal dry deposition of ozone", *Atmospheric Environment* **19**, 1627-1637.

Buckley R.L. & Kurzeija R.J. (1997) "An observational and numerical study of the nocturnal sea breeze: Part 1: Structure and circulation", *Journal of Applied Meteorology* **36**, 1577-1598.

Businger J.A. (1986) "Evaluation of the accuracy with which dry deposition can be measured with current micrometeorological techniques", *Journal of Climate and Applied Meteorology* **25**, 1100-1124.

Chimonas G. (1999) "Steps, waves and turbulence in the stably stratified planetary boundary layer", *Boundary-Layer Meteorology* **90**, 397-421.

Clark J.F. & Ching J.K.S. (1983) "Aircraft observations of regional transport of ozone in the northeastern United States", *Atmospheric Environment* **17**, 1703-1712.

Colbeck I. & Harrison R.M. (1985) "Dry deposition of ozone: some measurements of dry deposition velocity and vertical profiles to 100 meters.", *Atmospheric Environment* **19**, 1807-1818.

Collineau S. & Brunet Y. (1993) "Detection of turbulent coherent motions in a forest canopy part 1: wavelet analysis", *Boundary-Layer Meteorology* **65**, 375-379.

Corsmeier U., Kalthoff N., Kolle O., Kotzian M., & Fiedler F. (1997) "Ozone concentration jump in the stable nocturnal boundary layer during a LLJ-event", *Atmospheric Environment* **31**, 1977-1989.

Coulter R.L. (1990) "A case study of turbulence in the stable nocturnal boundary layer", *Boundary-Layer Meteorology* **52**, 75-91.

Das M. & Aneja V.P. (1994) "Measurements and analysis of concentrations of gaseous hydrogen peroxide and related species in the rural central piedmont region of North Carolina", *Atmospheric Environment* **28**, 2473-2483.

Davenport A.G., Grimmond C.S.G., Oke T.R., & Wieringa J. (2000) "Estimating the roughness of cities and sheltered country", *15th conference on Probability and Statistics / 12th Conference on Applied Climatology* **4B.2**, 96-99.

Derbyshire S.H. (1990) "Nieuwstadt's stable boundary layer revisited", *Quarterly Journal of the Royal Meteorological Society* **116**, 127-158.

Derbyshire S.H. (1994) "Stable boundary layers: Observations, models and variability part 1: Modelling and Measurement", *Boundary-Layer Meteorology* **74**, 19-54.

Derbyshire S.H. (1999) "Stable boundary-layer modelling: Established approaches and beyond", *Boundary-Layer Meteorology* **90**, 423-446.

Derwent R.G., Middleton D.R., Field R.A., Goldstone, M.E., Lester, J.N., Perry, R. (1995) "Analysis and interpretation of air quality data from an urban roadside location in central London over the period from July 1991 to July 1992", *Atmospheric Environment* **29**, 923-946.

Douglas S.G. & Kessler R.C. (1991) "Analysis of mesoscale airflow patterns in the South-Central Coast Air Basin during the SCCCAMP 1985 intensive measurement periods", *Journal of Applied Meteorology* **30**, 607-631.

Droppo J.G. (1985) "Concurrent measurements of ozone dry deposition using eddy correlation and profile flux methods", *Journal of Geophysical Research* **90**, 2111-2118.

Druilhet A, Attie J-L, de Abreu Sa L, Durand P, & Benech B (1994) Experimental study of inhomogeneous turbulence in the lower troposphere by wavelet analysis. In: Chui CK, Montefusco L, & Puccio L, (eds.), *Wavelets: Theory, Algorithms and Applications* Academic Press, pp. 543-559.

Farge M. (1992) "Wavelet transforms and their application to turbulence", *Annual Review of Fluid Mechanics* **24**, 395-457.

Finnigan J.C. (1999) "A note on wave-turbulence interaction and the possibility of scaling in the very stable nocturnal boundary layer", *Boundary-Layer Meteorology* **90**, 529-539.

Finnigan J.J., Einaudi F., & Fua D. (1984) "The interaction between an Internal gravity wave and turbulence in the stabily-stratified nocturnal boundary layer", *Journal of Atmospheric Science* **41**, 2409-2436.

Foken Th. & Wichura B. (1996) "Tools for quality assessment of surface-based flux measurements", *Agricultural and Forest Meteorology* **78**, 83-105.

Freytag F. (1987) "Results from the MERKUR experiment: Mass budget and vertical motions in a large valley during mountain and valley wind", *Meteorology and Atmospheric Physics* **37**, 129-140.

Frisch A.S., Orr B.W., & Martner B.E. (1992) "Doppler radar observations of the development of a boundary-layer nocturnal jet", *Monthly Weather Review* **120**, 3-16.

Fujita T.T. & Wakimoto R.M. (1982) "Effects of miso- and mesoscale obstacles on PAM winds obtained during project NIMROD", *Journal of Applied Meteorology* **21**, 840-858.

Galmarini S. & Attie J.-L. (2000) "Turbulent transport at the thermal inertial boundary layer top: Wavelet analysis of aircraft measurements", *Boundary-Layer Meteorology* **94**, 175-196.

Galmarini S., Duynkerke P.G., & De Arellano J.V.-G. (1997) "Evolution of nitrogen oxide chemistry in the nocturnal boundary layer", *Journal of Applied Meteorology* **36**, 943-957.

Gao W. & Li B.L. (1993) "Wavelet analysis of coherent structures at the atmosphere-forest interface", *Journal of Applied Meteorology* **32**, 1717-1725.

Garland J.A. & Derwent R.G. (1979) "Destruction at the ground and the diurnal cycle of concentrations of ozone and other gases", *Quarterly Journal of the Royal Meteorological Society* **105**, 169-183.

Garratt J.R. (1982) "Observations in the nocturnal boundary layer", *Boundary-Layer Meteorology* **22**, 21-48.

Greenhut G.K., Jochum A.M., & Neininger B. (1995) "Boundary-layer turbulent transport and production/destruction of ozone during summertime smog episodes over the Swiss plateau", *Boundary-Layer Meteorology* **73**, 357-372.

Gusten H., Heinrich G., & Sprung D. (1998) "Nocturnal depletion of ozone in the Upper Rhine Valley", *Atmospheric Environment* **32**, 1195-1202.

Gusten H., Heinrich G., Weppner J., Cvitas, T., Klasinc, L., Varotsos, C.A., Asimakopoulos, D.N. (1997) "Thessaloniki '91 field measurement campaign - 2. Ozone formation in the Greater Thessaloniki area", *Atmospheric Environment* **37**, 1115-1126.

Gusten H. & Heinrich G. (1996) "On-line measurements of ozone surface fluxes, 1. Methodology and instrumentation", *Atmospheric Environment* **30**, 897-909.

Haeger-Eugensson M. (1999) "Vertical interactions in a nocturnal multi-scale wind system influenced by atmospheric stability in a coastal area", *Theoretical and Applied Climatology* **64**, 69-82.

Hagelberg C.R. & Gamage N.K.K. (1994) "Structure-preserving wavelet decompositions of intermittent turbulence", *Boundary-Layer Meteorology* **70**, 217-246.

Hanna S.R. & Chang J. (1992) "Boundary-layer parameterization for applied dispersion modelling over urban areas", *Boundary-Layer Meteorology* **58**, 229-259.

Harrison R.M., Holmann C.D., McCartney H.A., & McIlveen J.F.R. (1978) "Short communication: nocturnal depletion of photochemical ozone at a rural site", *Atmospheric Environment* **12**, 2021-2026.

Hastie D.R., Narayan J., Schiller C., Niki, H., Shepson, P.B., Sills, D.M.L., Talyer, P.A., Moroz, Wm.J., Drummond, J.W., Reid, N., Taylor, R, Roussel, P.B. (1999) "Observational evidence for the impacts of the lake breeze circulation on ozone concentrations in Southern Ontario", *Atmospheric Environment* **33**, 323-335.

Hastie D.R., Shepson P.B., Reid N., Roussel P.B., & Melo O.T. (1996) "Summertime NO_x, NO_y, and ozone at a site in rural Ontario", *Atmospheric Environment* **30**, 2157-2165.

Hastie D.R., Shepson P.B., Sharma S., & Schiff H.I. (1993) "The influence of the nocturnal boundary layer on secondary trace species in the atmosphere at Dorset, Ontario", *Atmospheric Environment* **27A**, 533-541.

Hayden K.L., Anlauf K.G., Hoff R.M., Strapp, J.W., Bottenheim, J.W., Wiebe, H.A., Froude, F.A., Martin, J.B., Steyn, D.G., McKendry, I.G.. (1997) "The vertical chemical and meteorological structure of the boundary layer in the Lower Fraser Valley during Pacific '93", *Atmospheric Environment* **31**, 2089-2106.

Helmis C.G., Tombrou M., Asimakopoulos D.N., Soilemes, A., Gusten, H., Moussiopoulos, N., Hatzaridou, A. (1997) "Thessaloniki '91 Field measurement campaign - 1. Wind field and atmospheric boundary layer structure over greater Thessaloniki area under light background flow", *Atmospheric Environment* **31**, 1101-1114.

Heisenberg, W. (1958) *Physics and Philosophy,* Harper and Row, NY

Hicks B.B. & McMillen R.T. (1988) "On the measurement of dry deposition using imperfect sensors and in non-ideal terrain", *Boundary-Layer Meteorology* **42**, 79-94.

Holton J.R. (1992) *An Introduction to Dynamic Meteorology*, 3rd edn., Academic Press, pp. 1-507.

Horst T.W. & Weil J.C. (1994) "How far is far enough?: The fetch requirements for micrometeorological measurement of surface fluxes", *Journal of Atmospheric and Oceanic Technology* **11** , 1018-1025.

Howell J.F. & Sun J. (1999) "Surface-layer fluxes in stable conditions", *Boundary-Layer Meteorology* **90**, 495-520.

Howell J.F. & Mahrt L. (1997) "Multiresolution flux decomposition", *Boundary-Layer Meteorology* **83**, 117-137.

Howell J.F. & Mahrt L. (1994a) An adaptive decomposition: application to turbulence. In: Foufoula-Georgiou E & Kumar P (eds.) *Wavelets in Geophysics,* pp. 107-128.

Howell J.F. & Mahrt L. (1994b) "An Adaptive Multiresolution Data Filter - Applications To Turbulence And Climatic Time-Series", *Journal of the Atmospheric Sciences* **51**, 2165-2178.

Hubbard BB (1998) *The world according to wavelets. The story of a mathematical technique in the making*, 2nd edn., A K Peters, Wellesley, pp.1-330.

Hudgins L.L., Friehe C.A., & Mayer M.E. (1993) "Wavelet transforms and atmospheric turbulence", *Physical Review Letters* **71**, 3279-3283.

Jordan D.A., Hajj M.R., & Tieleman H.W. (1997) "Characterization of turbulence scales in the atmospheric surface layer with the continuous wavelet transform", *Journal of Wind Engineering and Industrial Aerodynamics* **71**, 709-716.

Kaimal J.C. & Finnigan J.C. (1994) *Atmospheric boundary layer flows their structure and measurement*, Oxford University Press, New York, pp. 1-289.

Kalthoff N., Horlacher V., Corsmeier U., Voltz_Thomas, A., Kolahgar, B., Giess, H., Mollmann-Coers, M., Knaps, A. (2000) "Influence of valley winds on transport and dispersion of airborn pollutants in the Freiburg-Schauinsland area", *Journal of Geophysical Research* **105**, 1585-1597.

Katul G., Hsieh C.I., Oren R., Ellsworth D., & Phillips N. (1996) "Latent and sensible heat flux predictions from a uniform pine forest using surface renewal and flux variance methods", *Boundary-Layer Meteorology* **80**, 249-282.

Katul G.G. & Parlange M.B. (1995) "The spatial structure of turbulence at production wave-numbers using orthonormal wavelets", *Boundary-Layer Meteorology* **75**, 81-108.

Kellerhals, M., (1996), "Dry Deposition of Ozone in the Lower Fraser Valley, British Columbia: Measurements and Comparison With a Model", pp. 1-136 , Unpublished thesis from University of British Columbia.

Kelly N.A., Wolff G.T., & Ferman M.A. (1984) "Sources and sinks of ozone in rural areas", *Atmospheric Environment* **18**, 1251-1266.

Kharabata S.K. & Schuepp P.H. (1999) "Source footprint considerations in the determination of volatile organic compound fluxes from forest canopies", *Journal of Applied Meteorology* **38**, 878-884.

Kleinman L., Lee Y.-N., Springston S.R., Nunnermacker, L., Zhou, X., Brown, R., Hallock, K., Klotz, P., Leahy, P., Lee, J. H.; Newman, L. (1994) "Ozone formation at a rural site in the southeastern United States", *Journal of Geophysical Research* **99**, 3469-3482.

Koracin D. & Berkowicz R. (1988) "Nocturnal boundary-layer height - observations by acoustic sounders and predictions in terms of surface-layer parameters", *Boundary-Layer Meteorology* **43**, 65-83.

Kristensen L., Mann J., Oncley S.P., & Wyngaard J.C. (1997) "How close is close enough when measuring scalar fluxes with displaced sensors?", *Journal of Atmospheric and Oceanic Technology* **14**, 814-821.

Kroening J.L. & Ney E.P. (1962) "Atmospheric ozone", *Journal of Geophysical Research* **67**, 1867-1875.

Kulkarni J.R., Sadani L.K., & Murthy B.S. (1999) "Wavelet analysis of intermittent turbulent transport in the atmospheric surface layer over a monsoon trough region", *Boundary-Layer Meteorology* **90**, 217-239.

Kumar P. & FoufoulaGeorgiou E. (1997) "Wavelet analysis for geophysical applications", *Reviews of Geophysics* **35**, 385-412.

Kunkel K.E. & Walters D.L. (1982) "Intermittent Turbulence measurements of the temperature structure parameter under very stable conditions", *Boundary-Layer Meteorology* **22**, 49-60.

Kurzeja R.J., Berman S., & Weber A.H. (1991) "A climatological study of the nocturnal planetary boundary layer", *Boundary-Layer Meteorology* **54**, 115-128.

Lalas D.P., Tombrou-Tsella M., Petrakis M., Asimakopoulos P., & Helmis C.G. (1987) "An experimental study of the horizontal and vertical distribution of ozone over Athens", *Atmospheric Environment* **21**, 2681-2693.

Lau K.-M. & Weng H. (1995) "Climate signal detection using wavelet transform: How to make a time series sing", *Bulletin of the American Meteorological Society* **76**, 2391-2402.

Lee X., Neumann H.H., Den Hartog G., Fuentes, J.D., Black, T.A., Mickle, R.E., Yang, P.C., Blanken, P.D. (1997) "Observation of gravity waves in a boreal forest", *Boundary-Layer Meteorology* **84**, 383-398.

Lee X. & Black T.A. (1994) "Relating eddy correlation sensible heat flux to horizontal sensor separation in the unstable atmospheric surface layer", *Journal of Geophysical Research* **99**, 18545-18553.

Lehning M., Richner H., Kok G.L., & Neininger B. (1998) "Vertical exchange and regional budgets of air pollutants over densely populated areas", *Atmospheric Environment* **32**, 1353-1363.

Lehning M., Richner H., & Kok G.L. (1996) "Pollutant transport over complex terrain: Flux and budget calculations for the POLLUMET field campaign", *Atmospheric Environment* **30**, 3027-3044.

Lenschow D.H., Xing-Sheng L., Zhu C.J., & Stankov B.B. (1988) "The stably stratified boundary layer over the great plains. 1. Mean and turbulent structure", *Boundary-Layer Meteorology* **42**, 95-121.

Li S.-M., Anlauf K.G., Wiebe H.A., Bottenheim, J.W., Shepson, P.B., Bisenthal, T. (1997) "Emission ratios and photochemical production efficiencies of nitrogen oxides, ketones and aldehydes in the Lower Fraser Valley during the summer Pacific 1993 oxidant study", *Atmospheric Environment* **31**, 2037-2048.

Lippmann M. (1989) "Health effects of ozone: A critical review 2-695", *Journal of Air and Waste Management Association* **39**, 67.

Loffler-Mang M., Kossmann M., Vogtlin R., & Fiedler F. (1997) "Valley wind systems and their influence on nocturnal ozone concentrations", *Beitraege zur Physik der Atmosphaere* 1-14.

Lu R. & Turco R.P. (1995) "Air pollutant transport in a coastal environment - Part 2. Three dimensional simulations over the Los Angeles Basin", *Atmospheric Environment* **29**, 1499-1518.

Mahrt L., Heald R.C., Lenschow D.H., & Stankov B.B. (1979) "An observational study of the structure of the nocturnal boundary layer", *Boundary-Layer Meteorology* **17**, 247-264.

Mahrt L. (1985) "Vertical structure and turbulence in the very stable boundary layer", *Journal of the Atmospheric Sciences* **42**, 2333-2349.

Mahrt L. (1989) "Intermittency of atmospheric-turbulence", *Journal of the Atmospheric Sciences* **46**, 79-95.

Mahrt L., Vickers D., Howell J.. Hojstrup, J., Wilczak, J.M., Edson, J. Hare, J (1996) "Sea surface drag coefficients in the Risø Air Sea Experiment", *Journal of Geophysical Research* **101**, 14327-14335.

Mahrt L. (1998) "Flux sampling errors for aircraft and towers", *Journal of Atmospheric and Oceanic Technology* **15**, 416-429.

Mahrt L., Sun J., Blumen W., Delany T., & Oncley S. (1998) "Nocturnal boundary-layer regimes", *Boundary-Layer Meteorology* **88**, 255-278.

Mahrt L. (1999) "Stratified atmospheric boundary layers", *Boundary-Layer Meteorology* **90**, 375-396.

Martin M., Plaza J., Bezares J.C., & Millan M. (1991) "Comparative study of seasonal air pollutant behaviour in a Mediterranean coastal site: Castellon (Spain)", *Atmospheric Environment* **25A**, 1523-1535.

Mayer M.E., Hudgins L.L., & Friehe C.A. (1994) Wavelet Spectra of Buoyant Atmospheric Turbulence. In: Chui CK, Montefusco L, & Puccio L (eds.), *Wavelets: Theory, Algorithms and Applications*, Academic Press, pp.533-541.

McElroy J.L. & Smith T.B. (1993) "Creation and fate of ozone layers aloft in Southern California", *Atmospheric Environment* **27A**, 1917-1929.

McElroy J.L. & Smith T.B. (1991) "Lidar descriptions of mixing-layer thickness characteristics in a complex terrain/coastal environment", *Journal of Applied Meteorology* **30**, 585-597.

McElroy J.L. & Smith T.B. (1986) "Vertical pollutant distributions and boundary layer structure observed by airbourne LIDAR near the complex southern California coastline", *Atmospheric Environment* **20**, 1555-1566.

McKendry I.G., Steyn D.G., Banta R.M., Strapp, W., Anlauf, K., Pottier, J.. (1990a) "Daytime air quality and local circulations in the Pitt Lake tributary valley, B.C", *Journal of Applied Meteorology* **37**, 393-404.

McKendry I.G., Steyn D.G., O'Kane S., Zawar-Reza P., & Heuff D. (1990b) "Lower tropospheric ozone measurements by light aircraft equipped with chemiluminescent sonde", *Journal of Atmospheric and Oceanic Technology* **15**, 136-143.

McKendry I.G. (1994) "Synoptic circulation and summertime ground level ozone concentration at Vancouver, B.C., Canada", *Journal of Applied Meteorology* **33**, 627-641.

McKendry I.G., Steyn D.G., Lundgren J., Hoff, R.M., Strapp, J.W., Anlauf, K.G., Froude, F.A., Martin, J.B., Banta, R.M., Olivier, L.D. (1997) "Elevated ozone layers and vertical down-mixing over the Lower Fraser Valley, BC", *Atmospheric Environment* **31**, 2135-2146.

McKendry I. (2000) "PM_{10} levels in the Lower Fraser Valley, British Columbia, Canada: An overview of spatiotemporal variations and meteorological controls", *Journal of Air and Waste Management Association* **50**, 443-452.

McKendry I. & Lundgren J. (2000) "Tropospheric layering of ozone in regions of urbanised complex and/or coastal terrain: a review", *Progress in Physical Geography* **24**, 329-354.

McMillen R.T. (1988) "An eddy correlation technique with extended applicability to non-simple terrain", *Boundary-Layer Meteorology* **43**, 231-245.

Millan M., Mantilla E., Salvador R., Carratala, A., Sanz, M., Alonso, L., Gangoiti, G., Navazo, M. (2000) "Ozone cycles in the Western Mediterranean Basin: Interpretation of monitoring data in complex coastal terrain", *Journal of Applied Meteorology* **39**, 487-508.

Millan M., Salvador R., & Mantilla E. (1996) "Meteorology and photochemical air pollution in Southern Europe: Experimental results from EC research projects", *Atmospheric Environment* **30**, 1909-1924.

Moore G.E., Killus J.P., & Whitten G.P. (1991a) "Composition of marine air offshore of the Western United States", *Journal of Applied Meteorology* **30**, 707-713.

Moore G.E., Douglas S.G., Kessler R.C., & Killus J.P. (1991b) "Identification and tracking of polluted air masses in the Southern-Central Coastal Air Basin", *Journal of Applied Meteorology* **30**, 715-732.

Moxley J.M. & Cape J.N. (1997) "Depletion of carbon monoxide from the nocturnal boundary layer", *Atmospheric Environment* **31**, 1147-1155.

Musselman R.C. & Massman W.J. (1999) "Ozone flux to vegetation and its relationship to plant response and ambient air quality standards", *Atmospheric Environment* **33**, 65-73.

Nai-Ping L., Neff W.D., & Kaimal J.C. (1983) "Wave and turbulence structure in disturbed nocturnal inversion", *Boundary-Layer Meteorology* **26**, 141-155.

Nappo C.J. & Johansson P. (1999) "Summary of the Lovanger international workshop on turbulence and diffusion in the stable planetary boundary layer", *Boundary-Layer Meteorology* **90**, 345-374.

Nester K. (1995) "Influence of sea breeze flows on air pollution over the Attica Peninsula", *Atmospheric Environment* **29**, 3655-3670.

Neu U. (1995) "A parameterization of the nocturnal ozone reduction in the residual layer by vertical downward mixing during summer smog situations using sodar data", *Boundary-Layer Meteorology* **73**, 189-193.

Neu U., Kunzle T., & Wanner H. (1994) "On the relationship between ozone storage in the residual layer and daily variation in near surface ozone concentration - a case study", *Boundary-Layer Meteorology* **69**, 221-247.

Percival D.B. & Walden A.T. (2000) *Wavelet Methods for Time Series Analysis*, 1st edn., University of Cambridge, pp.1-595.

Perrier V., Philipovitch T., & Basdevant C. (1995) "Wavelet spectra compared to Fourier spectra", *Journal of Mathematical Physics* **36**, 1506-1519.

Pisano J.T., McKendry I., Steyn D.G., & Hastie D.R. (1997) "Vertical nitrogen dioxide and ozone concentrations measured from a tethered balloon in the Lower Fraser Valley", *Atmospheric Environment* **31**, 2071-2078.

Prevot A.S.H., Dommen J., Baumle M., & Furger M. (2000) "Diurnal variations of volatile organic compounds and local circulation systems in an Alpine valley", *Atmospheric Environment* **34**, 1413-1423.

Pryor S.C., McKendry I.G., & Steyn D.G. (1995) "Synoptic-scale meteorological variability and surface ozone concentrations in Vancouver, British Columbia", *Journal of Applied Meteorology* **34**, 1824-1833.

Pryor S.C. & Steyn D.G. (1995) "Hebdomadal and diurnal cycles in ozone time series from the Lower Fraser Valley, B.C.", *Atmospheric Environment* **29**, 1007-1019.

Rees J.M., Denholm-Prince J.C.W., King J.C., & Anderson P.S. (2001) "A climatological study of internal gravity waves in the atmospheric boundary layer overlying the Brunt Ice Shelf, Antarctica", *Journal of Atmospheric Science* **57**, 511-526.

Reich P.B. & Amundson A.G. (1985) "Ambient levels of ozone reduce net photosynthesis in tree and crop species", *Science* **230**, 566-570.

Reitebuch O., Strassburger A., Emeis S., & Kuttler W. (2000) "Nocturnal secondary ozone concentration maxima analysed by sodar observations and surface measurements", *Atmospheric Environment* **34**, 4315-4329.

Rogers D.P., Johnson D.W., & Friehe C.A. (1995a) "The stable internal boundary layer over a coastal sea. Part 1: Airborne measurements of the mean and turbulence structure", *Journal of the Atmospheric Sciences* **52**, 667-683.

Rogers D.P., Johnson D.W., & Friehe C.A. (1995b) "The stable internal boundary layer over a coastal sea. Part 2: Gravity waves and the momentum balance", *Journal of the Atmospheric Sciences* **52**, 684-696.

Roussel P.B., Lin X., Camacho F., Laszlo, S., Taylor, R., Melo, O.T., Shepson, P.B., Hastie, D.R., Niki, H. (1996) "Observations of ozone and precursors levels at two sites around Toronto, Ontario, during SONTOS '92", *Atmospheric Environment* **30**, 2145-2155.

Samson P.J. (1978) "Nocturnal ozone maxima", *Atmospheric Environment* **12**, 951-955.

Sato K. & Yamada M. (1994) "Vertical structure of atmospheric gravity waves revealed by the wavelet analysis", *Journal of Geophysical Research* **99**, 20623-20631.

Schmid H.P. (1997) "Experimental design for flux measurements: matching scales of observations and fluxes", *Agricultural and Forest Meteorology* **87**, 179-200.

Schmid H.P. (1994) "Source areas for scalars and scalar fluxes", *Boundary-Layer Meteorology* **67**, 293-318.

Seibert P., Feldmann H., Neininger B., Baumle M., & Trickl T. (2000) "South Foehn and ozone transport in the Eastern Alps - case study and climatological aspects", *Atmospheric Environment* **34**, 1379-1394.

Seinfeld J.H. & Pandis S.N. (1997) *Atmospheric Chemistry and Physics of Air Pollution: From Air Pollution to Climate Change*, John Wiley & Sons, pp.1-1326.

Smedman A.S., Bergstrom H., & Högström U. (1995) "Spectra, variances and length scales in a marine stable boundary layer dominated by a low level jet", *Boundary-Layer Meteorology* **76**, 211-232.

Smedman A.S. (1998) "Observations of a multi-level turbulence structure in a very stable atmospheric boundary-layer", *Boundary-Layer Meteorology* **44,** 231-253.

Starn T.K., Shepson P.B., Bertman S.B. *et al.* (1998) "Night-time isoprene chemistry at an urban-impacted forest site", *Journal of Geophysical Research* **103**, 22437-22447.

Steinberger E.H. & Ganor E. (1980) "High ozone concentrations at night in Jerusalem and Tel-Aviv", *Atmospheric Environment* **14**, 221-225.

Steyn D.G., Bottenheim J.W., & Thompson R.B. (1997) "Overview of tropospheric ozone in the Lower Fraser Valley, and the Pacific '93 field study", *Atmospheric Environment* **31**, 2025-2036.

Stull R.B. (1988) *An Introduction to Boundary Layer Meteorology*, 1st edn., Kluwer Academic Publishers, Dordrecht, p.666.

Svensson G. (1996) "A numerical model for chemical and meteorological processes in the atmospheric boundary layer. Part 2: A case study of the air quality situation in Athens, Greece", *Journal of Applied Meteorology* **35**, 955-973.

Teichmann U., Spindler G., & Theiss D. (1997) "Test of a parameterization for nocturnal ozone reduction in the residual layer by downward mixing during summer smog situations", *Boundary-Layer Meteorology* **83**, 505-509.

Thorpe A.J. & Guymer T.H. (1977) "The nocturnal jet", *Quarterly Journal of the Royal Meteorological Society* **103**, 633-653.

Torrence C. & Compo G.P. (1998) "A practical guide to wavelet analysis", *Bulletin of the American Meteorological Society* **79**, 61-76.

Trevino G. & Andreas E.L. (1996) "On wavelet analysis of nonstationary turbulence", *Boundary-Layer Meteorology* **81**, 271-288.

Van Dop H., Guicherit R., & Lanting R.W. (1977) "Some measurements of the vertical distribution of ozone in the atmospheric boundary layer", *Atmospheric Environment* **11**, 65-71.

Vecchi R. & Valli G. (1999) "Ozone assessment in the southern part of the Alps", *Atmospheric Environment* **33**, 97-109.

Vickers D. & Mahrt L. (1997) "Quality control and flux sampling problems for tower and aircraft data", *Journal of Atmospheric and Oceanic Technology* **14**, 512-526.

Wakamatsu S., Ogawa Y., Murano K., Goi K., & Aburamoto Y. (1983) "Aircraft survey of the secondary photochemical pollutants covering the Tokyo Metropolitan area", *Atmospheric Environment* **17**, 827-835.

Weber A.H. & Kurzeja R.J. (1991) "Nocturnal planetary boundary-layer structure and turbulence episodes during the project stable field program", *Journal of Applied Meteorology* **30**, 1117-1133.

Whitcher, B., Byers, S.D., Guttorp, P., and Percival, D.B., (2001), "Testing for Homogeneity of Variance in Time Series: Long Memory, Wavelets and the Nile River", *National Research Center for Statistics and the Environment*

Whiteman C.D., Bain X., & Zhong S. (1997) "Low-level jet climatology from enhanced rawinsonde observations at a site in the Southern Great Plains", *Journal of Applied Meteorology* **36**, 1363-1376.

Wieringa J. (1993) "Representative roughness parameters for homogeneous terrain", *Boundary-Layer Meteorology* **63**, 323-363.

Wotawa G., Kroger H., & Stohl A. (2000) "Transport of ozone towards the Alps - results from trajectory analyses and photochemical model studies", *Atmospheric Environment* **34**, 1367-1377.

Wotawa G. & Kromp-Kolb H. (2000) "The research project VOTALP - general objectives and main results", *Atmospheric Environment* **34**, 1319-1322.

Xu D., Yap D., & Taylor P. (1996) "Meteorologically adjusted ground level ozone trends in Ontario", *Atmospheric Environment* **30**, 1117-1124.

Zaveri R.A., Saylor R.D., Peters L.K., McNider R., & Song A. (1995) "A model investigation of summertime diurnal ozone behaviour in rural mountainous locations", *Atmospheric Environment* **29**, 1043-1065.

Zhang J. & Rao S.T. (2000) "The role of vertical mixing in the temporal evolution of ground-level ozone concentrations", *Journal of Applied Meteorology* **38**, 1674-1691.

Zhang J., Rao S.T., & Daggupaty S.M. (1998) "Meteorological processes and ozone exceedances in the Northeastern United States during the 12-16 July 1995 episode", *Journal of Applied Meteorology* **37**, 776-789.

Zurita E. & Castro M. (1983) "A statistical analysis of mean hourly concentrations of surface ozone at Madrid (Spain)", *Atmospheric Environment* **17**, 2213-2220.

Appendix 1: Data availability

Ozone

Monitor Labs ML 9811

Available : (188) July 7 1540 – (259) 16 September 1035, 1998.

Missing data: (191) July 10th 1735 – (196) July 15th 1330

Ozone switching system and NO_x measurements - available only between the following dates

July 22nd (JD 203) 2135 – July 23rd (JD 204) 1555 (NB no NOx /NO /NO_2 data)

July 26th (JD 207) 1400 – July 29th (JD 210) 1120 (NB no NOx /NO /NO_2 data)

August 8th (JD 220) 1430 – August 10th (JD 222) 1040 (NB no NOx /NO /NO_2 data)

August 12th (JD 224) 1615 – August 15th (JD 225) 1800 (NB no ozone)

August 15th (JD 225) 1800 - August 14th (JD 226) 1200

August 30th (JD 242) 1505 – September 1st (JD 244) 1345

Radiation and climatological data

Available : July 3rd 0115 and September 4th 1400, 1998.

Missing: July 29th (JD 210) 1115 – July 31st (JD 212) 0115, 1998

August 27th (JD 239) 1415 – August 27th (JD 239) 2345, 1998

Richardson number data

Available: July 17th (JD 198) 0855h – September 4th (JD 247) 1455, 1998

Missing: July 23rd (JD 204) 1315 – July 24th (JD 205) 0910, 1998

July 29th (JD 210) 1035 – August 1st (JD 213) 0950, 1998

August 6th (JD 218) 1520 - August 7th (JD 219) 0405, 1998

August 14th (JD 226) 1135 - August 15th (JD 227) 0740, 1998

August 27th (JD 239) 1455 – August 28th (JD 240) 0400, 1998

High frequency data

a) sonic anemometer:

Available data: July 17 1998 1230 - Sept 3 1998 2400

Missing (m) or incomplete (i)

98072058 i
98072174 I
98072176 m
98072178 i
98072284 i
98072658 i
98072662 i
98072692 i
98072694 m
98072696 m
98072702 m
98072704 i
98072862 i
98072864 m
98072866 i
98072870 i
98072872 i
98072930 i
98080460 i
98080462 i
98081044 i
98081046 m
98081048 i
98081264 m
98081266 i
98081302 m
98081448 i
98081450 i
98082148 i

98082454 i

98082456 m

98082458 i

98082758 i

98082760 i

b) The times when the GFAS fast response ozone sensor and Krypton Hygrometer were operated and are included in the data sets are:

July 21 1998 1900 - July 23 1998 1530

July 26 1998 1620 - July 29 1998 1100

Aug 08 1998 1711 - Aug 10 1998 1030

Aug 12 1998 1600 - Aug 14 1998 1200

Aug 30 1998 1550 - Sept 01 1998 1430

NB Periods when the GFAS system went down are not known exactly. Care was exercised when using the data.

Appendix 2: Tethersonde flights

Julian day	Date (1998)	Time Up	Time Down	Start O_3	End O_3	Max O_3
202	***Tuesday July 21***	2017	2100	28.1	32.8	71.3
		2307	2349	12.8	30.4	57.6
		2353	2440	19.1	17.8	59.3
203	***Wednesday July 22***	0044	0143	16.1	17.4	56.2
		0452	0552	14.3	17.4	58.3
		0605	0632	20.6	20.6	52.8
		0634	0713	15.9	21.6	53.0
		0718	0758	18.8	22.9	59.4
		0845	0935	23.2	37.5	73.9
		0950	1037	32.0	36.0	77.4
		1432	1523	74.4	79.8	90.9
		1917	2033	73.2	45.2	85.8
		2044	2142	45.0	40.7	67.4
		2315	2410	7.6	13.6	41.2
204	***Thursday July 23***	0015	0114	11.9	18.1	46.3
		0116	0122	17.5	23.2	30.1
		0123	0209	22.9	22.5	37.2
		0210	0300	21.7	15.4	34.8
		0458	0604	10.6	13.7	30.8
		0623	0717	10.9	11.5	33.7

		0745	0835	13.4	5.5	41.0
		0922	1020	18.1	19.8	28.7
		1345	1432	35.7	42.3	56.4
207	***Sunday July 26***	1620	1711	78.7	82.7	83.9
		1715	1724	78.1	0.2	83.7
		1726	1759	73.8	82.4	83.9
		1837	1909	68.8	65.1	79.8
		1930	2009	54.8	45.4	93.1
		2037	2120	41.6	52.2	82.6
		2142	2219	48.4	61.0	72.7
		2250	2309	66.6	66.7	70.4
		2355	2437	11.8	13.3	99.0
208	***Monday July 27***	0055	0132	24.1	34.0	92.2
		0136	0225	27.3	41.9	87.5
		0308	0345	22.8	43.2	89.8
		0459	0540	43.4	39.2	89.5
		0644	0724	22.5	17.5	90.6
		0819	0857	34.4	56.1	97.2
		0940	1029	59.9	65.4	103.4
		1125	1159	84.7	96.4	97.7
		1650	1742	97.5	93.5	98.8
		1910	1947	81.6	78.3	92.1
		2009	2243	74.2	66.1	91.5

		2110	2146	72.2	61.7	89.7
		2230	2323	57.1	49.0	97.0
209	***Tuesday July 28***	0005	0044	48.1	26.3	85.9
		0130	0213	53.0	47.1	91.2
		0315	0401	42.2	21.1	75.9
		0440	0514	26.3	22.3	57.0
		0531	0609	20.0	26.7	63.7
		0647	0734	25.2	26.3	62.6
		0810	0840	34.8	35.3	58.6
		0949	1020	46.5	39.8	63.9
		1125	1156	49.6	60.4	61.9
		1700	1739	88.4	76.4	95.9
		1830	1857	82.0	83.3	99.3
		1946	2026	57.2	44.7	92.1
		2230	2303	40.9	35.9	86.2
		2327	0005	34.0	29.8	78.6
210	***Wednesday July 29***	0028	0108	23.1	36.0	81.7
		0136	0223	19.5	31.2	91.8
		0232	0256	35.0	22.0	42.4
220	***Saturday August 8***	1659	1732			
		1822	1853	50.0	46.5	51.5
		1940	2011	46.1	41.0	53.7
		2155	2227	42.2	40.5	?96.0?

		2303	2334	38.1	30.5	54.0
221	***Sunday August 9***	0002	0034	28.0	18.5	53.0
		0111	0153	19.4	23.5	50.5
		0229	0309	21.0	21.2	49.5
		0358	0431	25.9	30.3	42.7
		0528	0613	22.1	18.5	47.5
		0655	0748	17.0	29.5	44.3
		0844	0922	35.0	33.2	41.4
		1035	1105	37.6	33.7	38.9
		1654	1740	71.3	77.4	89.2
		1846	1927	65.6	64.9	-
		2000	2028	43.9	36.8	76.8
		2209	2251	28.1	29.3	49.5
		2324	2355	17.9	28.4	39.1
222	***Monday August 10***	0544	0624	15.0	15.1	38.6
		0724	0757	14.0	21.3	31.5
		0900	0935	26.6	24.2	37.2
224	***Wed August 12***	1625	1702	45.3	41.2	46.4
		1750	1824	39.8	39.1	41.2
		1912	1945	38.3	34.6	42.2
		2115	2146	36.5	37.2	43.2
		2218	2248	33.3	33.0	39.7
		2333	2405	25.4	22.1	36.8

225	***Thursday August 13***	0048	0120	20.1	21.0	36.3
		0204	0240	14.6	15.1	36.4
		0336	0412	14.5	18.0	40.7
		0436	0521	20.3	17.9	41.3
		0558	0637	14.5	14.6	44.7
		0711	0742	17.9	19.6	45.1
		0820	0852	27.0	31.1	48.2
		0934	1007	34.8	37.9	54.6
		1036	1108	40.3	44.1	50.0
		1711	1741	77.0	65.9	76.4
		1836	1908	55.8	49.5	56.3
		1945	2015	44.5	46.8	51.9
		2103	2140	35.2	20.1	42.7
		2240	2311	28.5	17.1	43.9
		2350	2425	29.8	17.4	39.6
226	***Friday August 14***	0121	0203	32.4	38.6	41.9
		0305	0354	27.9	25.9	34.8
		0440	0513	29.8	22.8	35.5
		0559	0629	33.5	22.9	35.1
		0740	0810	23.0	22.8	35.6
		0849	0925	24.0	23.0	30.3
		1027	1103	28.9	30.0	52.2
242	***Sunday August 30***	1702	1731	57.7	61.6	63.8
		1802	1832	62.9	57.3	64.3

		1913	1945	44.7	46.0	59.3
		2004	2032	40.8	33.0	58.1
		2210	2246	25.8	25.4	59.7
		2317	2357	16.7	16.0	58.3
243	***Monday August 31***	0044	0103	10.6	10.6	12.8
		0115	0152	11.5	14.5	55.3
		0250	0329	12.2	14.6	60.3
		0428	0450	14.5	16.3	60.1
		0538	0627	14.9	18.7	63.5
		0831	0932	18.2	26.2	56.3
		1030	1058	47.3	53.4	64.3
		1520	1548	76.1	76.5	79.6
		1842	1917	69.0	65.1	108.4
		1815	1955	62.7	52.8	103.6
		2151	2230	19.5	16.4	83.0
		2305	2337	10.3	22.8	76.6
244	***Tuesday September 1***	0008	0048	35.3	38.8	88.4
		0122	0206	57.1	29.1	93.9
		0233	0306	6.7	11.5	102.2
		0352	0413	15.9	-	81.4
		0429	0514	12.9	46.8	106.1
		0539	0612	11.4	12.6	97.3
		0644	0720	9.3	31.7	85.6

		0801	0835	11.5	19.1	90.7
		0907	0937	23.3	29.6	89.2
		1020	1051	31.5	52.7	87.8
		1211	1226	70.9	-	84.9
		1242	1309	82.1	87.1	106.2

Appendix 3: Sonic Wind direction corrections

The sonic anemometer was orientated to ensure minimal flow distortion from the prevailing winds. However, unfortunately the exact compass direction of the sonic was not recorded during the experiment. This information although not directly important to the field campaign would have been useful for determining which blocks of data had to be discarded due to poor fetch. To overcome this omission, the wind directions recorded by the sonic were correlated with the data from the wind vane for the 15 averages and a linear correction was made. Whilst this is clearly an inferior means of determining direction, the use of wide angle ranges and both data sources to discriminate between data sets suggests that any errors introduced by this omission will be minimal.

Procedure:

Data for 19/07/98,23/07/98,16/08/98,02/09/98 were chosen for analysis. These were windy days when variations in wind direction with height were likely to be minimal. 15 and 30 min averages of the wind direction measured by the wind vane were compared to the 15 and 30 min average from sonic.

Linear regression gave

$Y = 0.88+97.8\, r2 = 0.75$	all data (183 30 minute data records)
$Y= 1.02 + 83.03 \quad r2=0.99$	cases with wind speed < 2m/s

Appendix 4: Summary of data processing routines and data available on CDROM

Sonic and GFAS data

All the high frequency data was stored in binary format using software developed by Zoran Nesic for the UBC Soil Sciences. The data can be converted from binary to ASCII using a program written by Vincent Kujala **gill2txt.c**. The following processing routines are designed to run on a windows platform using MSDOS and DJGPP software. Many of these programs must be compiled with **lgblnk.for**. This is a freely available program designed to mirror some common UNIX based commands.

Data quality control programs

- Calculate mean and variance for 20 sub periods within each 30 min file using **stats.for** and subroutines **sepson.for**
- Calculate median of each group using **medians.for**
- Test for wind direction and stationarity using **nonstat.for**
- Calculate 5, 10 and 15 minute fluxes using **fl30cl05.for, fl30cl10.for fl30cl15.for**
- Calculate the error using Foken and Wichura methods **readfl30.for**

Calculate fluxes, averages and standard stability parameters

- Calculate eddy correlation, friction velocity and general statistics using **wkgflux.for**

Wavelet based programs

- Matlab routine to calculates the discrete form of the wavelet transform using the Haar wavelet - **dwave.m**
- Matlab routine to calculates the continuous form of the wavelet transform using the Haar wavelet - **cwave.m**
- Matlab routine to reconstruct signal at different scales - **reconstruct.m**

- Matlab routine to calculate the spectra from the wavelet transform for comparison with the spectra from the FFT - **dwave_spectra.m**. Note KM14 is just 2*pi/2^j where j = 1:14.
- Matlab routine to calculate fluxes using the MODWT form of the wavelet transform based on Whitcher (1997) code **wavecomp.m**
- Matlab routine to calculate continuous form of the wavelet transform, red and white noise based on Torrence and Compo (1998) code **TCwaven.m**
- Matlab routine to calculate co-spectra for the time series based on Torrence and Compo (1998) code **cospectra.m**
- Calculate number and duration of flux events from 30 minute reconstructed and filtered data provided by matlab routine tcwaves using **multiscales.for**

Code from Whitcher (1997)

http://www.cgd.ucar.edu/~whitcher/software/

wavecov.mlab % info file

dwt.c

idwt.c

modwt.c

imodwt.c

dwt_dbp

myacf.m

myccf.m

myfilter.m

Mexopts.sh

modwt_dbp

modwt_brick_wall

wave_var

mynorm = norminv

wave_cov.m

wave_cor.m

wave_cross_cov.m

wave_cross_cor.m

Code from Torrence and Compo (1998)

http://paos.colorado.edu/research/wavelets/

Chisquare_inv.m

chisquare_solv.m

wave_signif.m

wave_bases.m

wave_test.m

wavelet.m

Tethersonde data

Raw data stored as '.dat' files for each flight (ascending and descending limb). Data files which have been adjusted to read the correct heights above ground level are stored as '.out' files.

All other meteorological and chemical data

All other parameters were stored on Cambell Scientific data loggers using PC208 software. The data are stored as '.txt files' in the appropriate directories.

Appendix 5: Tethersonde flight paths

In order to determine the validity of the data shown in the contour plots the time versus height plots of the tethersonde flights for each night contoured are provided below.

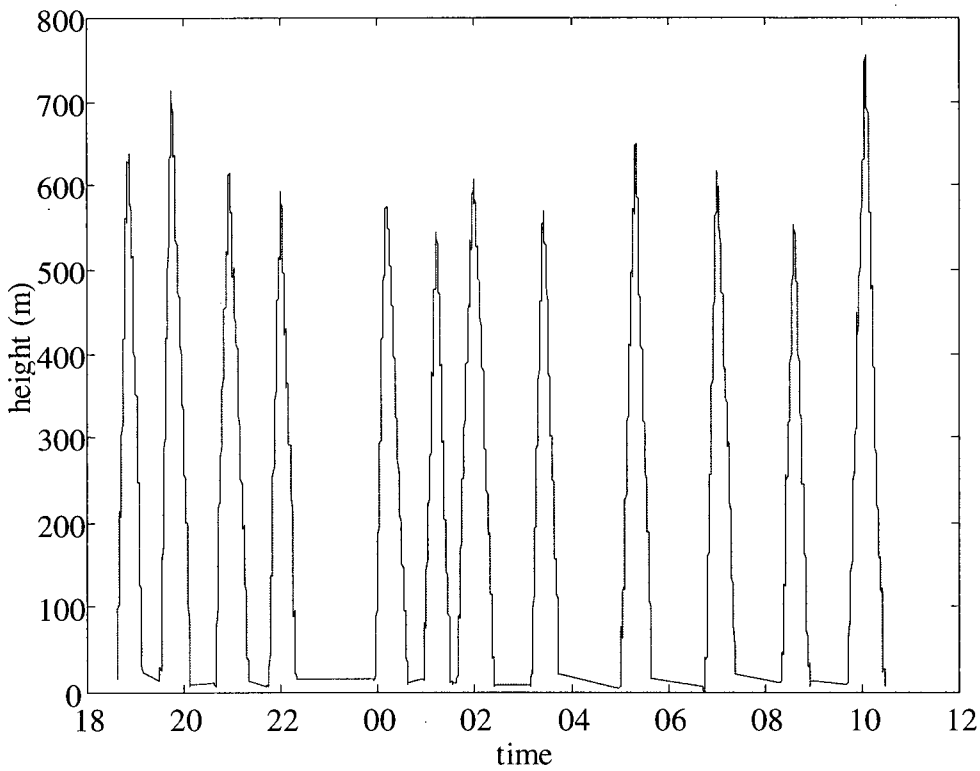

Figure A5.1 The time and height of tethersonde measurements used to calculate contours for July 26th - 27th 1998

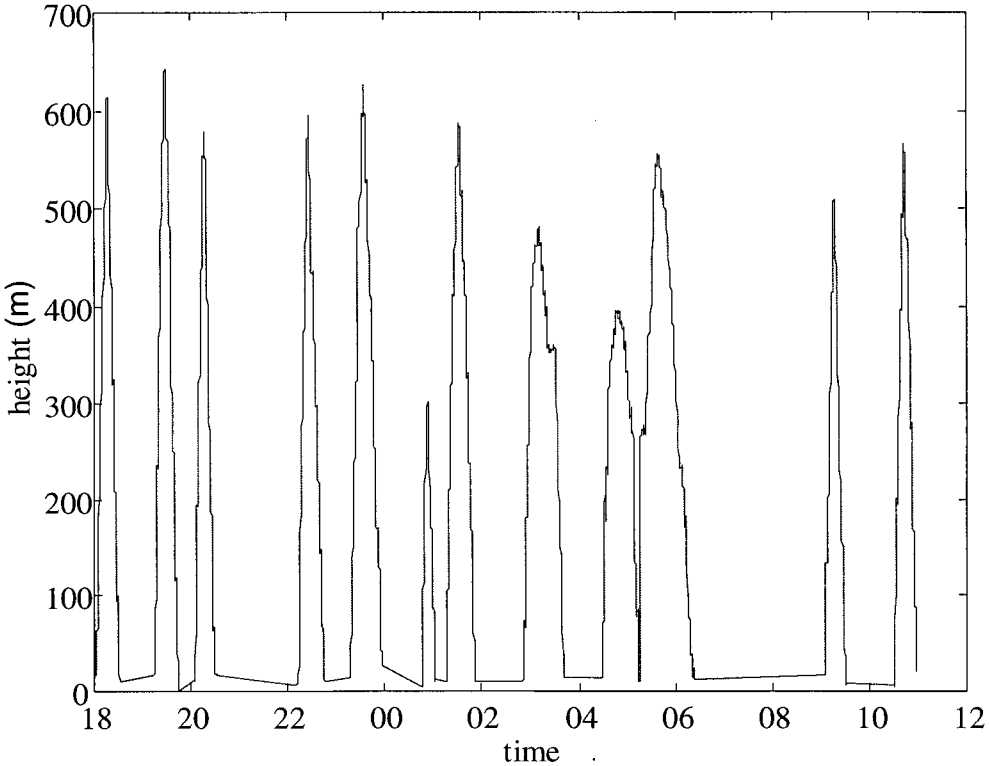

Figure A5.2 The time and height of tethersonde measurements used to calculate contours for August 30th - 31st 1998

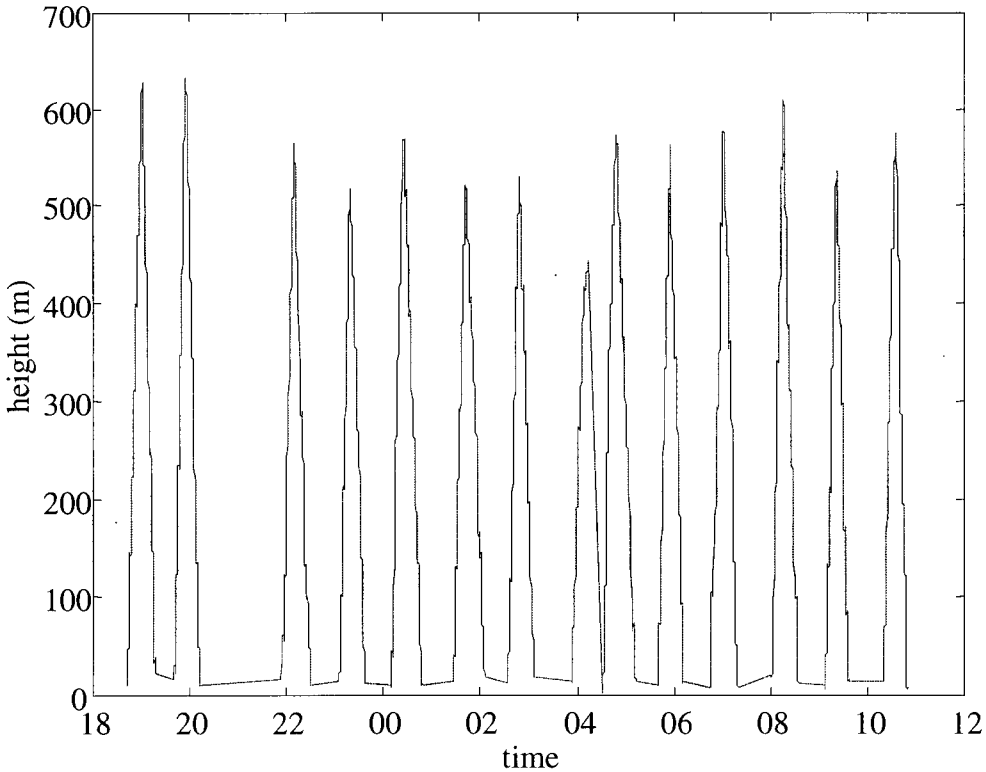

Figure A5.3 The time and height of tethersonde measurements used to calculate contours for August 31st - September 1st 1998

Appendix 6: Real examples of low-level jet classification types

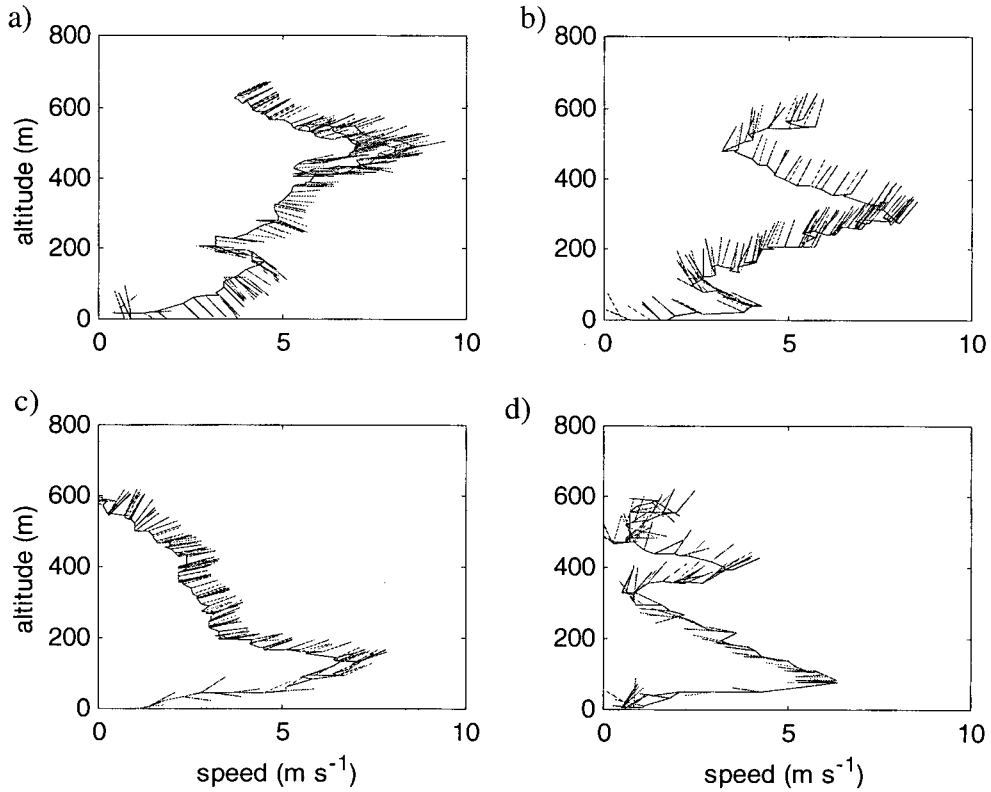

Figure A6.1 Real examples of low-level jet classification types 1 - 4 for a) type 1 LLJ observed at 0452 July 22 1998, b) type 2 LLJ observed at 0538 August 31 1998, c) type 3 LLJ observed at 0136 July 29 1998 and d) type 4 LLJ observed at 0644 September 1 1998